Path Tracking Control of Automated Vehicles: Theory and Experiment

Mostafa G. Mehrabi

A Thesis

in

The Department

of

Mechanical Engineering

Presented in Partial Fulfilment of the Requirements

for the Degree of Doctor of Philosophy at

Concordia University

Montreal, Quebec, Canada

September 1993

ISBN 0-612-01375-8

Path Tracking Control of Automated Vehicles:

Theory and Experiment

Mostafa G. Mehrabi

ABSTRACT

This thesis deals with theoretical and experimental studies on path tracking control of automated vehicles. Two (yaw and lateral) and three (yaw,lateral and roll) degrees of freedom nonlinear dynamic models are studied for the motion of a vehicle. Their linearized versions are also obtained, being more appropriate for analytical study and motion controller synthesis.

It is shown that the coupling between the roll, the yaw and the lateral motions is characterized by a dimensionless entity named "roll number". When the roll number is small, 3-DOF and 2-DOF models possess the same dynamic pattern. The former, thus, can be reduced to the latter avoiding the complexities of the higher order system.

The transient response of a vehicle in plane motion and the parameters involved is another issue considered here in this thesis. In this regard, two other

quantities called "velocity constant" and "yaw number" are introduced. These quantities can be effectively utilized in characterizing when to use a dynamic model or a simpler kinematic model to represent the motion of the vehicle.

A parametric study is carried out by using sensitivity theory as a tool. This provides one with a better understanding of the severity of changes in both transient and steady state responses of the system due to parameter variations.

Control algorithms for path following of a vehicle are investigated for various wheelbase configurations. For a tricycle model vehicle (front wheel steered) a nonlinear controller is proposed and the path following of the vehicle is studied by simulation. By employing the linear model (for tricycle model, front steered vehicle) an optimal controller is designed that minimizes a quadratic measure of performance consisting of the integral of the errors (errors in position and orientation of the vehicle) and the input (front wheel steering angle). The performance of the controlled system is studied by simulation. For a tricycle model with two independent side tractive wheels a controller is designed and the simulation results are presented for path following.

A prototype vehicle is built (CONCIC III) at Centre for Industrial Control, Department of Mechanical Engineering of Concordia University that serves as a testbed for the experimental studies. All the experimental results reported are

carried out on CONCIC III.

The optimal controller is implemented to path tracking control of CONCIC III. The analytical results obtained from the nonlinear dynamic model and those obtained from the actual motion of the vehicle are compared and the validity of the model and the associated assumptions are verified. A comparison is made between the linear and nonlinear models to show the accuracy of the linear model. Finally, path following of the vehicle for various initial conditions, trajectories and disturbances are examined and the results are reported.

ACKNOWLEDGEMENT

I would like to record my deep sense of gratitude and thanks to my thesis supervisors Dr. R.M.H. Cheng and Dr. A. Hemami for their excellent guidance and directive supervision, constructive criticism, moral and financial support during the course of this research. I feel extremely fortunate to have had the opportunity of working with them and sharing their experience and insight. The combination of freedom and unhesitating support they provided was invaluable.

I am very delighted to thank Dr. R. Rajagopalan for many useful discussions, suggestions, comments and encouragement I have received from him throughout this research.

I owe many thanks to Mr. Gilles Huard for his assistance in providing the necessary assistance in various phases of development of CONCIC III vehicle. Without his help, this work was impossible.

I would like to thank Dr. S. Rakheja for his valuable suggestions and comments I received.

The author highly appreciates the members of Machine Shop of the

Department of Mechanical Engineering for providing the assistance in building the experimental vehicle.

I would like to thank all my colleagues and the members of the Centre for Industrial Control (CIC) for keeping my spirits alive which made this thesis possible. Special gratitude is due to Mrs E. Morris for her assistance during the course of this study.

The author acknowledge the Natural Science and Engineering Research Council of Canada (NSERC) awarded to Dr. R.M.H. Cheng for developing CONCIC III experimental vehicle.

Last but not least I owe many thanks to my family and specially my wife for her patience, encouragements and help during this work.

Finally, I am also very grateful to my parents for supporting and encouraging me at all stages of my studies.

Dedicated to

My Family

TABLE OF CONTENTS

LIST OF FIGURES

LIST OF TABLES

List of the Notations

U	Longitudinal axis attached to the vehicle centre of mass
W	Lateral axis attached to the vehicle centre of mass
X,Y	Fixed coordinate system
V	Vehicle velocity
F_y	Lateral Force
F_x	Tractive Force
F_z	Normal Force
M_y	Rolling resistance moment
M_z	Aligning moment
M_x	Overturning moment
C_α	Cornering stiffness of the tire
$\frac{\partial F}{\partial x}$	Partial derivative of function F with respect to x
t_p	Pneumatic trail of the tire
C_γ	Camber stiffness
V_u	Forward velocity of the vehicle
V_w	Lateral velocity of the vehicle
p	Roll velocity

M Mass of the vehicle

M_s Sprung mass of the vehicle

h Distance between the roll centre and the centre of mass of the sprung mass

I_z Yaw moment of inertia of the vehicle

I_u Roll moment of inertia

K_p Stiffness Coefficient of roll motion

D_p Damping Coefficient of roll motion

$(F_{Rfl})_{L,R}$ Reaction forces of the front(f) Left(L) and Right(R) wheels

$(F_{Rrl})_{L,R}$ Reaction forces of the rear(r) Left(L) and Right(R) wheels

a Distance between front wheel and the centre of mass of the vehicle

b Distance between rear wheel and the centre of mass of the vehicle

q Roll angle

$\dot{x}$ Derivative of variable x with respect to time

m_w Mass of the wheel

r_w Radius of the wheel

$(F_{Rre})_{L,R}$ Rolling(R) resistance(re) of the Left(L) and Right(R) wheels

$(F_{Tf})_{L,R}$ Tractive(T) effort of the front(f), Left(L) and Right(R) wheels

$(F_{sf})_{L,R}$ Side forces(s) of the front(f), Left(L) and Right(R) wheels

$(C_f)_{L,R}$ Coefficeint of Cornering(C) stiffness(s) of the front(f), Left(L) and Right(R) wheels

f_r Coefficient of rolling(r) resistance of the tire

$(N_f)_{L,R}$ Vertical reactions of the front(f), Left(L) and Right(R) wheels

$(W_f)_{L,R}$ Vertical loads of the front(f), Left(L) and Right(R) wheels

W Total weight of the vehicle

a_u Forward acceleration/deceleration of the vehicle

g Constant of gravity

J_f Moment of inertia of the front(f) wheel

$(T_f)_{L,R}$ Torque of the front(f), Left(L) and Right(R) wheels

$(F_{Tr})_{L,R}$ Tractive(T) effort of the rear(r), Left(L) and Right(R) wheels

J_r Moment of ineria of the rear(r) wheel

$(T_r)_{L,R}$ Torque of the rear(r), Left(L) and Right(R) wheels

$(F_{sr})_{L,R}$ Side(s) forces of the rear(r), Left(L) and Right(R) wheels

$(C_r)_{L,R}$ Coefficeint of Cornering(C) stiffness(s) of the rear(r), Left(L) and Right(R) wheels

F_{sf} Side(s) forces of the front(f) wheel

F_{sr} Side(s) forces of the rear(r) wheel

$T_i(s)$ Transfer function between input-outpt pairs

$Z_j(s)$ Numerator polynomial of a transfer function (zeros)

Ps(s) Characteristic polynomial (poles)

t Time

x State vector

Δx Change in the state vector

x_i i'th state variable

u Input vector

g_i Tunning factor

q_i Positive scaler weighting factor

R Positive scaler weighting factor

z State vector

ω_i State variable

K Gain matrix

K_i Gain of the controller

K'_i Gain of the controller

G_i Gain of the controller

F_{cf} Frictional force of the front wheel

F_{cr} Frictional force of the rear wheel

U_A Coordinates of point A in body axis

$\Delta l_{f,r}$ Distance traveled by front(f) and rear(r) wheels

T Kinetic Energy

x_u Coordinate of centre of mass(vehicle) in U- direction

y_u Coordinate of centre of mass(vehicle) in W- direction

ψ Heading angle of the vehicle

β Side slip angle of the vehicle

γ Camber angle

Ω Yaw rate of the vehicle

$\delta_{fw,rw}$ Instantaneous Steering angles of the front(f) and rear(r) wheels

$\delta_{f,r}$ Steering angles (command) of the front(f) and rear(r) wheels

$(\omega_f)_{L,R}$ Angular velocities of the front(f), Left(L) and Right(R) wheels

$(\beta_f)_{L,R}$ Slip angles of the front(f), Left(L) and Right(R) wheels

$(\beta_r)_{L,R}$ Slip Angles of the rear(r), Left(L) and Right(R) wheels

$(\omega_r)_{L,R}$ Angular velocities of the rear(r), Left(L) and Right(R) wheels

$\beta_{f,r}$ Slip angles of the front(f) and rear(r) wheels

λ_i Eigenvalues

α_i i'th system parameter

α_0 Nominal parameter vector

$\Delta\alpha$ Change in the parameter vector

$\lambda_q^*(t)$ Trajectory sensitivity vector

$\lambda_{ij}(t)$ Trajectory sensitivity function

ε_d Position error

ε_θ orientation error

ρ Radius of the curve

$\Delta\psi$ Incremental orientation change of the vehicle

$\psi_{f,r}$ Angular position of front(f) and rear(r) wheels

CHAPTER 1
INTRODUCTION

1.1 Introduction

Automated Guided Vehicles (AGV) and Wheeled Mobile Robots (WMR) are self-propelled vehicles that are expected to follow a specified trajectory such as reflective tape or paint, or buried wires carrying different frequencies for path distinction. Alternatively, they can use a route map stored in memory. These systems have been used for various purposes for applications such as nuclear and explosive materials handling, security, hospital services, etc. or in three general areas of distribution, assembly, and manufacturing. The distribution applications typically involve the movement of materials to and from the production area or within warehousing operations. In manufacturing, their applications are limited to material handling between manufacturing cells. In assembly lines, they have had a larger impact. In this case, the workpieces are transported through the assembly/build process. For instance, in electronic industry where the demands for various types of productions are high, AGVs offer the flexible programmable transporting systems needed to meet the new demands of the production lines.

In automotive industries, AGVs have been used for both assembly applications as well as manufacturing process such as body assembly, motor assembly and welding stations [1].

AGVs are constrained by their fixed track and the only flexibility provided is switching or merging of the alternative routes. For many applications, a fixed track is perfectly adequate. Wheeled Mobile Robots (WMR) are the systems that can offer other tasks with a higher degrees of autonomy. So, instead of being confined to move along a fixed track they can move more freely and are more maneuverable. Their typical applications are working in hazardous environments, remote control applications, rescue works, hospital, undersea operations and similar areas.

Automated Transit Vehicles (ATVs) are a class of urban transportation systems ; like AGVs they need some reference trajectory to follow. However, their working environment is different (highways) and operate at a higher range of speeds as compared to the mobile robots and automated guided vehicles. ATVs have drawn a great deal of attention recently and the study of their performance will be an active topic for future research. This will be supported by the fact that a considerable amount of funds are being devoted to research and development of these systems in the United States, Europe or Japan. While two operational tests are under way in Europe and in Japan, several projects are being

sponsored by various agencies [2].

1.2 Review of Autonomous Vehicle Research

In this section, a historical background is provided to illustrate the advances in research and development of the above systems during the recent years. A brief review of the studies so far made in their theoretical and experimental aspects of kinematic modelling, dynamic modelling, motion control and tracking stability will be given and the aims and important areas of the future research will be explained. It should be mentioned that the research in this area is growing very rapidly and by no means the list of the projects mentioned in this section are complete.

1.2.1 Historical Background

Probably, the preliminary stages of developments on autonomous vehicles started in the early 1950's with their use in automotive industry. However, many factors hindered their early growth; among them are limited on-board computing power, lack of or nonexistence of the electronic devices such as integrated circuits (IC) to be used in their controllers, lack of sensor technology, etc.[1,3]. During the 1960s, with the advances in electronic industry, more compact controllers were in the market and also more computing power was

available; however, despite all these advances, they were too expensive to use them in manufacturing. During the seventies, the research was slowed down partly because of some of the reasons discussed above such as lack of on-board instrumentation and also little real-world applications. However, it was in the early eighties that the development of experimental works in advanced robotics was picked up rapidly and the AGVs were being used widely in industry, particularly in automotive industries and assembly lines. The major factors were the improvements in microprocessors and sensor technology as well as anticipations of new applications in both industry and hostile environments.

1.2.2 A Review of Experimental Automated Vehicle Projects

Literature survey suggests that the pioneering research on mobile robots started in Stanford University where two versions of an autonomous mobile robot were built. The main focus of the research has been the study of the processes for real time control of mobile robots interacting with complex environments by using Artificial Intelligence (AI) [4]. It is believed that mobile robots are very appropriate tool and powerful support for Artificial Intelligence (AI) oriented robotics where a variety of problems like perception, decision making, communications, etc. should be viewed and solved within the constraints and limitations of the robot like computing power, on-line processing of data, operation ability, etc. One of the critical problems directly associated with the

above limitations is their path planning problem which has been the subject of numerous studies [5-6]. In this regard, many experimental vehicles have been built and various algorithms for their path planning are proposed [7-10]. In the following section, attention is paid to explanations of some of these experimental projects and their aims and importance.

The Stanford Cart [11] was a remotely controlled mobile robot. The robot used an on-board camera that could locate the surrounding objects. It planned an obstacle-avoiding path to a desired destination on the basis of the images received. The motion of the robot was very slow (approximately one meter in every 10 to 15 minutes) and, as reported, it could take as much as 5 hours to execute an approximately 20 meter long trajectory. The cart has been used to investigate the problems such as 3D image processing, obstacle avoidance and path planning.

The Carnegie Melon University (CMU) rover [4] was a more capable mobile robot being built to develop and extend Stanford work and provide a more flexible testbed to explore new directions in research. It was equipped with a camera and an array of ultrasonic sensors to provide the robot with the necessary information about its surrounding environment. The CMU rover is intended to support a variety of research in the areas of mobile robots such as vision, decision making, path planning, real world modelling and similar issues.

At University of Tokyo [12], a mobile robot has been built with a tricycle wheelbase configuration equipped with differential driven rear wheels and a caster in the front. Two cameras provide the vision for the robot. It has been used for experimental studies to improve the flexibility and autonomy as well as obstacle avoidance of the vehicle. A scheme for path planning has been used that allows the robot to determine the minimum time route from the present position to the target.

At the Jet Propulsion Laboratory (JPL) in their research program on Mars rover a small scale of the vehicle has been built and used to study the issues like visual navigation, hazard avoidance, computation requirements etc. [13]. This vehicle can be teleoperated and controlled from the earth, however, because of the long signal time to the Mars, it possesed some degrees of autonomy. It has been equipped with stereo cameras and scanning laser to extract the information from the surrounding. The images are sent to the earth where they are viewed by a human operator and accordingly a safe path is designated for the vehicle.

The above projects are explained just to exemplify various developments in the area of automated vehicles. In addition to them, there are some reports on other projects and developments as are cited in references [14-19].

1.2.3 Review of the Literature

Generally speaking, the direction of research in the area of automated vehicles can be classified as (but not limited to) : guidance and motion control, sensing, navigation, motion planning, and design and building of a prototype.

In guidance and motion control, the problems concerned are associated with moving the vehicle around predefined desired trajectories. Therefore, like any other control system, it is required to have enough information regarding their kinematics, dynamics as well as certain levels of knowledge of designing feedback control systems [10,25-26,59,61,94-96]

Sensing is required for an automated vehicle in order to extract the necessary information about the surrounding environment, from which the vehicle can recognize its instantaneous position relative to the path and surrounding obstacles. Relevant to this topic, various techniques have been introduced [97-100].

One of the fundamental requirements for automated vehicles are their navigation as the vehicle should know its position and heading at every instant. There are various navigation schemes proposed in the literature [100,15,26]. For

instance in reference [100] inertial guidance has been used while Jullier[15], has employed odometery to update the position and heading of the vehicle.

Path planning problem is another area of research in automated vehicles that has received a lot of attention [6,9,95]. Generally, path planning can be stated as having specified the present location and final goal of the vehicle as well as the location of the surrounding obstacles, define a collision-free path within the constraints of motion of the mobile robot.

Research in the area of automated vehicle requires a multidisciplinary knowledge; building such a unit requires some or all of the expertise explained above. In addition, one also encounters difficulties in their hardware design such as structural design, necessary circuitry involved, as well as the development of the required software.

Due to main stream and objectives of this thesis, more attention is paid to review of previous works relevant to different proposed motion control policies, kinematic and dynamic modelling and their associated problems. In this section, it is tried to summarize and briefly discuss the achievements of some previous studies relevant to the above named topics respectively.

As it was explained before, these systems are supposed to accurately follow

a specified path. In this sense, any deviations from the path is undesirable and a good controller become necessary for a stable and accurate tracking ability. In this regard, there are some studies that have been carried out investigating the problems like their motion control and tracking stability [21,26-27]. Bronstein and Koren [26], a motion control strategy has been proposed for a tricycle model nursing robot with two left and right traction wheels; this motion control policy minimizes the position errors. The vehicle is designed to perform only two distinct kinds of motion: straight-line motion when both motors are running at the same speed in the same direction, and rotations about the vehicle centre points, when both motors are running at the same speed but in opposite directions. While, this algorithm has some advantages for typical works expected from a nursing robot, where a point to point motion is satisfactory, however, by applying this motion control policy the robot is unable to follow curved trajectories, since at any instant it can either move straight or turn "on the spot" and their simultaneous executions is not possible.

In [20] some preliminary results obtained from an experimental tricycle vehicle are described. A cart has been equipped with a single front wheel, which serves for both steering and driving the cart, and two passive rear wheels for stability purposes. The cart motion is represented by a set of kinematic relations while enough information regarding the importance of the cart's dynamics are not provided.

In continuation of the previous works carried out in [22], [21] recently has formulated motion controller design of (WMR) where use is made of a Lyapunov function to specify the structure of the controller to be designed for these systems. This analysis is based on a kinematic model common to the vehicles which are not omni-directional.

Regarding the motion control of WMRs, there are some other studies reported in the literature where basically the analysis are carried out by using simple kinematic models without any clear indication of the importance of the cart's dynamics at lower speeds. Let us cite references [8,12,15,16,23] among many other contributions. In addition, controllers based on neural networks and fuzzy control theories that have been already implemented to other systems such as robotic manipulators [28], chemical processes [29], two axis positioning table [30], and so on [31] are finding their ways toward the motion control of wheeled mobile robots [32-33]. For instance, in the study made in [33], a neuromorphic controller has been designed for the steering control of an AGV unit. steering. After being investigated with a realistic dynamic model of the vehicle [34-36], it has been successfully implemented on the experimental CONCIC II vehicle developed at Centre for Industrial Control of Concordia University [34,36-44].

The study of their kinematic modelling started with the pioneering work of Muir and Neuman [45-47]. In their approach, the kinematic of the vehicle was

developed based on a kinematic model for each wheel, and a condition was proposed to determine wether ideal rolling is possible. This methodology has been implemented to an experimental vehicle with omnidirectional wheels called Uranus developed at Robotic Institute of Carnegie Melon University.

In a very similar approach, the kinematics of the vehicles with directional sliding wheels are studied in [48]. In their study, the kinematic equations relating velocities of the wheels and the vehicle body are developed and from them, controllability of the vehicle is studied.

In another study as reported in [43-44], a generic form of kinematic modelling has been introduced that can be used for various wheelbase configurations employed in WMRs. Furthermore, a criteria called path controllability is introduced that can be used to identify a suitable combination of driving and steering wheels to avoid the redundancy in these systems.

In [49], the relationship between the rigid body motion of the robot and the steering and drive rates of various wheels are developed and as a result, the position and orientation of the robot are obtained. Also, a condition is provided that specifies when ideal rolling fails however, no experimental results is provided.

In addition to the above studies, by noting that WMRs are a typical example of mechanical systems with nonholonomic constraints, there are some other reports that kinematic models are developed and utilized to study some nonlinear control laws for these systems and WMRs in particular. The problem of parking is investigated extensively in the literature [50-52].

While motion control and kinematic modelling of these systems have been the subject of many studies, comparatively little work has been done for their dynamic modelling and even fewer experimental studies have been reported in the literature [14]. The complexity in dynamics of these vehicles arise from the constraints that reflect the non-slippage motion of the wheels [24,53]. Literature survey suggests that some earlier attempts of dynamic modelling of WMRs adopt the Lagrangian formalism for nonholonomic systems in order to obtain the equations of motion [24,54]. In their analysis, the wheels are assumed to be rigid, and nondeformable disks [54], and all interactions between the wheel and the ground is assumed to occur through a point contact. In reality, most wheels are made of a deformable material (rubber for instance), so that the interaction with the ground is through a contact patch [14,55-56]. Furthermore, it is rather difficult if not impossible to come up with closed form solutions for typical control applications; in addition, it is more difficult to analyse the dominant parameters affecting their motion. However, as it is shown in [14,25,34-36,57-61], some concepts commonly recognized in the area of vehicle dynamics can be effectively

used in the motion analysis of these systems. For instance, referrence [36] has formulated the dynmaics of a differential drive AGV.

In this regard, there are numerous studies concerning the handling and stability of vehicles, leading to the development of models with different levels of complexities [69-75]. On close examination, one may conclude that there are basically two popular classes of models arising from these researches for moderate levels of lateral accelerations: namely 3-DOF models which incorporate the lateral, the yaw and roll motion [76-78], and 2-DOF models that omit the roll motion [58,79-82]. Nisonegar [25] has used a 3-DOF model to compare the dynamic performance of single- and dual-axle steered automated transit vehicles. In their analysis, it is assumed that the feedback system or controller receives the tracking error measurements from the sensors mounted in the front and rear of the vehicle. It is found that for straight line tracks, the performance of the dual-axle vehicle exhibits very little improvement over single-axle vehicle and their tracking errors are comparable. However the results of the study have shown that significant reduction in tracking error during a curved trajectory can be achieved with dual-axle controllers. In [77], a 3-DOF model has been used to represent the vehicle dynamics to study the performance of four wheel steering vehicle. Different steering control strategies are compared by studying the vehicle response through simulation. In another study reported by [78], a 3-DOF dynamic model has been used to investigate the effects of suspension properties

on vehicle stability in a cross wind. Vehicle behaviour when subjected to a side wind is studied both analytically as well as experimentally; the results can be used as working guidelines for further studies.

Two degrees of freedom models are also employed by various researchers. In [79], the vehicle is represented with two degrees of freedom, yaw and lateral velocity. This model has been used to study the stability of the vehicle-pilot system and to get an insight to the way a driver controls his vehicle and to determine the vehicle characteristics that produce the most accurate and safe control. In another study made in [72], a two degrees of freedom model is used to compare the dynamics of a rear wheel steering vehicle with that of a front wheel steering. It is shown that the response of a vehicle to steering input for the rear wheel of the vehicle differs significantly at lower speeds than at higher speeds whereas as the speed increases, both transient and steady state responses become less dependent on which wheel is steered. As the vehicles equipped with four wheel steering (4WS) system are expected to improve the handling characteristics, many researchers' attention has been focused on this subject. The vehicle dynamic models mostly used for these typical applications have two degrees of freedom by considering yaw and lateral velocities [81]. Reference [81] provides a comprehensive review of four wheel steering studies and has tried to identify the essential elements of the 4WS technology in terms of vehicle dynamics and control techniques. In reference [82], a similar model has been

used to design an advanced method for a 4WS vehicle. The proposed technique is based on the theory of model following control where the steering response of the vehicle can follow the outputs of a virtual vehicle model. Relevant to this topic, references [77,80] exemplify some other works carried out in this area.

Noting that the directional response of a vehicle will be affected by the interaction of the tire and the ground, a knowledge of the forces and moments generated by pneumatic (rubber) tires at the ground is essential to understanding the vehicle dynamics. In this regard, there are numerous studies made within the last two decades to describe the characteristics of a tire and the forces and moments produced as a result of this interaction [83-89]. References [55-56,87] provide some general views on the mechanism of generations of the forces and moments at the surface of contact of a tire and ground. Also, the parameters that may affect the interaction are discussed. Reference [88], systematically investigate the effects of different tire design on the dynamic response of the vehicles. The study in this article is based upon experimental data obtained from three tires of widely different structural characteristics. In another study made in reference [111], an analytical formulation is derived for the tyre dynamic properties such as the lateral force, self-aligning moment, etc. that can be used for vehicle dynamic simulations. The formulations are validated against experimental results. It should be mentioned that the above references just exemplify some previous investigations relevant to tire properties. There are some other studies

regarding the tire performance and behaviour under different conditions. Let us cite references [82-85] among many other contributions.

1.2.4 Background of the Research on Automated Vehicles at Centre for Industrial Control (CIC) of Concordia University

To address the issue of experimentation, several prototype vehicles designated as CONCIC I, II and III have been built to supplement the research program at the Centre for Industrial Control of Concordia University in this area. The first vehicle (CONCIC I) was developed in 1985 [90]. CONCIC I is guided by camera vision and follows a floor guide path. It can be used as an automatic tractor or a unit load transporter. It has a tricycle wheel base configuration with one drive-steer wheel in the front and two casters at the back. The driving mechanism consists of a DC motor which is engaged to the driving wheel via a belt and chain transmission. The steering mechanism is made up of a DC motor which drives the steering axis via a chain drive. The controller has been designed and built as a modular structure comprising three microprocessors which execute specific operations such as motion control or analysis of the guide path image with the necessary hardware to communicate with the central computer. CONCIC I worked well in various types of paths. However, its tricycle wheelbase configuration imposes some limitations on turning radius and as a result the tracking at the intersections become more difficult. More technical

details of CONCIC I can be found in [90].

The second generation of the prototype vehicles that has been developed at Centre for Industrial Control (CIC) is CONCIC II. It has a very flexible mechanical design meeting various industrial needs as well as offering different wheelbase configurations by easy relocation of the wheels. Driving units consist of two motorized wheel set at mid-length and the casters at the front and rear. An optical camera is mounted in the front of the vehicle that recognize the location of the vehicle relative to the tape on the floor and the junctions. The vehicle is also equipped with ultrasonic sensors for obstacle detections as well as wireless devices to communicate with the control station [33,37-43]. Dynamic properties of CONCIC II have been studied by [34-36,91], where a two degrees of freedom model has been developed for the vehicles with two side differential driving wheels. A control strategy has been developed and implemented for their motion control. The developed dynamic model has been validated against experimental results obtained from CONCIC II AGV. An animation program has been developed to facilitate the visualization of the performance of the vehicle [36].

CONCIC III is the third generation of the experimental vehicle that has been built to serve as a testbed for the necessary experimentations to be carried out regarding the dynamic modelling and control of automated transit vehicles

(ATV) [59,64-68]. The experimental results reported in this study are carried out using CONCIC III. This vehicle is equipped with two integral driving units located in the fore and aft locations and two side casters for stability. Each driving unit has a driving motor geared to a solid rubber wheel and a steering motor with a ring type reduction gear. The motors are permanent magnet (PM) brushless type DC motors exhibiting linear characteristics suitable for typical applications [36]. More detailed explanations of CONCIC III will be provided in later chapters.

1.3 Components of Automated Vehicle

Generally, the physical structure of automated vehicles consists of four components as follows:

i. The physical infrastructure which consists of the vehicle body and the actuators including the driving and steering units. The vehicle structure is a housing for all other elements of the system such as power units, on-board computing facilities, power invertors, control elements, sensors and guidance systems, electrical and electronic components, etc. The actuators such as driving and steering units provide the required motion of the vehicle. They consist of electrical motors with the necessary elements such as belts or gears to transmit the powers to the wheels.

ii. Control Components to monitor the proper motion of the vehicle. It consists of motion controller, digital to analog convertor, servo amplifiers, measuring devices to monitor the motion of the actuators such as encoders, and the necessary computing facilities.

iii. Electrical and electronic components which mainly consist of the necessary interfacing cards, safety features such as ultrasonic sensors for obstacle detection, power invertors and communication systems (if there are any).

iv. Guidance system that depends on the type of application. Its function is to specify the path by using sensors and accordingly report the relative deviation of the vehicle from the desired trajectory to the host computer. These information will be processed by the on-board computer to generate the necessary commands signals to the actuators for proper steering action. There are several guidance techniques such as inductive guidepath, optical guidepath, dead reckoning, beacon systems, inertial guidance, etc. proposed for autonomous vehicles with their own advantages and disadvantages that can be evaluated by a number of performance criteria such as range, accuracy, flexibility, cost, etc. [1-3]. Among these guidance technique, the first three are most commonly used, which are briefly described below.

In inductive guidepath, the tracks are specified by the live wires embedded under the floor and the magnetic field surrounding the wires is detected by a coupler (or antenna) mounted on the vehicle. The vehicle thus sense its position relative to the guidepath and makes necessary corrections to the offset if encountered. This method of guidance is expensive and less flexible than the others. In optical guidance, the vehicle follows the line (paint or tape) on the floor that are tracked either by the sensors like photosensor in the case of fluorescent line or by the use of a camera(s) mounted on the vehicle [41-42]. The flexibility of this technique is excellent as compared with inductive guidance. In dead reckoning scheme [16], the coordinates of the path to be followed by the vehicle are stored in the memory. This type of navigation scheme is probably the least expensive to implement but it suffers from accumulated error caused by slippage of the driving wheels and disturbances emcountered during the vehicle motion. Reference at specific stations are thus highly desirable such that the vehicle can update its position and orientation.

There are several ways of achieving steering action in WMRs different wheelbase configurations [11,15,16,26,41]. Probably, the more popular ones are the two driving wheels and no steering wheel with caster(s) in the front and/or in the back, two rear wheels driven via a differential mechanism from a single motor and the front steering wheel, and front wheel driving-steering wheel. References [15,26,41] have employed two driving wheels configuration (also

known as differential drive) with two driving motors in the back and a caster in the front. The advantage of this configuration is that they can rotate in the spot around the midpoint of the differential axle [41]. However, they cannot move sideways. References [10,90,20] have used another type of wheelbase configuration known as tricycle model with front wheel driving and steering system and two passive wheels at the rear. These vehicle cannot rotate at zero radius as in the previous case and they have limitations on the minimum radius of curvature they can follow. A similar system with the two rear wheels as driving and the front wheel as steering introduces a redundancy in the system as discussed in references [41,46]. There are some other wheelbase configurations with more number of driving-steering units. For instance, the case of the automobiles with two rear wheels driven by the differential system and the two front steering wheels or with four wheel steered vehicles [81]. It should be mentioned that there are some special types of wheels proposed for WMRs to offer a better maneuverability to the system [3,45-48]. For instance, the type proposed in [47-48] consists of a hub about which are mounted rollers making a 45 degrees angle to the wheel orientation. This form offer the wheel to move in any direction that in turn give the vehicle the ability to move in any direction. The vehicles with the property to move in any direction are called omnidirectional in the literature [47,48].

1.4 Summary

The synopsis of this chapter was given to review of some previous studies relevant to various aspects of automated vehicles. A historical background was provided to show the steps in their evolution. Their various directions of research and development were explained through review of some experimental projects and their major objectives and achievements. Different methods of guidance schemes employed were described. In this regard, the importance of the motion control strategy and its effect on the performance of these systems were explained and some previous control algorithms proposed by other researchers were examined. A review of different attempts in their kinematic modelling was provided and the explanation of various wheelbase configurations employed to produce steering action along with their advantages and disadvantages were discussed. The previous studies relevant to their dynamic modelling and descriptions of different approaches taken by other researchers were explained. In this regard, some previous studies carried out in the area of vehicle dynamics were reviewed and various dynamic models proposed to represent their motion were reported.

CHAPTER 2

SCOPE OF THE STUDY AND PROBLEM DEFINITION

2.1 Introduction

To carry out research in all aspects of automated vehicles and mobile robots, which is an application of multidisciplinary expertise, requires certain levels of knowledge in various topics. The diversity in research is more pronounced by referring to previous studies reported on their kinematic and dynamic modelling, obstacle avoidance, path planning, integrated sensing, motion control, navigation schemes, etc. [10,21,24,26,92-95].

Among the topics mentioned above, in this thesis attentions has been paid to dynamic modelling and motion control of the automated vehicles.

2.2 Objectives

The objectives of this thesis are: dynamic modelling and characterization of dynamics of the automated vehicles, investigation of the effects of variations of the vehicle parameters on its response, development of various control strategies for the most popular wheelbase configurations (tricycle models with steering wheels in the front and differential drive vehicles), design, implementation of the optimal controller and investigation of further improvements in path tracking of the vehicle, and, finally, experimental investigation of the accuracy of the linear and nonlinear dynamic models developed to represent the motion of the vehicle.

2.3 Scope of the Study

As a first step to analysis of motion control of automated vehicles, it is important to develop a good mathematical model which represents the motion of a vehicle obtained from its kinematic and dynamic relations. Regarding the kinematic modelling, by noting that most of the automated vehicles have wheelbase configurations that usually can be classified as a tricycle model [8,10,16] with a front steering (driving) wheel and two active (passive) rear wheels, or two side differential wheels [26,17,39,41] with front or/and rear casters,

they possess rather simple kinematics and the related equations can be derived in a straightforward manner. The kinematic equation of a car like vehicle is also similar and its derivation is not difficult [51,92,95]. However, exceptions to the above exist. The literature reports cases where special wheels have been employed to achieve a better maneuverability for the vehicle; these cases have more complex kinematics than those mentioned above[3,45-48].

The dynamics of automated vehicles are rather complicated since there are certain constraints involved that should be satisfied for pure rolling motion of the vehicle [53,54,91]. Literature survey reveals that there have been two basic approaches followed by researchers [24,25,54,96]. In the first approach, conventional Lagrange equations of motion for nonholonomic systems have been used. Based on this methodology, it is possible to formulate the problem and derive the equations of motion of automated vehicles. However, there are certain assumptions made in their derivation, like considering the tires as rigid disks and the region of contact of the tires and the ground is considered to be a point. To be more realistic, it is noticed that the tires are deformable materials and have certain elastic properties that have not been taken into account in such an approach. Furthermore, the procedure is very long and the final forms of equations appear in a nonlinear fashion that makes it difficult to obtain more insights to dynamic behaviour of the system.

In the other approach, the equations of motion are obtained by using Newton's law of motion and the expression of the forces are obtained by using certain concepts of vehicle dynamics [25,36,57-58,64-65]. The remarkable advantage of this approach is that while it takes into account the stiffness properties of tires, it also makes possible to obtain a linearized version of this model; such a linearized model appears to be very useful in predicting the dynamic and response properties of the system as well as its sensitivity to parameter variations [59,61-62,65]. Throughout this thesis the Newtons' law of motion is used for derivations of equations of motion [34,36,87].

Because the knowledge about the effect of the variations in the physical properties of a dynamical system on its behaviour is a valuable information, in this thesis a parametric study has been carried out. This study reveals the effects of changes of different parameters of the vehicle such as tire properties, mass, sprung mass, forward speed, etc. on its behaviour. This parametric investigation is based on sensitivity theory and the analysis is performed on a three degrees of freedom (3-DOF) dynamic model.

The analytical work in this thesis has given rise to the introduction of three defined entities: the "roll number", and the "yaw number" which are dimensionless and the "velocity constant". These entities are very useful for predicting the dynamic behaviour of an automated vehicles based on certain

physical properties such as mass, sprung mass, roll and yaw moment of inertia, stiffness properties of the wheels and forward velocity, and without need for a detailed analysis.

The "roll number" can be used to characterize two linear dynamic models: one with three degrees of freedom incorporating the lateral, yaw and roll motions, and the other with two degrees of freedom consisting of the lateral and the yaw motions only. These dynamic models (linear) have been used extensively in the literature [25,57,80,82,101] for control applications such as steering controller design of automated vehicles and design of four wheel steering systems for passenger cars and for the study of the effect of disturbances on the handling properties of vehicles. Elsewhere [79], the two degrees of freedom model has been used to analyze the interaction of the driver and vehicle and its effect on the stability of the pilot/vehicle system. In spite of the above mentioned studies, as yet, there is not a clear indication of when to use which of the above two models. As the result of this thesis shows, the "roll number" can be used in this respect. If it is sufficiently small, then a two degrees of freedom model is adequate for the typical applications mentioned above, otherwise the three degrees of freedom model can be used. The advantage of this number becomes more evident by noting that as the degree of a mathematical model representing a dynamical system increases, it becomes more complicated to study the issues such as the response properties, controller design, etc. while having a lower order model

without loosing the necessary information about the performance of the system makes the analysis much easier.

Literature survey reveals that throughout the studies so far reported regarding the guidance and motion control of automated vehicles, either the studies have been carried out by using the kinematic models without taking into account the transient behaviours associated with a vehicle motion [102,52,26] or they have employed dynamic models [25, 53-54,57,103]. Therefore, it is important to identify when and under what conditions the effect of transient part associated with dynamic properties of a vehicle can be neglected and a simple kinematic model is sufficient for their motion control. Furthermore, it is equally important to investigate and specify the dominant parameters that are affecting the vehicle transient response. In this study, it is tried to answer some of these typical questions. In this regard, two other numbers named "Velocity Constant" and "Yaw Number" have been introduced that effectively will specify the relative importance of the transient response of a vehicle. The number called "Velocity Constant" provides a basis to characterize the lateral velocity response, while the "Yaw Number" characterizes the yaw velocity response. The lateral and yaw velocities in turn are closely related to lateral offset and orientation error of a vehicle relative to a desired trajectory, respectively. The above numbers provide relations between various parameters of a vehicle that appear to be the more effective on its dynamic behaviour; for standard passenger cars these parameters

even take a simpler form. It is shown that the forward speed is the most dominant factor affecting the transient response of these systems as is also verified by a parametric study. Furthermore, it is possible to specify the speed ranges above which dynamic properties of the vehicle can not be neglected anymore.

Development of various control strategies for the motion control of automated vehicles constitute another subject that has been studied in this thesis. The two types of vehicle namely tricycle model with the steering wheel in the front and a vehicle with two differential side wheels are considered in this study. The above wheelbase configurations are among the most popular in practice [8,26,36,38]. A nonlinear control strategy is proposed for the control of the vehicles with front steering wheel. Its performance is compared with previous control algorithms by means of simulation.

Based on the linearized dynamic model of the vehicles with front wheel steering system and using optimal control theory, an optimal control law is derived that minimizes a quadratic measure of performance consisting of the integral of the errors (errors in position and orientation of the vehicle) and the input (front wheel steering angle). The performance of the controller is investigated by simulating the system on a digital computer.

The control problem of another class of vehicles equipped with two motorized side wheels, to produce both traction and steering, is also studied. The controller generates the control signals to adjust the angular velocities of the left and right wheels. The structure of such a controller is obtained by making use of the steady-state analysis of equations of motion.

Since there are relatively little experimental studies reported in the literature [14] regarding developments of suitable dynamic models and their respective testing and validations, in this work a great deal of attention is paid to experimental investigations and detailed studies of the results. In order to address some of the above issues, a prototype vehicle CONCIC III has been built at Centre for Industrial Control (CIC) of Concordia University and a good part of this thesis is devoted to experimental studies by using CONCIC III. CONCIC III is a vehicle with fore and aft steering and driving wheels and two side casters for the purpose of stability. In order to justify the validity of the developed mathematical models, as well as the assumptions made in their derivations, the actual motion of the vehicle is compared with that obtained by simulation on the mathematical model. This is achieved by using the magnitudes obtained from the experimentation for the torque on the driving wheels and the steering angles in the model in order to study the performance in path following. This is done for both the nonlinear model and the linearized version of this model and a comparison is made between the two (nonlinear and linear models) by using

experimental data. The latter (linear) is employed in deriving an optimal control policy for the motion control of the vehicle. The designed controller is implemented on the system and its performance is experimentally investigated. Furthermore, it is tried to invoke the possibilities of getting better performances by using the on line data generated while the vehicle is in motion. In this regard, a feedforward action is introduced in the controller by estimating the future posture (position and orientation of the vehicle) of the vehicle and its deviation from a desired trajectory. Also, the data has been used to make the necessary adjustments on the vehicle speed according to variations in the path curvature to obtain a fine motion.

2.4 Layout of the Thesis

This thesis consists of 10 chapters. Chapter 1 is devoted to some general explanations about automated vehicles. In this chapter, the issues like various areas of applications, working enviornement, comprising components and their function are explained and their relationships with each other are discussed. A historical background is provided to show their preliminary stages of research and development and the advances made in this regard. A general explanation of the issues that have recently drawn the attention of the researchers are given and the problems involved are briefly discussed.

In Chapter 2, a particular emphasize is given to review of the literature relevant to the issues considered in this thesis. This demonstrates the past and present status of the studies and their achievements. In this regard, the recent results of the studies relevant to guidance and motion control, kinematic modelling, dynamic modelling of automated vehicles and the problems involved are discussed. This in turn constitutes a basis for the problem definition and the scope of the study of the thesis which is dynamic modelling and motion control of automated vehicles.

Chapter 3 considers some basic concepts and definitions commonly used in the area of vehicle dynamics. In this regard, explanation of different forces and moments acting on the vehicle and the tires as well as the mechanism of their generation are given. Also, the factors that are influential on them are described. Part of this chapter is devoted to description of different dynamic models commonly used by vehicle dynamicists. Also, the various degrees of freedom encountered in their derivation and the statement of the assumptions involved are explained.

Chapter 4 is devoted to development of various dynamic models representing the motion of the vehicle. In this chapter, three degrees of freedom (3-DOF) nonlinear dynamic model is developed by considering yaw, lateral and roll motion. The linearized version of the above model is also obtained and the

assumptions involved are explained. In addition, two degrees of freedom (2-DOF) models (nonlinear and linear) which considers yaw and lateral motions of the vehicle are also developed and their respective assumptions are explained.

In Chapter 5, three new parameters are introduced namely dimensionless "roll number", dimensionless "yaw number" and "velocity constant". These three entities essentially provide one with the necessary information relevant to the dynamic properties of the vehicle without need for a detailed analysis. By using the "roll number" one can decide on which model to use: two degrees of freedom model (2-DOF) or (3-DOF) model. On the other hand, "velocity constant" and "yaw number" provide one with the necessary information regarding the transient behaviour of the vehicle.

In Chapter 6, a parametric study of automated transit vehicles is carried out by using sensitivity theory as it offers an efficient way of doing it. After giving a theoretical background of the approach, a three degrees of freedom model (3-DOF) is developed by taking into account the yaw, lateral and roll motion of the vehicle. The effects of inertia, stiffness and damping, geometric and kinematic parameters on the response of the vehicle are studied. This provides one with a better understanding of the important factors that should be considered in their design.

Chapter 7 is devoted to the study of different motion control policy. For the vehicles with front steering wheel, a new control strategy is proposed to determine the steering angle at each instant based on measured errors, the offset from the path and deviation in orientation. It is illustrated that by implementing the new control policy significant improvement in tracking capability can be achieved.

Based on a linear dynamic model developed for a tricycle model vehicle with front wheel steering system, an optimal controller has been designed for path tracking of the vehicle. It can be shown that the linearized system can be decoupled into two fast and slow mode subsystems where slow subsystem corresponds to a simpler kinematic model. Based on this result, an optimal control law is derived that minimizes a quadratic measure of performance consisting of integral of the errors (errors in position and orientation of the vehicle) and the input (front wheel steering angle).

On the basis of a kinematic studies of motion for a vehicle equipped with a pair of motorized wheels which, by having appropriate velocities, can provide traction forces as well as steering action, a steering control strategy is derived. The angular velocities for the right and left wheels are considered the two control inputs which must cause a system to follow a desired trajectory. Assuming these inputs to be linear functions of the two errors associated with path tracking

problem (position and orientation errors), a control policy is determined. The path tracking behaviour of a mobile robot using such a control law is demonstrated by computer simulation.

In Chapter 8, the mechanical structure as well as the components of the experimental vehicle CONCIC III is explained. Included in this chapter are the general descriptions of the architecture and the comprising units, mechanical and hardware structures, power units, special driving and steering unit arrangements, motion controller chips, arrangements of the servo controller units, data acquisition board and software specifications.

Chapters 9 is dedicated to development of the dynamic model and controller design for CONCIC III vehicle together with the implementation of the controller and study of the experimental results. In Chapter 9, a nonlinear dynamic model is developed for the vehicles with front and rear steering system and a linearized version of that is also obtained The latter (linearized version) has been utilized in development of an optimal controller which minimizes a quadratic measure of performance consisting of the integral of the errors (errors in position and orientation of the vehicle) and the inputs (steering angles of the front and rear wheels). This controller has been implemented on the vehicle as experimental results are provided in Chapter 9. In this chapter, the developed dynamic models (both linear and nonlinear) are validated against experimental

data and a comparison is made between them. The performance of the controller is investigated for path following of the vehicle for different trajectories. As well, a mechanism is introduced that regulates the speed of the vehicle according to the curvature of the path which is useful when the vehicle is negotiating sharper curved trajectories.

Chapter 10 is devoted to explanations of the conclusions and the recommendations for future work. In this chapter, the results obtained from this study are summarized and the conclusions arrived are described.

CHAPTER 3

VEHICLE DYNAMICS CONSIDERATIONS

3.1 Introduction

As mentioned in the previous chapter, there are two basic approaches for deriving equations of motion of automated vehicles. These are using Lagrange's equations for nonholonomic systems [24,53-54,69] and employing Newton's law of motion [25,34,36,59,61]. Throughout this study, the second methodology has been used for the purpose of analysis of motion and the synthesis of motion controllers. The advantage of the second approach is that while it takes into account the stiffness properties of the tire, it also makes possible to obtain a linear model to represent the motion of the vehicle. The linearized model while retains the important dynamic properties of a system simplifies any analytical study. When necessary, the relevant explanations and remarks are given to clarify the

advantages of the approach as well as its potential strength in leading to certain conclusions that otherwise may not be derived.

Due to dependency of the methodology upon the interpretation and understanding of the interactions of pneumatic rubber tires and the ground, the synopsis in this chapter is given to the review of some general notions usually used in vehicle dynamics and the descriptions of the mechanism of generation of the forces and moments in tires. In addition, the factors that may affect these mechanisms are elaborated and explained, while the relevant expressions deemed necessary for derivation of equations of motion of a vehicle are provided.

3.2 A Review of Vehicle Dynamics

Generally speaking, vehicle dynamics is a subject mainly concerned with the characteristics of a vehicle that are assessed from its ability in accelerating, decelerating, braking, handling, cornering, directional response and ride qualities [55-56,87]. Noting that the above properties are direct results of action of various forces on the vehicle, for the motion analysis of a vehicle it is required to develop a suitable dynamic model usually expressed in the form of differential or

algebraic equations. This model can be employed in evaluating the role of the parameters involved in the interested phenomenon as well as providing one with a means of identifying the more important factors and their influence on the vehicle performance. The latter can provide the predictions for future steps that may be followed for any possible improvement in the system.

3.2.1 Description of Dynamic Models with Two or Three Degrees of Freedom and Their Applications

As it implies, a dynamic model is an approximate mathematical representation of an actual system, developed based on some assumptions, in order to make a desired analysis simpler and feasible. The fact that a system may be represented by different models can be justified by noting the main stream of a study and its particular area of application [34-36,57,61,71-72,79,82-84,104-105]. For instance, in the process of modelling, although the vehicle has many components with distributed masses, for many analytical applications it is possible to represent it as a lumped mass. During acceleration and deceleration all the elements speed up or slow down and it is reasonable to assume that the

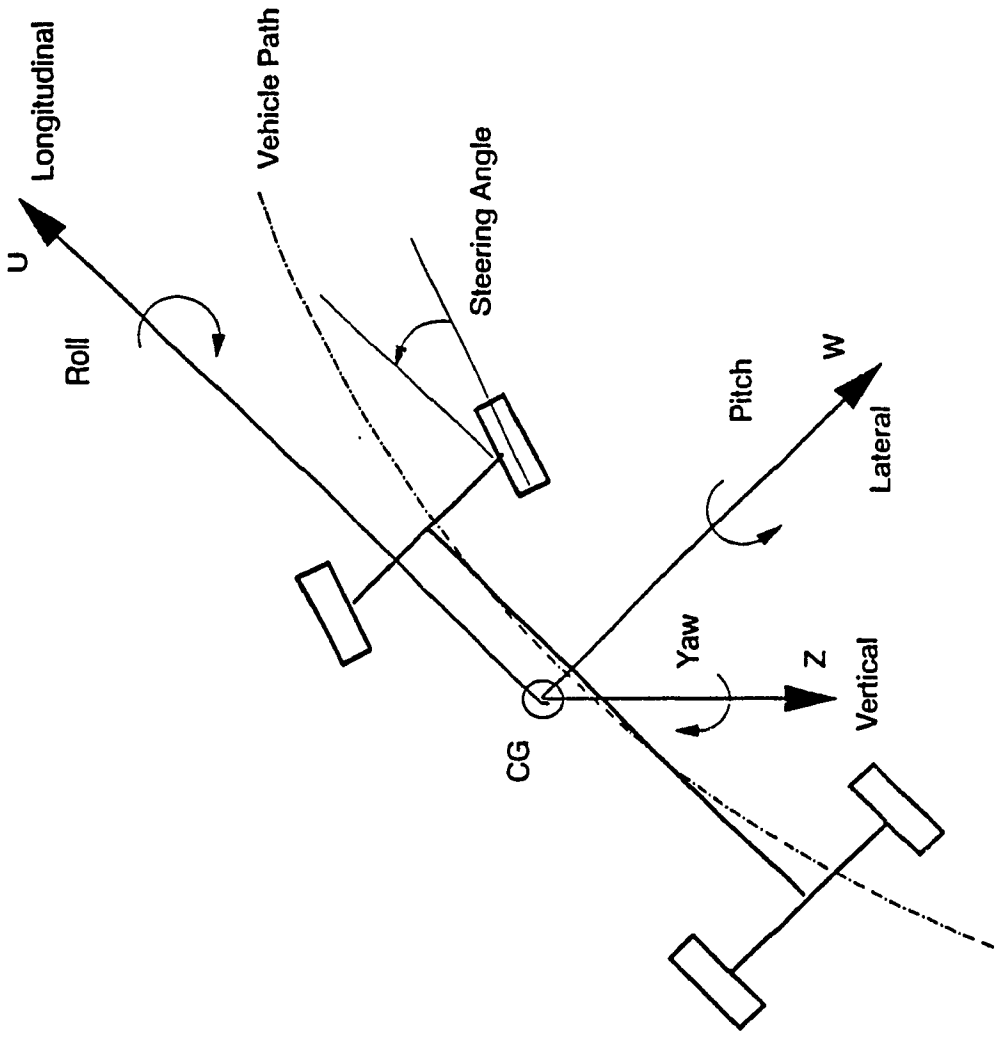

Fig.3.1 Definitions of Vehicle Axis System.

vehicle is a rigid body. However, for ride analysis, this may not be true and the vehicle and the wheels are considered to be as two or more separate lumped masses due to their relative motion [56,87].

In general, as a rigid body the vehicle has six (6) degrees of freedom as shown in Fig. 3.1, offering various choices in the number of degrees of freedom that can be included in dynamic models. Therefore, complex dynamic models can be developed for simulation purposes while simplified models are also proposed for some analytical studies by assuming certain conditions that are not far from

the reality of the system [56]. Within the scope of this thesis, the problems studied are closely related to directional response and handling characteristics of a vehicle, and in this regard, it is well accepted that a dynamic model that takes into account the lateral, yaw and roll motions of the vehicle are quiet adequate to represent the motion of the vehicle [56,78]. Even more simplified models that consider yaw and lateral motions are also reported to give satisfactory results [71-72,79-81]. Typical examples of such motions are lane change or nonemergency manoeuvre of the vehicle where the lateral accelerations

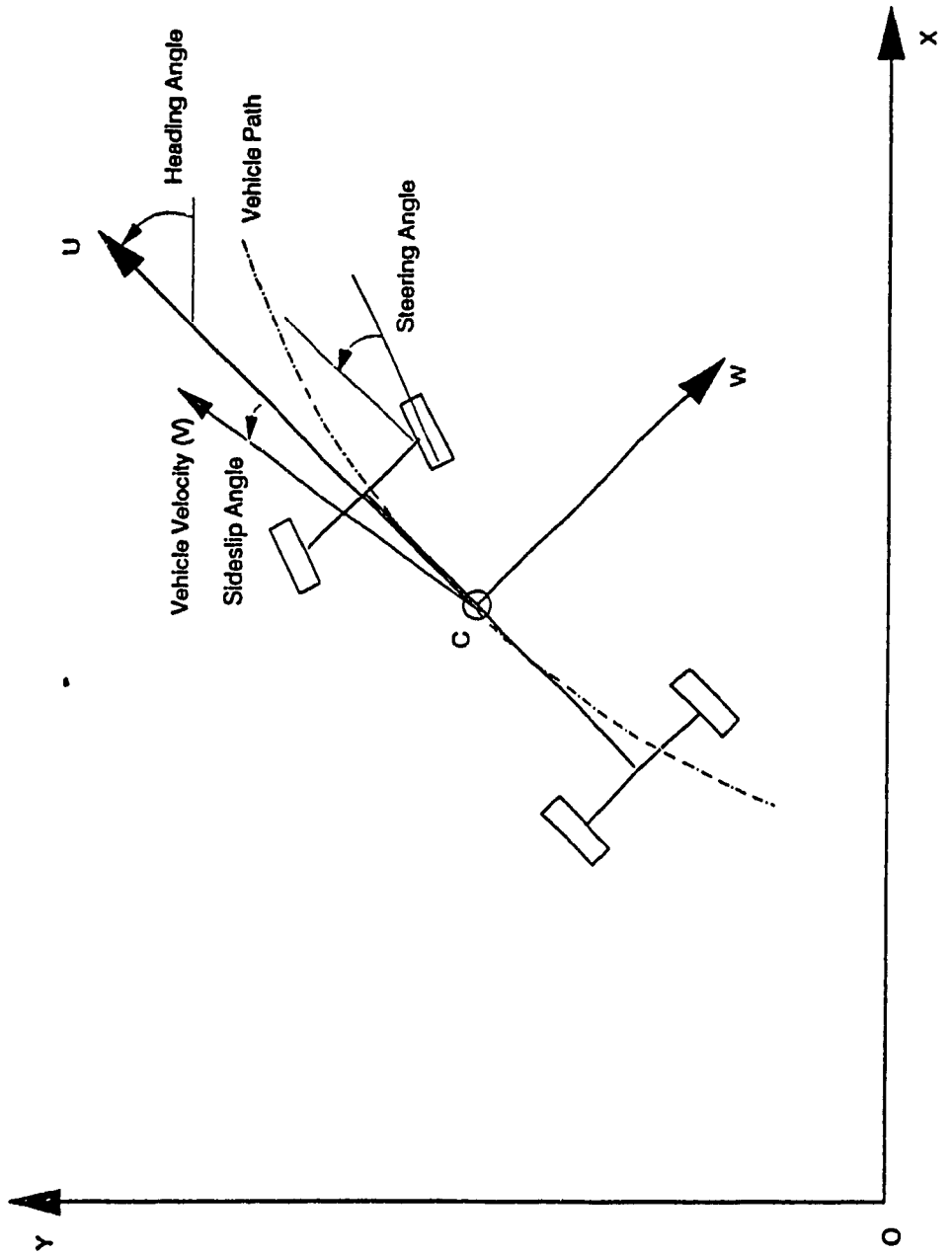

Fig.3.2 Vehicle and Fixed Coordinate Axis Systems

are approximately below 0.3g [58,71]. But, for the assessments of more sever manouvers such as vehicle performance during a combined steering and acceleration/ braking other models are proposed that are mainly used for simulation studies [70,76].

In analyzing the vehicle motion, two sets of coordinates are used, namely the coordinate system that are attached to the body of the vehicle and the world coordinate system that is fixed to the earth. Fig. 3.2 illustrates the two coordinate systems and the notations used. In this figure, U- and W- are the longitudinal and lateral axis attached to the vehicle body at the centre of gravity (c.g), ψ is the heading angle of the vehicle, X- and Y- are the fixed coordinate system, β is the sideslip angle defined as the angle between the vehicle's velocity vector (V) and the longitudinal axis (U-) and δ is the steering angle of the wheel. It is helpful to notice the definitions of some terms that are frequently used such as handling, cornering, and directional response. The last two terms refer to objective properties of a vehicle when changing direction and sustaining lateral acceleration in the process [55]. For instance, directional response is defined

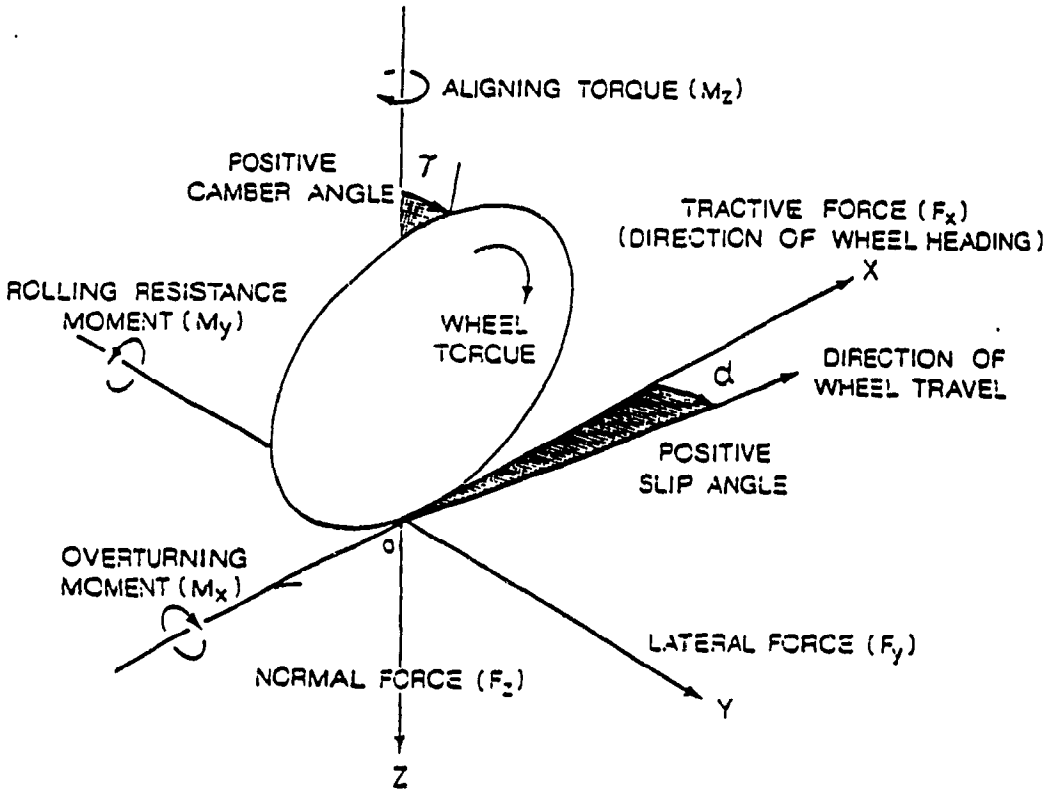

Fig. 3.3 Forces and Moments of Tire

(Courtesy of Gillespie and Wong [55,56])

as how fast the vehicle is responding to a steering input and cornering ability is quantified as the level of lateral accelerations that can be sustained in a stable condition. The term handling includes the contributions of the vehicle in a combined driver-vehicle performance in addition to the vehicle's explicit capabilities [55]. Elsewhere [56,106], the term handling has been used to define the response of the vehicle to steering command and all disturbances such as wind and load disturbances, as they affect the direction of motion of the vehicle.

Since the major forces acting on a vehicle (aside from gravitational and aerodynamic forces) are coming from the interactions of the wheel and the ground, there are a great deal of studies in the area of vehicle dynamics devoted to mechanistic understanding of this interaction [107-110,86,87]. Therefore, at this point it seems appropriate to discuss the properties of tires and the dominant forces acting on the vehicle, developed by the tires against the road.

3.2.2 A Description of the Forces and Moments of Tires

The ground reactions on the tire are described by three (3) forces and three moments as depicted in Fig. 3.3 [55-56,106]. The former are normal, tractive and lateral forces and the moments are rolling resistance, aligning and overturning moments as shown in the figure. These are described as follows:

- Lateral Forces (F_y): The component of the force acting on the tire by the road in the plane of the road and normal to the intersection of the wheel plane and the road plane toward the centre of curvature of the path followed by the wheel. Lateral forces are produced when the wheel is steered and to a great extent, the control of the vehicle is determined by these forces.

- Tractive Force (F_x): The component of the resultant force acting on the tire by the road in longitudinal axis (X). Tractive forces are developed during acceleration and deceleration.

- Normal Force (F_z): The component of the resultant force acting on the tire

by the road which is normal to the plane of the road.

- Rolling Resistance Moment (M_y): The moment acting on the tire by the road trying to turn the tire about an axis in the Y-direction.

- Aligning Moment (M_z): The moment acting on the tire by the road which is normal to the plane of the road and tries to turn the tire about an axis parallel to the Z-axis.

- Overturning Moment (M_x): The moment acting on the tire from the road trying to turn the tire about an axis in the X-direction.

In the next sections, more detailed description of the above forces and moments will be given.

3.2.2.1 Tractive Properties

During the vehicle braking or acceleration, tractive forces are developed due to the deformation of the tire tread. For instance, when the vehicle is

braking, the front elements are stretched as they are entering the contact area [55] and the rear treads are compressed. Compared with a free rolling tire, the distance travelled by the tire is larger and for braking and during acceleration, therefore. The severity of the braking or acceleration are measured by the skid and longitudinal slip of the wheels, respectively [55-56,106]. There are a number of parameters affecting the tractive effort of a tire, such as road condition (wet, dry, etc.), road characteristics (asphalt, concrete, etc.), normal load, inflation pressure, vehicle speed, and so on. For more information, the interested reader may consult references [108,55-56]

3.2.2.2 Cornering Properties

Vehicle handling characteristics to a great extent are related to the cornering properties of the tire. In essence, the tire should develop the necessary lateral forces required for the vehicle during a lane change manoeuvre, turning on a corner or generating the necessary forces in order to resist the environmental disturbances such as side winds. In explaining the mechanism of generation of lateral forces, there are two important angles defined namely slip angle and camber angle of the tire. The former is used to describe a lateral force called

cornering force (with camber angle equal to zero) while the latter contributes to a lateral force called camber trust that will be explained later in this section.

When a tire is not subjected to any side force, it will roll in the direction of the wheel plane. However, when it is subjected to a side force, it is drifted to the side and an angle is created between the direction of heading of the wheel and the direction of wheel travel, called slip angle [55-56,85-86]. This phenomenon, which is mainly due to elastic properties of the tire, can be more appreciated by looking at Fig. 3.4 [55]. As it is shown in this figure, where the tire is not in contact with ground, the tread elements are undeflected and they have the same direction as the heading. However, as the tread elements move forward and reach the contact surface, they are deflected toward the direction of travel and produce a lateral force as shown in the figure.

Further advancement of the tire generates larger forces, up to the point where the lateral force is larger than friction, and slip occurs (slip region in the figure). The corresponding lateral force distribution is also shown in the figure suggesting a kind of asymmetry in force distributions. The net resultant force

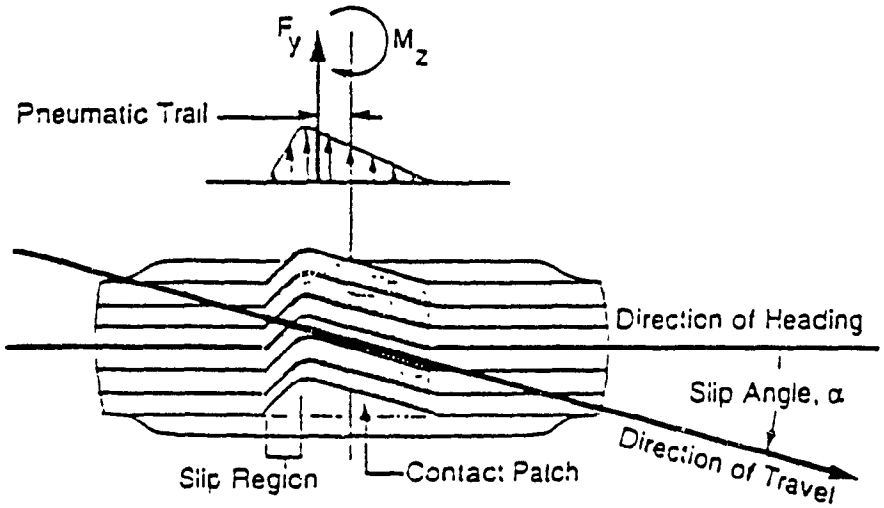

Fig. 3.4 Behaviour of a Tire Subjected to a Side Force

(Courtesy of Gillespie [55])

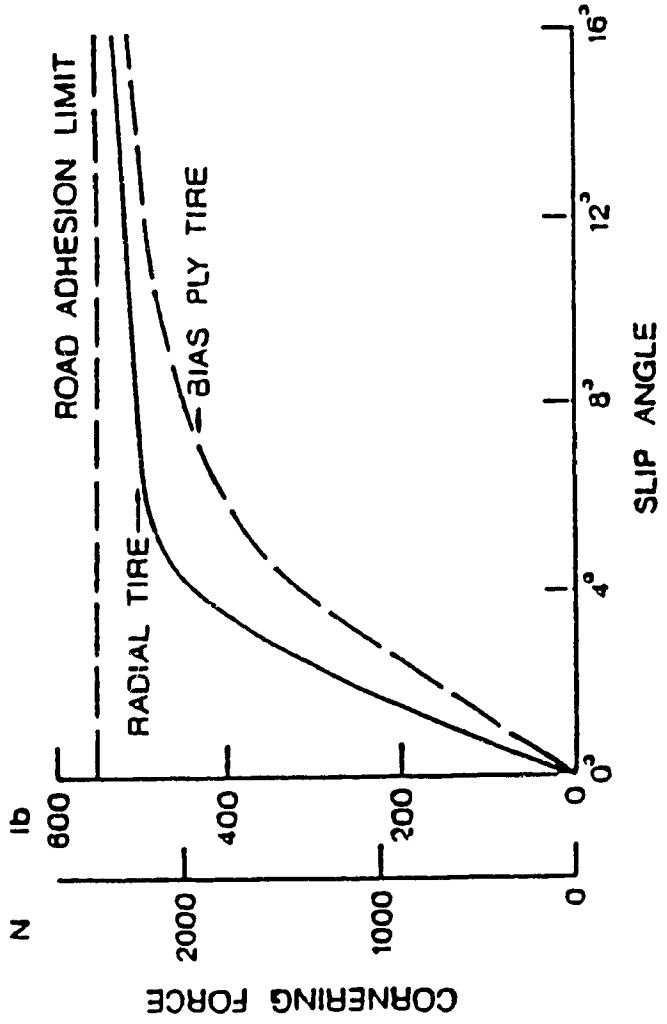

Fig. 3.5 Tire Lateral Force properties

(Courtesy of Wong [56])

generated (F_y) is a lateral force (with zero camber angle it is called cornering force) whose point of action is behind the contact patch at a distance called pneumatic trail of the tire [56]. As a result of this asymmetrical distribution of the forces, a moment called aligning moment (M_z) will be generated that tries to align the tire plane with the direction of motion, as will be explained later in this section.

There has been many studies carried out regarding the relationship between cornering force and the slip angle of a tire [85-86,89,111] and it has been generally accepted that an equation of the form:

$$C_\alpha = \frac{\partial F_{y\alpha}}{\partial \alpha} \tag{3.1}$$

provides a common basis for most of the studies. In the above equation, C_α is the cornering stiffness of the tire, $F_{y\alpha}$ is the lateral force and α is the slip angle. In addition, most of the studies suggest a typical cornering characteristics depicted in Fig. 3.5.[56]. As it is shown in this figure, cornering force is linearly

dependent on slip angle of the tire up to approximately 4 degrees and beyond that it reaches a maximum value where the tire begins sliding in the lateral direction. There are many parameters affecting the cornering properties of a tire such as type of tire, normal load, inflation pressure, etc. As reported in [107], any increase in normal load of the tire, increases the cornering force in a nonlinear fashion whose typical characteristics curves. Also, it has been generally accepted that as inflation pressure is increased, the cornering force of the tire is increased as well [87,55]. However, overinflation does not increase the cornering force due to the reduction in contact area.

As it was explained before, as a result of asymmetric nature of the distribution of the lateral force, a moment is produced called self aligning moment (M_z). The expression for this moment is:

$$M_z = t_p F_{y\alpha} \tag{3.2}$$

In the above equation, t_p is pneumatic trail of the tire [108,56]. The magnitude of this moment has a small contribution to the total yaw moment of the vehicle while it may contribute to the reactions in the steering system [89,111,55]. There are many factors affecting this moment like path curvature, normal load, nonzero

camber angle, etc.[89,111]. The self aligning moment increases in a nonlinear fashion as the normal load increases.

Another factor contributing to cornering properties of the vehicle is a lateral force called camber trust produced as a result of non-zero angle between the wheel plane and perpendicular plane of the road surface (as shown in Fig. 3.1). The relationship between camber angle and camber trust can be stated as [55]:

$$C_\gamma = \frac{\partial F_{y\alpha}}{\partial \gamma} \tag{3.3}$$

where C_γ is camber stiffness and γ is the camber angle. Camber trust has a linear characteristic for small camber angle [56] and like cornering force is affected by a number of parameters such as normal load, inflation pressure, type of the tire, etc. For more information, the interested reader is referred to [85,89,108,111].

3.2.2.3 Rolling Resistance

Rolling resistance of a tire is one of the major resistive forces acting on a

vehicle and, unlike other resistive forces that act under certain conditions, it exists from the instant a tire starts rolling. As reported in [56], there are at least seven mechanisms responsible for rolling resistance of a tire such as energy losses due to deflection of the tire sidewalls and the tread elements, scrubbing in the contact area, tire slip in longitudinal and lateral directions, air drag on the inside and outside of the tire and energy loss on bumps. When a tire is rolling the front treads of the tire in the contact area are compressed causing a higher normal pressure at the front than rear of the tire as shown in Fig. 3.6. This asymmetry produces a moment about the centre of the tire called rolling resistance moment of the tire; it should be balanced with a force called the rolling resistance force of the tire acting at the contact patch of the tire with the ground. This force is usually expressed in terms of the coefficient of rolling resistance of the tire, defined as the ratio of rolling resistance to normal force of the tire [56,106].

There are numerous factors affecting the rolling resistance of a tire such as tire temperature, inflation pressure, velocity, tire diameter, etc. For instance, variations of coefficient of rolling resistance with inflation pressure is shown in Fig. 3.7 [55-56,106].

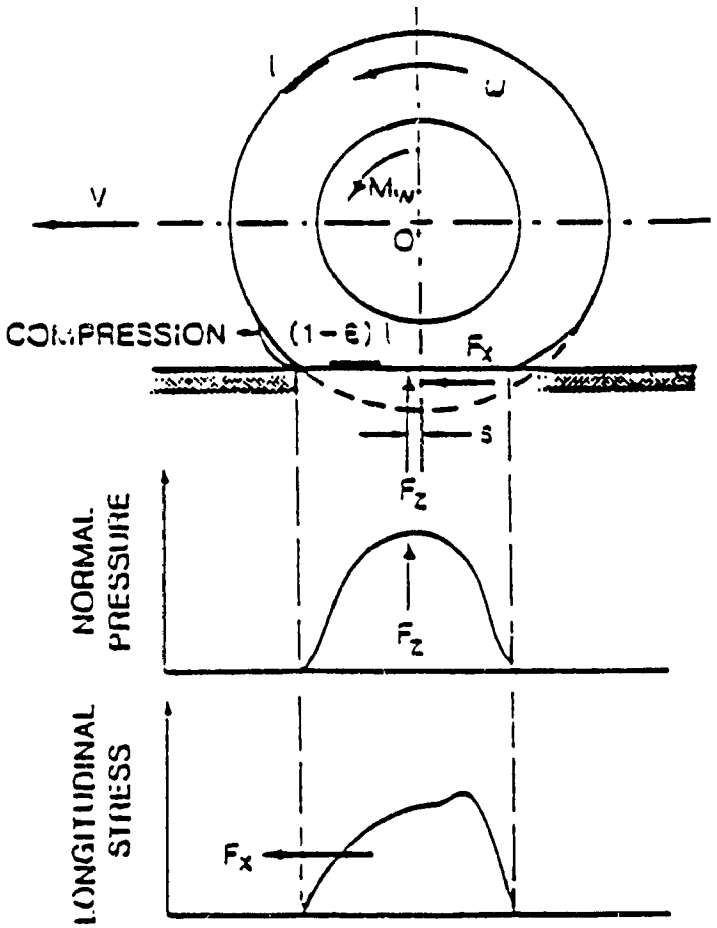

Fig. 3.6 Behaviour of a Tire Under a Driving Torque

(Courtesy of Wong [56])

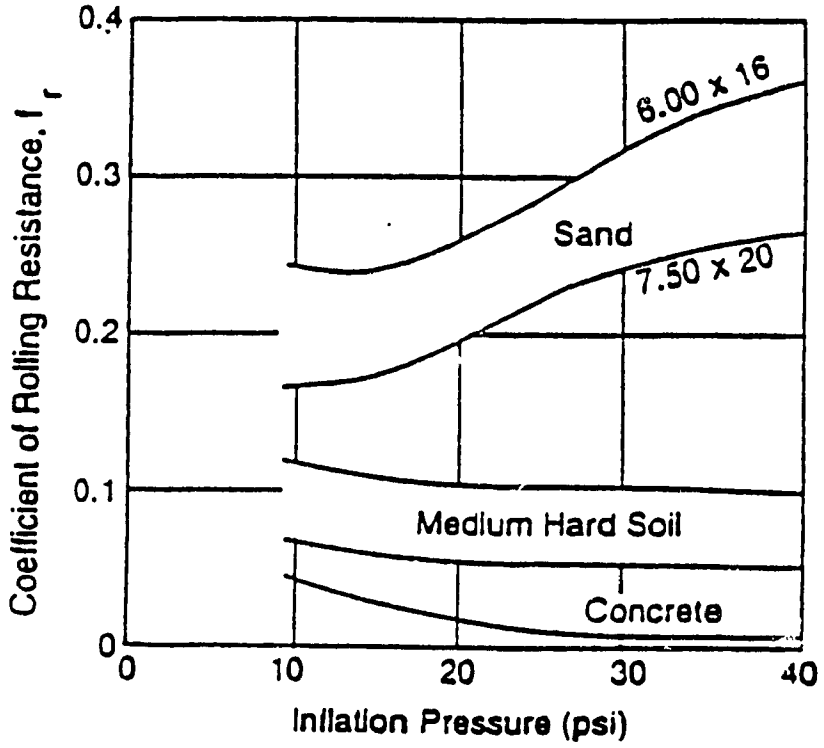

Fig. 3.7 Variations of Coefficient of Rolling Resistance

of a Tire with Inflation Pressure

(Courtesy of Gillespie [55])

In addition to the above forces and moments which are mainly produced from the interaction of the tire and the ground, there are some other forces whose sources are different than those and in deriving the equations of motion of a vehicle, generally they have to be considered in all the derivations. Typical examples of these forces are: aerodynamic forces, gravitational forces, drawbar resistance, etc.

3.3 Summary

In this chapter, an overview of some terms and concepts commonly used in the studies relevant to vehicle dynamics was provided. Explanation of various degrees of freedom dynamic models used in representing a vehicle motion with their relevant assumptions and limitations were discussed. A general description of the forces and moments acting on a tyre was given. Mechanisms of generations of the forces and moments produced in the contact area of the tyre and the ground were explained. From literature survey, it was observed that a great deal of effort has been given to analytical and experimental studies to describe the mechanics and characteristics fundamental to all types of tire. In this

regard, some previous reports and articles were reviewed and their main focus and major achievements were explained. It was noticed that there are a lot of factors like normal load, type of tire, inflation pressure, size, speed, temperature, surface, surface conditions, etc. affecting the behaviour of a tire that makes it very difficult to come up with a model encompassing all these parameters.

CHAPTER 4

DYNAMIC MODELLING OF AUTOMATED VEHICLES

4.1 Introduction

A primary objective of development of a dynamic model is to provide a suitable tool for the analysis of motion of a system when subjected to applied forces. To a great extent, all mathematical models are obtained based on some assumptions as they are often necessary to simplify the intended study [25,34,36,58-59,78,92]. For developing a proper dynamic model, on one hand, an adequate number of parameters need to be taken into account. On the other hand, the model should not be unduly complicated, so that further analysis turns into an almost impossible task. This is quite important when it comes to the design and analysis of a control system where simpler models are preferred. In practice, for automated vehicles, while it is quite acceptable to use a more

complicated model for simulation studies, a simpler model (of a lower order for instance) is preferred for the purpose of determining the structure of a controller. A compromise is often required.

Because the knowledge of dynamics of automated vehicles is required to investigate their handling characteristics and directional stability, various dynamic models with a range of levels of complexity have been proposed by a number of researchers [25,58,78,87,101]. Nonetheless, one detects that there are basically two classes of models: 3-DOF models which incorporate the lateral, the yaw and the roll motions, and 2-DOF models that consider the lateral and yaw motions only [36,58,59,65,96].

The focus of this chapter is directed toward the developments of the (2- and 3-DOF) nonlinear and linear models. After a general explanations of the forces and moments involved and their expressions, the 2- and 3-DOF nonlinear dynamic models are derived. It is shown that by making some assumptions, it is possible to obtain the linearized versions of the above models that are quite useful for analytical purposes. Their explanations are provided in order to show the scope and limitations of the above models.

In the following sections, two nonlinear dynamic models namely 3-DOF and 2-DOF models are developed to represent the motion of a double steering

vehicle with front and rear steering wheels. By setting the rear wheel steering angle to zero, the similar relationships are obtained for a front wheel steering vehicle.

4.2 Development of the (3-DOF) Nonlinear Model

The directional response and the stability of a vehicle can be deduced from its response to the steering inputs or disturbances [56]. More precisely, it may be investigated how well the vehicle follows a prescribed path, and if it is "hunting" about the path, how large the overshoots are, and whether the amplitude of hunting oscillations are diverging (unstable) or converging (stable). This type of behaviour is mainly influenced by geometric parameters of the vehicle, such as the location of centre of mass, the mass, and the moments of inertia of the vehicle, the suspension system and the interaction forces between the wheels and the ground, etc. Fig. 4.1 shows schematically the freebody diagram of the vehicle for the yaw motion of the vehicle and Fig. 4.2 shows the roll motion which is represented by a sprung mass (M_s) linked by a suspension system to an unsprung mass. The equations are referenced to the coordinate system attached to the vehicle body (hereafter called body axes) by noting that the forces are more easily specified in this coordinate system. The acceleration is also specified in body axes and at the end, a transformation is

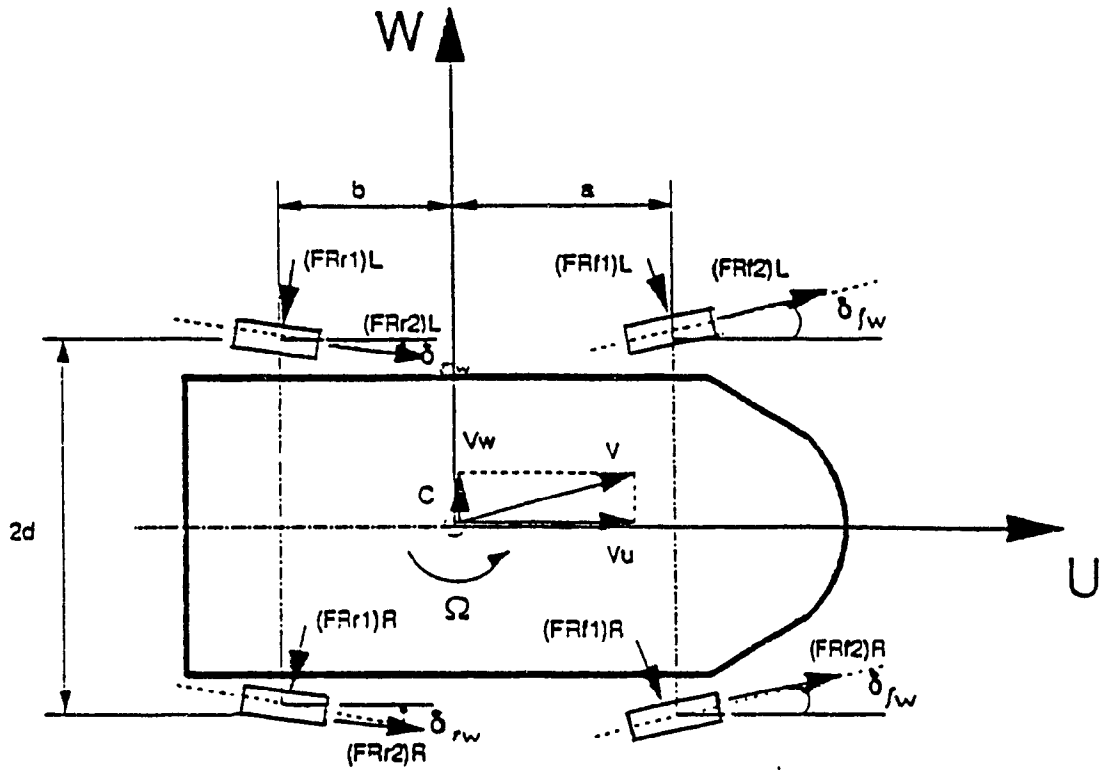

Fig. 4.1 Freebody Diagram of the Vehicle.

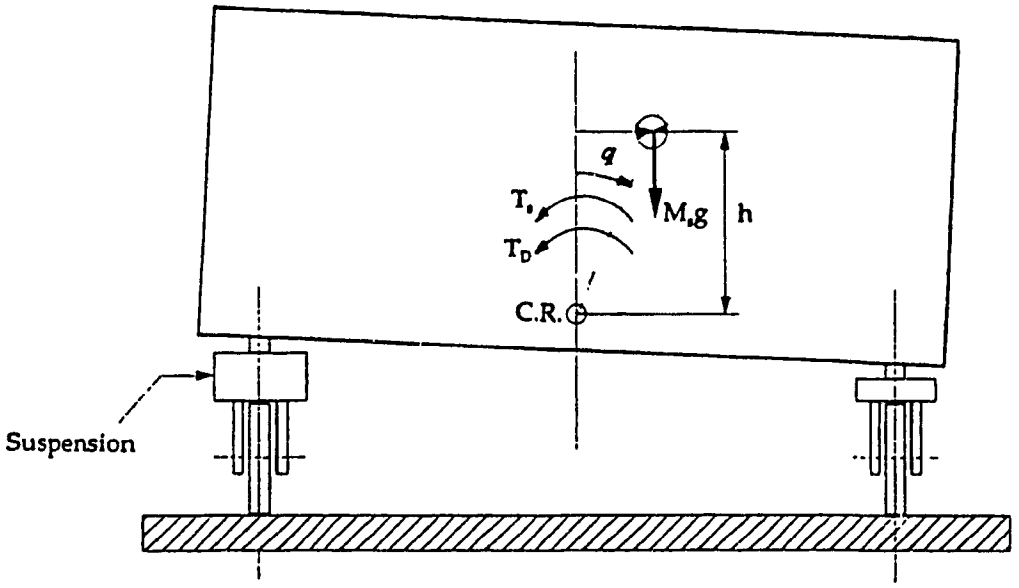

Fig. 4.2 Roll Motion of the Vehicle.

needed to express the position and orientation of the vehicle in world coordinates.

Let U- and W-, respectively, be the body axis of the vehicle. The sum of the forces along U- direction are as follows [34,36,56,87]:

$$\begin{aligned} M(\dot{V}_U - V_W\,\Omega) = & -[(F_{Rf2})_L + (F_{Rf2})_R]\cos\delta_{fw} \\ & +[(F_{Rf1})_L + (F_{Rf1})_R]\sin\delta_{fw} \\ & +[(F_{Rr2})_L + (F_{Rr2})_R]\cos\delta_{rw} \\ & -[(F_{Rr1})_L + (F_{Rr1})_R]\sin\delta_{rw} \end{aligned} \tag{4.1}$$

Similarly the sum of the forces along W- direction are:

$$\begin{aligned} M(\dot{V}_W + V_U\Omega) + M_s h\ddot{q} = & -[(F_{Rf2})_L + (F_{Rf2})_R]\sin\delta_{fw} \\ & -[(F_{Rf1})_L + (F_{Rf1})_R]\cos\delta_{fw} \\ & -[(F_{Rr1})_L + (F_{Rr1})_R]\cos\delta_{rw} \\ & +[(F_{Rr2})_L + (F_{Rr2})_R]\sin\delta_{rw} \end{aligned} \tag{4.2}$$

The moments of the above forces about a vertical axis passing through the vehicle centre of mass (yaw motion) are as follows:

$$\begin{aligned} I_z\dot{\Omega} = & +a[+(F_{Rf2})_L + (F_{Rf2})_R]\sin\delta_{fw} - d[-(F_{Rf2})_R + (F_{Rf2})_L]\cos\delta_{fw} \\ & +a[+(F_{Rf1})_L + (F_{Rf1})_R]\cos\delta_{fw} + d[+(F_{Rf1})_L - (F_{Rf1})_R]\sin\delta_{fw} \\ & -b[+(F_{Rr1})_L + (F_{Rr1})_R]\cos\delta_{rw} - d[-(F_{Rr1})_R + (F_{Rr1})_L]\sin\delta_{rw} \\ & +b[+(F_{Rr2})_L + (F_{Rr2})_R]\sin\delta_{rw} + d[-(F_{Rr2})_L + (F_{Rr2})_R]\cos\delta_{rw} \end{aligned} \tag{4.3}$$

The moments about roll axis are due to suspension system (see Fig. 4.2) which are specified as T_s (torque produced by suspension stiffness which is generally assumed to be proportional to roll angle [55]) and T_D (torque due to damping of suspension system [77]), moment due to rolling of the sprung mass, inertial moment of the sprung mass, and the moment due to lateral acceleration of the vehicle. Summation of the moments about the axis for roll motion are as follows:

$$I_x\ddot{q} + M_s h(\dot{V}_W + V_U\,\Omega) = -K_p q - D_p\dot{q} + M_s g h q \tag{4.4}$$

where V_u and V_w are the forward and lateral velocities of the vehicle (in its own frame), Ω is the yaw rate of the vehicle about the vertical axis, p is the roll velocity, M and M_s are the mass and sprung mass of the vehicle, h is the distance between the roll centre and the centre of mass of the sprung mass, I_z and I_u are the yaw and roll moments of inertia, K_p and D_p are the equivalent roll stiffness (N.m/rad) and damping (N.m.s/rad) coefficients of the entire suspension system and g is the constant of gravity. The forces $(F_{Rf1})_{L,R}$, $(F_{Rf2})_{L,R}$, $(F_{Rr1})_{L,R}$, $(F_{Rr2})_{L,R}$ are the reaction forces of the front wheels (Left/Right) and rear wheels (Left/Right), δ_{fw} and δ_{rw} the instantaneous steering angles of the front and rear wheels (assumed equal for left and right) respectively, a,b and d are as shown in Fig. 4.1 and q is the roll angle. Only small magnitudes of the roll angle are considered. It should be noted that although equations (4.1-4.4) mathematically represent a dynamic system with four degrees of freedom, because of the nonholonomic constraints (see section 4.5), V_u, V_w and Ω are not independent. This system has got only three degrees of freedom, that is, two degrees in plane motion and one degree for the roll motion.

Fig. 4.3 shows, the freebody diagram of the front wheel (the corresponding Left(L) and Right(R) symbols not shown) and the forces acting on it. Writing the sum of the forces in the plane of the wheel and perpendicular to that gives:

$$m_w r_w (\dot{\omega}_f)_{L,R} \cos \delta_{fw} = [(F_{Tf})_{L,R} - (F_{Fre})_{L,R} - (F_{Rf2})_{L,R}] \cos \delta_{fw} - [(F_{sf})_{L,R} - (F_{Rf1})_{L,R}] \sin \delta_{fw} \quad (4.5)$$

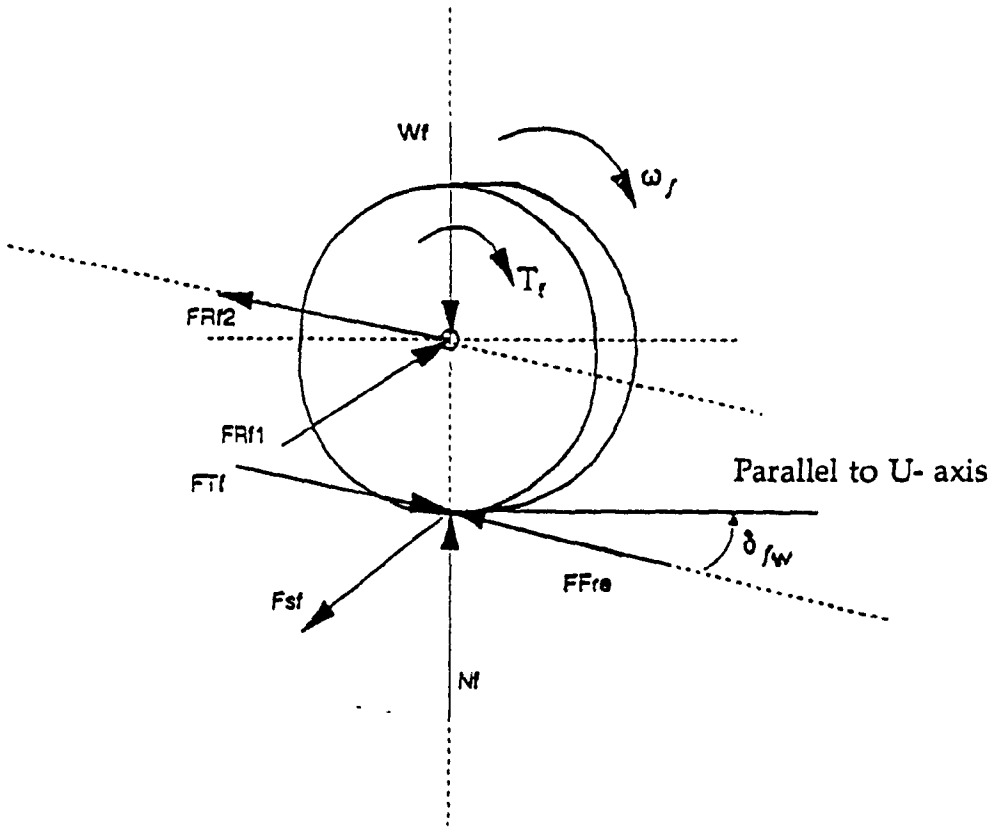

Fig. 4.3 Free body Diagram of the Front Wheel

$$m_w r_w (\dot{\omega}_f)_{L,R} \sin \delta_{fw} = [(F_{Tf})_{L,R} - (F_{Fre})_{L,R} - (F_{Rf2})_{L,R}] \sin \delta_{fw} - [(F_{sf})_{L,R} - (F_{Rf1})_{L,R}] \cos \delta_{fw} \quad (4.6)$$

where m_w, r_w, $(\omega_f)_{L,R}$ are the mass, radius (both assumed equal for the left and right wheels) and the angular velocities, $(F_{Rre})_{L,R}$ the rolling resistance and $(F_{Tf})_{L,R}$ the tractive effort of the front wheels (Left/Right). $(F_{sf})_{L,R}$ are the side-forces (cornering force) of the front tires (Left/Right) which are given as:

$$(F_{sf})_L = C_f (\beta_f)_L \quad (4.7)$$

$$(F_{sf})_R = C_f (\beta_f)_R \quad (4.8)$$

where C_f is the cornering stiffness of the front wheel (assumed equal otherwise $(C_f)_{L,R}$). As similar statement holds for the rear tires. The above linear relationships between the side forces and slip angles (equations 4.7-4.8) are valid for slip-angles that are no larger than 4° , and assuming that the cornering stiffness is constant within this range [56]. Furthermore, in view of the definition of slip angle of a tire to be the angle between the wheel velocity and wheel heading, the expressions for $(\beta_f)_L$ and $(\beta_f)_R$ are as follows:

$$(\beta_f)_L = \delta_{fw} - \tan^{-1} \frac{V_w + a\Omega}{V_u - d\Omega} \quad (4.9)$$

$$(\beta_f)_R = \delta_{fw} - \tan^{-1}\frac{V_w + a\Omega}{V_u + d\Omega} \tag{4.10}$$

where the terms in the numerator and denominator are the lateral and tangential components of the vehicle body at the front, respectively (see Figs. 3.3 and 4.6). The rolling resistance on each wheel is proportional to its vertical load and is given as:

$$(F_{Fre})_{L,R} = f_r\ (N_f)_{L,R} \tag{4.11}$$

where f_r is the coefficient of rolling resistance of the wheel (assumed the same for all wheels), and $(N_f)_{L,R}$ are the vertical reactions of the ground ($(N_f)_{L,R} \approx (W_f)_{L,R}$). $(W_f)_{L,R}$ are the vertical load on each front tire that consist of static load distributions on each tire and the dynamic load transfer. The latter depends upon some other variables such as tractive forces, rolling resistances of the tires, height of centre of gravity, etc. In its simplified form it can be obtained from (for the front and rear tires):

$$(W_f)_i = (W_f)_{i,static} + W\frac{a_u}{g}\frac{h'}{(a+b)} \quad , \quad i = L,R \tag{4.12}$$

$$(W_r)_i = (W_r)_{i,static} - W\frac{a_u}{g}\frac{h'}{(a+b)} \quad , \quad i = L,R \tag{4.13}$$

where W is the total weight of the vehicle, a_u is the forward acceleration/ deceleration of the vehicle, g is the constant of the gravity and h' is the height of centre of gravity.

Summation of the moments around axle of the front wheels (Left/Right) gives:

$$J_f (\dot{\omega}_f)_{L,R} = (T_f)_{L,R} - r_w[(F_{Tf})_{L,R} - (F_{Fre})_{L,R}] \tag{4.14}$$

where J_f is the moment of inertia of the front wheels (assumed equal) around its centre and $(T_f)_{L,R}$ are the applied torques.

Similar equations can be written for the rear wheels as follows:

$$\begin{aligned} m_w r_w(\dot{\omega}_r)_{L,R} \cos \delta_{rw} = {} & [(F_{Tr})_{L,R} - (F_{Rre})_{L,R} - (F_{Rr2})_{L,R}]\cos \delta_{rw} \\ & - [(F_{sr})_{L,R} - (F_{Rr1})_{L,R}]\sin \delta_{fw} \end{aligned} \tag{4.15}$$

$$\begin{aligned} m_w r_w(\dot{\omega}_r)_{L,R} \sin \delta_{rw} = {} & [(F_{Tr})_{L,R} - (F_{Rre})_{L,R} - (F_{Rr2})_{L,R}]\sin \delta_{rw} \\ & - [(F_{sr})_{L,R} - (F_{Rr1})_{L,R}]\cos \delta_{rw} \end{aligned} \tag{4.16}$$

$$J_r (\dot{\omega}_r)_{L,R} = (T_r)_{L,R} - r_w[(F_{Tr})_{L,R} - (F_{Rre})_{L,R}] \tag{4.17}$$

where $(\omega_r)_{L,R}$ are angular velocities, $(F_{Rre})_{L,R}$ the rolling resistances, $(F_{Tr})_{L,R}$ the tractive efforts, J_r and $(T_r)_{L,R}$ are the moment of inertia and the applied torques of the rear wheels (Left/Right) around their centre and $(F_{sr})_{L,R}$ are the side-forces (cornering force) of the rear wheels (Left/Right) obtained from:

$$(F_{sr})_L = C_r(\beta_r)_L \tag{4.18}$$

$$(F_{sr})_R = C_r(\beta_r)_R \tag{4.19}$$

where C_r is the cornering stiffness of the rear wheel (assumed equal for the left and right side) while the assumption of linear relationships between the side forces and slip angles (for small slip angles) are used. $(\beta_r)_L$ and $(\beta_r)_R$ are the slip angles of the rear (Left/Right) wheels obtained from:

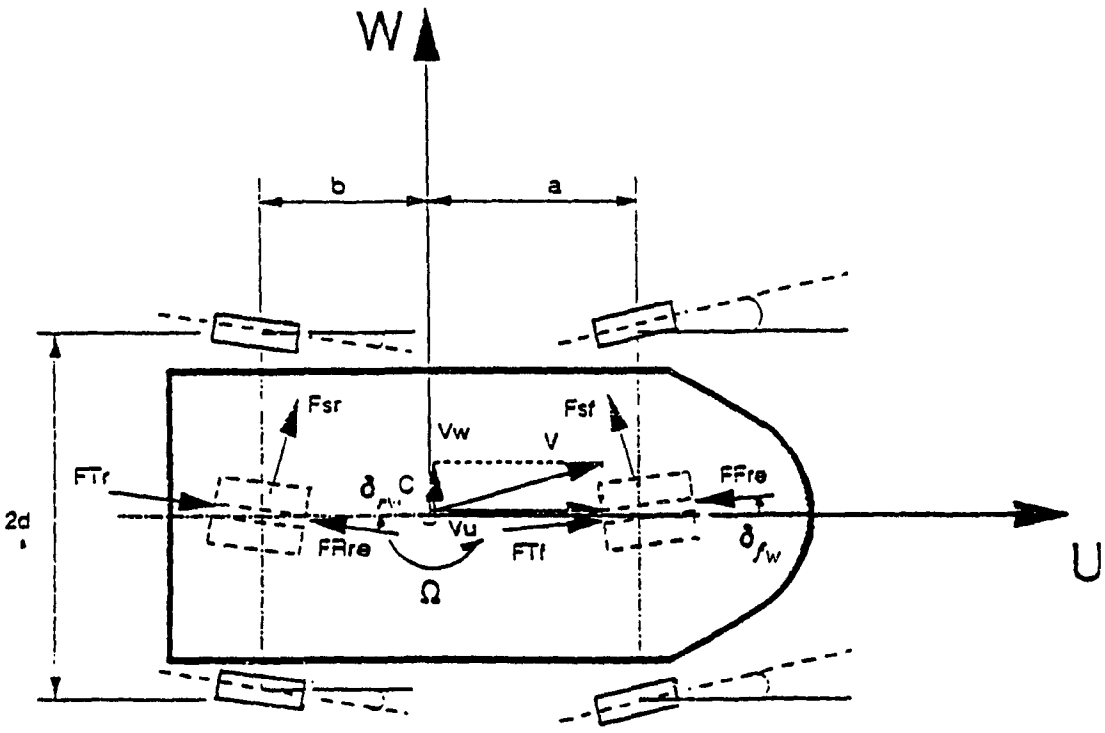

Fig. 4.4 Bicycle Model of the Vehicle

$$(\beta_r)_L = \delta_{rw} + \tan^{-1}\frac{b\Omega - V_w}{V_u - d\Omega} \tag{4.20}$$

$$(\beta_r)_R = \delta_{rw} - \tan^{-1}\frac{b\Omega - V_w}{V_u + d\Omega} \tag{4.21}$$

where δ_{rw} is the instantaneous steering angles of the rear wheels.

In derivation of the above dynamic model, it is assumed that the vehicle body possesses an approximately symmetrical structure about UZ and UW planes such that the product of inertia terms are small. Furthermore, the self aligning moments [55-56,87,111] of the wheels as well as the effects of gyroscopic moments are also considered to be negligible.

A simplified version of this model can be obtained by neglecting the inertia properties of the wheels by noting that their effects will be diminished at lower accelerations. Therefore, substituting from equations (4.5), (4.6), (4.14) and also equations (4.15-4.17) (with all the left hand sides equal to zero) into equations (4.1) to (4.3), the following equations can be obtained:

$$\begin{aligned} M(\dot{V}_U - V_W\Omega) = {} & [(F_{Tf}-F_{Fre})_L + (F_{Tf}-F_{Fre})_R]\cos\delta_{fw} \\ & -[(F_{sf})_L + (F_{sf})_R]\sin\delta_{fw} \\ & +[(F_{Tr}-F_{Rre})_L + (F_{Tr}-F_{Rre})_R]\cos\delta_{rw} \\ & +[(F_{sr})_L + (F_{sr})_R]\sin\delta_{rw} \end{aligned} \tag{4.22}$$

$$
\begin{aligned}
M(\dot{V}_W + V_u\Omega) + M_s h\ddot{q} = &[(F_{Tf}-F_{Fre})_L + (F_{Tf}-F_{Fre})_R]\sin\delta_{fw} \\
&+[(F_{sf})_L + (F_{sf})_R]\cos\delta_{fw} \\
&+[(F_{sr})_L + (F_{sr})_R]\cos\delta_{rw} \\
&-[(F_{Tr}-F_{Rre})_L + (F_{Tr}-F_{Rre})_R]\sin\delta_{rw}
\end{aligned} \tag{4.23}
$$

$$
\begin{aligned}
I_z\dot{\Omega} = &+a[+(F_{Tf}-F_{Fre})_L+(F_{Tf}-F_{Fre})_R]\sin\delta_{fw} \\
&-d[-(F_{Tf}-F_{Fre})_R+(F_{Tf}-F_{Fre})_L]\cos\delta_{fw} \\
&+a[+(F_{sf})_L+(F_{sf})_R]\cos\delta_{fw} \\
&+d[+(F_{sf})_L-(F_{sf})_R]\sin\delta_{fw} \\
&-b[+(F_{sr})_L+(F_{sr})_R]\cos\delta_{rw} \\
&-d[-(F_{sr})_R+(F_{sr})_L]\sin\delta_{rw} \\
&+b[+(F_{Tr}-F_{Rre})_L+(F_{Tr}-F_{Rre})_R]\sin\delta_{rw} \\
&+d[-(F_{Tr}-F_{Rre})_L+(F_{Tr}-F_{Rre})_R]\cos\delta_{rw}
\end{aligned} \tag{4.24}
$$

$$
I_u\ddot{q} + M_s\, h\, (\dot{V}_W + V_U\, \Omega) = -D_p\, \dot{q} + (M_s g h - K_p)q \tag{4.25}
$$

In addition, it is possible to further simplify the above developed models by collapsing the two pairs of front and rear wheels into two corresponding sets to obtain their bicycle (telescopic) models as shown in Fig. 4.4. The bicycle models are reasonably accurate at higher speeds where the term ($V_U > d\Omega$). In order to show the procedure, the revised forms of the equations of motion for previous case (the inertia properties of the wheels neglected) are written as follows:

$$
\begin{aligned}
M(\dot{V}_U - V_W\,\Omega) = &(F_{Tf}-F_{Fre})\cos\delta_{fw} - F_{sf}\sin\delta_f \\
&+(F_{Tr}-F_{Rre})\cos\delta_{rw} + F_{sr}\sin\delta_{rw}
\end{aligned} \tag{4.26}
$$

$$M(\dot{V}_W + V_U\Omega) + M_s h\ddot{q} = (F_{Tf} - F_{Fre})\sin\delta_{fw} + F_{sf}\cos\delta_{fw} + F_{sr}\cos\delta_{rw} - (F_{Tr} - F_{Rre})\sin\delta_{rw} \quad (4.27)$$

$$I_z\dot{\Omega} = +a(F_{Tf} - F_{Fre})\sin\delta_{fw} + aF_{sf}\cos\delta_{fw} - bF_{sr}\cos\delta_{rw} + b(F_{Tr} - F_{Rre})\sin\delta_{rw} \quad (4.28)$$

$$I_u\ddot{q} + M_s h(\dot{V}_W + V_U\,\Omega) = -D_p\dot{q} + (M_s gh - K_p)q \quad (4.29)$$

where the expressions for the side forces of the front and rear wheels are:

$$F_{sf} = C_f\,\beta_f \quad (4.30)$$

$$F_{sr} = C_r\,\beta_r \quad (4.31)$$

and β_f and β_r (the slip angles of the front and rear wheels) obtained from:

$$\beta_f = \delta_{fw} - \tan^{-1}\frac{a\Omega + V_w}{V_u} \quad (4.32)$$

$$\beta_r = \delta_{rw} - \tan^{-1}\frac{b\Omega - V_w}{V_u} \quad (4.33)$$

4.3 Development of the 2-DOF Nonlinear Model

The 2-DOF models are obtained by neglecting the effect of roll motion. Therefore, all the terms relevant to roll motion are neglected while the remaining equations are unchanged. For the telescopic model, the equations are as follows:

$$M(\dot{V}_U - V_W\,\Omega) = (F_{Tf} - F_{Fre})\cos\delta_{fw} - F_{sf}\sin\delta_{fw} + (F_{Tr} - F_{Rre})\cos\delta_{rw} + F_{sr}\sin\delta_{rw} \quad (4.34)$$

$$M(\dot{V}_W + V_U\Omega) = (F_{Tf}-F_{Fre})\sin\delta_{fw} + F_{sf}\cos\delta_{fw} + F_{sr}\cos\delta_{rw} - (F_{Tr}-F_{Rre})\sin\delta_{rw} \quad (4.35)$$

$$I_z\dot{\Omega} = +a(F_{Tf}-F_{Fre})\sin\delta_{fw} + aF_{sf}\cos\delta_{fw} - bF_{sr}\cos\delta_{rw} + b(F_{Tr}-F_{Rre})\sin\delta_{rw} \quad (4.36)$$

For other models developed in the previous section (with/without considering the inertia effects of wheels), derivations are similar. In the above equations namely equations (4.34-4.36), the definitions and the symbols remain the same as defined for the telescopic model.

In the following section, linear dynamic models representing the motion of a vehicle without acceleration or deceleration in longitudinal axis (U) are obtained. By making use of this assumption, the complexity of the mathematical models so far developed is tremendously reduced without loosing the important information regarding the dynamic behaviour of the vehicle.

4.4 Developments of Linear 3-DOF and 2-DOF Models

In developing the linear dynamic equations, it is a common practice to use

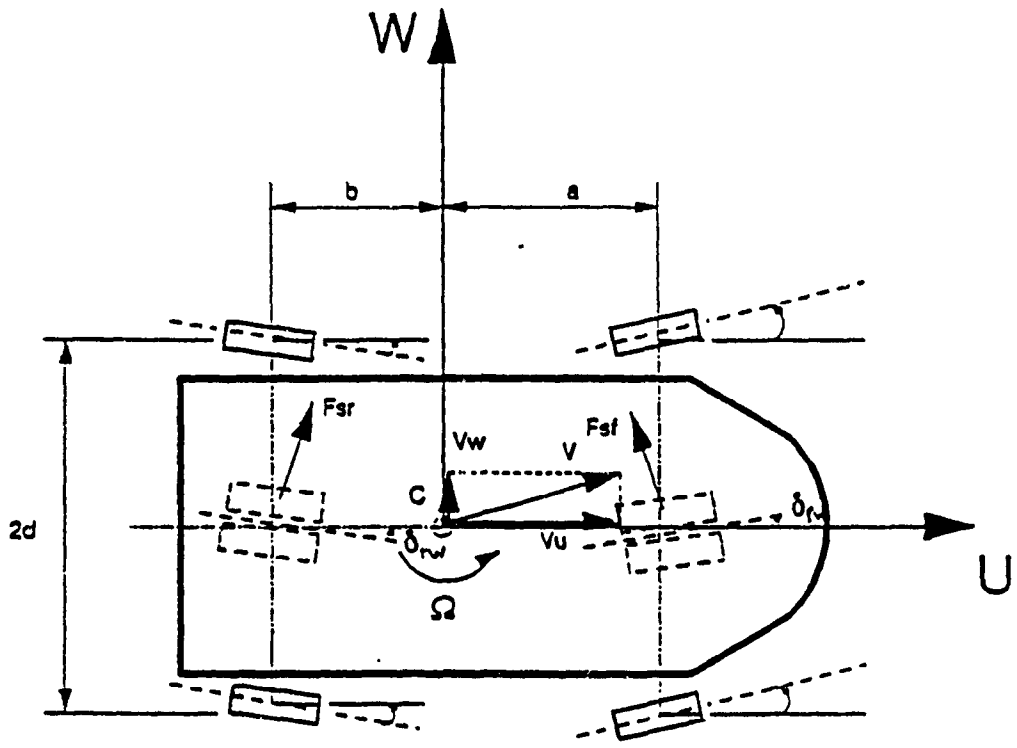

Fig. 4.5 A Telescopic (Bicycle) Model of the Vehicle

a bicycle (telescopic) model by collapsing the two pairs of front and rear wheels in two corresponding sets, one at the front and the other at the rear, as shown in Fig. 4.5. Based on the assumptions that the angles involved are small, such that the trigonometric approximation can be justified , the side forces F_{sf} and F_{sr} may be represented as:

$$F_{sf} = C_f \beta_f \tag{4.37}$$

$$F_{sr} = C_r \beta_r \tag{4.38}$$

where C_f and C_r are the cornering stiffness and β_f and β_r are the slip angles of the front and rear wheels, respectively, obtained from:

$$\beta_f = \delta_{fw} - \frac{a\Omega + v_w}{v_u} \tag{4.39}$$

$$\beta_r = \delta_{rw} + \frac{b\Omega - v_w}{v_u} \tag{4.40}$$

The above expressions for slip angles of the front and rear wheels are obtained based on the assumption that the forward speed of the vehicle is large enough such that ($V_u > d\Omega$). In these equations, δ_{fw}, δ_{rw}, V_w, Ω are as defined before and the geometric quantities a and b are as shown in Fig. 4.5.

Summation of the forces and moments around the centre of mass gives:

$$m(\dot{V}_w + V_u\Omega) + M_s h\ddot{q} = F_{sf} + F_{sr} \tag{4.41}$$

$$I_z\dot{\Omega} = aF_{sf} - bF_{sr} \tag{4.42}$$

$$I_u\ddot{q} + M_s h(\dot{V}_w + V_u\Omega) = -D_p\ddot{q} + (M_s gh - K_p)q \tag{4.43}$$

The symbols used in the above equations are the same as in section (4.3).

Neglecting the roll motion of the vehicle, by referring to Fig. 4.5, the following equations can be obtained for 2-DOF linear model by writing the sum of the forces and moments about the centre of mass of the vehicle:

$$M(\dot{V}_w + V_u\Omega) = F_{sf} + F_{sr} \tag{4.44}$$

$$I_z\dot{\Omega} = aF_{sf} - bF_{sr} \tag{4.45}$$

where the expressions for the side forces, namely F_{sf} and F_{sr} and slip angles are the same as equations (4.37-4.40) for the front and rear wheels.

In derivation of the above equations, it is assumed that the vehicle body possesses an approximately symmetrical structure about UZ and UW planes such that the product of inertia terms are small (the same assumptions made in previous section). In addition, the effects of inertia properties of the wheels are considered to be small; otherwise the formulation can be carried out in an approach provided in the previous section. Furthermore, trigonometric

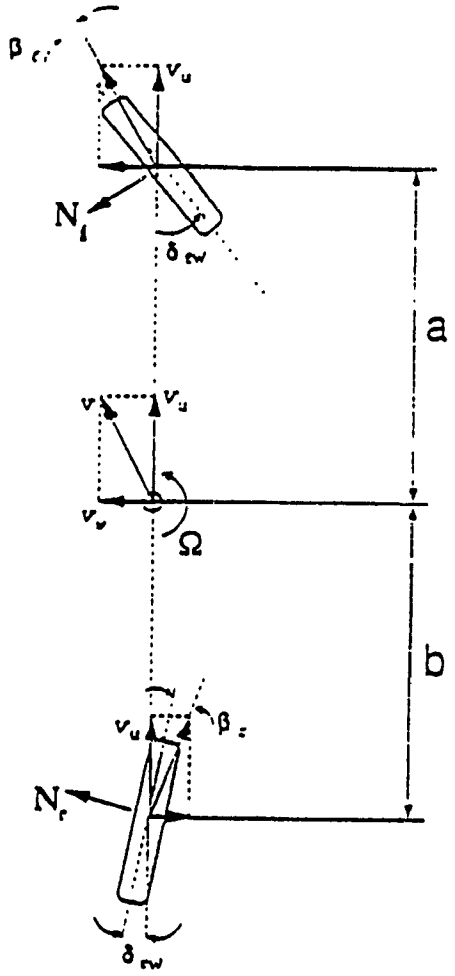

Fig. 4.6 Kinematic Constraints of the Wheels

for Telescopic Model

approximation is used for roll angle and also the self aligning moments of the wheels are also considered to be negligible; if there are any, they can be added to the right hand side of equation (4.42) and (4.45).

The survey of the literature published in this area shows that the above model is quite adequate if the vehicle does not go through severe lane change manoeuvre: specifically, if the lateral acceleration of the vehicle is less than 0.3 g (3 m/s^2) [25,71-72].

4.5 Description of Nonholonomic Constraints

For non-slippage motion of the vehicle, there are some rolling constraints involved that should be included in the model. These constraints are shown in Fig. 4.6 which is a bicycle model of a vehicle. For pure rolling motion, the velocities of the wheels at the point of contact should be zero at the direction normal to the wheel (shown by vector N) and equal to its angular velocity in the direction perpendicular to N. Therefore, the following equations can be written between the velocity of the vehicle in U- and W- directions and the components of the velocity of the wheels (front and rear) in the same directions:

$$r_w \omega_f \cos \delta_{fw} = V_U \tag{4.46}$$

$$r_w\ \omega_f \sin \delta_{fw} = V_W + a\Omega \tag{4.47}$$

$$r_w\ \omega_r \cos \delta_{rw} = V_U \tag{4.48}$$

$$r_w\ \omega_r \sin \delta_{rw} = V_W - b\Omega \tag{4.49}$$

The above equations are the nonholonomic constraints that should be satisfied for the motion of the vehicle without any slippage. By dividing both sides of equations (4.46-4.47) and (4.48-4.49), the following expressions can be written:

$$\tan \delta_{fw} = \frac{V_W + a\Omega}{V_U} \tag{4.50}$$

$$\tan \delta_{rw} = \frac{V_W - b\Omega}{V_U} \tag{4.51}$$

Comparing equations (4.32) and (4.33) with (4.50) and (4.51), respectively, it is seen that with good approximations they are the same by noting that the slip angles of the front and rear wheels are small (usually less than 4 degrees). Therefore, it can be stated that by including the expressions for slip angles of the wheels in the derivations of equations of motion of the vehicle, the nonholonomic constraints are also satisfied. Although the telescopic model of the vehicle was used to simplify the explanations, however, the above procedure is the same for other cases as well.

4.6 Summary

In this chapter, the derivations of the nonlinear and linear dynamic models representing the motion of a vehicle were explained in detail. The equations of motion were developed by the using the freebody diagram of the vehicle. The nonlinear models developed here, although more accurate in principle but, their applications are mostly limited to simulation studies. It was shown that by making some assumptions, it is possible to obtain a simplified linear dynamic model which offer a good choice for any analytical study. As well, whenever required they can be represented in the state space format which is an ideal choice for control application purposes.

The nonholonomic (nonintegrable) constraints associated with the motion of the vehicle in the absence of slippage were explained. It was shown that inclusion of the expressions for the slip angles of the wheels indirectly satisfies the nonholonomic constraints.

CHAPTER 5

CHARACTERIZATION OF DYNAMICS OF AUTOMATED VEHICLES

5.1 Introduction

For the purpose of characterizing the directional response of a vehicle, its "open-loop" behaviour is studied which refers to the response of the vehicle to steering input. Therefore, it is necessary to have a dynamic model representing the vehicle motion as a function of the applied input which is the steering angle. Let consider a vehicle moving on a flat surface without any acceleration / deceleration in longitudinal direction. Basically two classes of models so far have been used to represent the motion of the vehicle [25,58,78,104]: namely, 3-DOF models, which incorporate the lateral, the yaw and the roll motions, and 2-DOF models that consider lateral and yaw motion only [58,61,96,101]. However, there is as yet no clear-cut criterion or indicator available as to which class of model to

be used under what circumstances. In fact, the following questions seem to persist:

1. Under the assumptions made to derive the two dynamic models, how closely do the two models match?

2. The roll motion is somehow coupled with the other two, lateral and yaw motions. The question is how strong is this coupling, and in what way? Which parameters of the vehicle are dominant in this coupling?

3. Under what conditions could the significance of the roll motion be reduced?

The focus of this chapter is directed toward the comparison of the two models (2- and 3-DOF) as well as investigation of the vehicle parameters that significantly affect its dynamics in plane motion. This study has led to a better understanding of the issues listed above. It should be mentioned that due to main emphasize of the chapter and to simplify the analysis, the effects of the other elements such as dynamics of the steering system are not involved. Throughout the analysis, it is assumed that instantaneous steering angles of the wheels (δ_{fw}, δ_{rw}) follow the command to the steering system (δ_f, δ_r) at any instant.

This chapter introduces a dimensionless entity called "roll number" for dynamic modelling of automated vehicles. It can be used to characterize between two linear models, one with three degrees-of-freedom incorporating the lateral, yaw and roll motions, and the other with two degrees-of-freedom consisting of

the lateral and the yaw motions only.

Another issue that is addressed here is the investigation on the importance of transient responses of yaw and lateral velocities and their relevant effects on plane motion of the vehicle. In this regard, "velocity constant" and "yaw number" are introduced. These entities are functions of the parameters of the vehicle and characterize its transient behaviour in plane motion. They can be utilized in deciding as when to use a dynamic model or a simpler model based on kinematics, to represent the motion of the vehicle.

The equations of motion of the vehicle employed in this chapter are the same as those in previous chapter (section 4.4) namely, equations (4.37) to (4.45) and are relabled as (5.1) to (5.9).

5.3. Comparison of the two models

It was found that rewriting the dynamic equations in the Laplace domain makes it easier to compare the merits of the two models. For the 3-DOF model the transfer functions between the steering angles signals at the front and rear wheels as inputs, and the lateral and yaw velocities as outputs can be defined as in the following:

$$T_1(s) = \frac{\Omega(s)}{\delta_f(s)} = \frac{Z_1(s)}{P_s(s)}$$
$$T_2(s) = \frac{\Omega(s)}{\delta_r(s)} = \frac{Z_2(s)}{P_s(s)} \qquad (5.1)$$

$$T_3(s) = \frac{V_w(s)}{\delta_f(s)} = \frac{Z_3(s)}{P_s(s)}$$
$$T_4(s) = \frac{V_w(s)}{\delta_r(s)} = \frac{Z_4(s)}{P_s(s)} \qquad (5.2)$$

and

$$q(s) = \frac{-hM_s[sV_w(s) - V_u\Omega(s)]}{F(s)} \qquad (5.3)$$

where $T_{i(i=1,4)}(s)$ are the transfer functions, $Z_{i(i=1,4)}(s)$ are the numerator polynomials (zeros) for different input-output pairs and $P_s(s)$ the characteristic polynomial (poles) of the system. The expressions for $Z_{i(i=1,4)}(s)$ are as follows:

$$Z_1(s) = V_u C_f [\, F(s)\, [-aMV_u\, s + (aC_f - bC_r) - a(C_f + C_r)] + Z_{11}(s)] \qquad (5.4)$$

$$Z_2(s) = V_u C_r [\, F(s)\, [bMV_u s + (aC_f - bC_r) + b(C_f + C_r)] + Z_{21}(s)] \tag{5.5}$$

$$Z_3(s) = V_u C_f [\, F(s)\, [V_u I_z s + (a^2 C_f + b^2 C_r) - a(aC_f - bC_r)] + Z_{31}(s)] \tag{5.6}$$

$$Z_4(s) = V_u C_r [\, F(s)\, [V_u I_z s + (a^2 C_f + b^2 C_r) + b(aC_f - bC_r)] + Z_{41}(s)] \tag{5.7}$$

with $Z_{11}(s)$, $Z_{21}(s)$, $Z_{31}(s)$, $Z_{41}(s)$ after rearranging the terms being:

$$Z_{11}(s) = -aV_u \,[\, (I_u M - M_s^2 h^2) s^3 + Ms[D_p s + (K_p - M_s gh)] \,] \tag{5.8}$$

$$Z_{21}(s) = bV_u \,[\, (I_u M - M_s^2 h^2) s^3 + Ms[D_p s + (K_p - M_s gh)] \,] \tag{5.9}$$

$$Z_{31}(s) = -aV_u^2 \,[\, (I_u M - M_s^2 h^2) s^2 + M[D_p s + (K_p - M_s gh)] \,] \tag{5.10}$$

$$Z_{41}(s) = bV_u^2 \,[\, (I_u M - M_s^2 h^2) s^2 + M[D_p s + (K_p - M_s gh)] \,] \tag{5.11}$$

and

$$F(s) = s^2 I_u + D_p s + (K_p - M_s gh) \tag{5.12}$$

The characteristic equation of the system ($P_s(s)$) is obtained as:

$$P_s(s) = F(s)\,[\; M(aC_f - bC_r)V_u^2 - (C_f + C_r)I_z V_u s + (aC_f - bC_r)^2 - M(a^2C_f + b^2C_r)V_u s - I_z M V_u^2 s^2 - (C_f + C_r)(a^2C_f + b^2C_r)\;] + M_s^2 h^2 V_u\, P_{s1}(s) \tag{5.13}$$

where $P_{s1}(s)$ is given by:

$$P_{s1}(s) = [\; I_z V_u s^2 + (a^2C_f + b^2C_r)s - (aC_f - bC_r)V_u\;] \tag{5.14}$$

Rearranging the terms in equation (5.14) leads to:

$$P_s(s) = -V_u P_{s1}(s)\,[\; (I_u M - M_s^2 h^2)s^2 + M[D_p s + (K_p - M_s g h)\;]] - F(S)\,[\; -(aC_f - bC_r)^2 + (C_f + C_r)I_z V_u s + (C_f + C_r)(a^2C_f + b^2C_r)\;] \tag{5.15}$$

The zeros of the 2-DOF model are obtained by dividing $Z_1(s)$, $Z_2(s)$, $Z_3(s)$, $Z_4(s)$ to F(s) after substituting $Z_{11}(s)$, $Z_{21}(s)$, $Z_{31}(s)$, $Z_{41}(s)$ equal to zero and its poles are obtained from P'(s) as:

$$P'(s) = I_z M V_u^2 s^2 + [I_z V_u (C_f + C_r) + M V_u (a^2C_f + b^2C_r)]\, s + [(C_f + C_r)(a^2C_f + b^2C_r) - (bC_r - aC_f)(bC_r - aC_f - MV_u^2] \tag{5.16}$$

The details of the manual derivations are given in Appendix A. The derivations have been verified by using the symbolic software MAPLE [112].

Let us examine closely the following term that appears in the numerators and denominators of all the transfer functions so derived:

$$I_u M - M_s^2 h^2 = [1 - (\frac{M_s^2 h^2}{I_u M})] I_u M \qquad (5.17)$$

Define the dimensionless ratio $(M_s^2 h^2)/(I_u M)$, as "roll number".

When this number is small as compared to 1, a third-order system may be reduced to a second order by neglecting the small effect of the corresponding terms. This is because if the "roll number" is small and considered to be negligible, the roots of the numerator, zeros (equations (5.8-5.12) and the roots of the denominator, poles (equation(5.13) have a common factor, namely,

$$F(s) = s^2 I_u + D_p s + (K_p - M_s g h) \qquad (5.18)$$

This factor F(s) depends exclusively on those parameters that are relevant to the roll dynamics.

In order to obtain a clear insight to the problem, the pole_zero loci of both

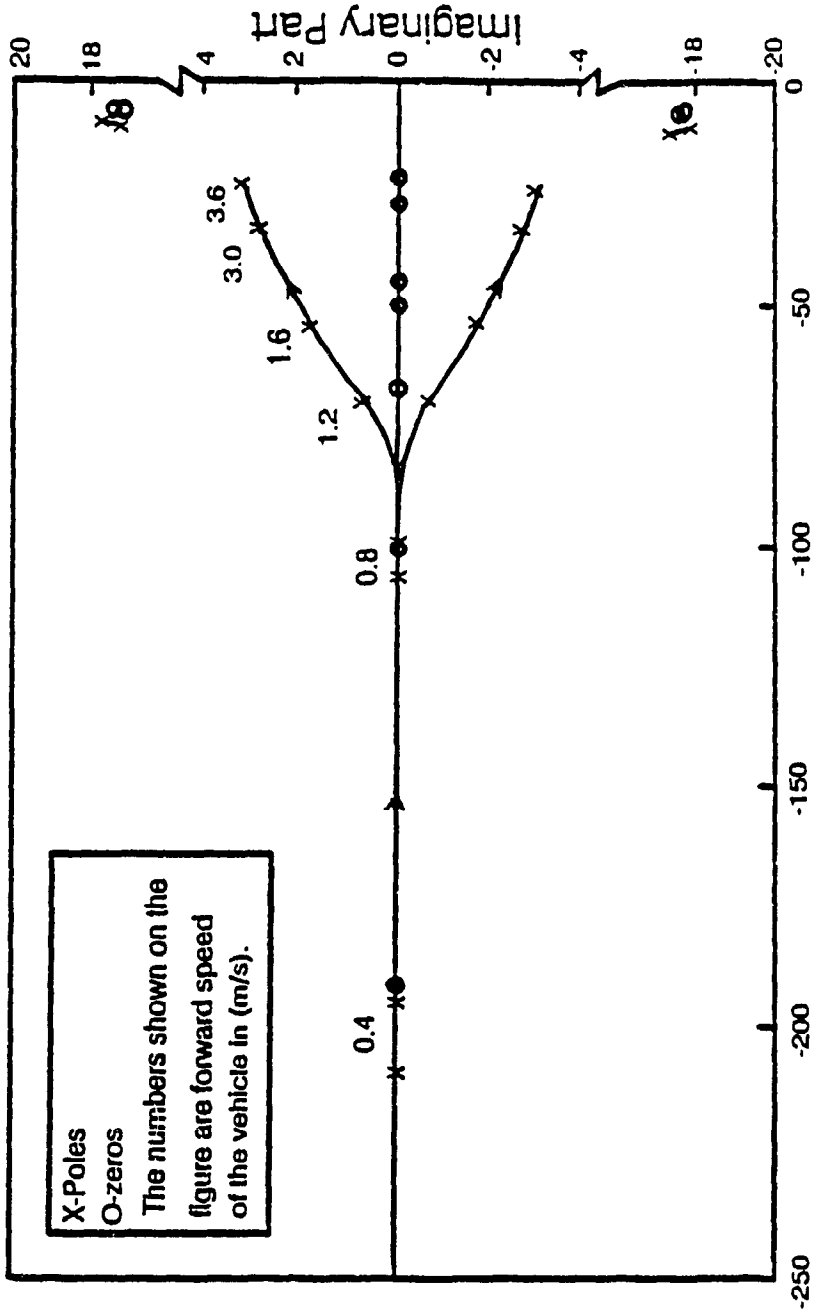

Fig. 5. 1.a Pole-zero loci for 3-DOF Model as a Function of Forward Speed (Front Wheel Steering Input- Angular Velocity Output)

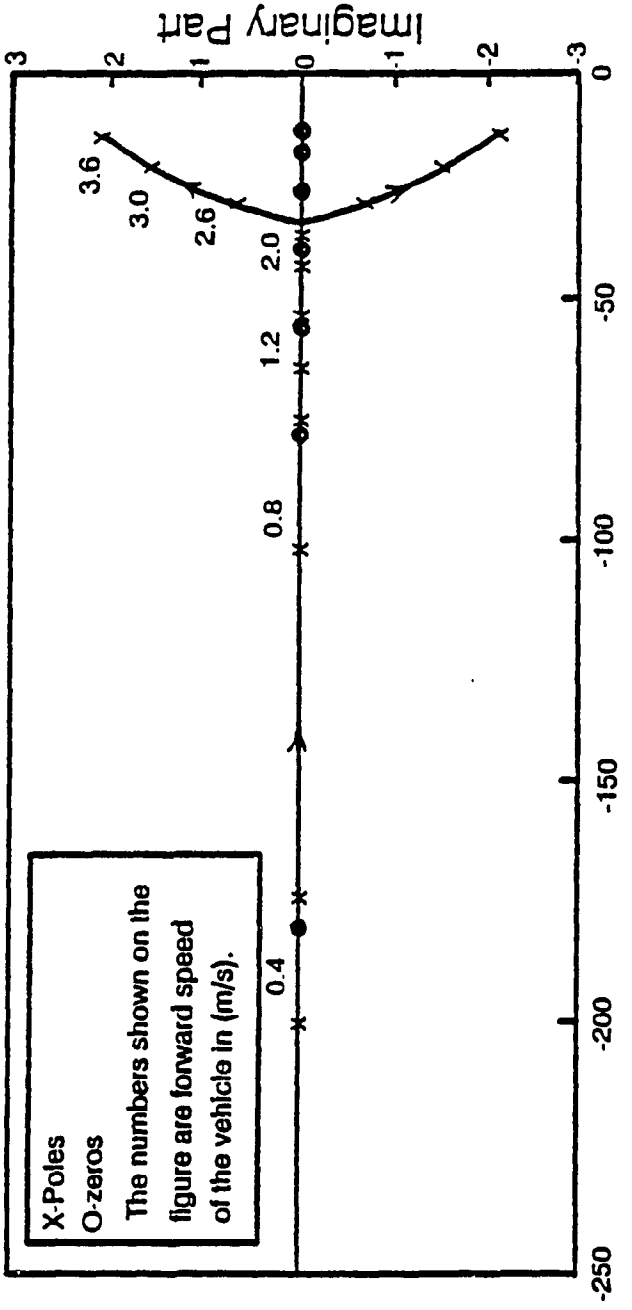

Fig. 5.1.b Pole-zero for 2-DOF Model as a Function of Forward Speed (Front Wheel Steering Input- Angular Velocity Output)

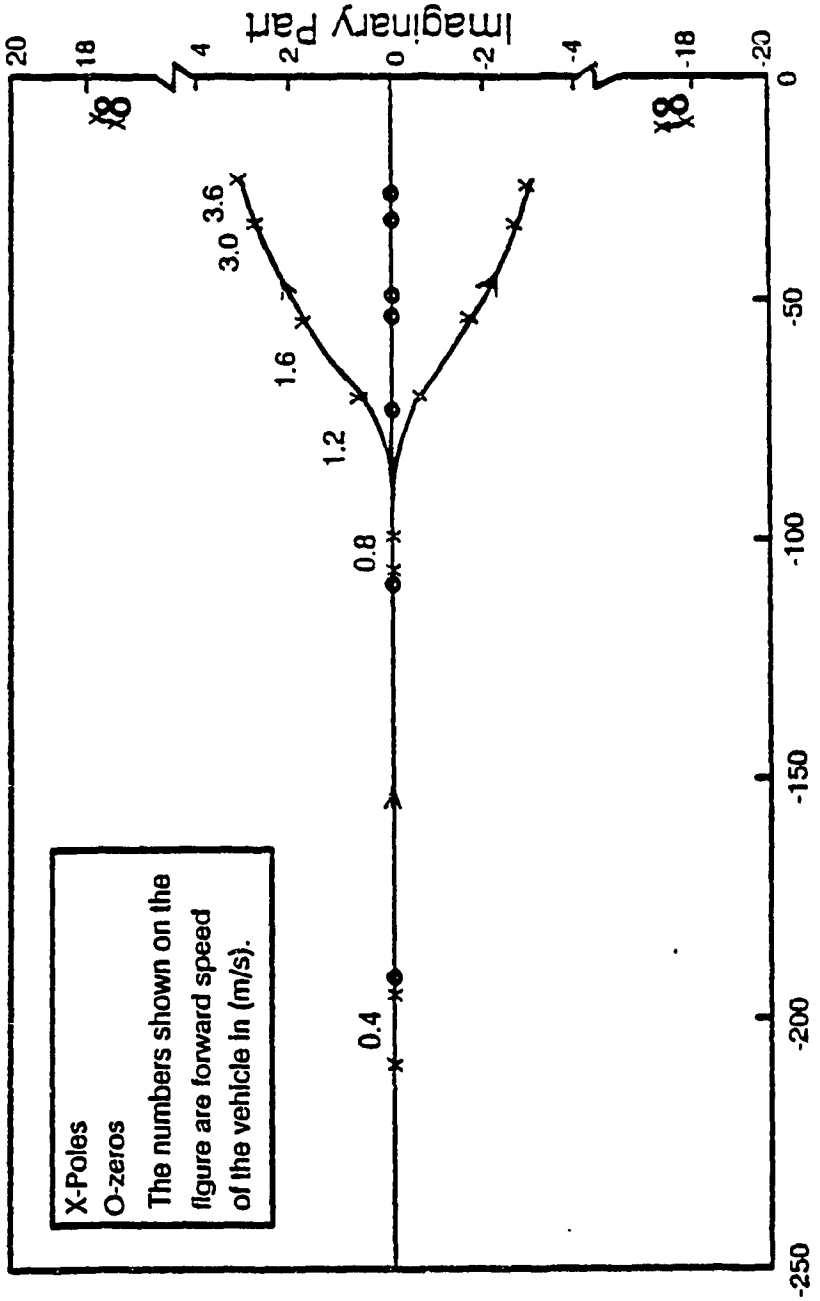

Fig. 5.2.a Pole-zero loci for 3-DOF Model as a Function of Forward Speed (Rear Wheel Steering Input- Angular Velocity Output)

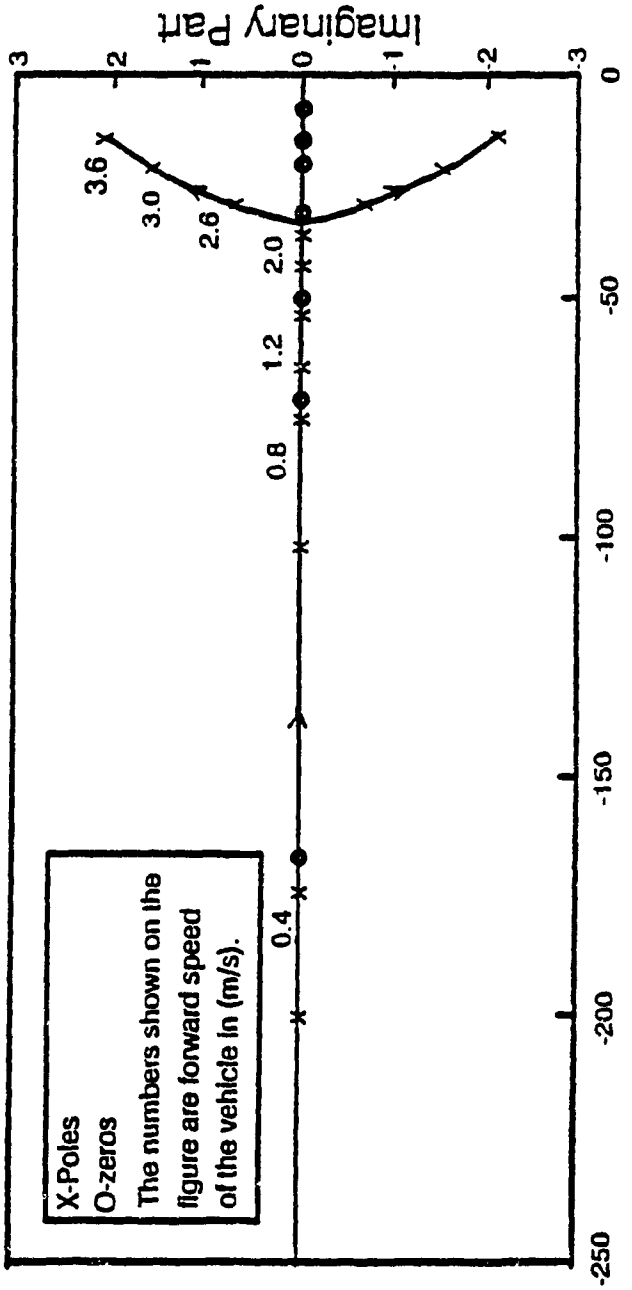

Fig. 5.2.b Pole-zero loci for 2-DOF Model as a Function of Forward Speed (Rear Wheel Steering Input- Angular Velocity Output)

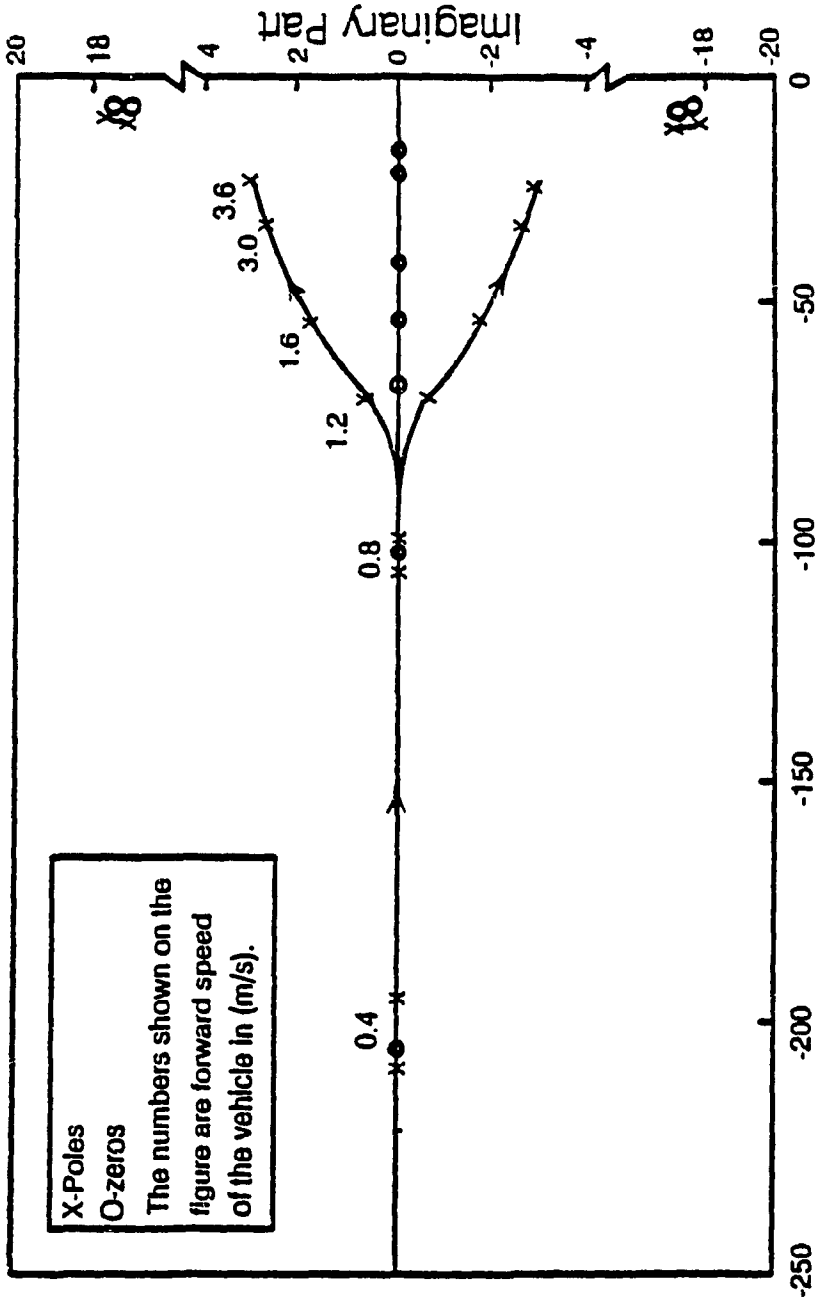

Fig. 5.3.a Pole-zero loci for 3-DOF Model as a Function of Forward Speed (Front Wheel Steering Input- Lateral Velocity Output)

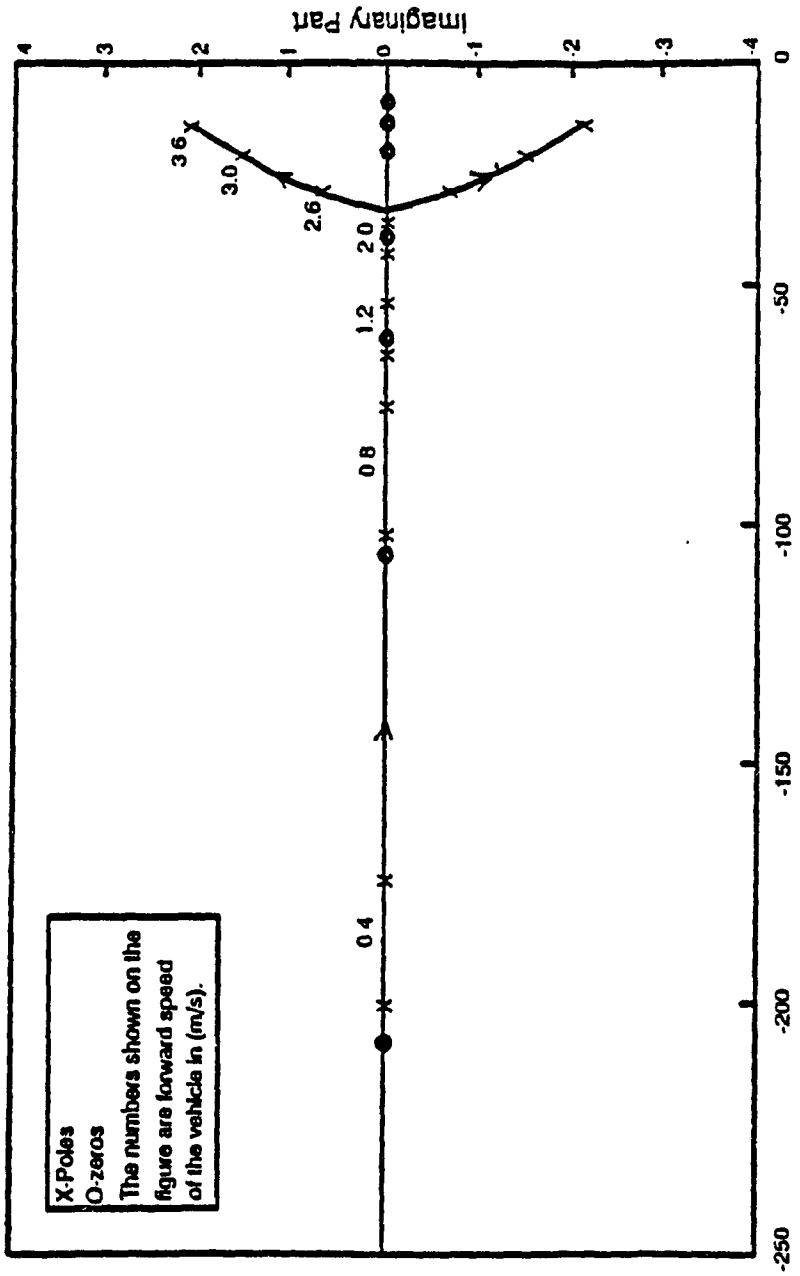

Fig. 5.3.b Pole-zero loci for 2-DOF Model as a Function of Forward Speed (Front Wheel Steering Input- Lateral Velocity Output)

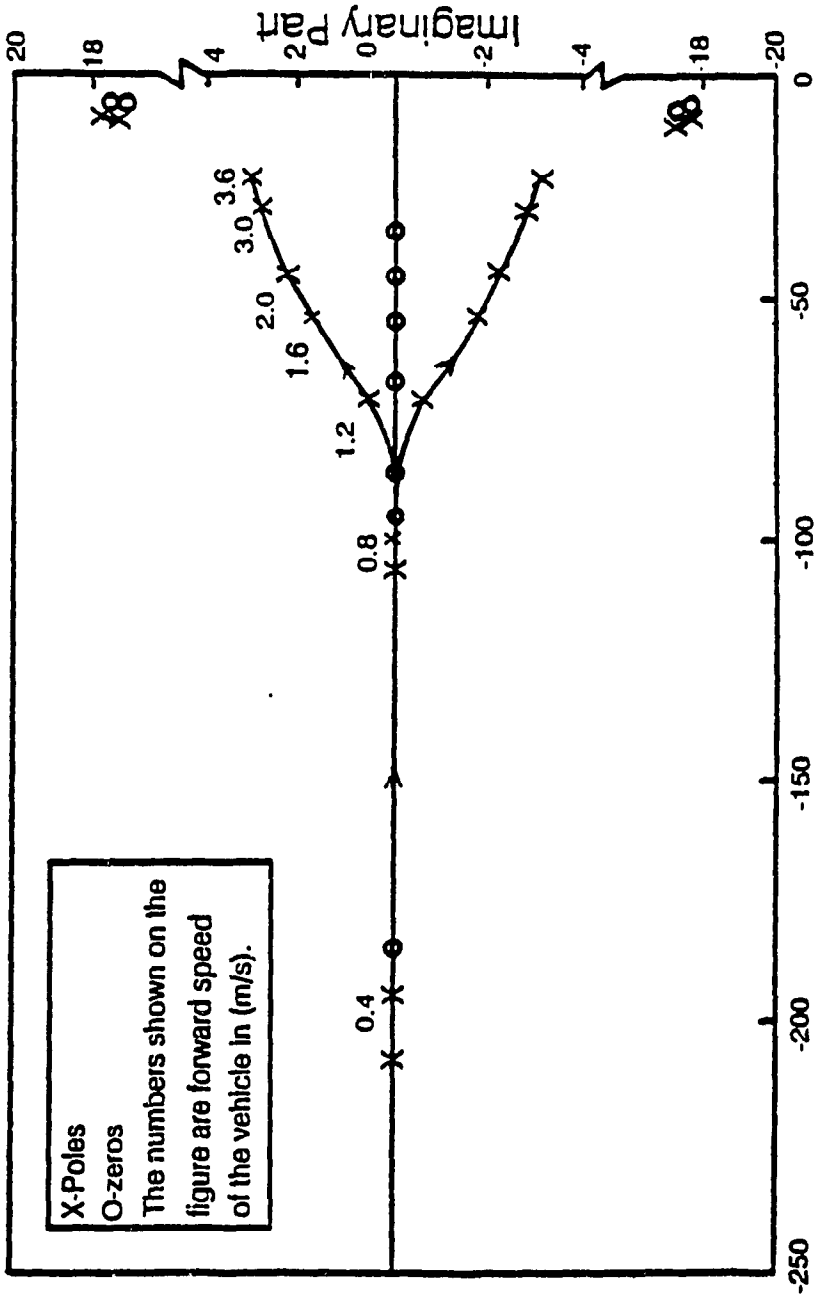

Fig. 5.4.a Pole-zero loci for 3-DOF Model as a Function of Forward Speed (Rear Wheel Steering Input- Lateral Velocity Output)

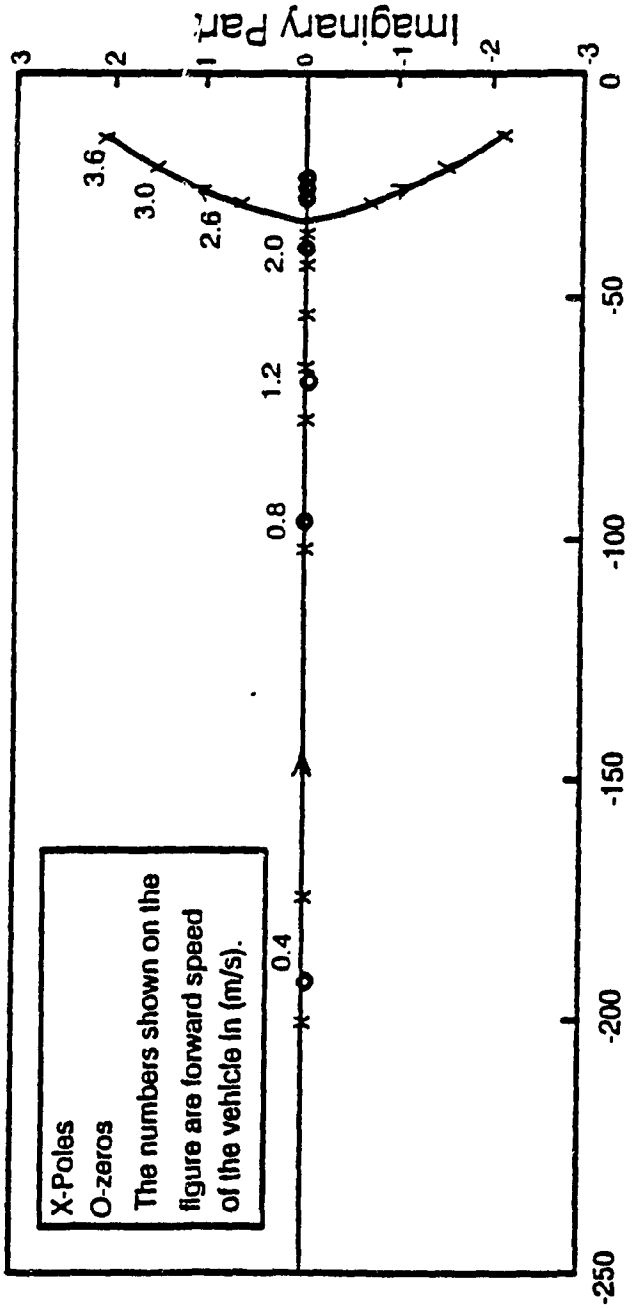

Fig. 5.4.b Pole-zero loci for 2-DOF Model as a Function of Forward Speed (Rear Wheel Steering Input- Lateral Velocity Output)

models for the various input-output pairs are plotted, for a range of values of the forward speed of the vehicle, as shown in Figs. (5.1.a,b -5.4.a,b). The parameters used in this study are taken from a prototype vehicle (CONCIC III) that was developed in the Centre for Industrial Control at Concordia University [59,65]. A comprehensive list of its parameters is given in Appendix B. The plots are obtained by calculating the roots of the polynomials in denominator (poles) and numerator (zeros) of equations (5.10) to (5.11) while all vehicle parameters except its forward speed are kept constant. For CONCIC III experimental vehicle, the roll number is approximately 0.15, thus qualifying it to be considered as functionally equivalent to a 2-DOF system as explained above.

The following observations are made from the pole-zero loci plots:

1. At higher forward speeds, the same trends in poles locations can be observed for both models: the poles that start off by being on the real axis "move" toward the imaginary axis until they split to become complex conjugate pairs, while the two imaginary poles are relatively insensitive to the magnitude of the vehicle speed. One may therefore conclude that, for both models, the real poles (poles that lie on the real axis) have minor significance in the transient response of the vehicle at lower speeds, on account of the high decaying rate. However, at higher speeds, these real poles contribute more and the dynamics involved can

no longer be neglected. The response of the system may become more oscillatory at higher speeds.

2. Two complex conjugate zeros of the system are located very close to two complex poles. These pole- and zero- pairs effectively cancel one another and contribute little to the total response of the vehicle. How close they are is to a great extent dictated by the magnitude of the roll number (the zeros are strong functions of the parameters of the roll dynamics, and are quite insensitive to other parameters). This observation is supported by the results of the parametric study described in chapter 6, where it will be shown that those parameters of the vehicle which contribute to the roll motion do not considerably affect the lateral and the yaw velocities. It is apparent that these same two velocities are influenced more by the forward speed of the vehicle than by other geometric-kinematic parameters [66-67].

3. Comparing the two plots for the same input-output pairs reveals that in both models, almost the same poles dominate. However, the 2-DOF model tends to yield a more damped response. This is more obvious when we examine the splitting points of the real poles for both models.

Therefore, it is possible to use the properties of roll number to decide which model to be used. In the next section, the way the parameters of a vehicle

affect its dynamic behaviour in plane motion is described. This leads to the criteria based on which one can decide whether or not the dynamics of the vehicle can be neglected.

5.4 Characterization of Transient Response for Plane Motion

As it was shown in the previous section, under the condition of small roll number, the contribution of roll motion in response of a vehicle is small. The state-space representation of equations of plane motion for 2-DOF (steering dynamics is neglected) can be obtained by substituting from (5.1-5.4) into (5.9-5.10) in the form of

$$\dot{x} = Ax + Bu \tag{5.19}$$

where

$$x^T = [V_w \ \Omega] \tag{5.20}$$

$$u^T = [\delta_f \ \ \delta_r] \tag{5.21}$$

and

$$A = \begin{bmatrix} -\dfrac{C_f + C_r}{MV_u} & \dfrac{bC_r - aC_f}{MV_u} - V_u \\ \dfrac{bC_r - aC_f}{I_z V_u} & -\dfrac{b^2 C_r + a^2 C_f}{I_z V_u} \end{bmatrix}$$

$$B = \begin{bmatrix} \frac{C_f}{m} & -\frac{C_r}{m} \\ \frac{aC_f}{I_z} & \frac{bC_r}{I_z} \end{bmatrix} \tag{5.22}$$

According to (5.22), the characteristics equation of this system is obtained from matrix (A) as:

$$\lambda^2 + \left(\frac{C_f + C_r}{MV_u} + \frac{b^2C_r + a^2C_f}{I_zV_u}\right)\lambda + \left(\frac{C_f + C_r}{MV_u}\right)\left(\frac{b^2C_r + a^2C_f}{I_zV_u}\right) - \left(\frac{bC_r - aC_f}{I_zV_u}\right)\left(\frac{bC_r - aC_f}{MV_u} - V_u\right) = 0 \tag{5.23}$$

Any vehicle is either of the following three types: understeer, neutral steer and oversteer [55,56,87]. For a neutral steer vehicle, when it is accelerated with a fixed steering angle, the turning radius remains the same. For understeer vehicle, the turning radius increases and for oversteer vehicle, turning radius decreases [55,56,87]. For a neutral steer vehicle a $C_f = b\ C_r$ and the eigenvalues of matrix A are:

$$\lambda_1 = -\frac{C_f + C_r}{MV_u} \tag{5.24}$$

$$\lambda_2 = -\frac{alC_f}{I_z V_u} \tag{5.25}$$

where (l=a+b) is the wheelbase of the vehicle. Equations (5.24) and (5.25) can be further simplified to (by assuming $C_f = C_r$):

$$\lambda_1 = \frac{-2C_f}{MV_u}, \quad \lambda_2 = \frac{-alC_f}{I_z V_u} \tag{5.26}$$

The transient response of understeer vehicle and oversteer vehicle (below critical speed), can be evaluated by using (λ_1, λ_2) as a basis. How fast the transient part of the response of the vehicle (open loop response) to a steering input diminishes is characterized by the decaying rates of the eigenvalues of matrix A. Obviously, λ_1 and λ_2 represent the contributions of lateral and yaw velocities on transient part of the response respectively. Let us define λ_1 as "velocity constant" (due to its dimension which is second^{-1} and also its correspondence with lateral velocity) and the ratio of (λ_1, λ_2) :

$$\Lambda = \frac{\lambda_2}{\lambda_1} = \frac{alM}{2I_z} \tag{5.35}$$

as "yaw number". Let's compare the above values (λ_1, λ_2) with (λ_3, λ_4) obtained from the solution of characteristic equation of matrix A. As examples, Figs.(5.5-

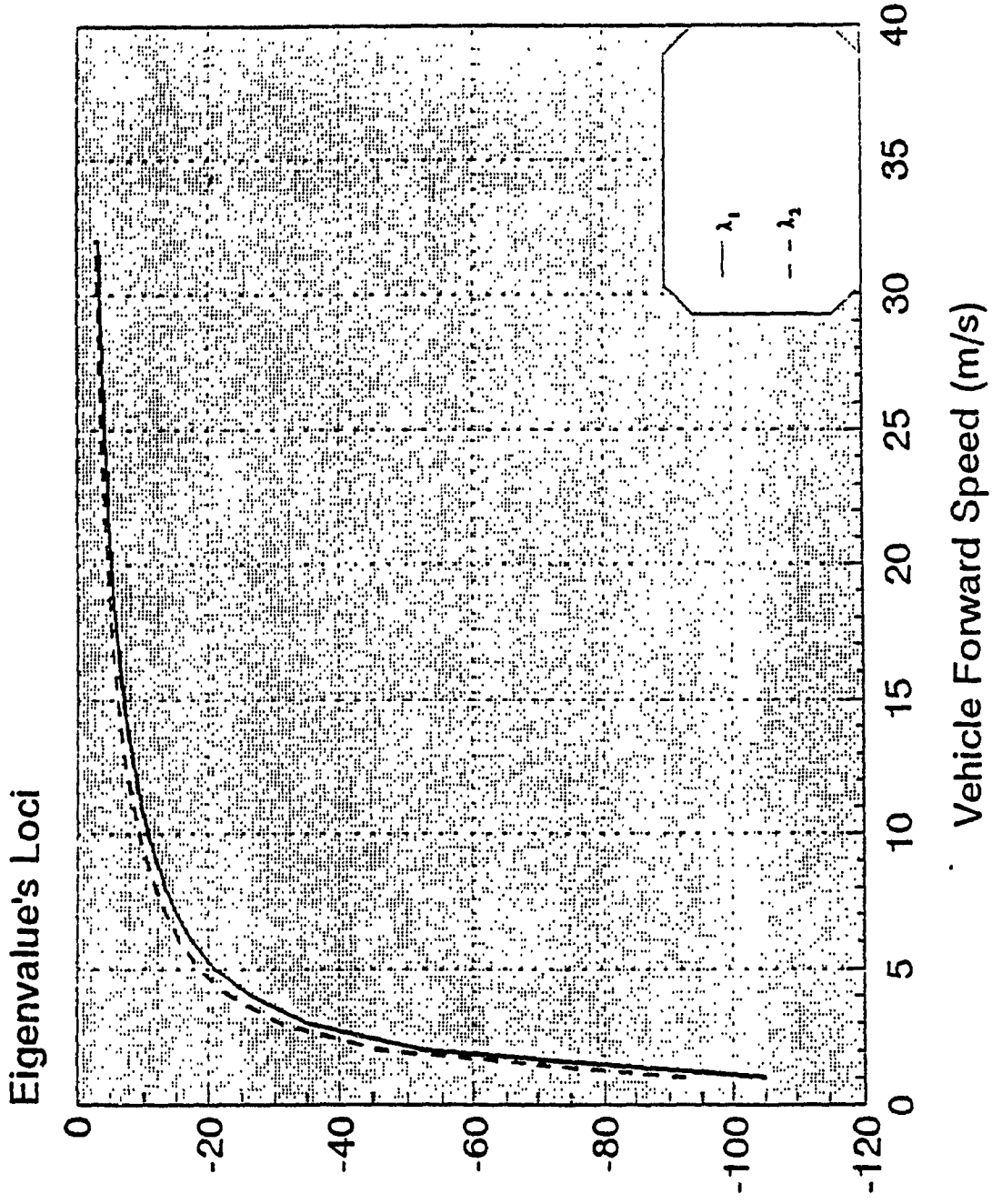

Fig. 5.5 Variations of λ_1 and λ_2 as a Function of Forward Speed of the Vehicle (understeer)

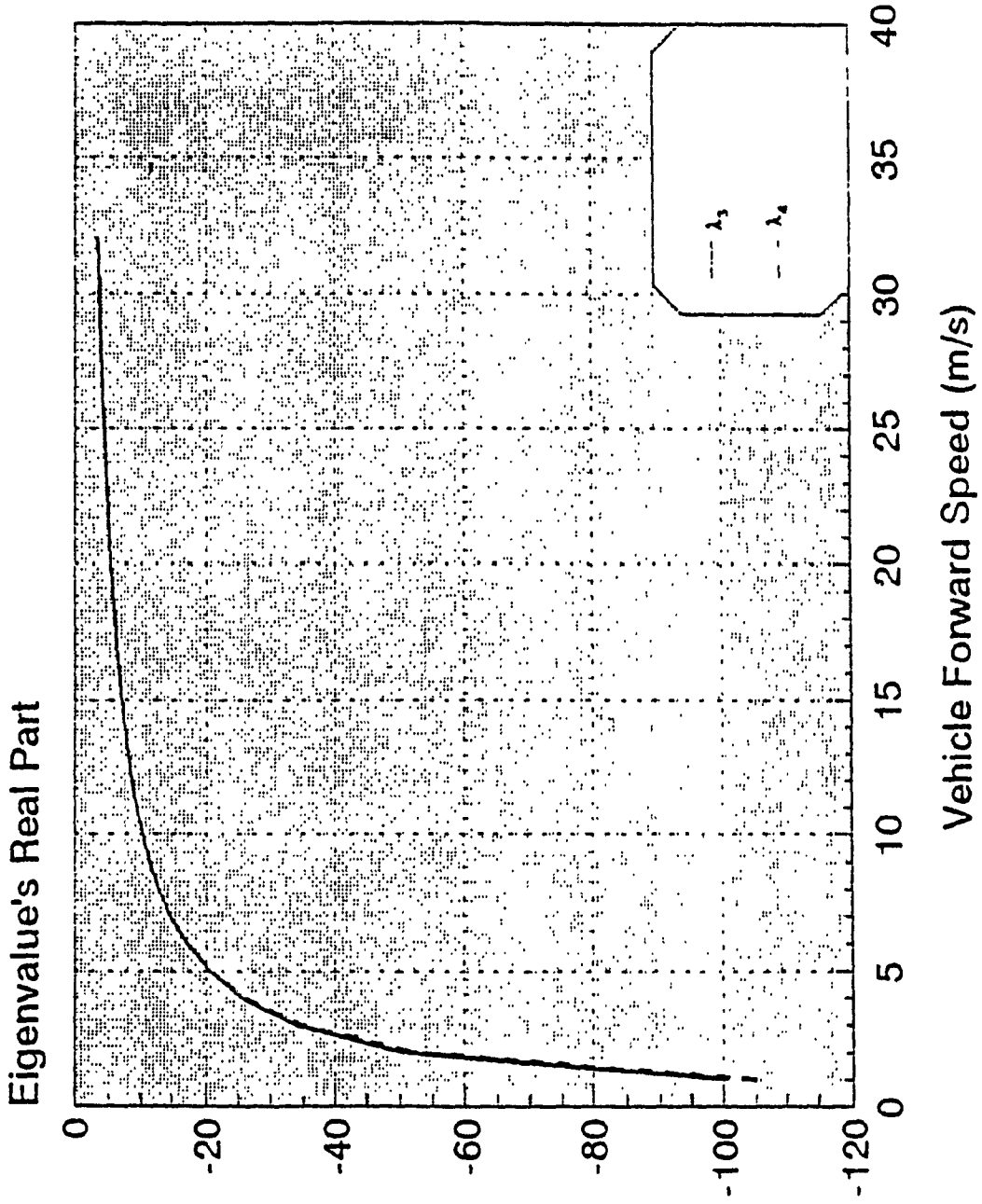

Fig. 5.6 Variations of λ_3 and λ_4 as a Function of Forward Speed of the Vehicle (understeer)

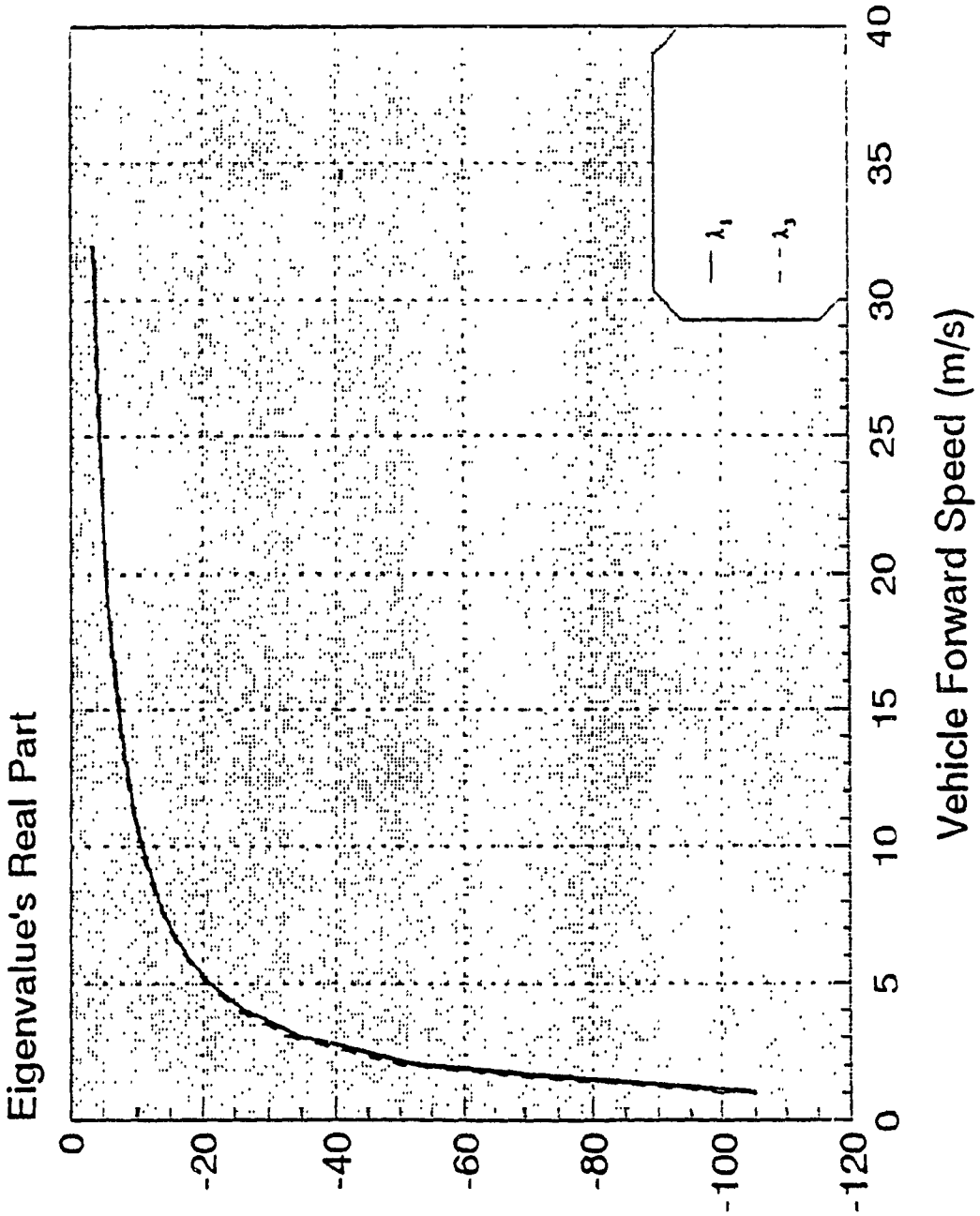

Fig. 5.7 Comparison of λ_1 and λ_3 as a Function of Forward Speed of the Vehicle (understeer)

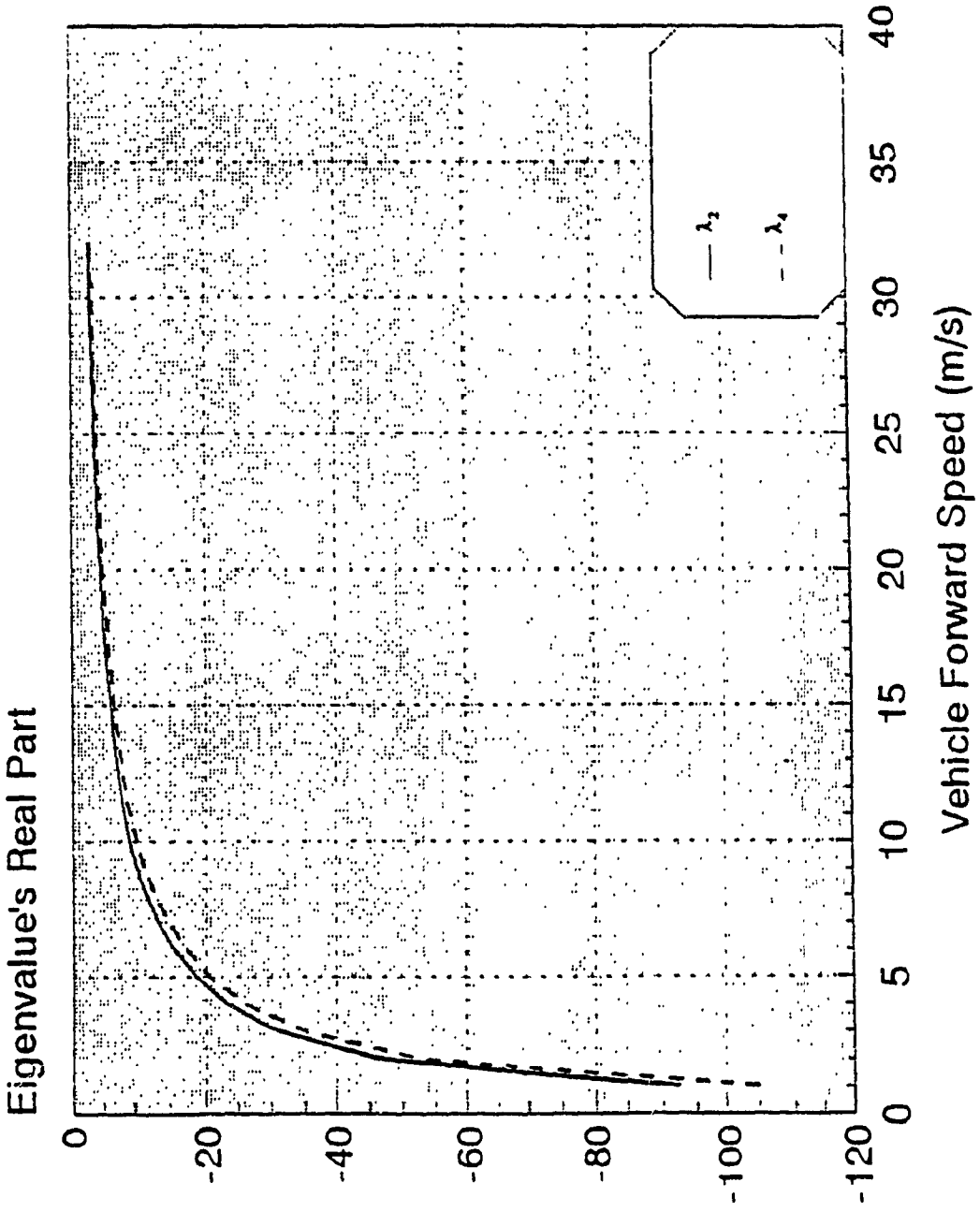

Fig. 5.8 Comparison of λ_2 and λ_4 as a Function of Forward Speed of the Vehicle (understeer)

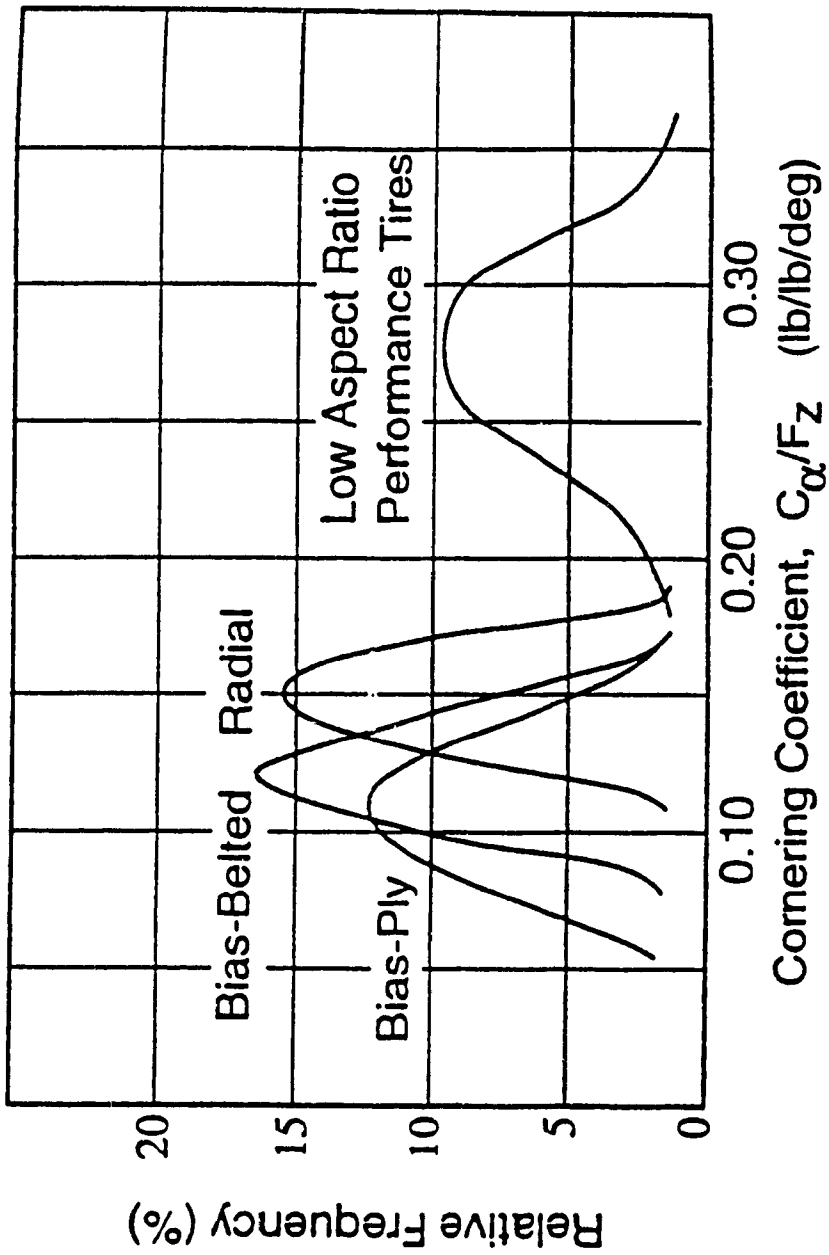

Fig. 5.9 Frequency Distribution of Cornering Coefficient for Passenger-Car Tires
(Courtesy of Gillespie [55])

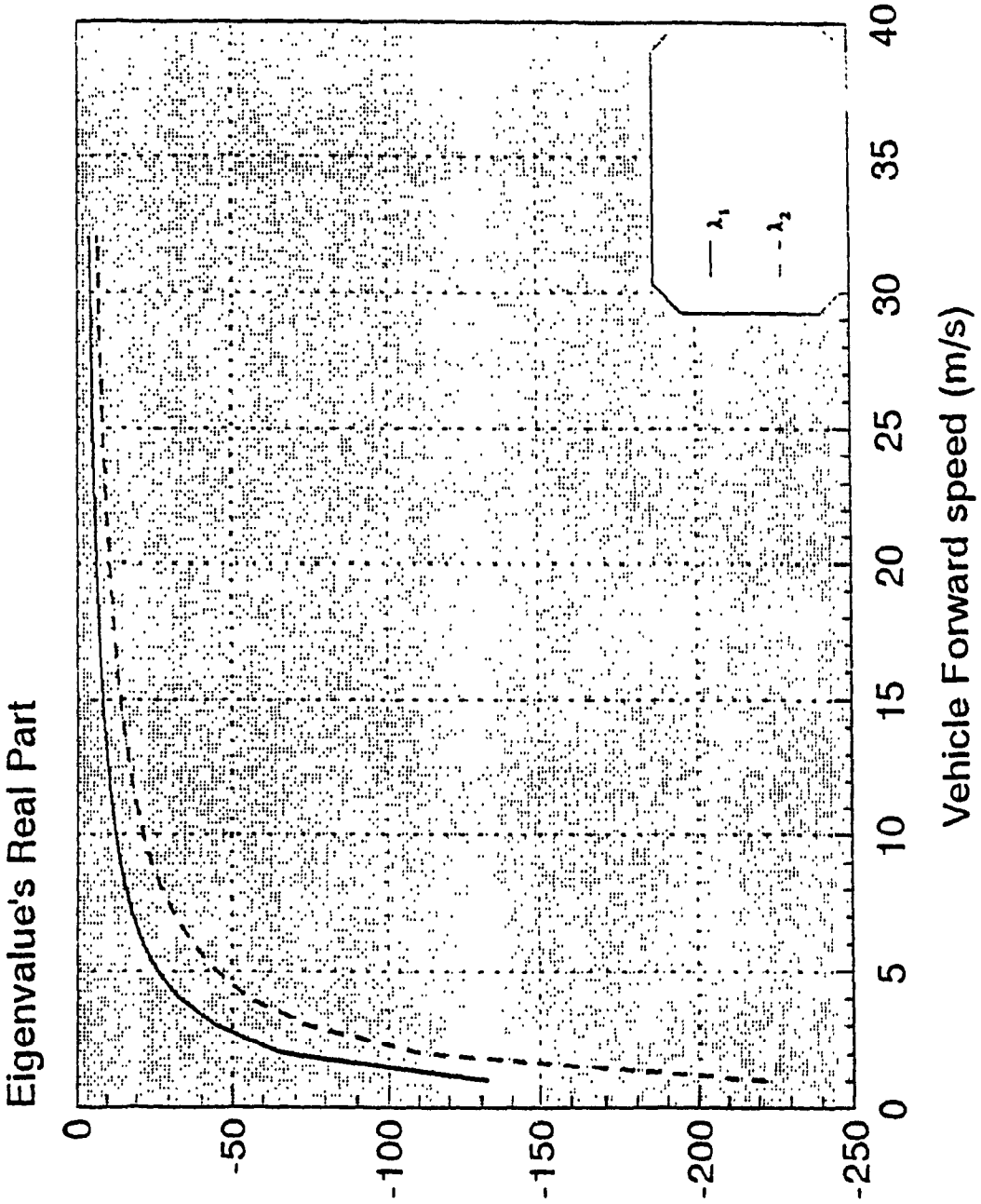

Fig. 5.10 Variations of λ_1 and λ_2 as a Function of Forward Speed of the Vehicle (oversteer)

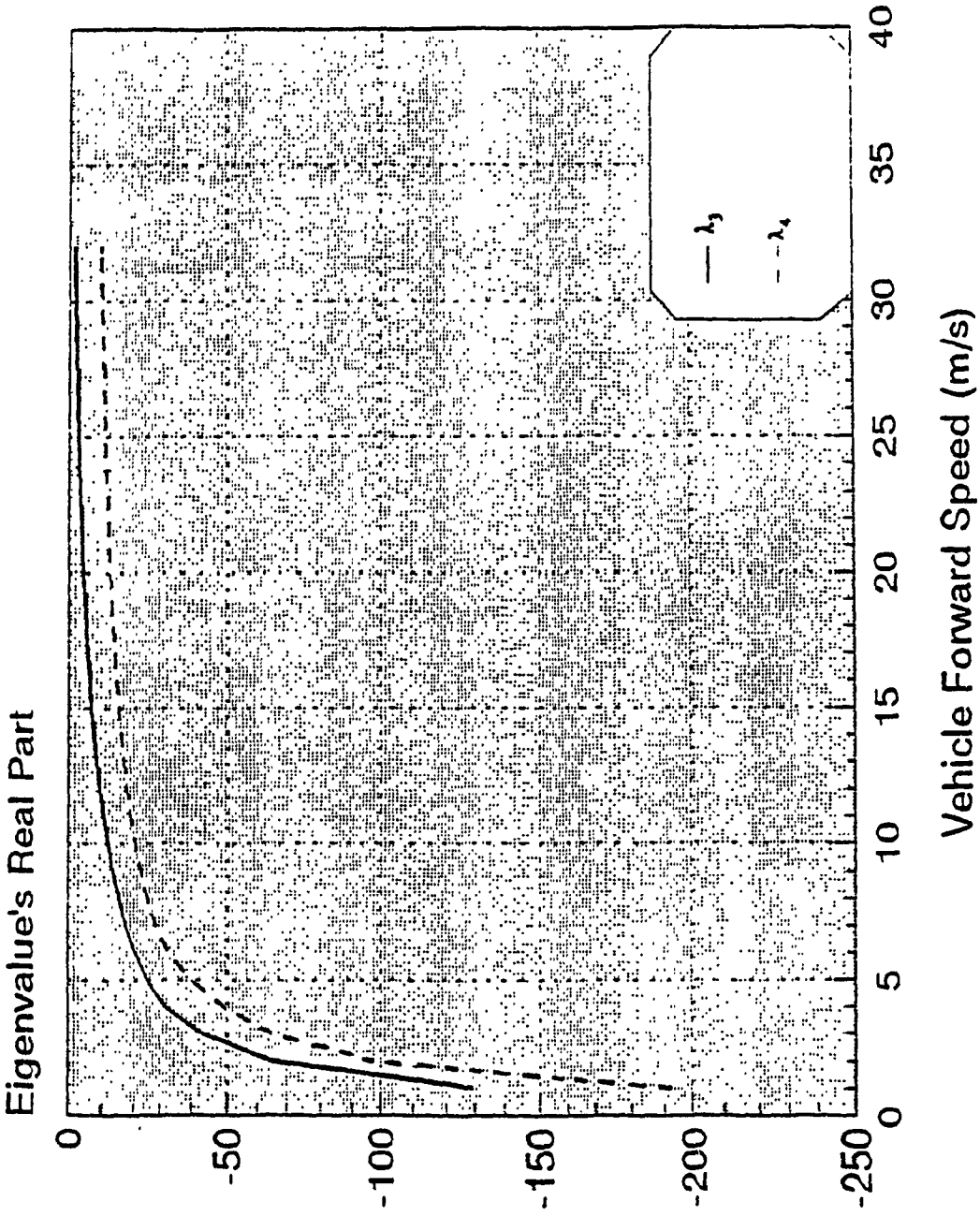

Fig. 5.11 Variations of λ_3 and λ_4 as a Function of Forward Speed of the Vehicle (oversteer)

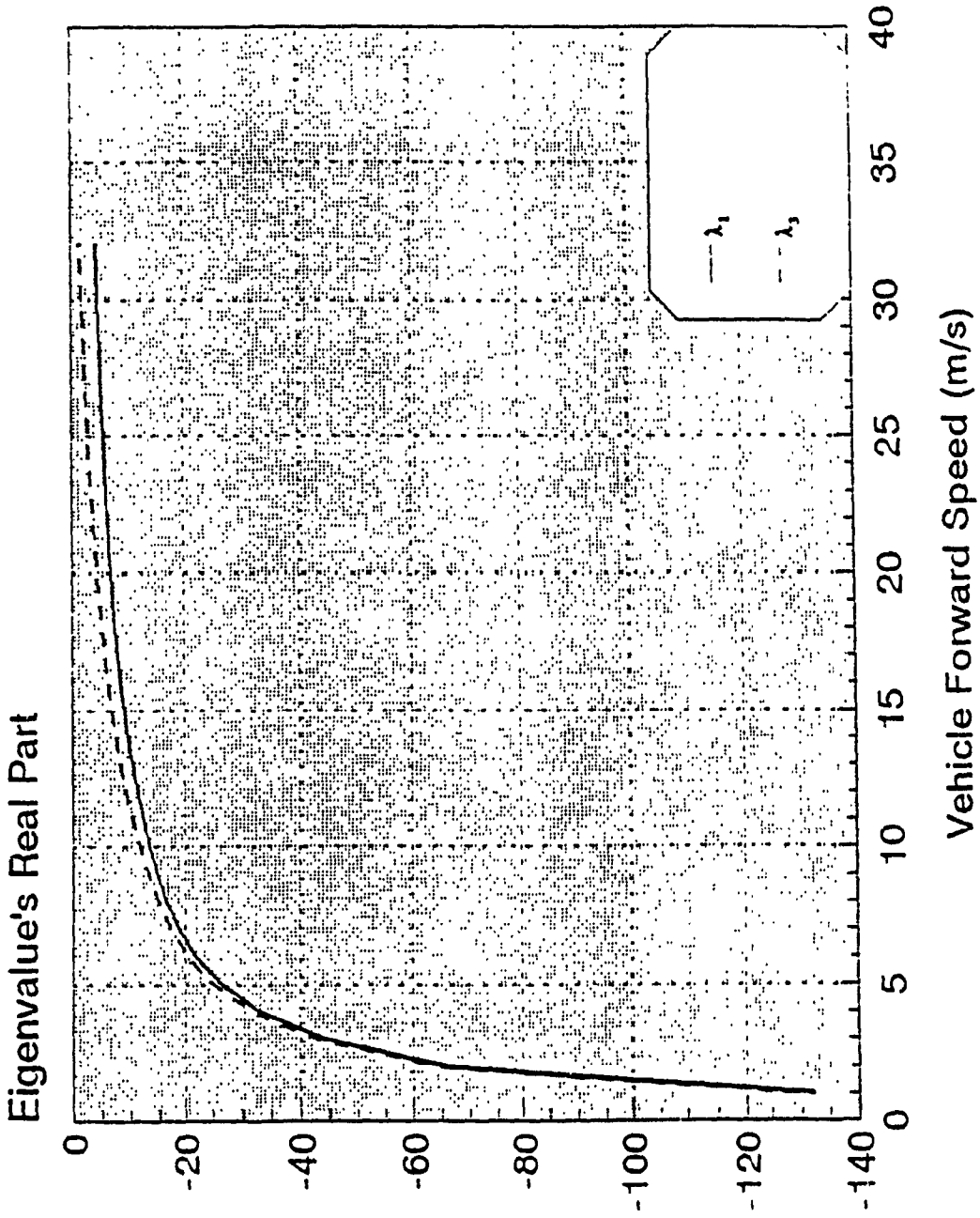

Fig. 5.12 Comparison of λ_1 and λ_3 as a Function of Forward Speed of the Vehicle (oversteer)

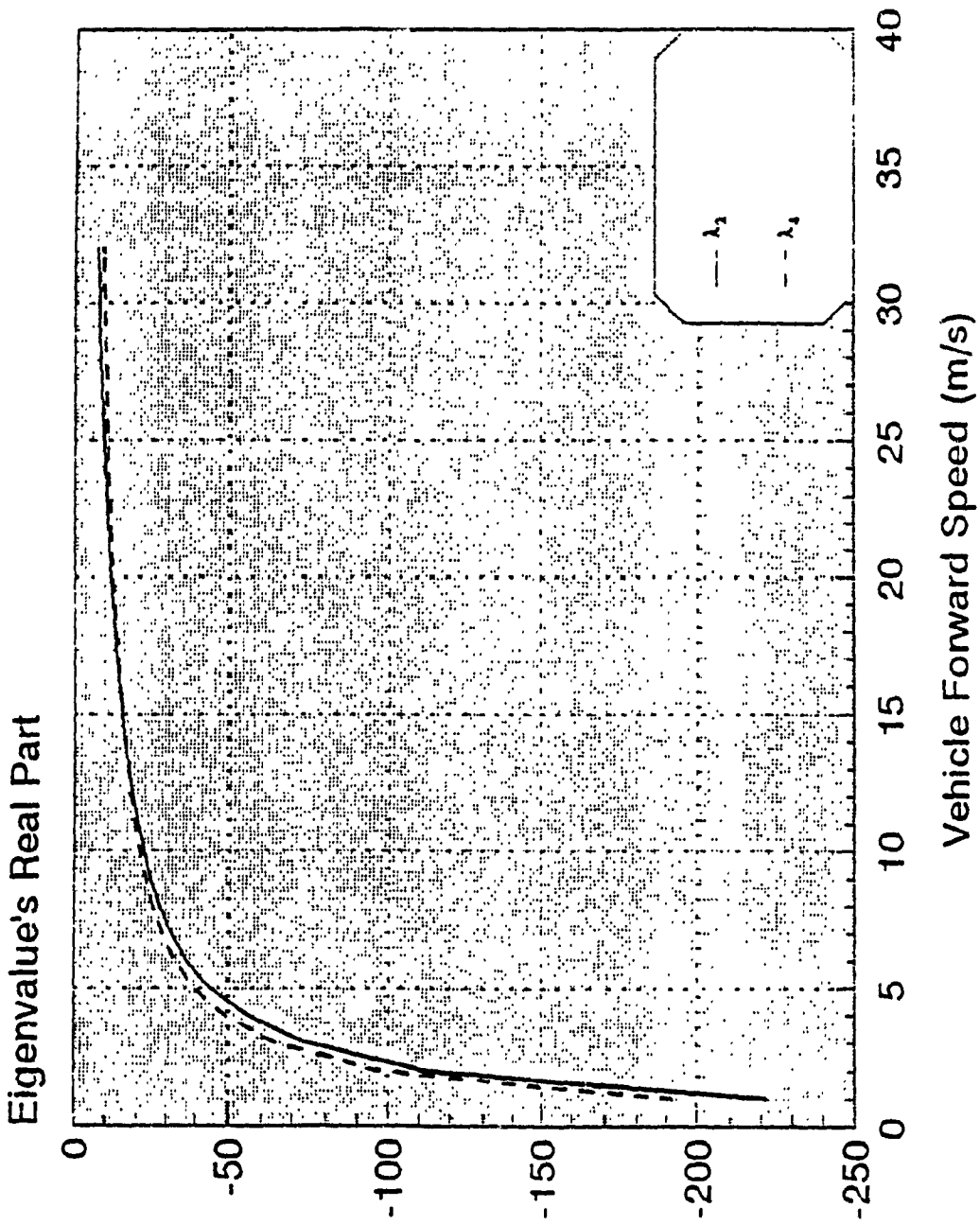

Fig. 5.13 Comparison of λ_2 and λ_4 as a Function of Forward Speed of the Vehicle (oversteer)

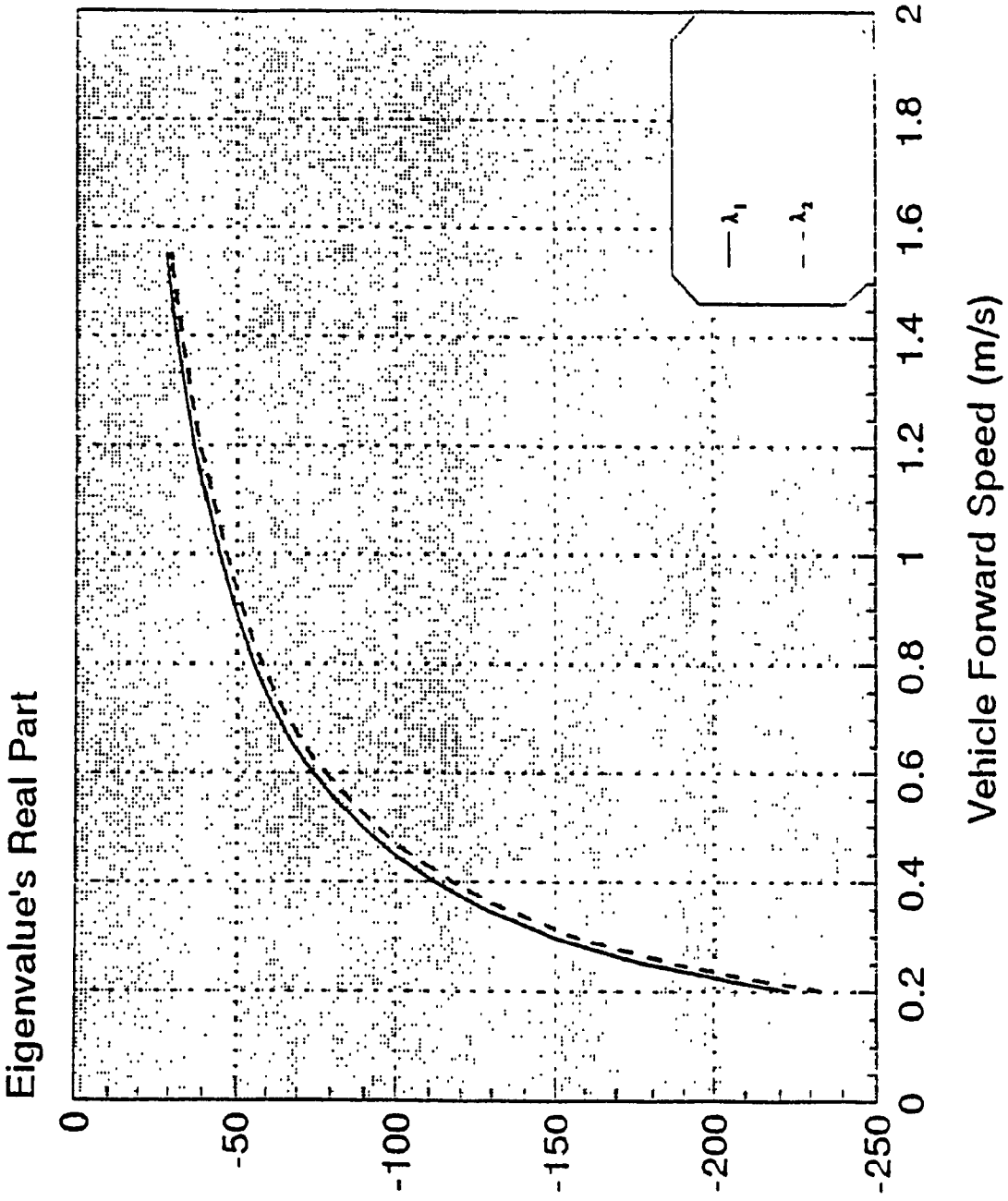

Fig. 5.14 Variations of λ_1 and λ_2 as a Function of Forward Speed of the Vehicle (CONCIC III)

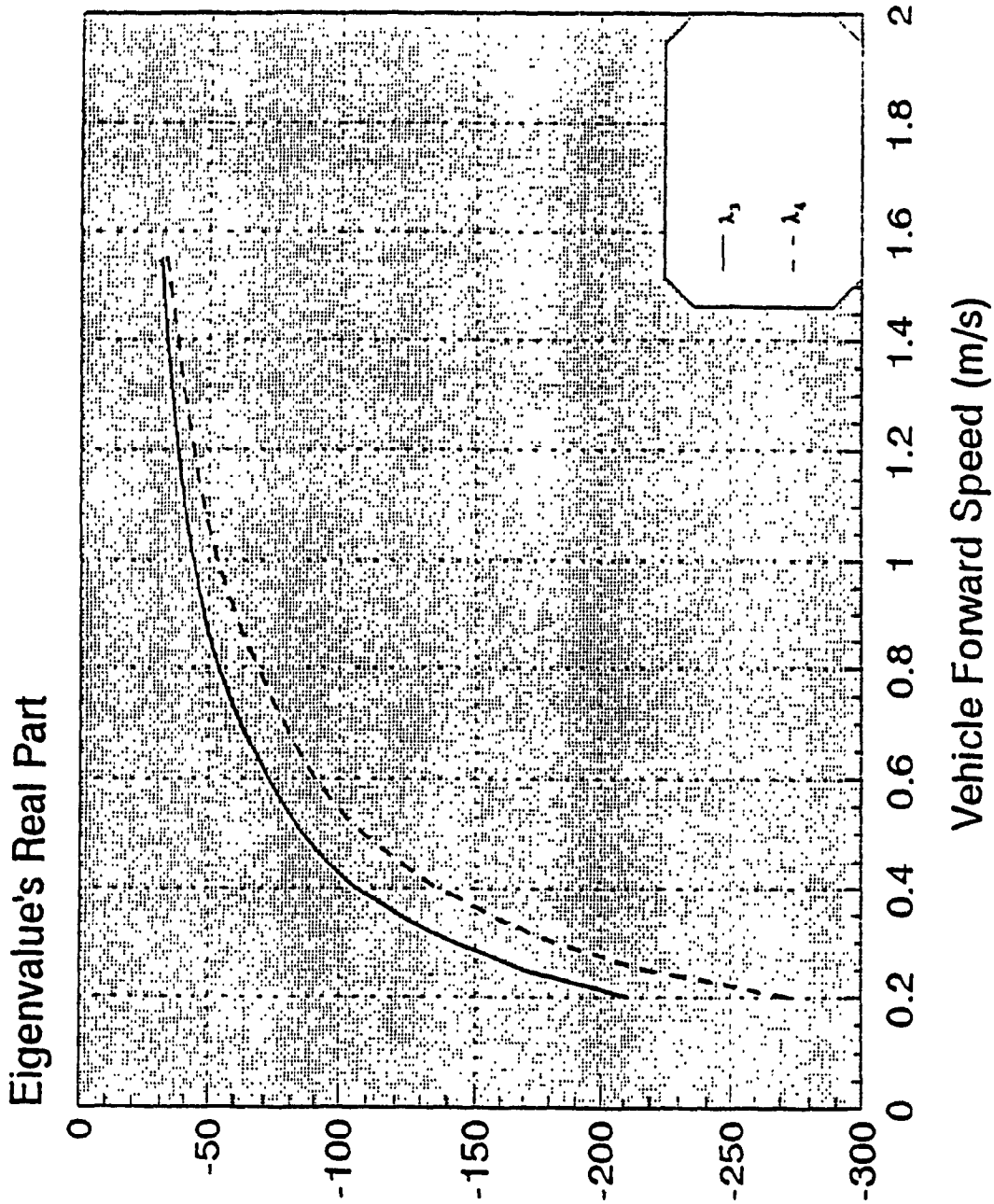

Fig. 5.15 Variations of λ_3 and λ_4 as a Function of Forward Speed of the Vehicle (CONCIC III)

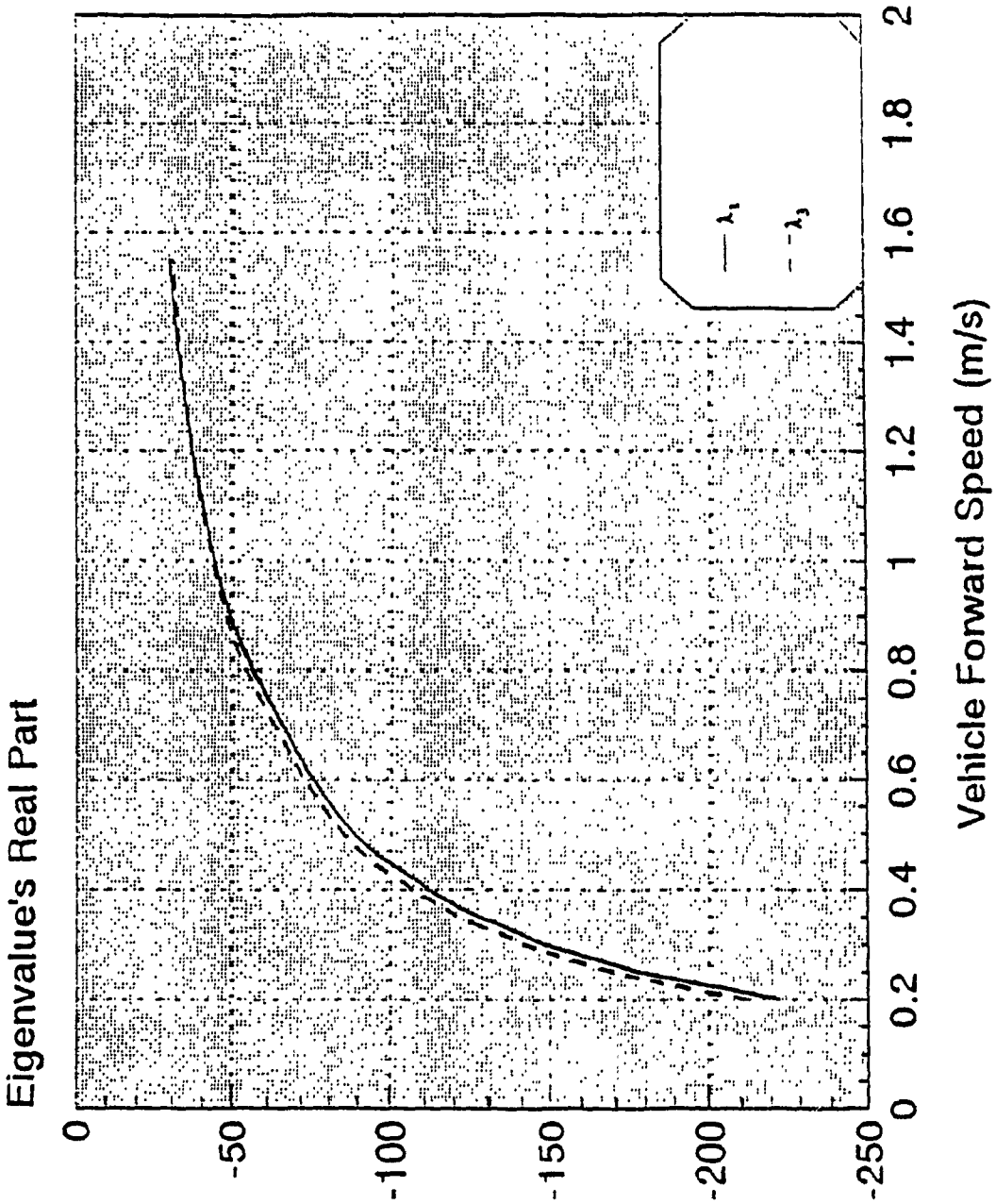

Fig. 5.16 **Comparison of λ_1 and λ_3 as a Function of Forward Speed of the Vehicle (CONCIC III)**

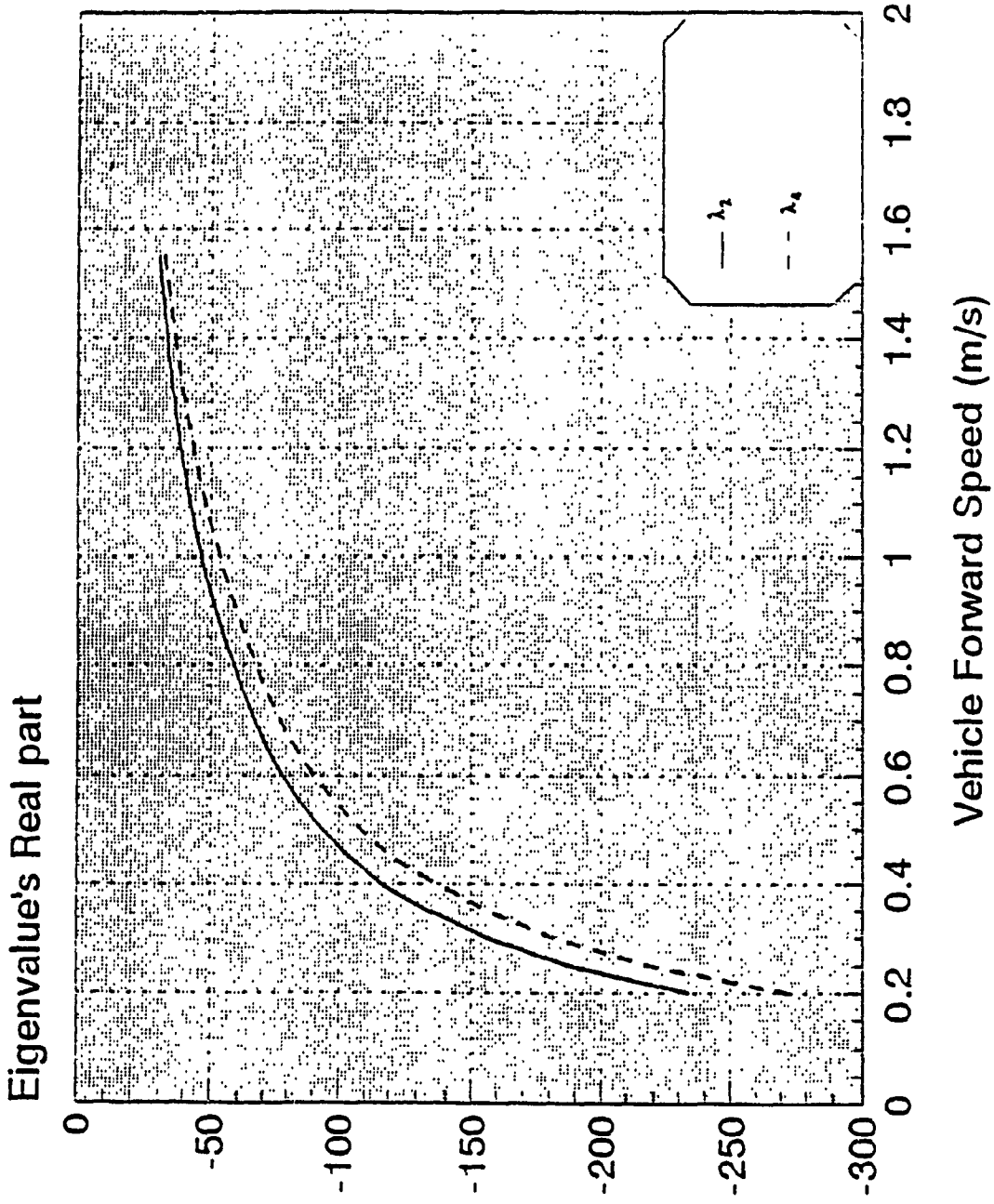

Fig. 5.17 Comparison of λ_2 and λ_4 as a Function of Forward Speed of the Vehicle (CONCIC III)

5.8) and (5.10-5.17) demonstrate the variations of (λ_1, λ_2) and (λ_3, λ_4) with the forward speed of the vehicle and their comparison for three different vehicles [82,106,59,65]. Figs.(5.5-5.8) show the results obtained for an understeer vehicle [82] whose parameters are given in Appendix C. The following observations are made from the figures (for λ_1, λ_2 and λ_3, λ_4):

1. As the speed of the vehicle increases, in all cases, the values of (λ_1, λ_2) and (λ_3, λ_4) are decreased with a very sharp decrease at lower speeds and a fairly flat change at higher speeds. This can also be deduced from equation (5.34) (due to its hyperbolic nature).

2. Although the pairs of (λ_1, λ_2) and (λ_3, λ_4) are relatively far at lower speeds (where they do not have any contribution to transient response due to their high decaying rate), but they are fairly close at higher speeds and effectively they converge to each other. This phenomenon suggests that in the region where the transient response of the vehicle is important (i.e. at higher speeds), just by checking one eigenvalue one can extract the necessary information about dynamic behaviour of the vehicle. However, if necessary, "yaw number" can be used to obtain the other eigenvalue.

3. As it is observed from Figs.5.7 and 5.8, the values of (λ_1, λ_3) and (λ_2, λ_4)

are fairly close particularly at higher speeds. Therefore, (λ_1, λ_2) and (λ_3, λ_4) can be used interchangeably.

4. The "Velocity constant" is more specific for the typical passenger cars, since the cornering coefficients (cornering stiffness divided by normal load of the tire) of the type of tires usually used have a specific range. Typical variations of the cornering coefficients are shown in Fig. 5.9 [55]. This figure suggests that the values of cornering coefficients lie approximately between (5.7-11.5 N/N/rad; after conversion). Therefore, by using these values (depending upon the type of the tire) and the weight of the vehicle, the values of cornering stiffness are obtained, which makes equation (5.26) more specific for typical passenger cars.

The sets of Figs.(5.10-5.13) and (5.14-5.17) show the results for an oversteer vehicle [106] whose parameters are given in Appendix C and for CONCIC III respectively. It is observed that a slight decrease in decaying rates of the variations of the eigenvalues for CONCIC III vehicle can be noticed at lower speeds.

5.5 Summary

In this study, a comparison was made between 2-DOF and 3-DOF mathematical models of a vehicle. To study the dynamic

behaviour associated with each of the two models, transfer functions of the system were used. The pole-zero loci plots have been found to be extremely valuable to arrive at some important insight to the nature of the path following characteristics of such a system. A dimensionless number, designated as the "roll number" was defined, with the property that for a system whose roll number is small, the 3-DOF model is effectively reduced to a 2-DOF model as a result of pole-zero cancellation. By checking this number for any vehicle one can avoid the complexities associated with the studies of steering controller design, directional response, directional stability as well as structural design if the simpler model would suffice.

The study was further extended to more detailed analysis of dynamic behaviour of the system by using the 2-DOF model. It was shown that further analysis and simplification of the 2-DOF model, while carrying the important information about the original model, gives rise to two other quantities called "velocity constant" and "yaw number". These two quantities represent those parameters of a vehicle that influence its plane motion. They can be effectively used in deciding when to use a dynamic or a simpler kinematic model to represent the motion of the vehicle. By making use of the above numbers it can be stated that the forward speed of a vehicle is a critical parameter affecting its dynamic behaviour.

CHAPTER 6

PARAMETRIC STUDY AND SENSITIVITY ANALYSIS OF AUTOMATED VEHICLES

6.1 Introduction

The problem of investigating the sensitivity of dynamical systems with respect to parameter changes takes an important place in today's engineering design. In particular, in design of control systems, one of the necessary properties is low sensitivity to parameter variation or uncertainties that exist in the system. Therefore, for their design the knowledge of how the changes in parameters of a dynamic system affect its performance and whether such variations cause severe changes or they have minor effects are necessary. In this regard, sensitivity methods can be employed as useful tools for typical parametric investigation.

The information provided by sensitivity study can be utilized in twofold. The first one to design and build a control system with a variable structure in order to achieve certain adaptation properties such as self tuning and adaptive control. References [113-117,121-123] exemplify some of these studies. The other aspect is to investigate the changes in dynamics of a system as a result of variations (or deviations) in its parameters. In this regard, literature survey reveals that there are some reports on the applications of sensitivity theory on optimal design of hydraulic systems or its applications on design of electrical circuits [117-120]]. For this thesis, more emphasis is given to the latter, although the former can also be considered in order to investigate the possibility of designing more intelligent vehicles with certain levels of adaptations.

In this chapter, a parametric study of automated vehicles is carried out by using sensitivity theory. A sixth order dynamic model is developed in state space format to represent the motion of a 3-degrees of freedom (3-DOF) vehicle by considering lateral, yaw and roll motions. The effects of steering system dynamics are taken into account by representing it as a first-order-lag. The effect of the variations of different parameters of the system on its dynamic behaviour are studied by classifying them into three vectors with the elements consisting of inertia, stiffness and damping and geometric-kinematic parameters. The effects of every element of these vectors on various state variables are studied. A

comparison is made among the state variables to reveal the relative influence of the parameter-induced variations. This helps one in better understanding of which state will be more affected due to changes in a particular parameter. And if it is so, how severe this variation is, both in transient and steady-state responses. Then the effects of a particular vector on the performance of the system is studied. This will provide one with a global view over the severity of the changes and helps in a qualitative study of the overall parameter changes on the motion of the vehicle.

First, a summary of some previous developments of the methodology is provided and its application in different areas are explained.
In addition, definitions of some basic terms commonly used in this methodology as well as a brief outline of the underlying theory are described.

6.2 Theoretical Background

The early developments in sensitivity analysis were started with the study of the effects of changes in coefficients of a differential equation on its solution. The early work on sensitivity analysis of control systems was started with Bode [117,122] who introduced this concept into modern control theories and defined a proper sensitivity definition in frequency domain for systems with the feedback control. Later on, a number of studies were devoted to sensitivity analysis in

time domain due to development of state-space method in modern control theory. References [114-116,121] exemplify some of the techniques used for design of optimal control systems.

It is a common practice in this theory to talk about the sensitivity functions [117,122-123]. Let's assume that dynamic model of a system is represented by

$$\dot{x} = f(x, t, u, \alpha_0), \quad x(0) = x_0 \tag{6.1}$$

where x is the state vector, f is a vector function, u is the input vector, α_0 is the nominal parameter vector and x_0 is the vector of initial conditions. This equation is called nominal state equation [117,122]. If the parameter vector is perturbed from its nominal value by $\Delta\alpha$, then we have:

$$\dot{x} = f(x, t, u, \alpha_0+\Delta\alpha), \quad x(0) = x_0 \tag{6.2}$$

with the same initial conditions. This equation is called the actual state equation. The change of the state vector due to $\Delta\alpha$ is:

$$\Delta x = x(t, \alpha_0+\Delta\alpha) - x(t, \alpha_0) \tag{6.3}$$

By first-order approximation the above equation can be written as [117,122]:

$$\Delta x(t,\alpha) = \sum_{j=1}^{r} \frac{\partial x}{\partial \alpha_j}\Big|_{\alpha_0} \Delta \alpha_j \tag{6.4}$$

In this case, the trajectory sensitivity vector is defined as:

$$\lambda_j(t,\alpha_0) = \frac{\partial x(t,\alpha)}{\partial \alpha_j}\Big|_{\alpha_0}, \quad j=1,2,\ldots,r \tag{6.5}$$

where $\alpha = [\alpha_1\ \alpha_2\ \alpha_3 \ldots \alpha_r]^T$ is the parameter vector. it should be noted that λ_j has the same dimension as the state vector and the components:

$$\lambda_{ij}(t,\alpha) = \frac{\partial x_i(t,\alpha)}{\partial \alpha_j}\Big|_{\alpha_0} \tag{6.6}$$

are called the trajectory sensitivity functions and accordingly the trajectory sensitivity matrix will be defined as [117,119]:

$$\begin{vmatrix} \frac{\partial x_1}{\partial \alpha_1} & \frac{\partial x_1}{\partial \alpha_2} & \cdots & \frac{\partial x_1}{\partial \alpha_r} \\ \cdots & \cdots & \cdots & \cdots \\ \frac{\partial x_n}{\partial \alpha_1} & \frac{\partial x_n}{\partial \alpha_2} & \cdots & \frac{\partial x_n}{\partial \alpha_r} \end{vmatrix} \tag{6.7}$$

Taking the partial derivatives of the actual state equation with respect to parameter α_j we get:

$$\frac{\partial \dot{x}}{\partial \alpha_j} = \frac{\partial f}{\partial x}\frac{\partial x}{\partial \alpha_j} + \frac{\partial f}{\partial \alpha_j} \tag{6.8}$$

or

$$\dot{\lambda}_j = \frac{\partial f}{\partial x}\Big|_{\alpha_0} \lambda_j + \frac{\partial f}{\partial \alpha_j}\Big|_{\alpha_0}, \quad \lambda(0)=0, \quad j=1,2,\ldots r \tag{6.9}$$

where

$$\lambda_j = \frac{\partial x}{\partial \alpha_j}\Big|_{\alpha_0} \tag{6.10}$$

and $(\partial f/\partial x)$ is the (nxn) Jacobi matrix.

In the case of a linear system represented by:

$$\dot{x} = Ax + Bu \tag{6.11}$$

the trajectory sensitivity equation can be obtained as[117,119]:

$$\dot{\lambda}_j = A_0\lambda_j + \frac{\partial A}{\partial \alpha_j}\Big|_{\alpha_0} x_0 + \frac{\partial B}{\partial \alpha_j}\Big|_{\alpha_0} u(t), \quad \lambda_j(t_0)=0 \tag{6.12}$$

where $A_0 = A(\alpha_0)$, $x_0 = x(t,\alpha_0)$. In this case, the trajectory sensitivity matrix can be obtained from:

$$\dot{\lambda} = A_0\lambda + \frac{\partial A}{\partial \alpha}\Big|_{\alpha_0} x_0 + \frac{\partial B}{\partial \alpha}\Big|_{\alpha_0} u(t), \quad \lambda(t_0)=0 \tag{6.13}$$

In addition, if a mathematical parameter such as α_i is a function of some other physical properties like a_i represented by:

$$\alpha_j = \alpha_j(a_1, a_2, \ldots, a_i) \tag{6.14}$$

Then, by applying chain rule, trajectory sensitivity functions can be obtained from:

$$\frac{\partial \lambda_{ij}}{\partial a_i} = \frac{\partial \lambda_{ij}}{\partial \alpha_1}\frac{\partial \alpha_1}{\partial a_i} + \frac{\partial \lambda_{ij}}{\partial \alpha_2}\frac{\partial \alpha_2}{\partial a_i} + \ldots + \frac{\partial \lambda_{ij}}{\partial \alpha_3}\frac{\partial \alpha_3}{\partial a_i} \tag{6.15}$$

It is often desired to compare the global sensitivity characterization of the systems. As an appropriate basis, L2-Norms of the sensitivity vectors offer a natural choice [117], since by definition it is the integral of a quadratic form that takes into account the contributions of all parameter-induced variations. In general, the integral of the quadratic form:

$$I_M = \int_{t_0}^{t_1} e(t)^T Z\, e(t) dt \tag{6.16}$$

where Z is a symmetric positive definite weighting matrix and t0 >0 and t1 >t0, are two positive instants, is called the L2_Norm. To characterize the sensitivity of a system by the L2-Norm, e(t) in equation (6.16) can be replaced by Δx [117].

Trajectory sensitivity functions can be classified in time domain, Laplace domain or performance index sensitivity depending upon the mathematical model

of the system [117,122]. For instance, the last one is suited for the analysis of the optimal control problems. In addition, the parameter variations may be classified as:

α_type variation, that has not any effect on the order of the system (this is the case of the current study)

β_type variation, which is due to the initial conditions.

λ_type variation, that affects the order of the system (order of the mathematical model).

The emphasize in this study is on α_type parameter variations whose definitions and basic theory were explained above. For β_type and λ_type parameter vectors, the underlying theory is the same and for further details, the interested reader is referred to [117,122-123].

6.3 State Space Representation of the System

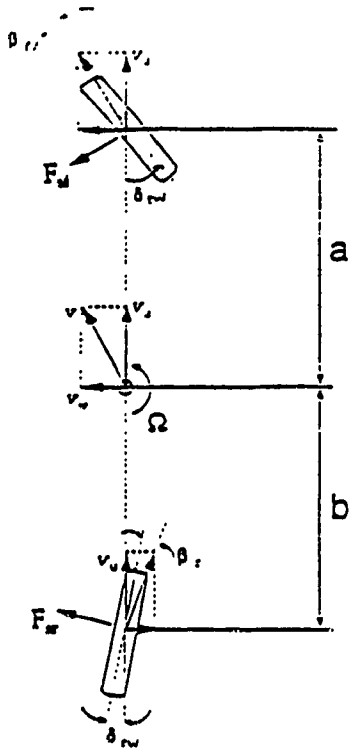

Fig. 6.1 Schematic Diagram of a Bicycle Model of the Vehicle

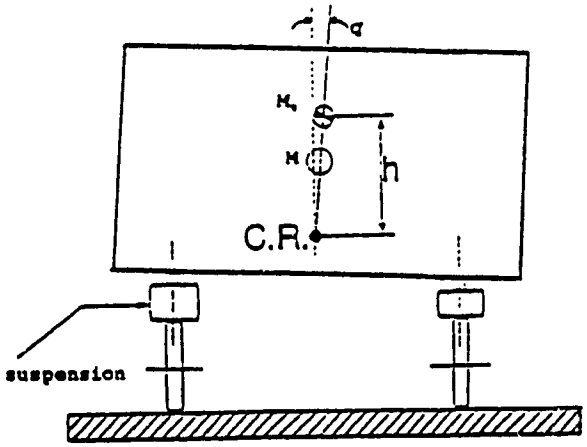

Fig. 6.2 Roll Motion of the Vehicle

The 3-DOF linear model is employed in this study and for the sake of convenience, it is reviewed again. Referring to the schematic diagram of the vehicle as shown in Figs.(4.1-2) and the assumptions unchanged, summation of the forces and moments about the centre of mass of the vehicle gives:

$$M(\dot{V}_w + V_u\Omega) + M_s h\ddot{q} = F_f + F_r \tag{6.17}$$

$$I_z\dot{\Omega} = aF_f - bF_r \tag{6.18}$$

$$I_u\ddot{q} + M_s h(\dot{V}_w + V_u\Omega) = -D_p\dot{q} + (M_s gh - K_p)q \tag{6.19}$$

with the expressions of the side forces of the tires as:

$$F_f = C_f \beta_f \tag{6.20}$$

$$F_r = C_r \beta_r \tag{6.21}$$

where the expressions for β_f and β_r (slip angles) as:

$$\beta_f = \delta_{fw} - \frac{a\Omega + V_w}{V_u} \tag{6.22}$$

$$\beta_r = \delta_{rw} + \frac{b\Omega - V_w}{V_u} \tag{6.23}$$

The notations used in equations (6.17 to 6.23) are the same as mentioned in chapter 4.

In equation (6.17), the first term implies the lateral acceleration due to changes in the lateral velocity and direction of the forward velocity vector, while the second term represents the induced force due to the tangential acceleration of the sprung mass. In equation (6.19), the first term is due to rolling acceleration while the second term shows the moment due to the force induced by the lateral acceleration. In addition, the effect of the front and rear steering actuator dynamics are represented by a first order lag model in the following form:

$$\dot{\delta}_{fw} = -\frac{1}{\tau}(\delta_{fw} + \delta_f) \tag{6.24}$$

where τ is the lag constant.

Substituting from equations (6.20 to 6.23) into (6.17 to 6.19) and carrying out the necessary manipulations, the dynamic equations of the system can be written in state-space form as:

$$\dot{x} = Ax + Bu \tag{6.25}$$

where

$$x^T = [V_w \quad \Omega \quad p \quad q \quad \delta_{fw} \quad \delta_{rw}] \tag{6.26}$$

is the state vector and

$$u^T = [\ \delta_f \quad \delta_r\ ] \tag{6.27}$$

is the input vector. In derivations of the above equations, δ_f and δ_r are incorporated in the states. Matrix A can be written as:

$$\begin{bmatrix} \frac{-I_u(C_f+C_r)}{I_s V_u} & \frac{I_u(bC_r-aC_f)}{I_s V_u} - V_u & \frac{M_s h D_p}{I_s} & \frac{-M_s h(M_s gh-K_p)}{I_s} & \frac{I_u C_f}{I_s} & \frac{I_u C_r}{I_s} \\ \frac{(bC_f-aC_r)}{I_z V_u} & \frac{(-a^2C_f-b^2C_r)}{I_z V_u} & 0 & 0 & \frac{aC_f}{I_z} & \frac{-bC_r}{I_z} \\ \frac{M_s h(C_f+C_r)}{I_s V_u} & \frac{-M_s h(bC_r-aC_f)}{I_s V_u} & \frac{-MD_p}{I_s} & \frac{M(M_s gh-K_p)}{I_s} & \frac{-M_s hC_f}{I_s} & \frac{-M_s hC_f}{I_s} \\ 0 & 0 & 1 & 0 & 0 & 0 \\ 0 & 0 & 0 & 0 & -T_{sf} & 0 \\ 0 & 0 & 0 & 0 & 0 & -T_{sr} \end{bmatrix} \tag{6.28}$$

where

$$I_s = I_u M - M_s^2 h^2 \tag{6.29}$$

and

$$B^T = \begin{bmatrix} 0 & 0 & 0 & -T_{sf} & 0 & 0 \\ 0 & 0 & 0 & 0 & 0 & -T_{sr} \end{bmatrix} \tag{6.30}$$

where T_{sf} and T_{sr} are equal to $(1/\tau)$ with typical value for τ=0.1 second.

6.4 Parametric Study

The properties of the developed dynamic model depend upon the elements of A and B matrices which in turn are functions of different parameters of the system. In this thesis, it is desired to study the effects of changes of M, M_s , I_z , I_u , a, b, h, V_u , C_f , C_r , K_p and D_p on the response of the system mainly specified by the state variables V_w, Ω and p. The above parameters are classified as vector of mass and inertia parameters

$$\alpha_1^T = [M \quad M_s \quad I_z \quad I_u] \tag{6.31}$$

vector of stiffness and damping coefficients

$$\alpha_2^T = [C_f \quad C_r \quad K_p \quad D_p] \tag{6.32}$$

and geometric and kinematic parameter vector

$$\alpha_3^T = [a \quad b \quad h \quad V_u] \tag{6.33}$$

The net parameter-induced changes of the state trajectories are obtained from equations (6.4-6.5) as:

$$\Delta x(t,\alpha) = \lambda(t,\alpha_0)\ \Delta\alpha \tag{6.34}$$

In this equation, Δx shows the net change of the states under the influence of $\Delta\alpha$ changes in the nominal value of the parameters. In this study, $\Delta x(t,\alpha)$ are

obtained for twenty percent (20%) increase in the nominal values of parameters.

The expressions for $(\partial A/\partial \alpha_1)$ are obtained by taking the partial derivatives of matrix A with respect to the elements of the vectors α_1, α_2, α_3 as they are necessary for the solution of sensitivity equations. Furthermore, wherever necessary (such as I_z), chain rule is utilized to obtain the elements of $\partial A/\partial \alpha_{11}$, $\partial A/\partial \alpha_{12}$,..., $\partial A/\partial \alpha_{34}$ matrices whose details are provided in Appendix D.

6.5 Simulation Results

Simulations are carried out by applying the step inputs of (10°) degrees to the front and rear wheels. Results are shown for 2.0 seconds, since all transient parts of the responses of the original system die out after almost 1.3 second and the states reach to their steady-state values after this time. The nominal values of the parameters used in this study belong to CONCIC III vehicle, as given in Appendix B. The time histories of the state variables are shown in Figs.(6.3-6.18) and the detailed discussion of the results are provided in the following sections.

6.5.1 Effects of Inertia Parameters

Figs.(6.3-6.7) show the effects of changes of various inertia properties of the system on its dynamic response. It is seen that mass is very effective on the

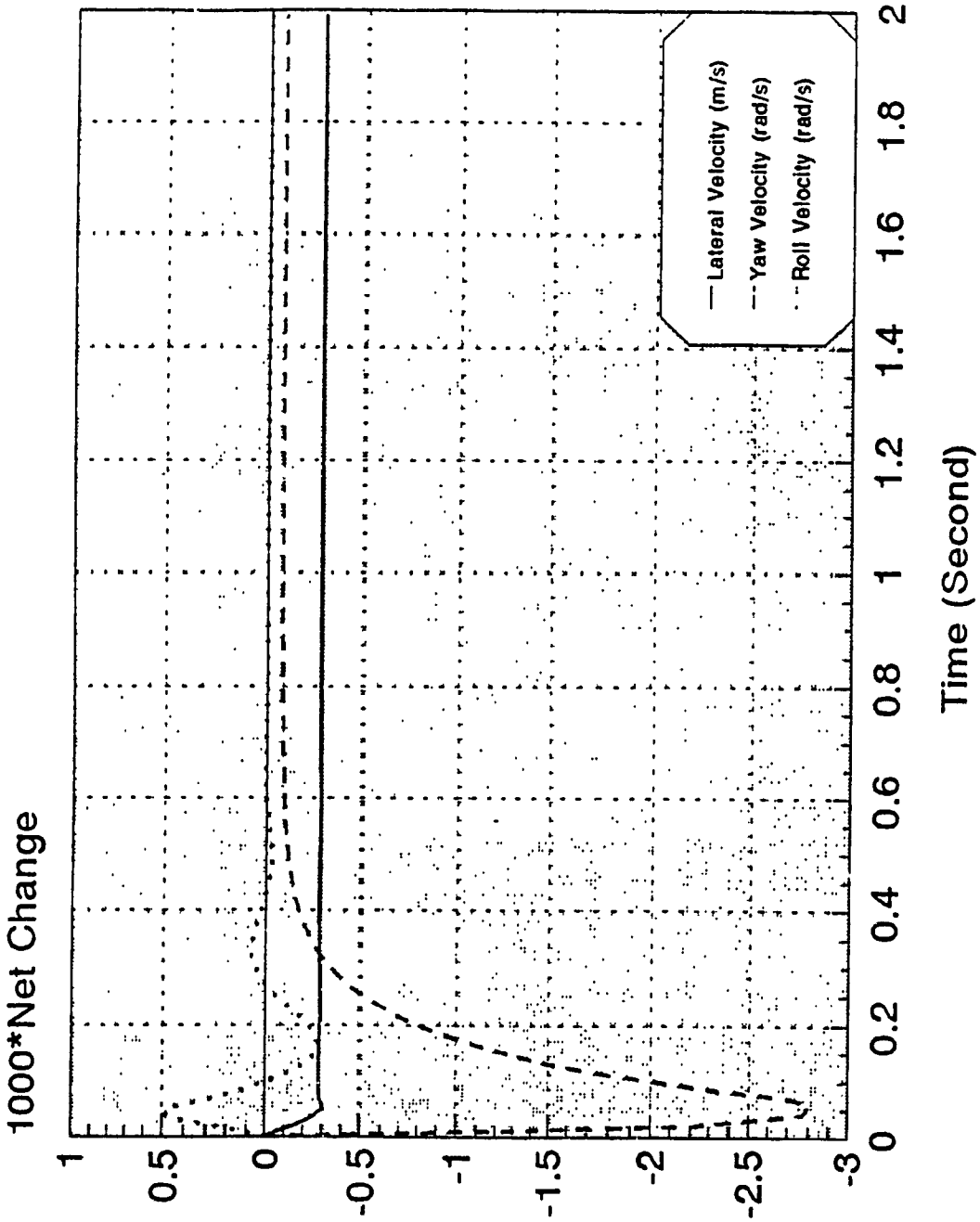

Fig. 6.3 Net Changes in the States (Δx) Due to Mass (M) Variation

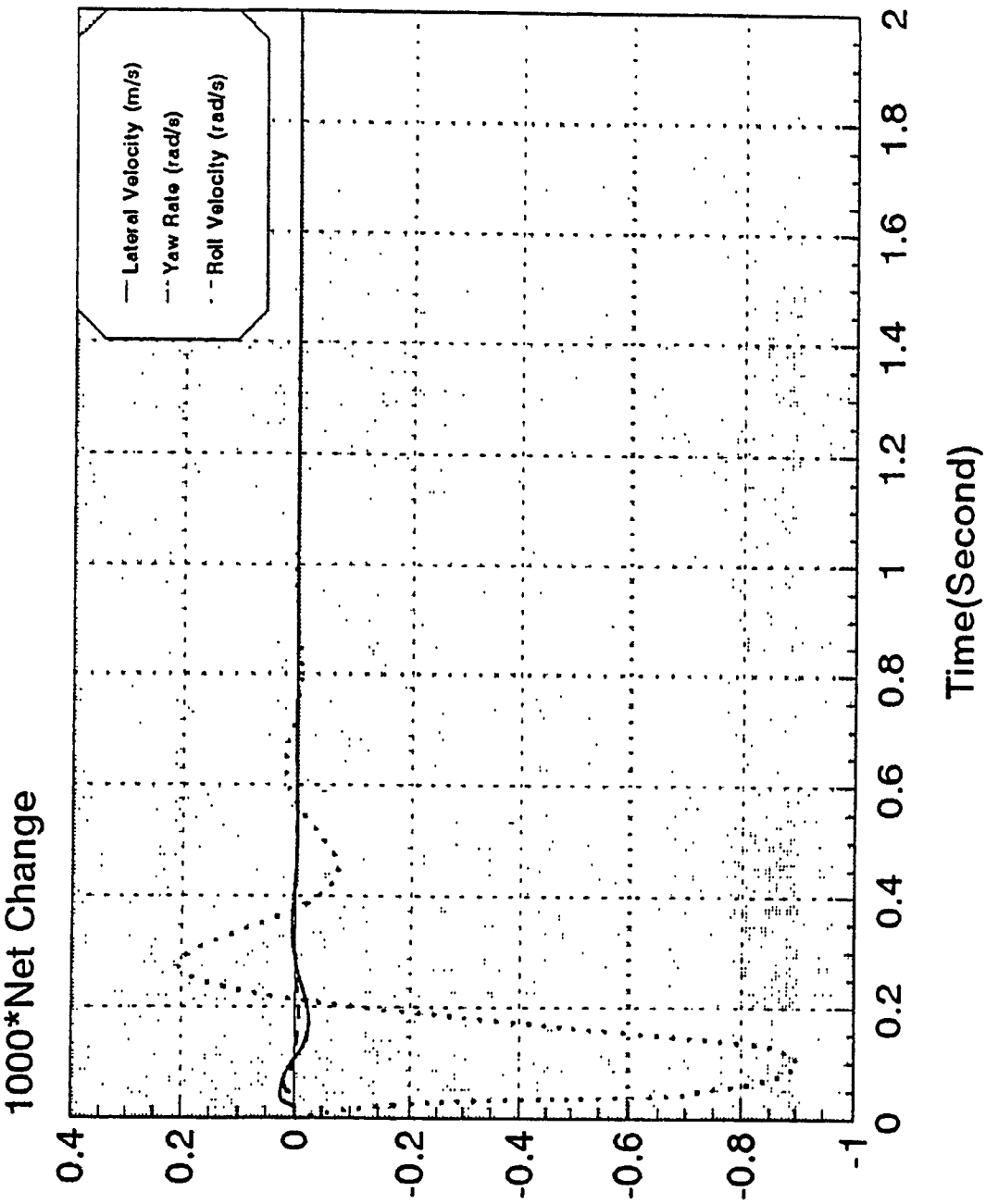

Fig. 6.4 Net Changes in the States (Δx) Due to Sprung Mass (M_s) Variation

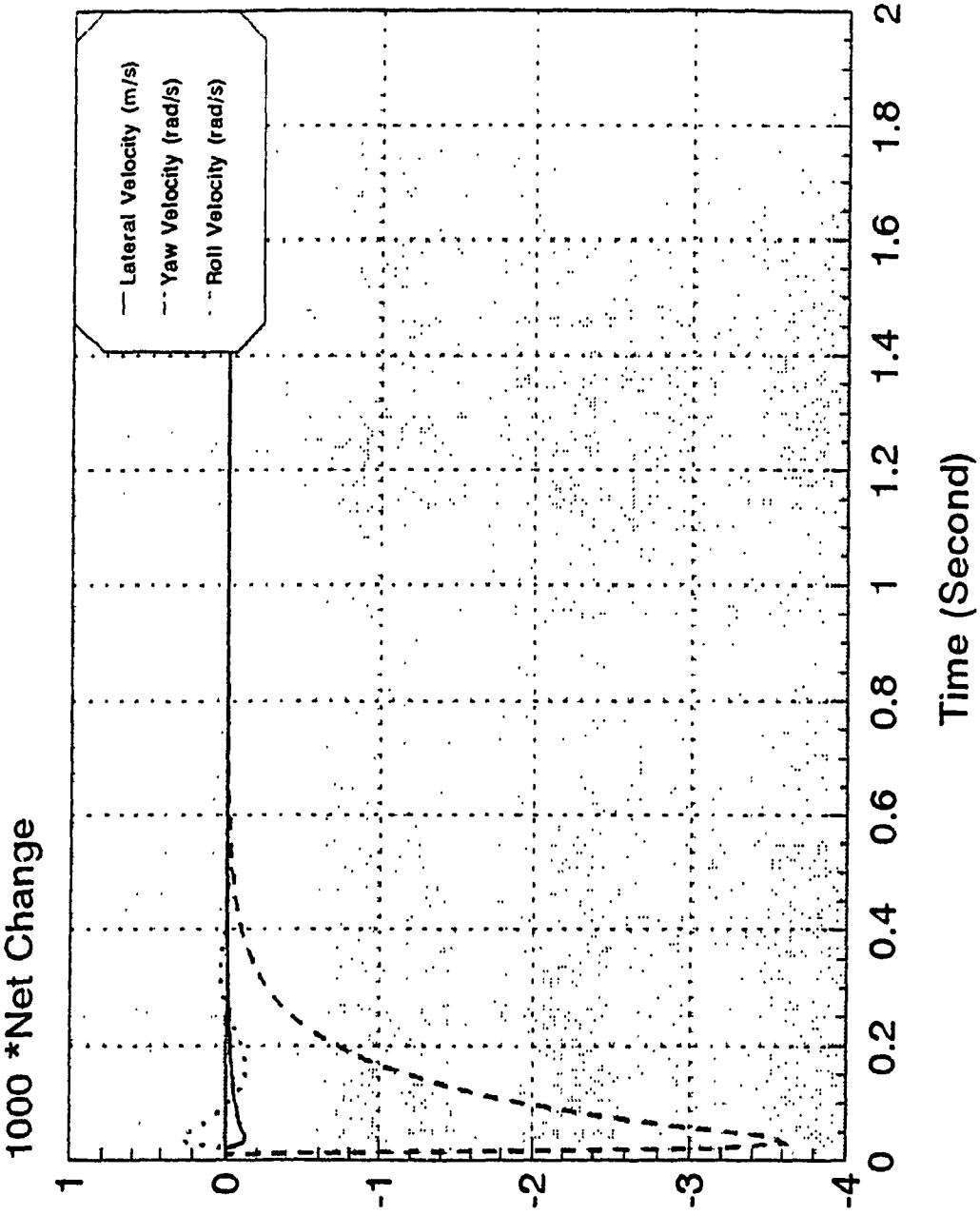

Fig. 6.5 Net Changes in the States (Δx) Due to Mass Moment of Inertia (I_z) Variation

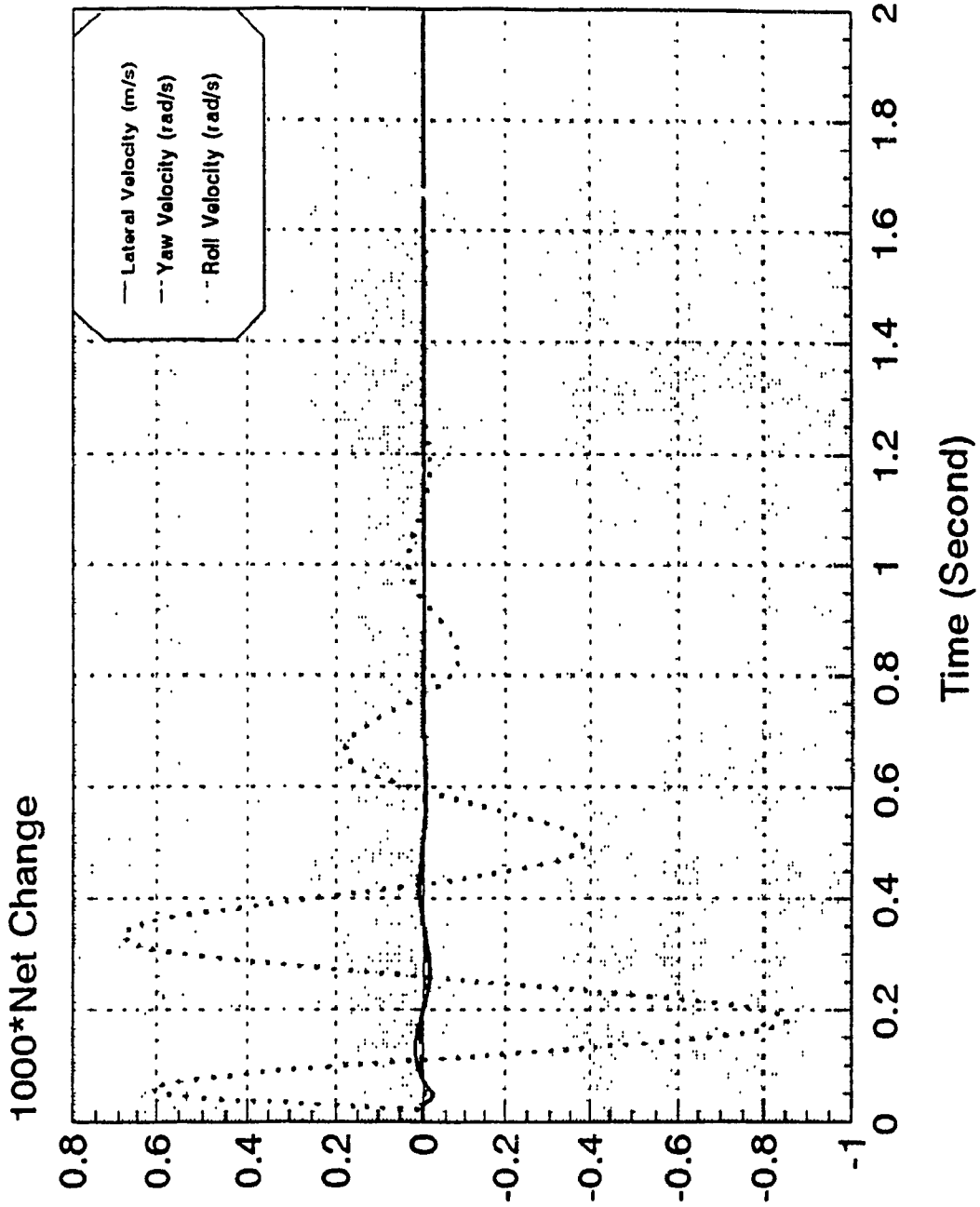

Fig. 6.6 Net Changes in the States (Δx) Due to Roll Moment of Inertia (I_x) Variation

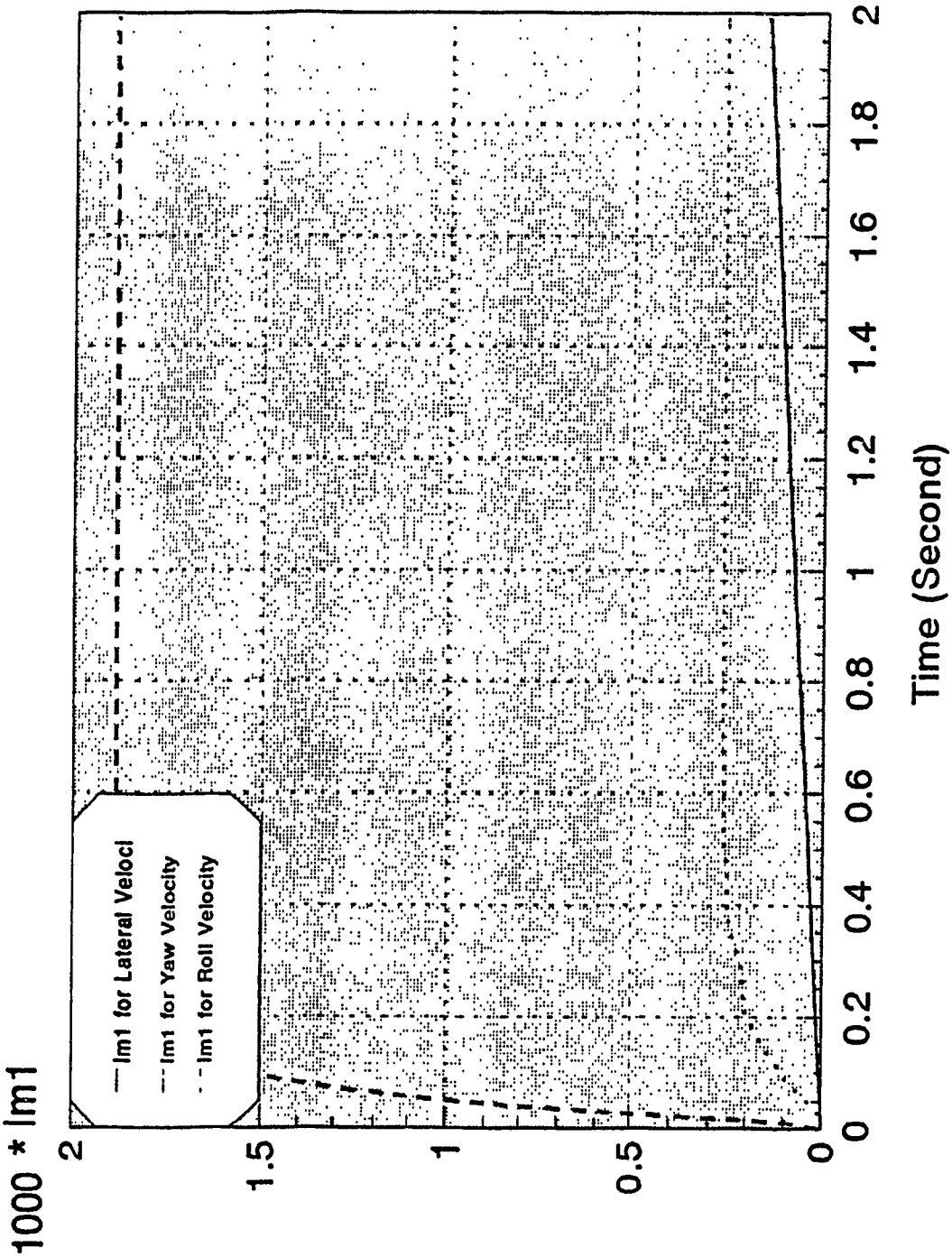

Fig. 6.7 Net Changes in the States (Δx) Due to Inertia Parameter Vector (α_1) Variation

lateral velocity and any increase in mass decreases the steady-state lateral velocity of the vehicle with little effect on transient response of roll motion (Fig. 6.3). The effect of sprung mass on the response of the system are shown in Fig. 6.4. As it is shown in this figure, sprung mass is very effective on transient response of roll motion with little effect on yaw and lateral velocities. The results of changes of motion of the vehicle due to variations of I_u and I_z are shown in Figs.(6.5-6.6). From Fig. 6.5, it is observed that I_u is very effective on transient part of roll motion with no effect on the steady-state values of state variables. Also, from Fig. 6.6 it is seen that yaw moment of inertia is very effective on yaw rate with very little effect on the other states.

In order to provide one with a global characterization of the system sensitivity, the overall effects of the parameter vectors on the motion of the vehicle are obtained by using the definition of sensitivity measure namely equation (6.16). In particular, sensitivity measure of the vehicle (I_{m1}) with respect to inertia parameter vector (α_1) is shown in Fig. 6.7. As it is shown in this figure, inertia parameters are very effective on transient response of yaw motion with less effect on roll and lateral velocities.

6.5.2 Effect of Stiffness and Damping Parameters

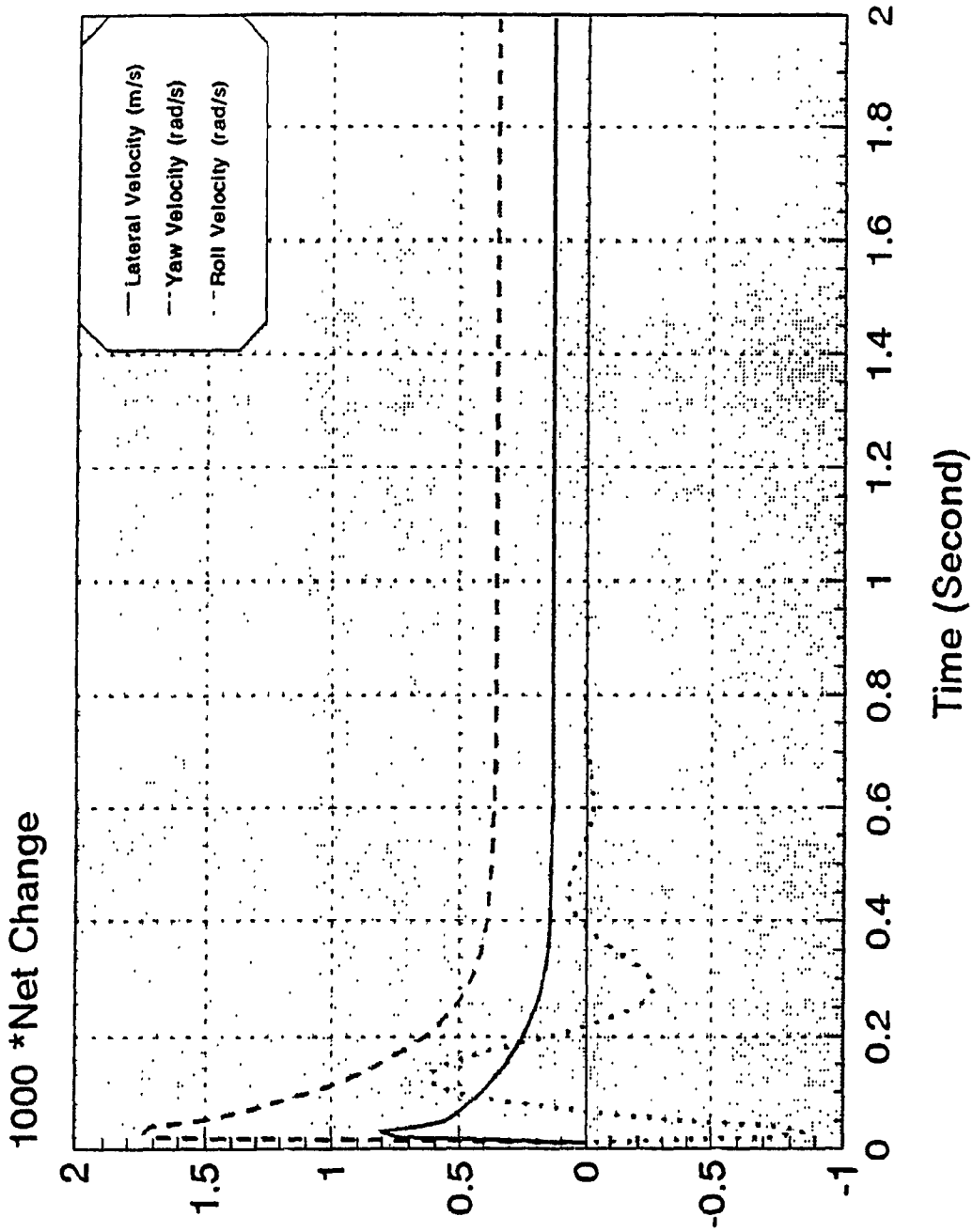

Fig. 6.8 Net Changes in the States (Δx) Due to Cornering Stiffness of the Front Wheel (C_f) Variation

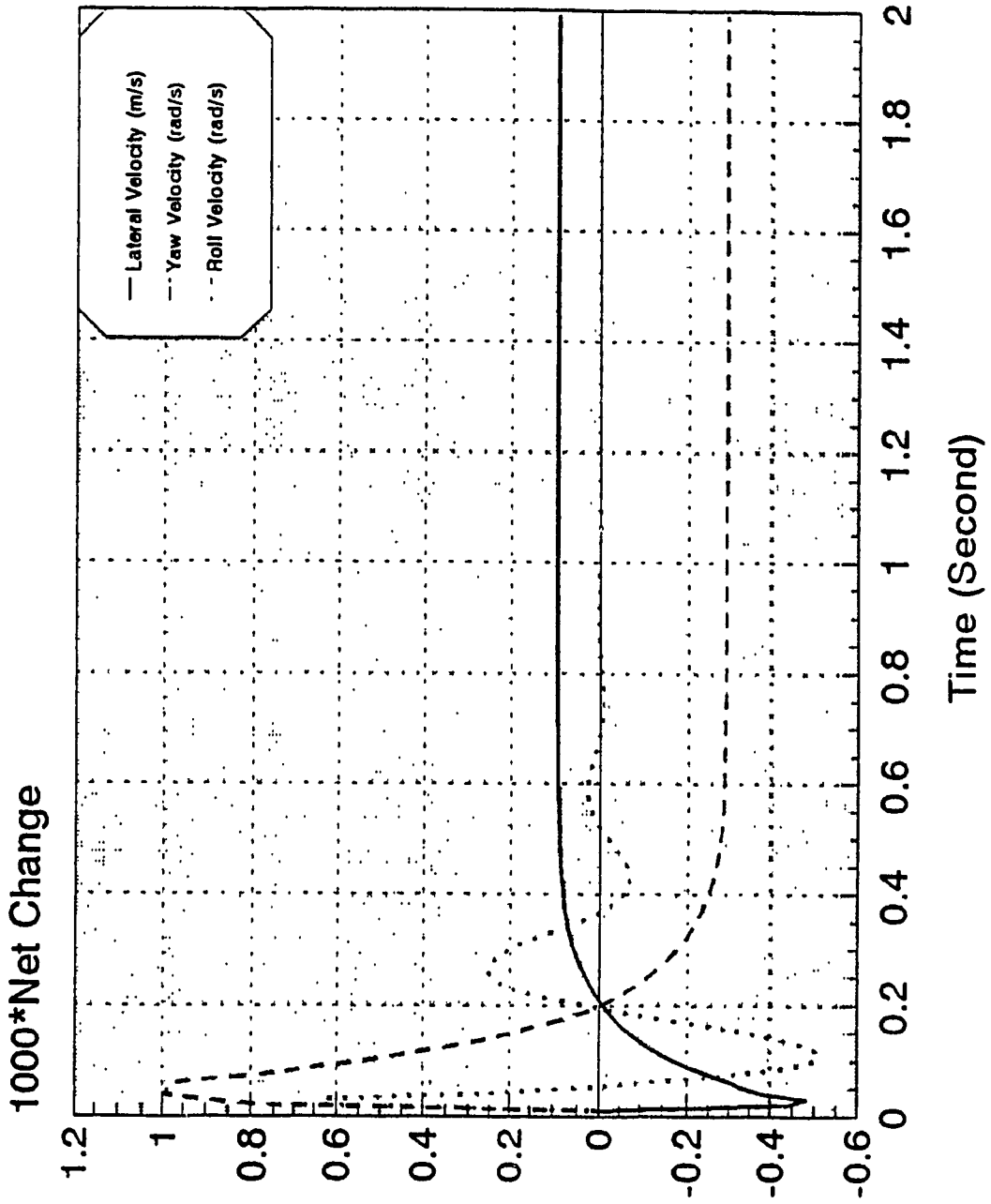

Fig. 6.9 Net Changes in the States (Δx) Due to Cornering Stiffness of the Rear Wheel (C_r) Variation

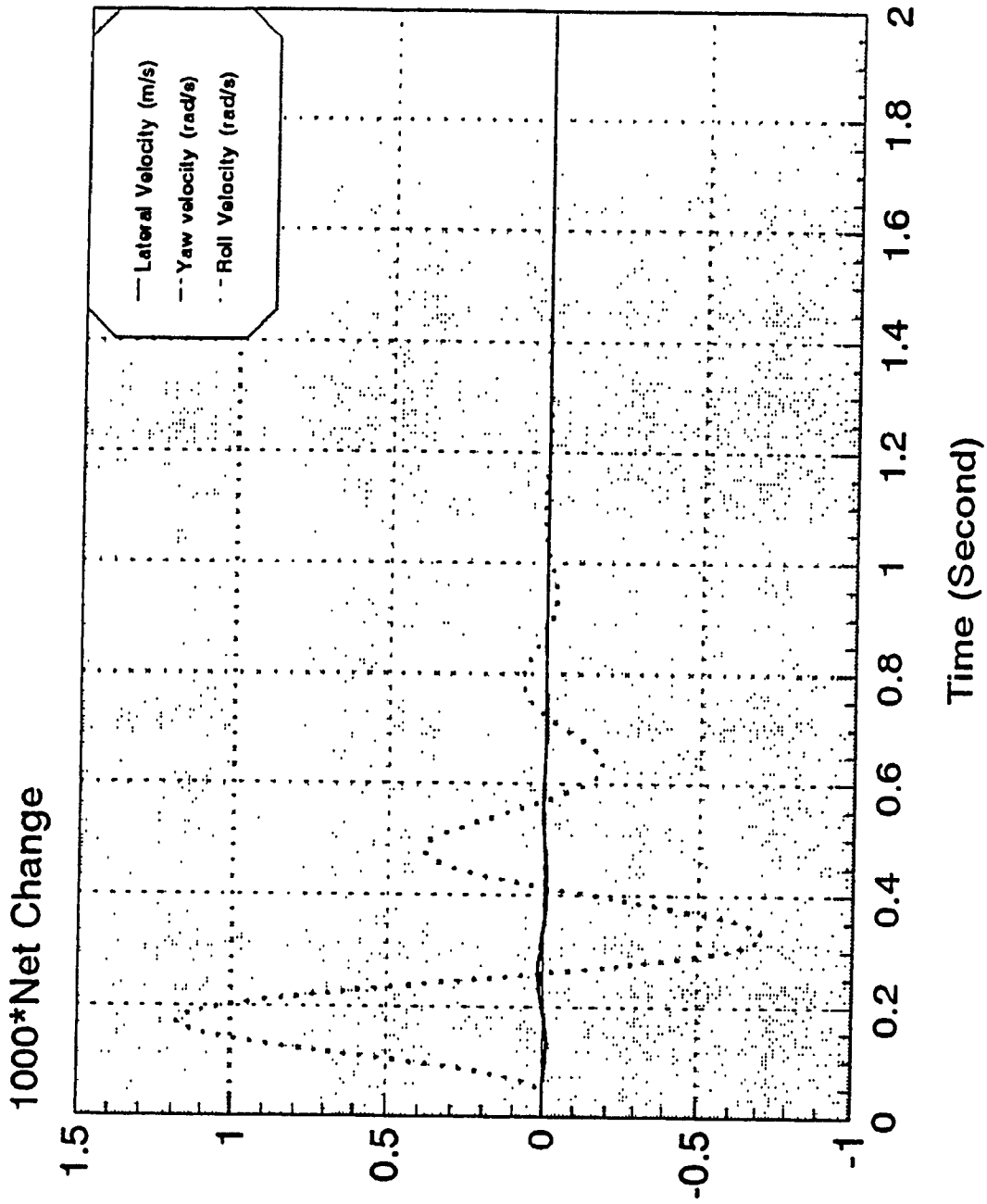

Fig. 6.10 Net Changes in the States (Δx) Due to Roll Stiffness (K_p) Variation

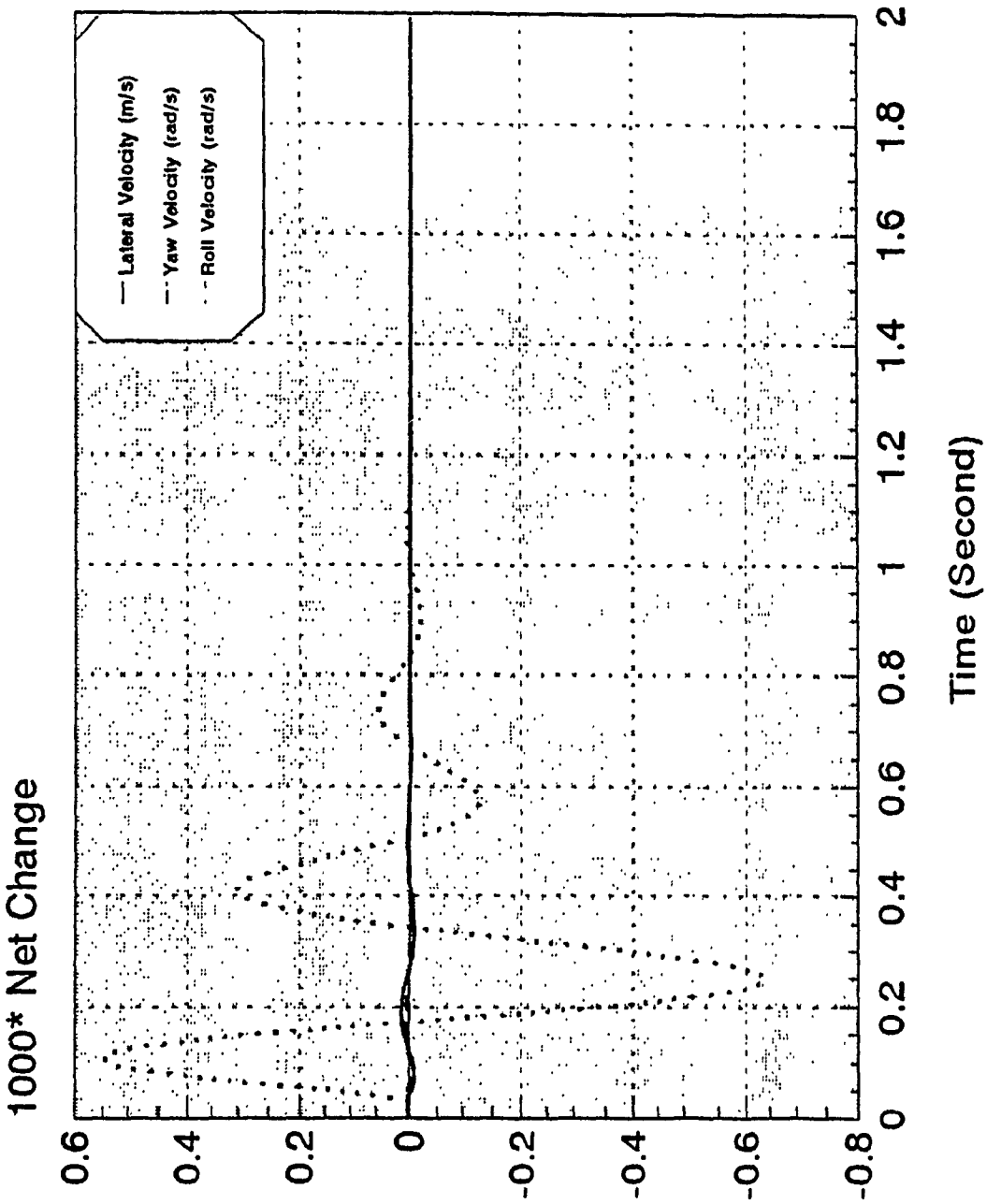

Fig. 6.11 Net Changes in the States (Δx) Due to Roll Damping (D_p) Variation

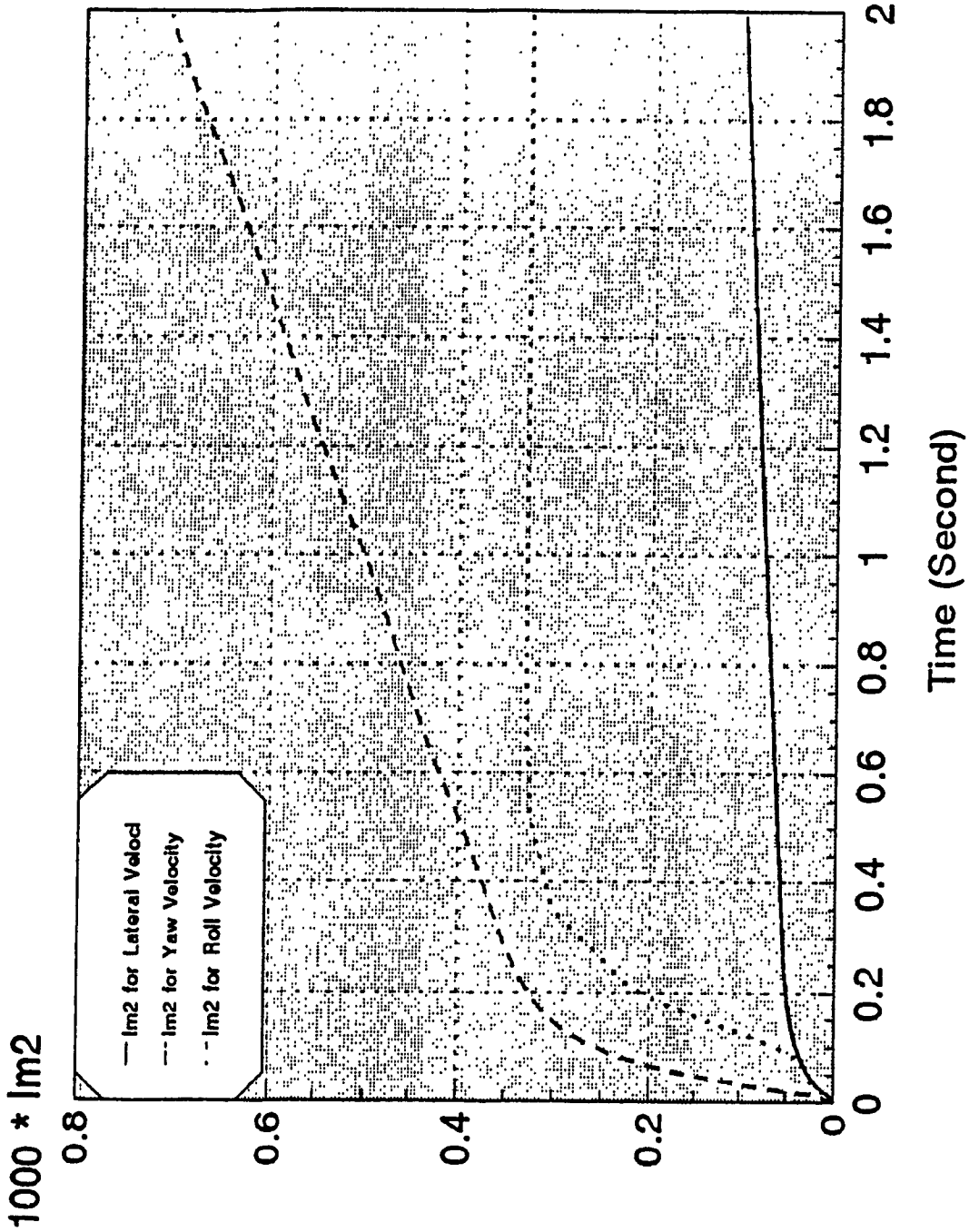

Fig. 6.12 Net Changes in the States (Δx) Due to Stiffness and Damping Parameter Vector (α_2) Variation

Figs.(6.8-6.12) show the variations of V_w, Ω and p as a result of changes in C_f, C_r, K_p, D_p. It is seen that the transient part of all state variables are sensitive to the changes in C_f and C_r with Ω being the highest. Comparison of Figs.6.8 and 6.9 reveals that cornering stiffness of the tires are effective on steady-state responses of lateral velocity and yaw rate of the vehicle with the adverse affect on the latter one. Figs.(6.10) and (6.11) show the effects of K_p and D_p. It is seen that transient part of rolling motion is very sensitive to the variations of these parameters while the lateral and yaw velocities are not affected.

The overall effects of stiffness parameter vector (α_2) on the behaviour of the system (I_{m2}) are illustrated in Fig. 6.12. As it is shown in this figure, stiffness and damping parameters very effective on the steady-state value of Ω with less effect on lateral velocity and no influence on steady-state value of roll motion.

6.5.3 Effects of Geometric and Kinematic Parameters

Geometric parameters are grouped together in vector α_3. As it is shown in Figs.6.13-6.14, a and b are very effective on the steady-state values of lateral and yaw motion with little effect on transient part of roll velocity. Therefore, any increase on a or b reduces the steady-state value of yaw rate whereas they have adverse effect on lateral velocity. Comparison of time histories of the states with

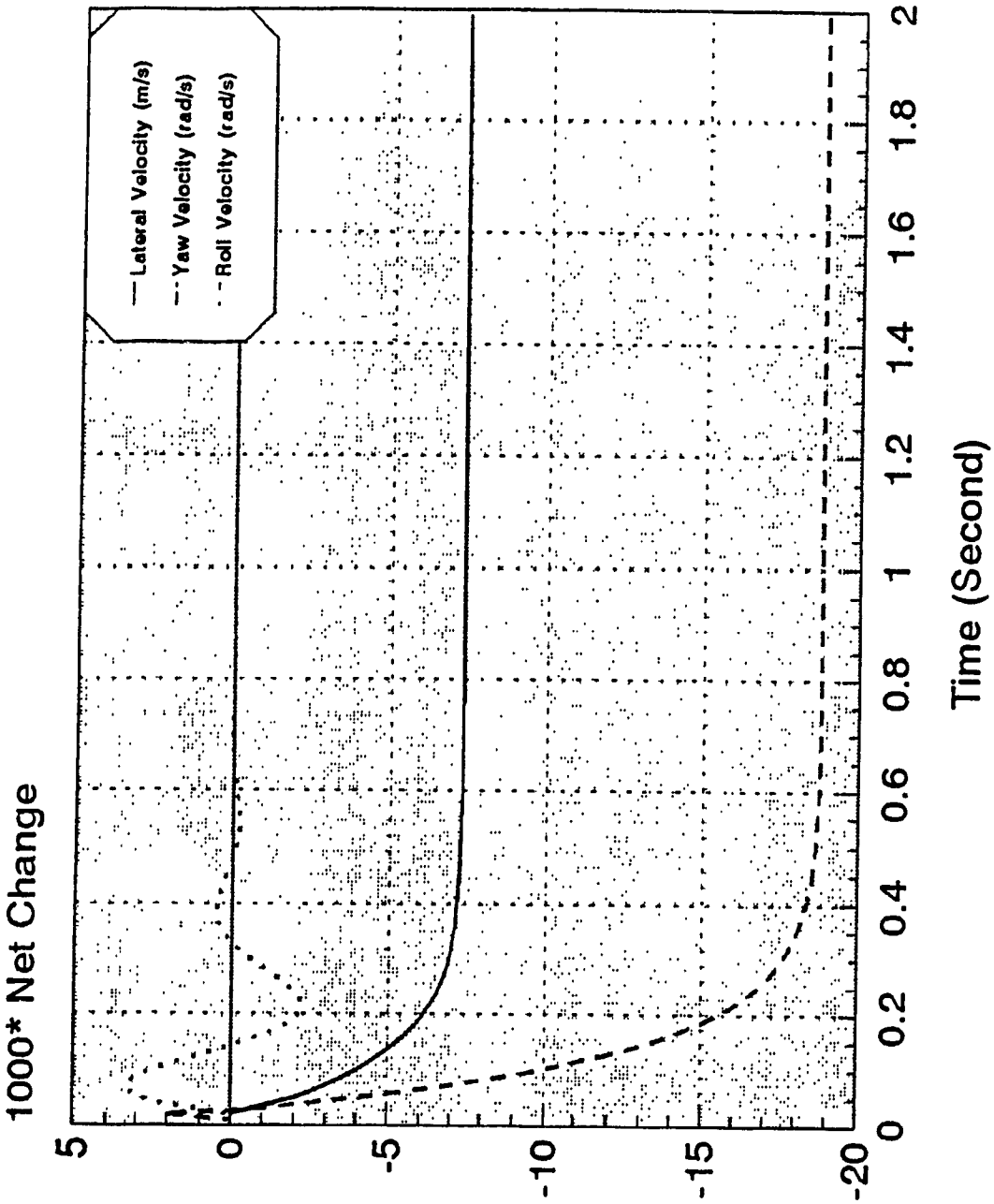

Fig. 6.13 Net Changes in the States (Δx) Due to Variation of a

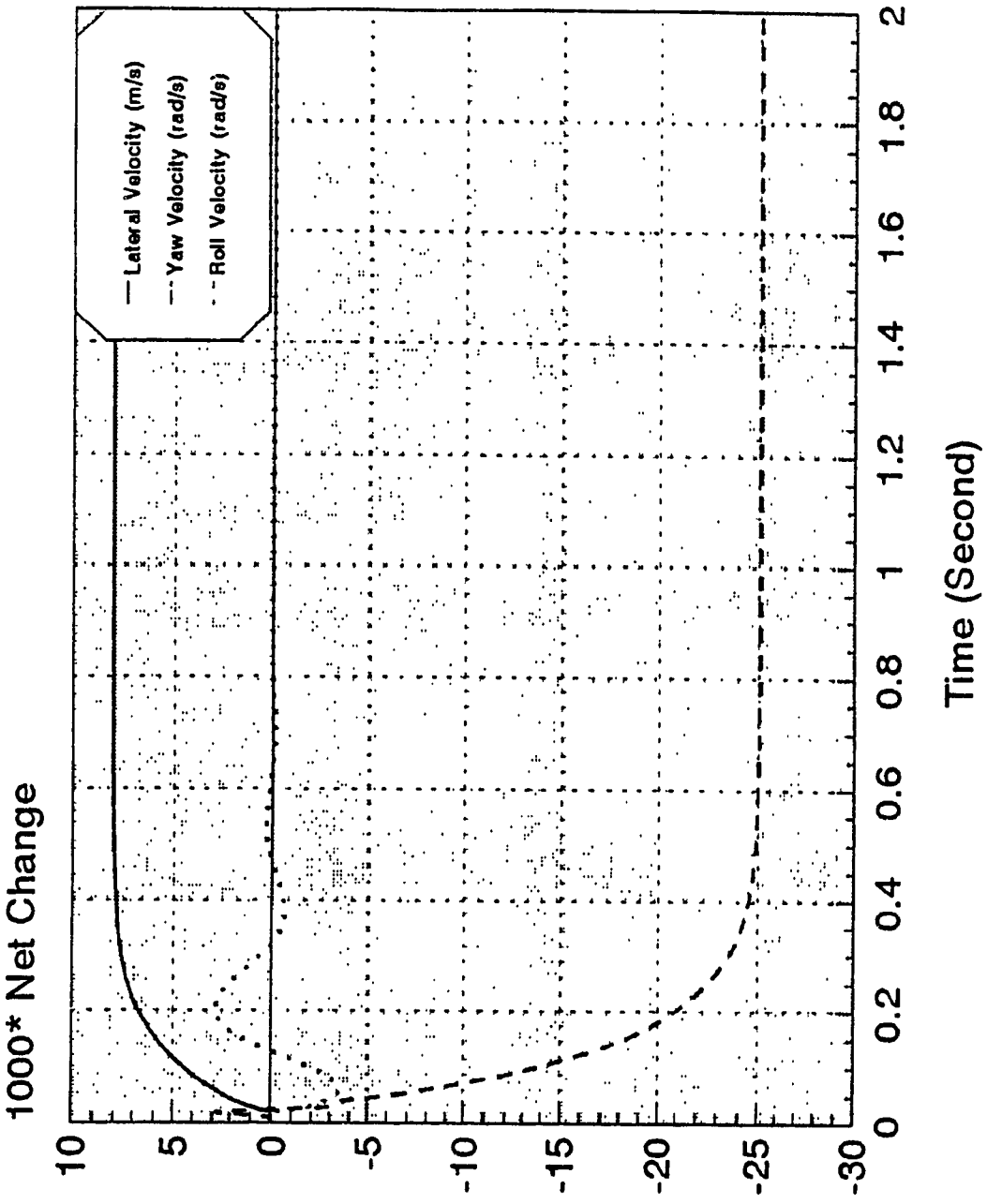

Fig. 6.14 Net Changes in the States (Δx) Due to Variation of b

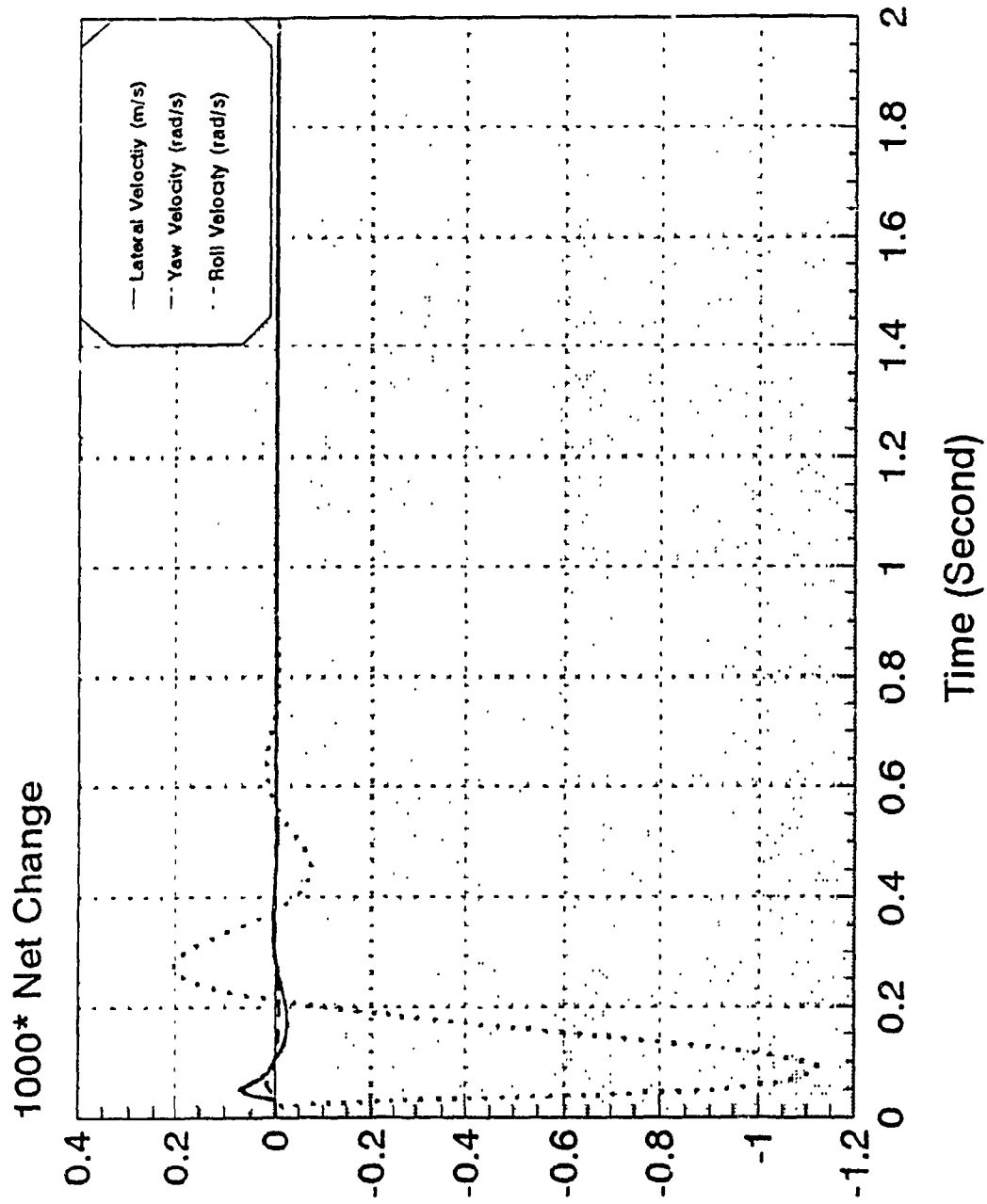

Fig. 6.15 Net Changes in the States (Δx) Due to Variation of h

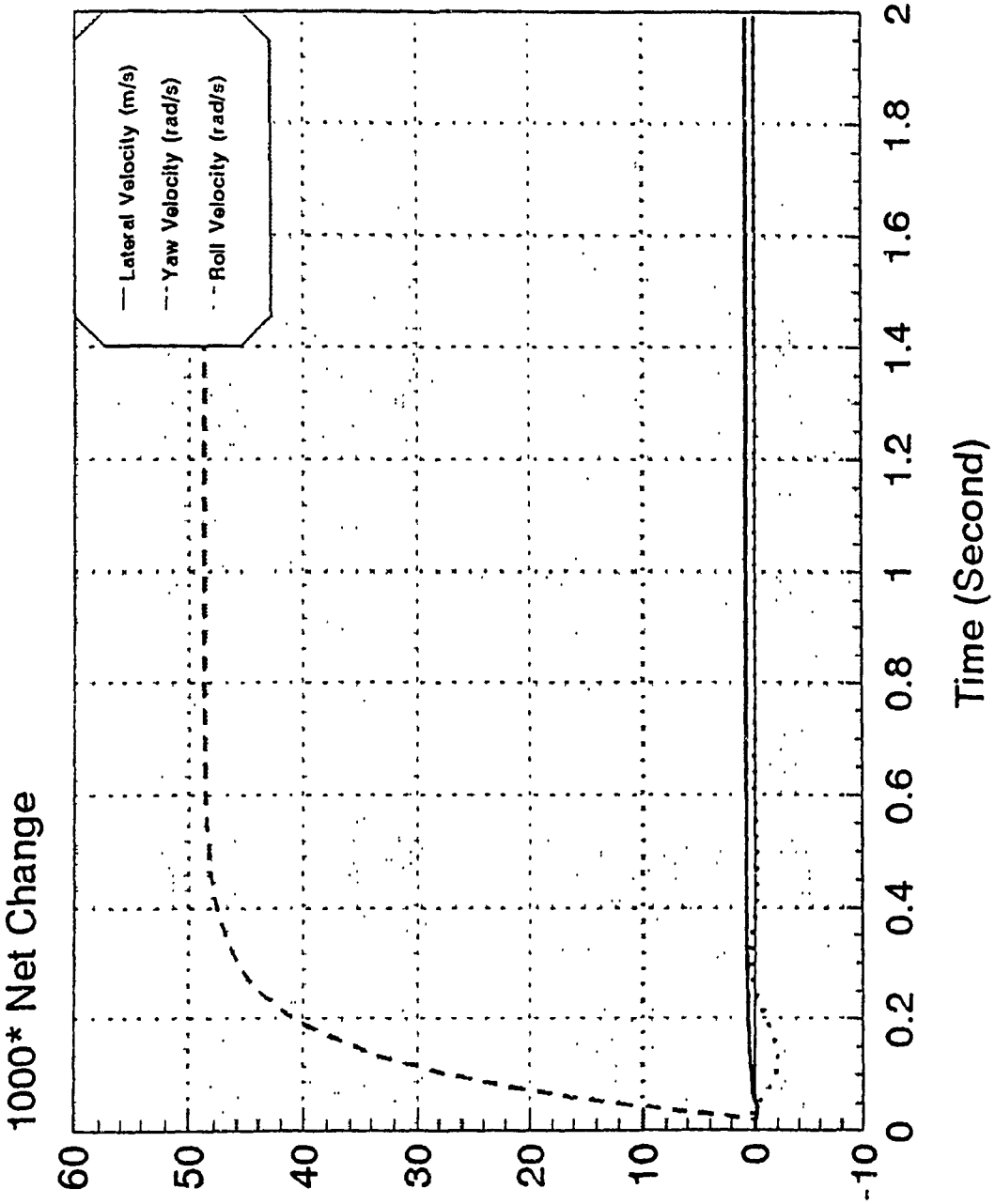

Fig. 6.16 Net Changes in the States (Δx) Due to Variation of Forward Speed (V_U) of the Vehicle

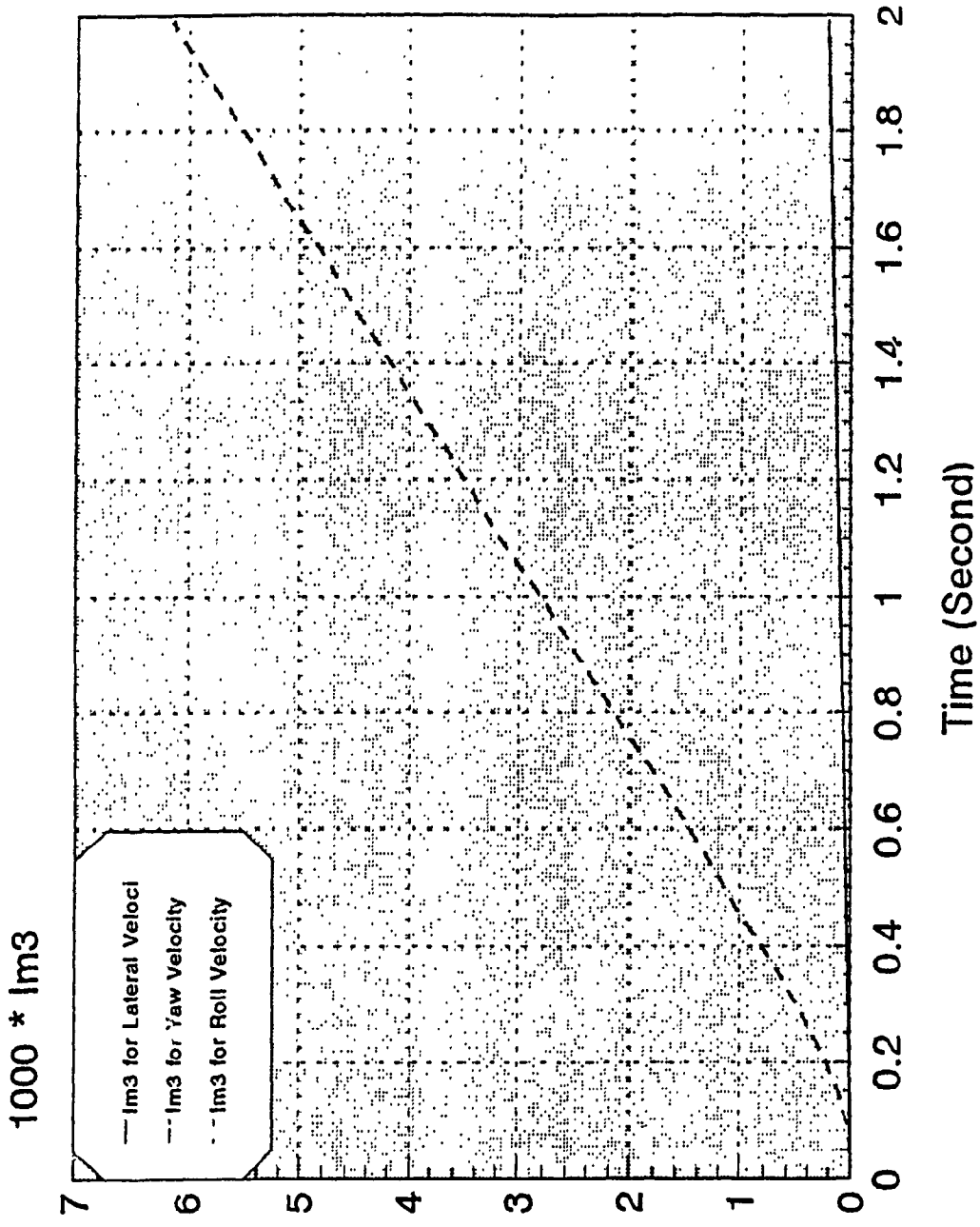

Fig. 6.17 Net Changes in the States (Δx) Due to Geometric-Kinematic Parameter Vector (α_3) Variation

those observed for the cases of C_f and C_r suggests that the vehicle motion is more sensitive to the changes in a and b. Fig. 6.15 shows the effect of changes of h on the response. It is seen that h is very effective on the transient part of roll motion without almost any influence on V_w and Ω. The effect of forward velocity of the vehicle on its motion are illustrated in Fig. 6.16. It is seen that the steady-state values of yaw and lateral motion of the vehicle are influenced by the variations of this parameter while the roll motion has been affected very little. Among them, yaw rate is the most affected state and any increase in forward speed considerably increases yaw rate of the vehicle.

The overall effects of geometric parameters on the response of the system is shown in Fig. 6.17. It is seen that generally speaking, these parameters are the most effective, both in transient and steady-state response, among all the others like stiffness or inertia with yaw rate being the most sensitive to the variations (the vertical scale are different from inertia and stiffness-damping vector).

6.6 Summary

In this chapter, a parametric study of automated vehicles was carried out by using sensitivity theory as a tool. The linear three degrees of freedom (3-DOF) dynamic model was employed for the purpose of this study.

A general observation was that the vehicle parameters directly related to roll motion like sprung mass (M_s), roll moment of inertia (I_u), roll damping (D_p), etc. do not have a significant contribution on the yaw and lateral motion. This result was obtained by comparing the parameter-induced variations of the state variables. The above observations support the properties of "roll number" introduced in the previous chapter.

Among the parameters studied, it was observed that the geometric-kinematic parameters were the most influential on the motion of the vehicle. Therefore, in the primary stages of the design this factor should be considered. As well, it appeared that the forward speed was the most significant parameter affecting the motion of the vehicle with yaw rate being the most sensitive mode. This result is compatible with those obtained from the analysis of motion in the previous chapter.

Sensitivity measures were utilized to obtain a global sensitivity characterization of the system. Among the parameter vectors, geometric-kinematic parameters were the most influential on the performance of the vehicle with yaw rate being the most sensitive in all cases. Furthermore, it appeared that the inertia parameters were mostly influential on transient parts of the responses as it was observed from Fig. 6.7.

CHAPTER 7

SYNTHESIS OF STEERING CONTROLLERS FOR AUTOMATED VEHICLES

7.1 Introduction

Satisfactory performance of automated vehicles requires an efficient control scheme to generate the control signals such that by a proper steering action, the errors in position and orientation when a desired path is to be followed converge to zero. For such systems it is necessary at each instant to control the angle of the steering wheel so that any deviation from the path is corrected in a stable manner, in a reasonable time and without oscillations about the path (hunting). The control strategy must define the steering angle (the angle of the steering wheel with the vehicle longitudinal axis) as a function of the two measurable errors

hereafter referred to by the positional error (the distance from the vehicle mass centre to the line tangent to the path at the point nearest to the mass centre) and orientation error (the angle between the vehicle longitudinal axis and the line tangent to the path).

Although there are various wheelbase configurations that can be employed for these systems however, the most popular ones are tricycle models, differential drive and double steering vehicles. This chapter is devoted to developments of a number of control strategies for the above wheelbase configurations.

For tricycle model vehicles with steering wheel in the front, a nonlinear control strategy is developed. Simulations demonstrate improvement in path tracking behaviour of the vehicle.

By using optimal control theory, the structure of a controller is obtained by using a linearized dynamic model of the vehicles with front wheel steering systems. It is shown that the system can be decoupled into two fast and slow subsystems and the controller design is based on the slow subsystem. In design of the controller, a quadratic measure of performance consisting of the integral of the errors (errors in position and orientation of the vehicle) and the input (front wheel steering angle) are minimized.

For the vehicles with differential drive configuration, a controller is designed that employs a linear feedback of the position and orientation errors as command to control the velocities of the side wheels. The performance of the controlled system is shown by the simulation.

Throughout this chapter, in order to simplify the controller design for the above mentioned vehicles (front wheel steered vehicles), the effects of the steering dynamics are neglected. It is assumed that instantaneous wheel steering angle (δ_{fw}) follow the command (δ_f) at any instant. However, these effects (steering dynamics) can be taken care of by using the proceedure provided at the end of this chapter (section 7.5).

7.2 Synthesis of a Nonlinear Controller

The results of previous studies [27] show that in cases where the steering wheel is in the front, a control law based on a proportional feedback of the position error only is not sufficient and can lead in hunting rather than following the path. Inclusion of the orientation error feedback results in improving the tracking behaviour. However, as the results of this study show, it is possible to further improve the performance of the controlled system by making advantage of incorporation of other variables such as the angular velocity of the vehicle.

7.2.1 Dynamic Relations

Figure 7.1 shows the various dimensions and angles between the body axis (UCW) and the world coordinate system (XOY). V_u and V_w are the longitudinal and lateral components of the velocity V of the vehicle mass centre in (UCW) frame, and V_x and V_y represent the components of V in the X- and Y- direction, respectively. Similarly, a_u, a_w, a_x and a_y are used for components of the

·.cceleration in the two coordinate systems. ψ is the orientation of the vehicle at each instant of time and Ω is the angular velocity in both (UCW) and (XOY). The positional offset and the orientational error are denoted by ε_d and ε_θ, respectively (Fig. 7.1).

The relationship for transformation of components of any vector like V, the velocity, in the two coordinate frames is in the form of

$$V_x = V_U \sin \psi - V_W \cos \psi \tag{7.1}$$

$$V_y = V_U \cos \psi + V_W \sin \psi \tag{7.2}$$

The schematic diagram of a three wheeled vehicle considered in this study is depicted in Fig. 7.2. The resultant of the forces exerted from tires to the vehicle have components in the longitudinal (U) and lateral (W) directions.

Considering only the plane motion of the system and neglecting roll motion due to small roll number (0.15) (the parameters belong to CONCIC II vehicle [36,41] and are given in Appendix E), the equations of motion of the vehicle at any time can be written as:

$$F_{Tl} - F_{Rre} + F_{Tr} - F_{Rre} - F_{sf} \sin\delta_{fw} - F_{Fre} = M a_u \tag{7.3}$$

$$(F_{sr})_L + (F_{sr})_R + F_{sf} \cos\delta_{fw} - F_{Fre} \cos\delta_{fw} = M\, a_w \tag{7.4}$$

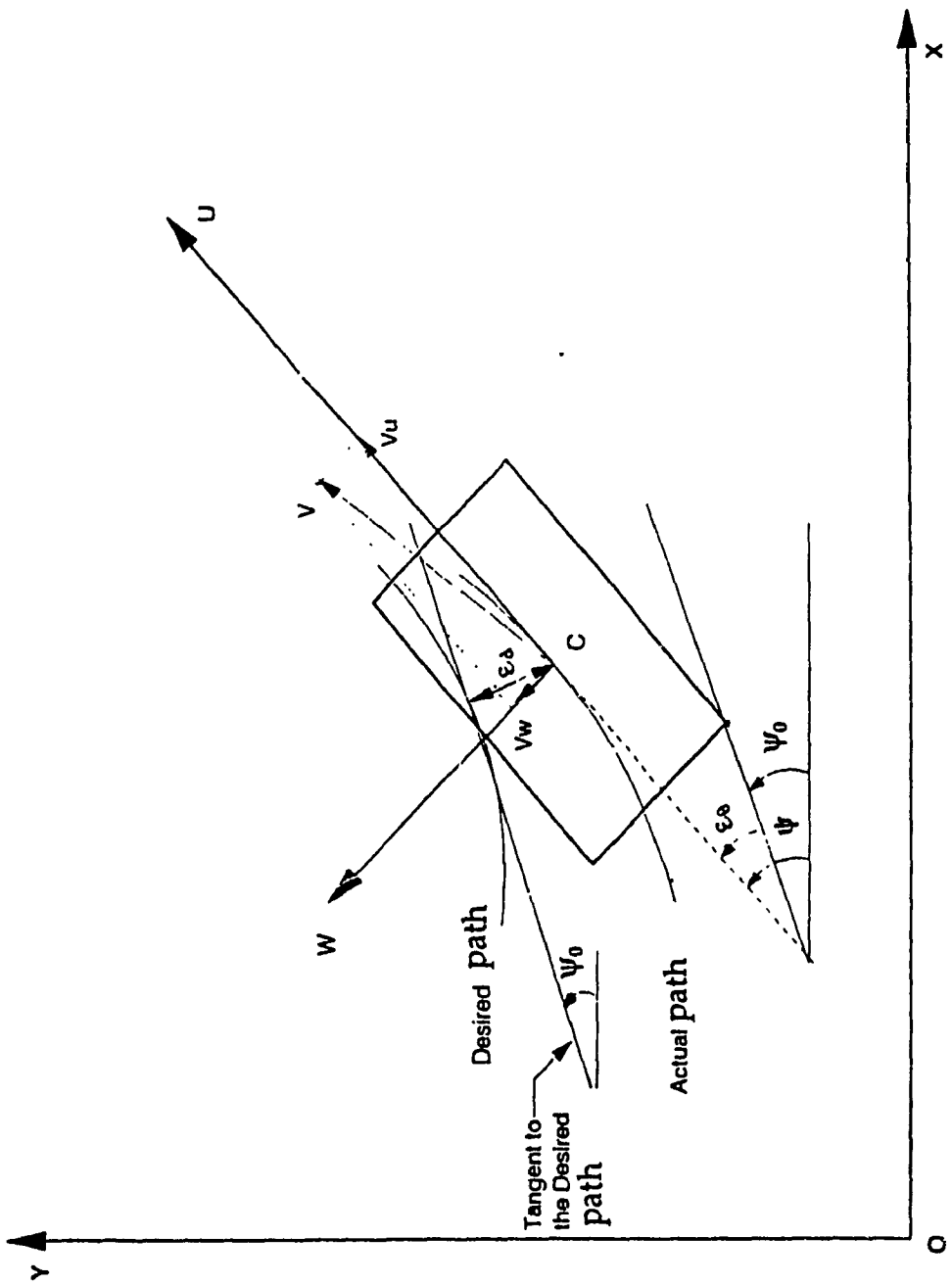
X
O
Y
U
V
W
Vu
Vw
C
ϵ_δ
ϵ_θ
ψ_0
ψ
ψ_0
Desired path
Actual path
Tangent to the Desired path

Fig. 7.1

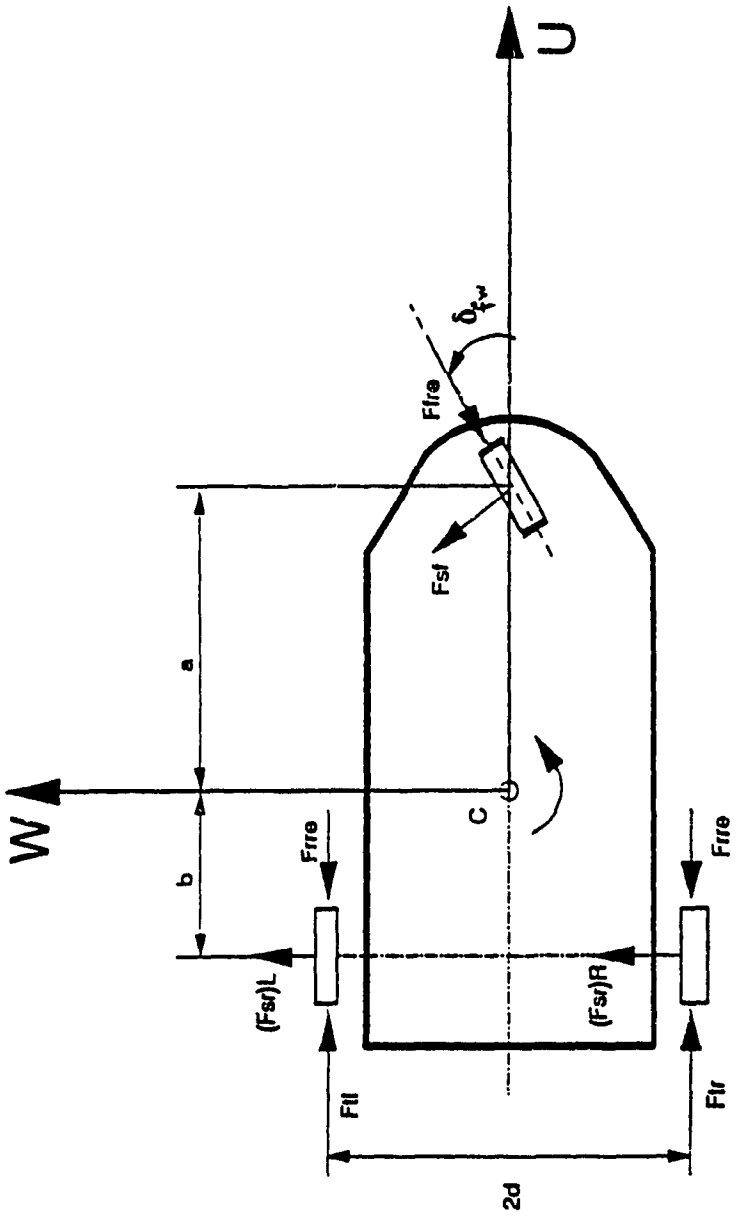

Fig. 7.2 Schematic Diagram of the Vehicle

$$a\,F_{sf}\cos\delta_{fw} - b\,[(F_{sr})_L + (F_{sr})_R] - a\,F_{Fre}\sin\delta_{fw} - I_z\dot{\Omega} \qquad (7.5)$$

Where a and b are the distances between the centre of mass and the front and rear wheels respectively (see Fig.7.2), δ_{fw} is the instantaneous steering angle, i.e., the angle between the steering wheel and the vehicle longitudinal axis (CU) as shown in Fig. 7.2, I_z is the moment of inertia about a vertical axis passing through the centre of mass, Ω is the yaw rate of the vehicle, F_{Tl} and F_{Tr} are tractive forces in the left and right rear wheels, F_{Fre} and F_{Rre} are the rolling resistance of the front and rear wheels acting against the vehicle motion, and F_{sf}, $(F_{sr})_L$ and $(F_{sr})_R$ are the side forces of the front and rear wheels (left and right), respectively. F_{Fre} and F_{Rre} depend on the weight of a vehicle and can be determined from:

$$F_{ire} = f_r\,N_i \qquad (i=F,R) \qquad (7.6)$$

where f_r is the coefficient of rolling resistance and N_i is the vertical load on the i'th wheel. Also, accelerations in U- and W- directions can be expressed as (see Fig.7.1):

$$a_u = \dot{V}_u - V_w\,\Omega \qquad (7.7)$$

$$a_w = \dot{V}_w + V_u\,\Omega \qquad (7.8)$$

where V_u and V_w are the components of the velocity in the vehicles coordinate

system. Assuming that the side slip angles are small and thus the corresponding side forces are determined from:

$$F_{sf} = C_f \beta_f \tag{7.9}$$

$$(F_{sr})_i = C_r (\beta_r)_i \qquad i=L,R \tag{7.10}$$

where C_f and C_r are the cornering stiffness and β_f, $(\beta_r)_i$ are the slip angles of the front and rear wheels (i= L,R) with their expressions as follows:

$$\beta_f = \delta_{fw} - \tan^{-1} \frac{V_w + a\,\Omega}{V_u} \tag{7.11}$$

$$(\beta_r)_i = \tan^{-1} \frac{b\,\Omega - V_w}{V_u \pm d\,\Omega} \tag{7.12}$$

7.2.2 Motion Control Policy

The function of the controller is to bring the two errors namely position error (ε_d) and orientation error (ε_θ) **(Fig.7.1)** to zero smoothly, fast and without oscillation. By noting that β_f is a very small angle (typically less than 4 degrees), therefore, according to (7.11) by setting β_f equal to zero, the best approximation for instantaneous steering angle δ_{fw} is:

$$\delta_{fw} \approx \tan^{-1} \frac{V \sin \varepsilon_\theta + a\,\Omega}{V \cos \varepsilon_\theta} \tag{7.13}$$

But in equation (7.13) no use is made of the position error. By adding another term, proportional to the offset ε_d, the structure of the controller would be of the following form

$$\delta_f = K_1 \tan^{-1} \frac{V \sin e_\theta + a\,\Omega}{V \cos e_\theta} + K_2\, e_d \qquad (7.14)$$

Note that by cancelling the term ($a\Omega$) in equation (7.14) we obtain the proportional controller as proposed and used by other researchers. The inclusion of (Ω) in the feedback improves the behaviour of a vehicle in path tracking, as it is shown in the simulation results in the next section.

7.2.3 Simulation Results

In this section, a control law in the form of equation (7.14) has been implemented to a front steered vehicle. A tuning factor (g_1) has been also included such that the steering angle is determined according to

$$\delta_f = g_1 \left[K_1 \tan^{-1} \frac{V \sin e_\theta + a\,\Omega}{V \cos e_\theta} + K_2\, e_d \right] \qquad (7.15)$$

In the simulation, first the effect of changing the ratio between the tuning parameter (g_1) is investigated. For a number of initial conditions, that

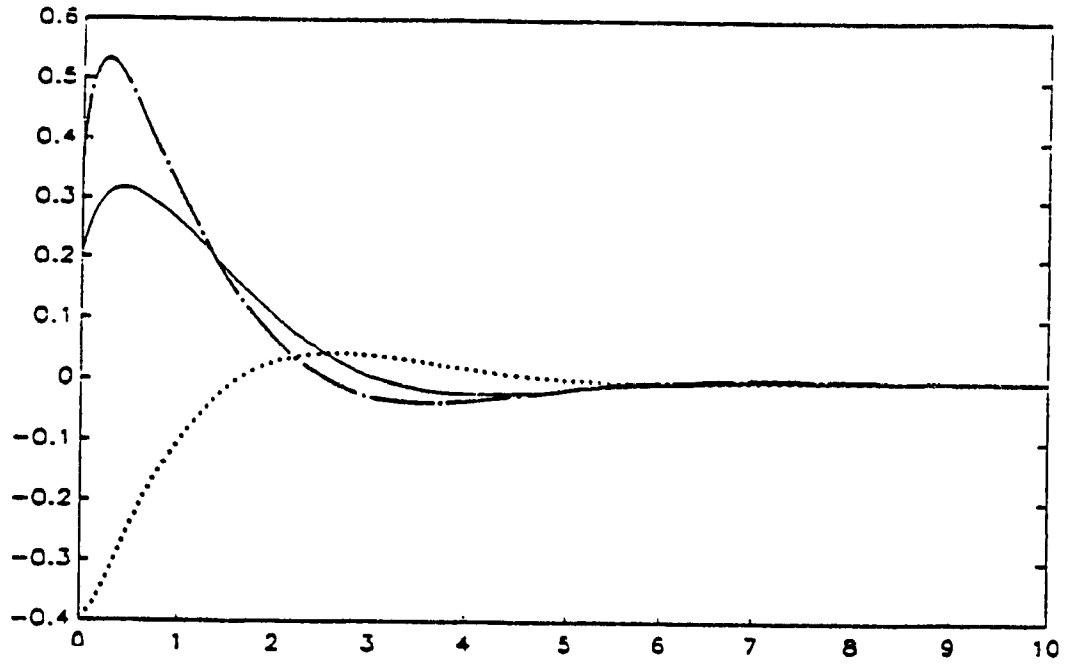

Fig. 7.3 Variations of ε_d____ , ε_θ.... (for C.G.), ε_d_._._ (for axle centre)

Initial Conditions ε_d =0.2 m, ε_θ=-π/8 rad

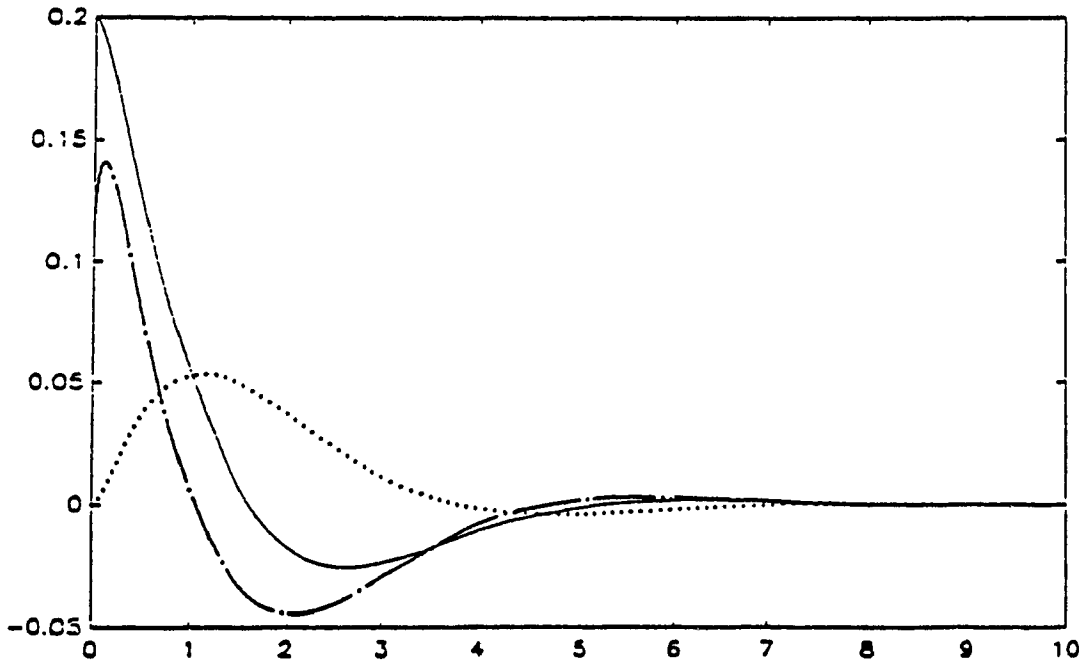

Fig. 7.4 Variations of ε_d____ , ε_θ.... (for C.G.), ε_d_._._ (for axle centre)

Initial Conditions ε_d =0.2 m, ε_θ=0 rad

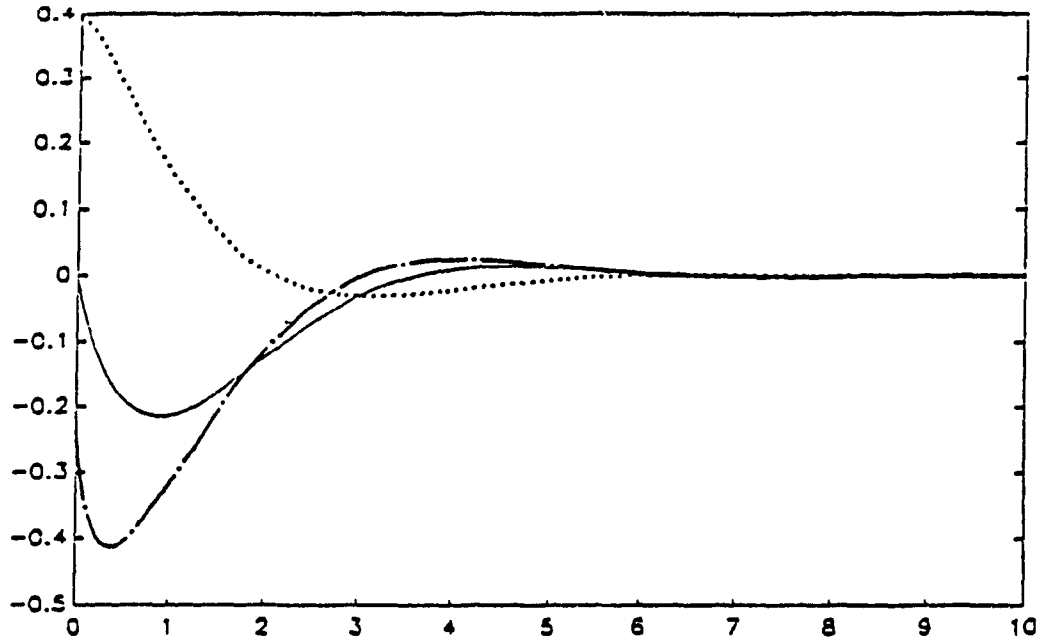

Fig. 7.5 Variations of ε_d____ , ε_θ.... (for C.G.), ε_d_._._ (for axle centre)

Initial Conditions ε_d =0.0 m, ε_θ=π/8 rad

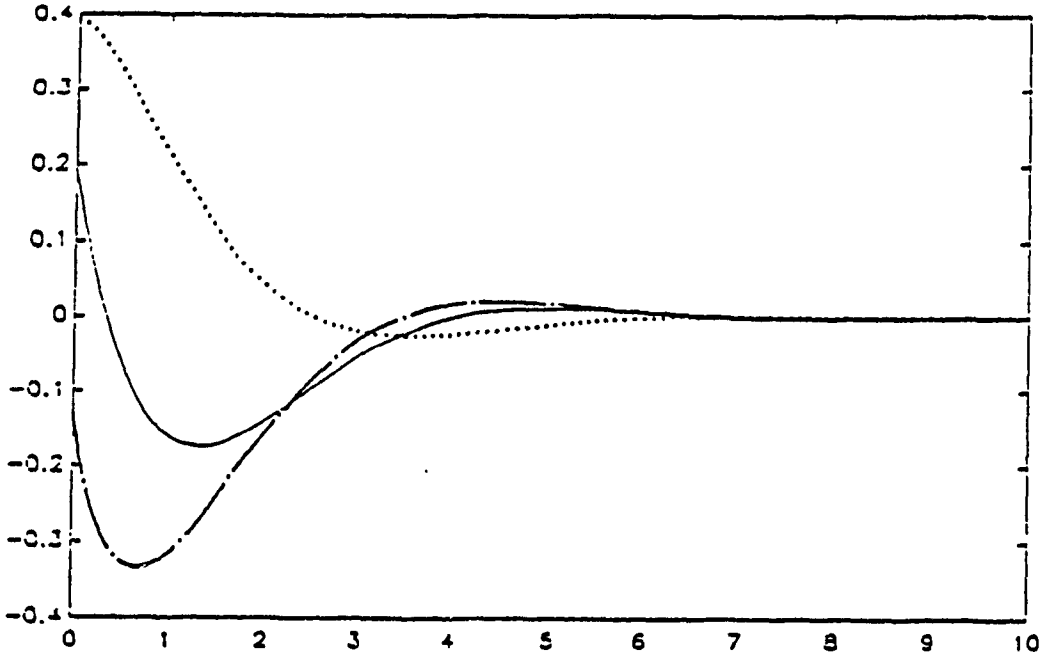

Fig. 7.6 Variations of ε_d____ , ε_θ.... (for C.G.), ε_d_._._ (for axle centre)

Initial Conditions ε_d =0.2 m, ε_θ= π/8 rad

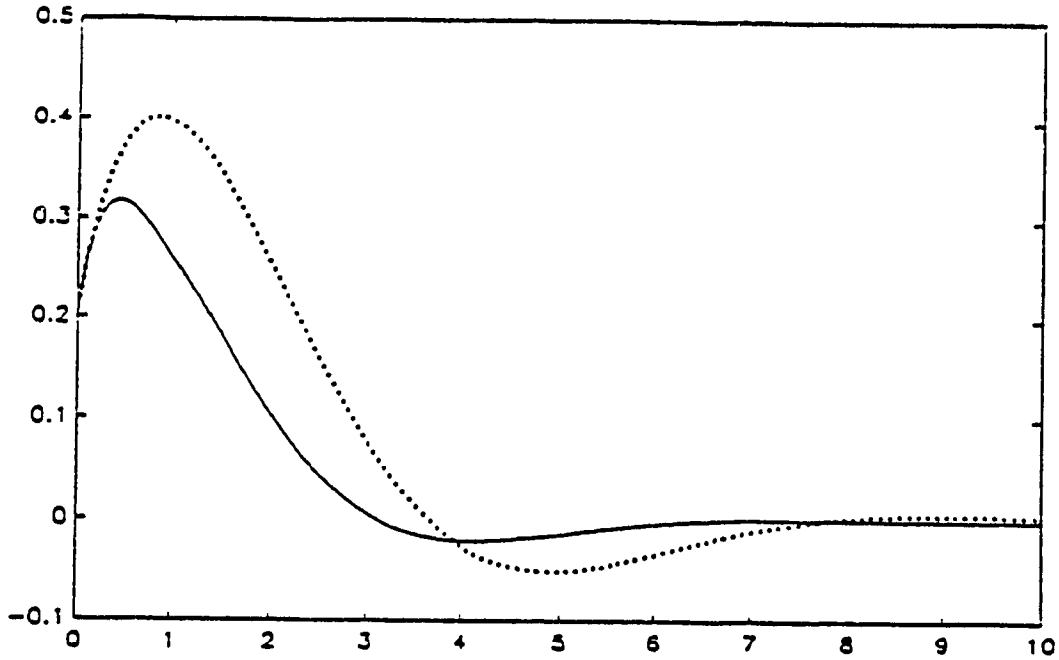

Fig. 7.7.a ε_d____, Nonlinear Controller, ε_d....., Linear Controller

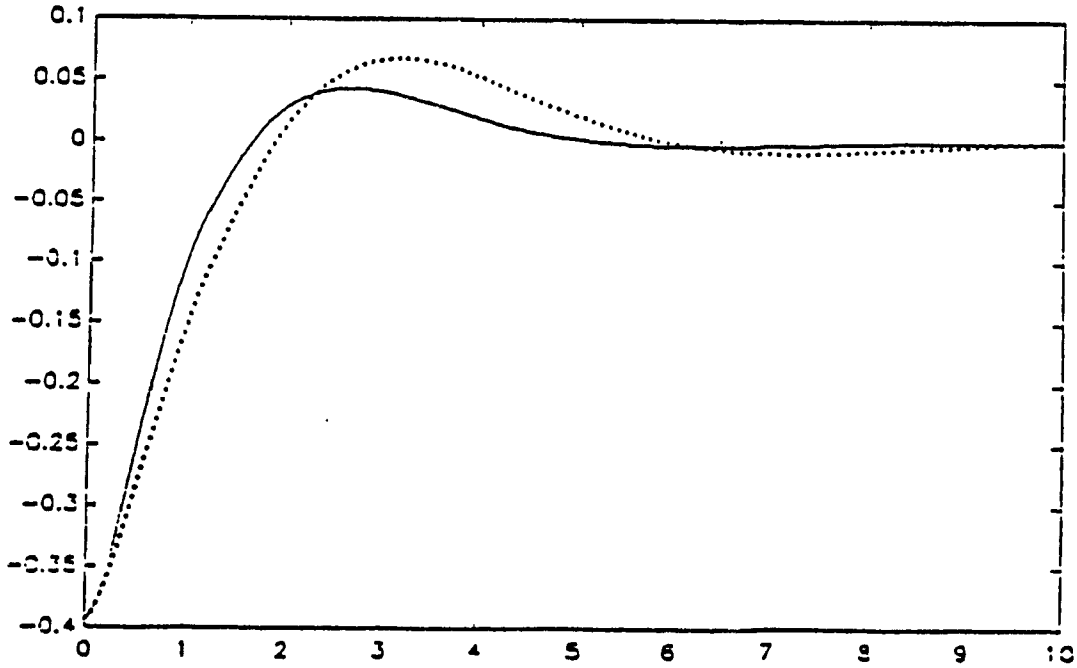

Fig. 7.7.b ε_θ____, Nonlinear Controller, ε_θ....., Linear Controller

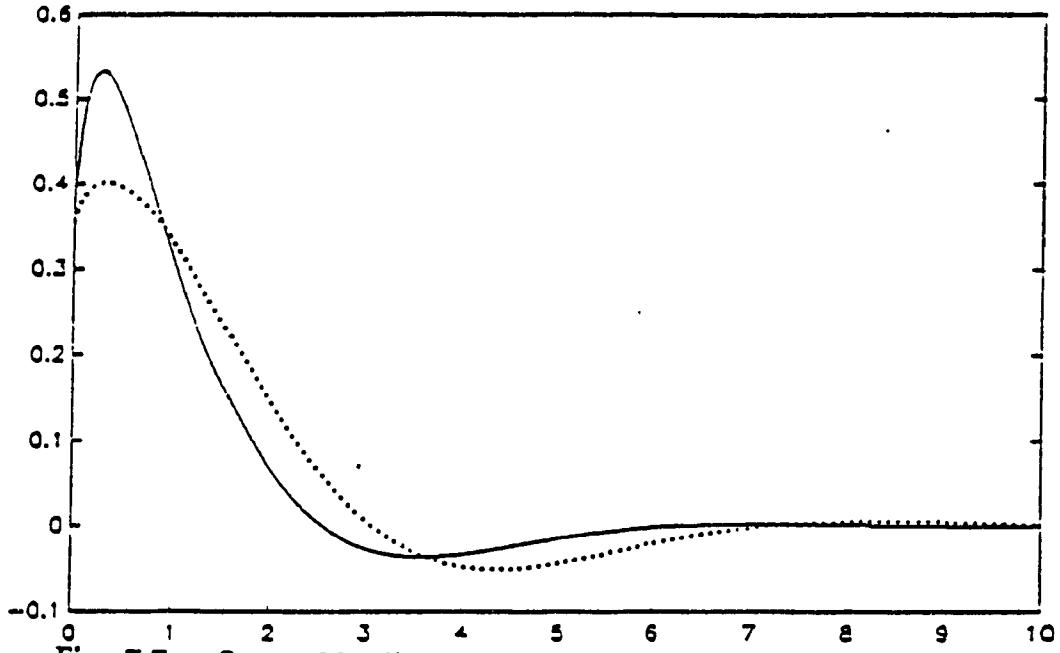

Fig. 7.7.c δ_f ——, Nonlinear Controller, δ_f....., Linear Controller

is, initial errors in the offset and orientation of the vehicle, the simulation studies are carried out. Figures (7.3) to (7.7.a-c) illustrate samples of the simulation results. Simulation result show that for the system under study, for equal values of K_1 and K_2 better performance is obtained. The most appropriate value for parameter g_1 can then be determined based on any particular system's requirement by examining a number of values for g_1. Taking the overall results, in the example used in this study a value of g_1 around (0.6-0.7) has shown to be more appropriate for a fixed gain. For larger values of g_1 ($g_1 > 1.5$) the system's behaviour becomes oscillatory in both offset and orientation settling. In all the graphs shown, g_1=0.6 and K_1=K_2=1.0.

Comparison with the results of simulation when the steering angle is adjusted according to a linear function of the errors (proportional control) reveals that a better performance is obtained when the nonlinear control law in equation (7.15) is implemented. The results of this comparison are shown in Figures (7.7a) to (7.7c) for the offset, orientation error and steering angle, respectively. In the simulation results shown, the initial offset (ε_d) is 0.2 m, the initial orientation error (ε_θ) is 22.5 degrees ($\pi/8.0$ rad) and the value of δ_f is in radians. In Figures (7.7-a,b,c) the continuous line corresponds to the control law in equation (7.15) and the curve shown by "....." corresponds to the proportional control law. The above simulation results are for the forward speed of the vehicle of 1.0 m/s.

7.3 Synthesis of an Optimal Controller

In view of the fact that the steering angle (the system input) has physical limitations it seems reasonable to look for a controller that can minimize the tracking errors during the motion of the vehicle as well as the control input. Therefore, this problem can be viewed as an optimal control problem to minimize a performance index.

In this section based on a simplified linear dynamic model for the plane motion of a 3-wheeled vehicle with front steering wheel, an optimal controller is sought such that a quadratic measure of performance consisting of the integral of the errors (errors in position and orientation of the vehicle) and the input (front

wheel steering angle) are minimized. In this way the feedback gains will be explicitly determined in terms of physical specifications.

The results are implemented for simulation studies of a vehicle and the simulation results are presented.

7.3.1 State Space Representation of Vehicle Path Tracking

Referring to telescopic (bicycle) model of the vehicle depicted in Fig. 7.8 and the assumptions (like small angles for trigonometric approximations, linear behaviour of the side forces with slip angles) remaining the same as the case for linear model, summations of the forces and moments about the centre of mass of the vehicle give:

$$C_f \beta_f + 2 C_r \beta_r = M \dot{V}_w + M V_u \Omega \tag{7.15}$$

$$a C_f \beta_f - 2 C_r \beta_r = I_z \dot{\Omega} \tag{7.16}$$

where β_f and β_r are the slip angles of the front and rear tires defined in equations (4.39) and (4.40), repeated here for the sake of convenience:

$$\beta_f = \delta_{fw} - \frac{V_w + a\Omega}{V_u} \tag{7.17}$$

$$\beta_r = \frac{b\Omega - V_w}{V_u} \tag{7.18}$$

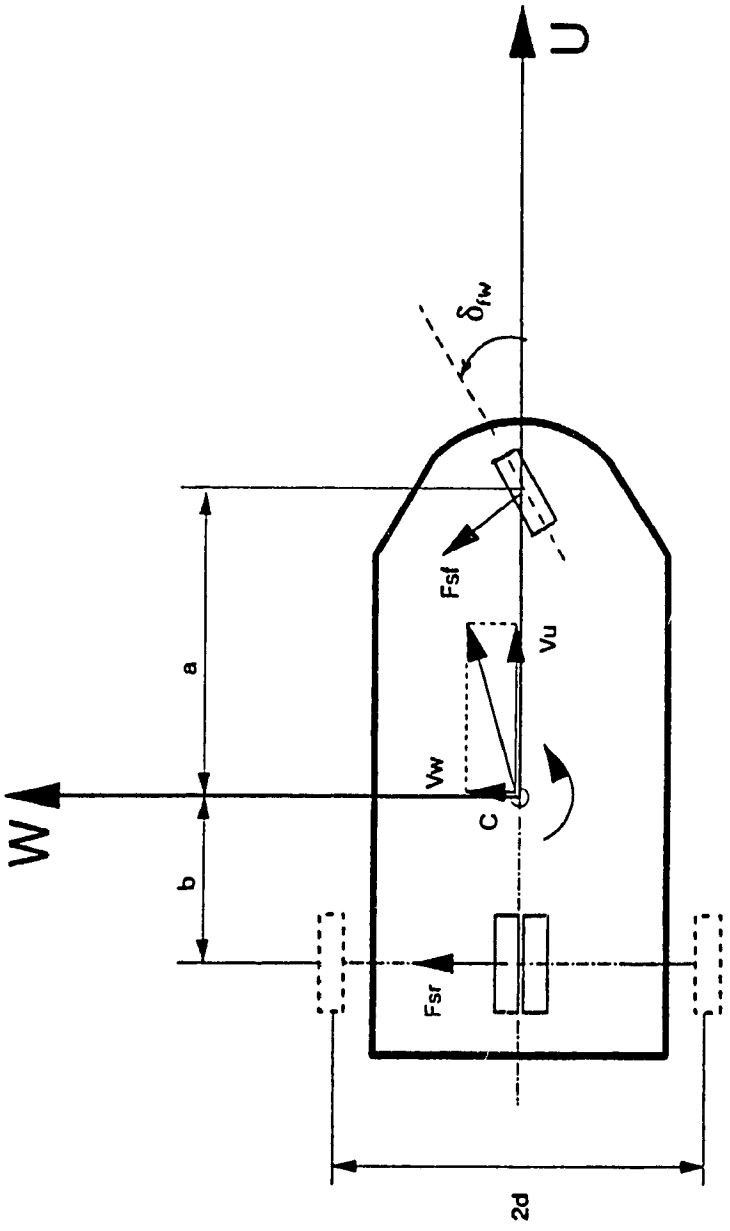

Fig. 7.8 Telescopic Model of the Vehicle

Two successive positions of the vehicle are shown in Fig. 7.9. Point P is the instantaneous centre of rotation which is determined by the intersection of a line perpendicular to the front and rear tires. The location of this point depends on the steering angle δ_{fw}. The non-slippage condition for this class of vehicle implies that the rear wheels have no lateral velocity; in this sense, point M′ the middle point on the rear axle has no lateral velocity. The velocities of all other points on the vehicle can be assumed to consist of the forward velocity of point M′ and a rotation about this point with the angular velocity Ω. If the velocity components of the mass centre in the forward and lateral directions are denoted by V_u and V_w, then the new position of the vehicle can be considered as a forward translation with velocity V_u, a lateral translation with velocity V_w and a rotation by an angle $\Delta\psi$. For a straight line path (desired), since the slope (ψ_0 in Fig.7.1) is constant, therefore:

$$\dot{e}_\theta = \psi = \Omega \tag{7.19}$$

Also, from coordinate transformation relationships Fig. 7.10 reveals that (for straight line path)

$$\dot{e}_d = V_w \cos \epsilon_\theta + V_u \sin \epsilon_\theta \tag{7.20}$$

where ϵ_d and ϵ_θ are position and orientation errors.

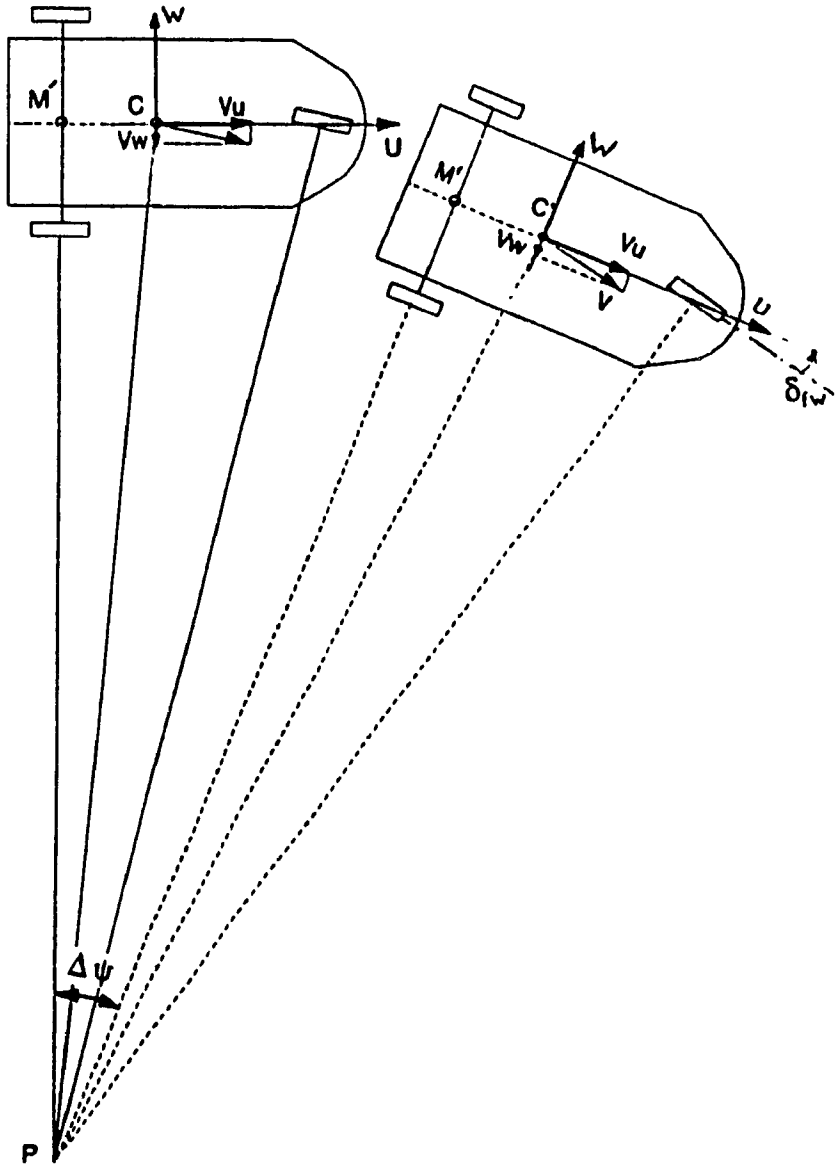

Fig. 7.9

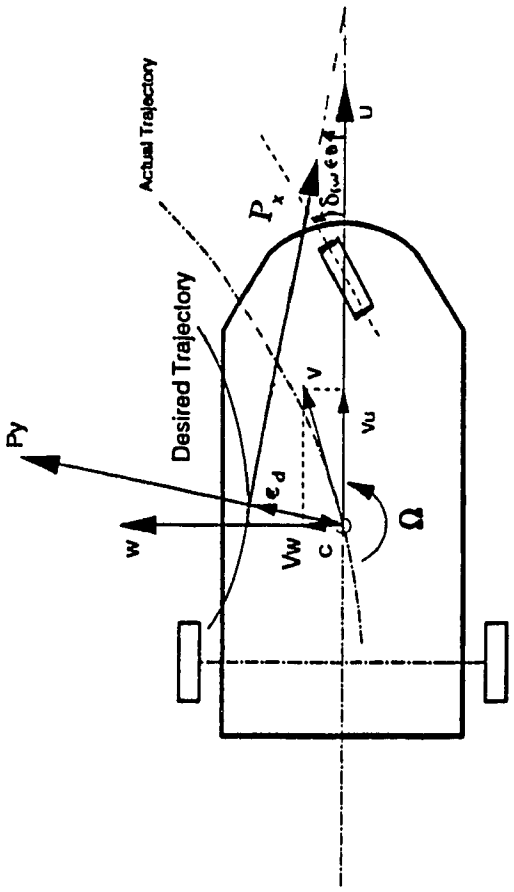
Actual Trajectory
Desired Trajectory
U
P_x
$\delta_{(w)}$
v
vu
Py
ϵ_d
w
Vw
c
Ω

Fig. 7.10

For small ε_θ ($\sin \varepsilon_\theta = \varepsilon_\theta$, $\cos \varepsilon_\theta = 1$), equation (7.20) can be simplified to

$$\dot{e}_d = V_w + V_u \varepsilon_\theta \tag{7.21}$$

substituting for β_f and β_r from equations (7.17-7.18) in equations (7.15) and (7.16) and using equations (7.19) and (7.21) the linearized equations of the system in the state space from can be written as:

$$\dot{x} = Ax + B\delta_f \tag{7.22}$$

where

$$x^T = [\, e_d \; V_w \; \Omega \; \varepsilon_\theta \,] \tag{7.23}$$

and

$$A = \begin{bmatrix} 0 & 1 & 0 & 0 \\ 0 & \dfrac{-C_f - 2C_r}{MV_u} & \dfrac{2bC_r - aC_f}{MV_u} - V_u & 0 \\ 0 & \dfrac{2bC_r - aC_f}{I_z V_u} & \dfrac{-2b^2 C_r - a^2 C_f}{I_z V_u} & 0 \\ 0 & 0 & 1 & 0 \end{bmatrix} \tag{7.24}$$

$$B = \begin{bmatrix} 0 & \dfrac{C_f}{M} & \dfrac{aC_f}{I_z} & 0 \end{bmatrix}^T \tag{7.25}$$

This system has two open loop poles (eigenvalues of matrix A) at origin, and the other two are in the form of:

$$\lambda_{2,3} = \frac{1}{2}[\alpha + \sqrt{\sigma^2 + 4\upsilon}] \tag{7.26}$$

where

$$\alpha = \frac{-1}{M I_z V_u} [\, C_f(I_z + Ma^2) + 2(I_z + Mb^2)C_r \,] \tag{7.27}$$

which is always negative,

$$\sigma = \frac{(Ma^2 - I_z)C_f + 2(Mb^2 - I_z)C_r}{MI_z V_u} \tag{7.28}$$

and

$$\upsilon = \frac{(2bC_r - aC_f)^2}{M I_z V_u^2} - \frac{(2bC_r - aC_f)}{I_z} \tag{7.29}$$

Typical values of α,σ and υ for physical systems show that these two poles are far from origin and in the left half plane of the complex plane; that is, the system possesses two fast modes and two slow modes. The fast modes correspond to the lateral and angular velocities of the vehicle (V_w and Ω), whereas the slow modes correspond to the first and fourth states; that is, the position error (offset) and the orientation error.

7.3.2 Synthesis of the Optimal Controller

For the system defined by equations (7.22) - (7.25), an optimal controller

to minimize the performance index:

$$J = \int_0^{\infty} (q_1 \varepsilon_d^2 + q_2 \varepsilon_\theta^2 + R\delta_f^2) dt \tag{7.30}$$

is sought. q_1, q_2, and R are positive scalars weighting factors for the two errors, ε_d and ε_θ, and the control effort represented by the steering angle δ_f. However, for such a system with slow and fast modes, the effect of fast modes disappear almost instantly. For this class of system, an optimal control based on only the slow subsystem will suffice, as the results of this study show.

In order to decouple the slow and fast modes, a linear transformation of the states in the form of [124]:

$$z = P^{-1}x \tag{7.31}$$

where P is the matrix whose column are the eigenvectors of A, changes equation (7.22) into:

$$\dot{z} = P^{-1}APz + P^{-1}B\,\delta_f \tag{7.32}$$

where $P^{-1}AP$ is in the Jordan canonical form (due to the repeated eigenvalues).

The subsystem associated with slow modes has the following form:

$$\dot{z}_{1A} = \begin{bmatrix} 0 & 1 \\ 0 & 0 \end{bmatrix} z_{1A} + \begin{bmatrix} b_1' \\ b_2' \end{bmatrix} \delta_f \tag{7.33}$$

The unique optimal controller for a linear system in the form of

$$\dot{z}(t) = A \cdot z(t) + B \cdot u(t) \tag{7.34}$$

where z(t) is the state vector and u(t) is the input vector, to minimize the cost function (7.30) is given by [124]:

$$u(t) = -R^{-1}B^{T}Kz(t) \tag{7.35}$$

where K is a constant positive definite matrix which results from solving the algebraic Ricatti equation:

$$-KA - A^{T}K + KBR^{-1}B^{T}K - Q = 0 \tag{7.36}$$

where Q is a positive definite matrix of compatible dimension of the weighting factors for each state.

In the next section numerical computations are performed to synthesize an optimal controller for the prototype vehicle CONCIC II. The results of simulation for implementation of this controller are also presented.

7.3.3 Illustrative Example and Simulation results

As for observing the effect of the controller designed based on the analysis in this section, the specifications of an automated guided vehicle [36,41] is used. These data are given in Appendix E.

For this system, when the forward velocity V_u = 0.4m/sec, the open loop

plant matrix is:

$$A=\begin{bmatrix} 0 & 1 & 0 & 0.4 \\ 0 & -375 & -37.5 & 0 \\ 0 & -319.5 & -140 & 0 \\ 0 & 0 & 1 & 0 \end{bmatrix} \tag{7.37}$$

which has the following eigenvalues:

$$\begin{aligned} \lambda_{1,4} &= 0.0 \\ \lambda_2 &= -96.5 \\ \lambda_3 &= -418.0 \end{aligned} \tag{7.38}$$

The input vector has the values:

$$b = [0 \;\; 50 \;\; 153.4 \;\; 0]^T \tag{7.39}$$

and matrix P whose columns are the eigenvectors of A (equation (7.37)) is:

$$P=\begin{bmatrix} 0.4 & 0.0014 & -0.0016 & 0 \\ 0 & -0.1348 & 0.6571 & 0 \\ 0 & 0.9908 & 0.7538 & 0 \\ 0 & -0.01 & -0.0018 & 1 \end{bmatrix} \tag{7.40}$$

the transformed system according to equation (7.31) is:

$$\begin{aligned} z_1 &= 2.5x_1 + 0.0088x_2 - 0.0023x_3 \\ z_2 &= -1.0015x_2 + 0.873x_3 \\ z_3 &= 1.3164x_2 + 0.1791x_3 \\ z_4 &= -0.0076x_2 + 0.0091x_3 + x_4 \end{aligned} \tag{7.41}$$

As it is seen from equation (7.41) with good approximation

$$z_1 \sim 2.5x_1 \sim 2.5\varepsilon_d$$
$$z_4 \sim x_4 \sim \varepsilon_\theta \tag{7.42}$$

The subsystems that result from linear transformation (7.31) are in the form of:

$$\dot{z}_{1,4} = \begin{bmatrix} 0 & 1 \\ 0 & 0 \end{bmatrix} z_{1,4} + \begin{bmatrix} 0.08 \\ 1 \end{bmatrix} \delta_f \tag{7.43}$$

$$\dot{z}_{2,3} = \begin{bmatrix} -96.5 & 0 \\ 0 & -418.5 \end{bmatrix} + \begin{bmatrix} 83.9 \\ 93.3 \end{bmatrix} \delta_f \tag{7.44}$$

The design of the optimal controller for the subsystem in equation (7.43) for weighting factors of 0.16 for q_1 and unity for q_2 and R, leads to the following gain matrix (K):

$$K = \begin{bmatrix} 0.52 & 0.36 \\ 0.36 & 1.3 \end{bmatrix} \tag{7.45}$$

which is the solution to Riccati equation (7.36). Using equation (7.35) and substituting for (z_1, z_2) in terms of ε_d and ε_θ from equation (7.42) gives rise to the following control law:

$$\delta_f = -(\varepsilon_d + 1.3\varepsilon_\theta) \tag{7.46}$$

The results of simulation studies for various initial conditions (for straight line paths) after implementing control law (7.46) are illustrated in Figs.7.11 to 7.14. It is seen that for all initial conditions, the errors in position and orientation converge to zero.

In deriving the above control law, the desired path was assumed to be a straight line and therefore the slope remains constant $(\psi_0 = constant = \psi_0 = 0)$. In the case of a curved path, there would be a steady state error because of the changes in the path curvature. In order to remove this error, an integral action can be incorporated in the controller. In view of this, a new state, that is, the integral of the error in the form of:

$$\dot{e} = \epsilon_d \tag{7.47}$$

can be added to the slow subsystem. Therefore, the design of the optimal PI controller will be based on the new state space representation of the system, namely equations (7.43) and (7.47) and the performance index in the form of:

$$J = \int_0^\infty (q_1\epsilon^2_d + q_2\epsilon^2_\theta + q_3 e^2 + R\delta^2_f)dt \tag{7.48}$$

For the weighting factors of $q_1=q_2=2$ and unity values of (q_3) and (R), one can solve a set of algebraic Riccati equation to get:

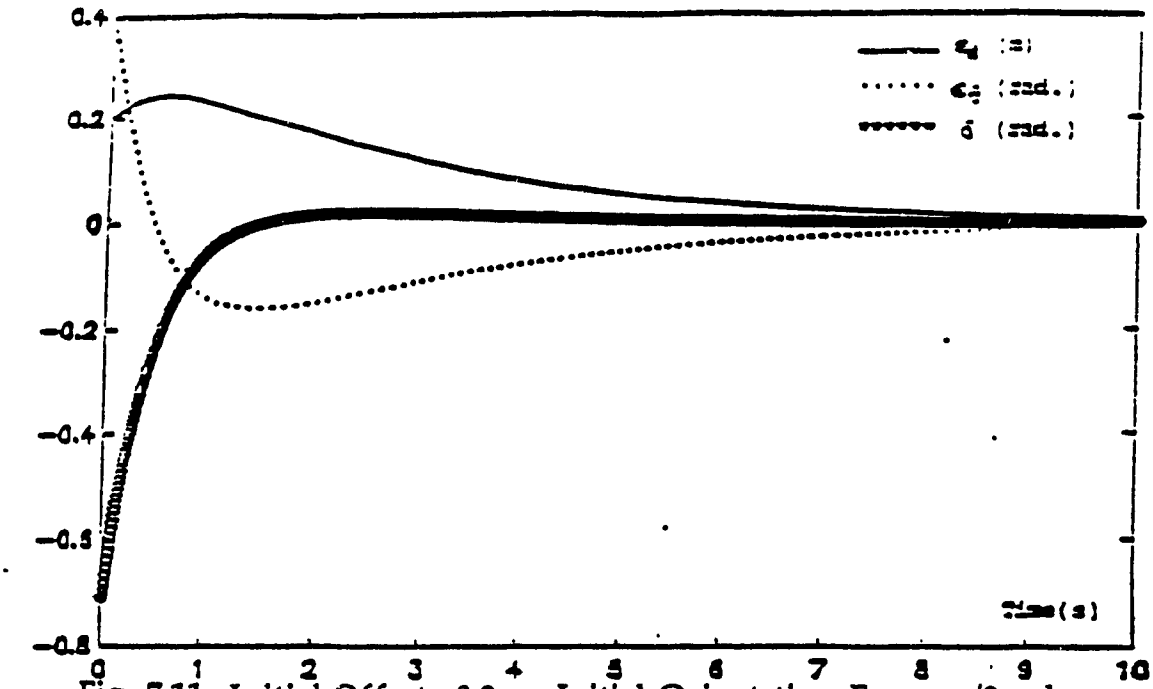

Fig. 7.11 Initial Offset =0.2 m, Initial Orientation Error= $\pi/8$ rad

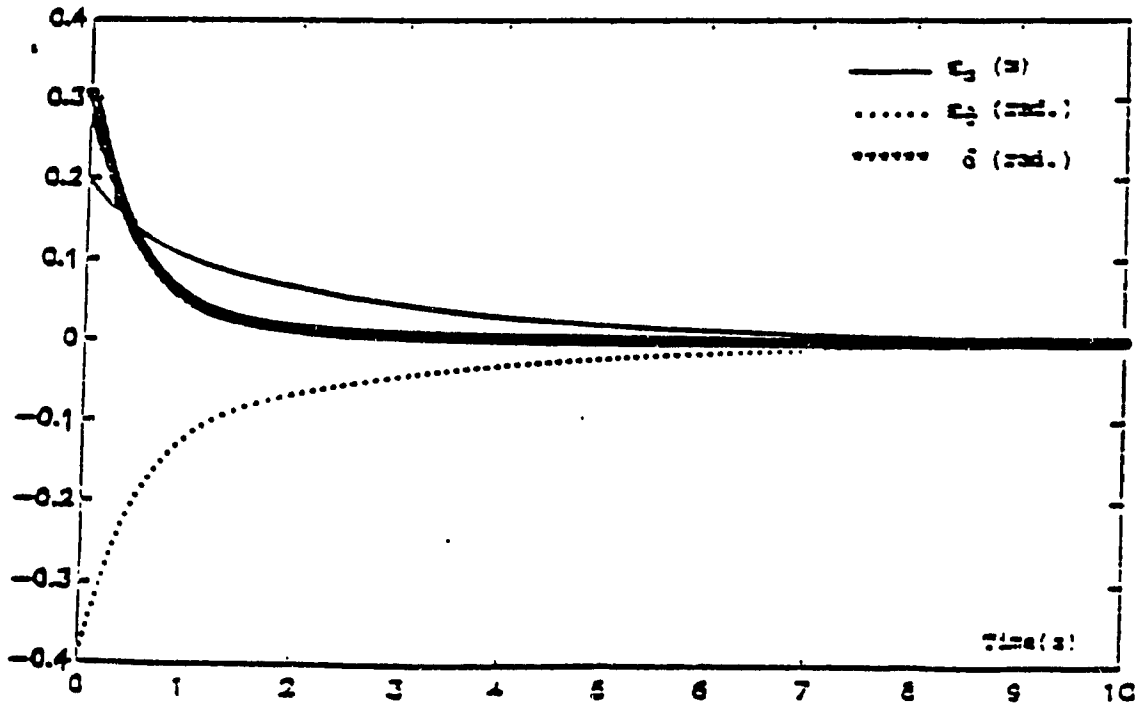

Fig. 7.12 Initial Offset =0.2 m, Initial Orientation Error= $-\pi/8$ rad

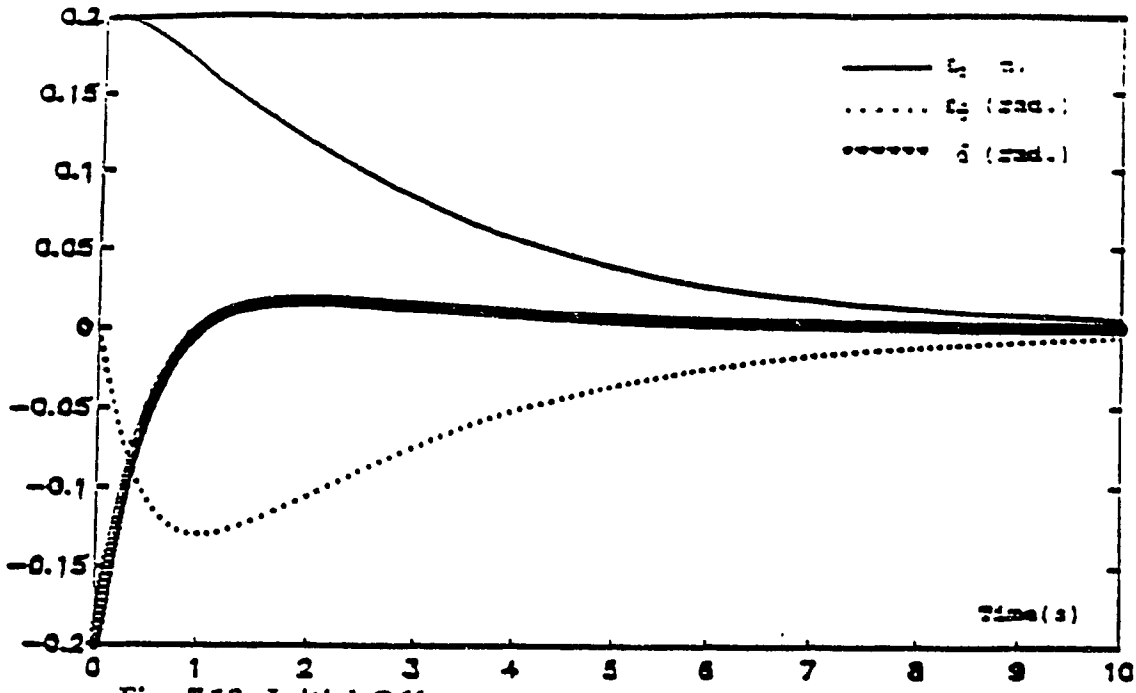

Fig. 7.13 Initial Offset =0.2 m, Initial Orientation Error= 0

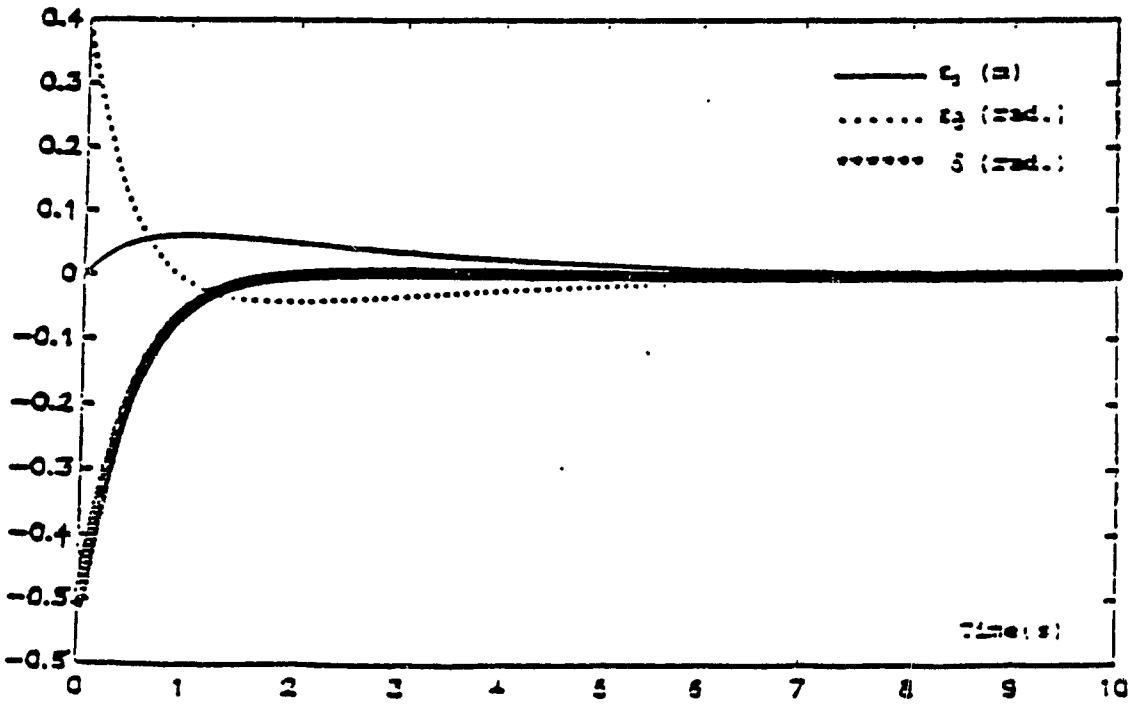

Fig. 7.14 Initial Offset =0.0 m, Initial Orientation Error= $\pi/8$ rad

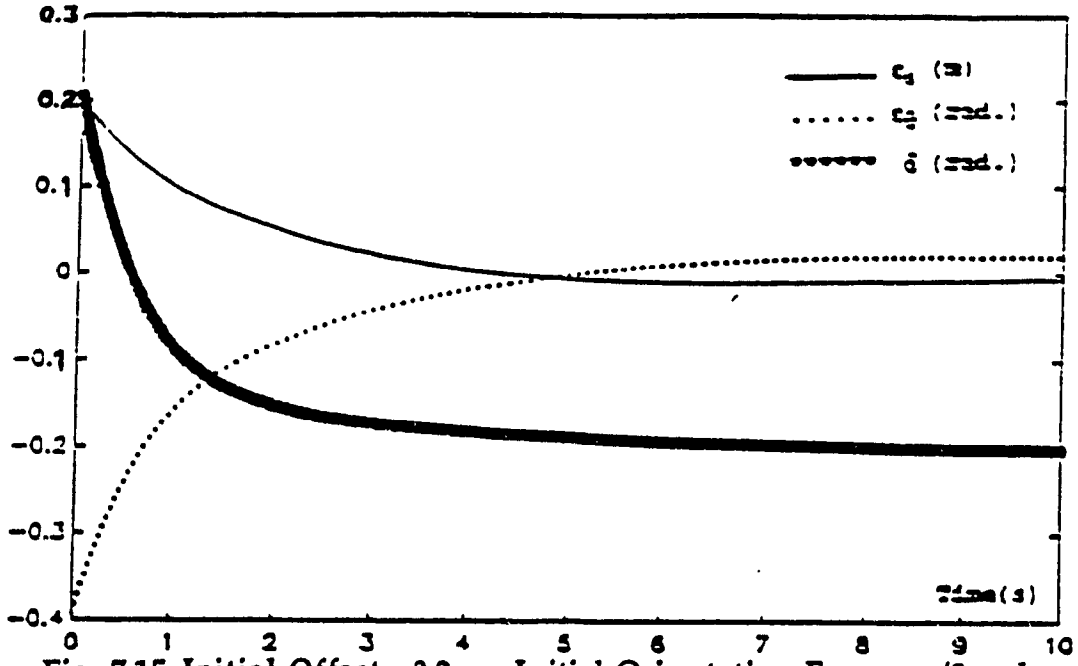

Fig. 7.15 Initial Offset =0.2 m, Initial Orientation Error= -π/8 rad

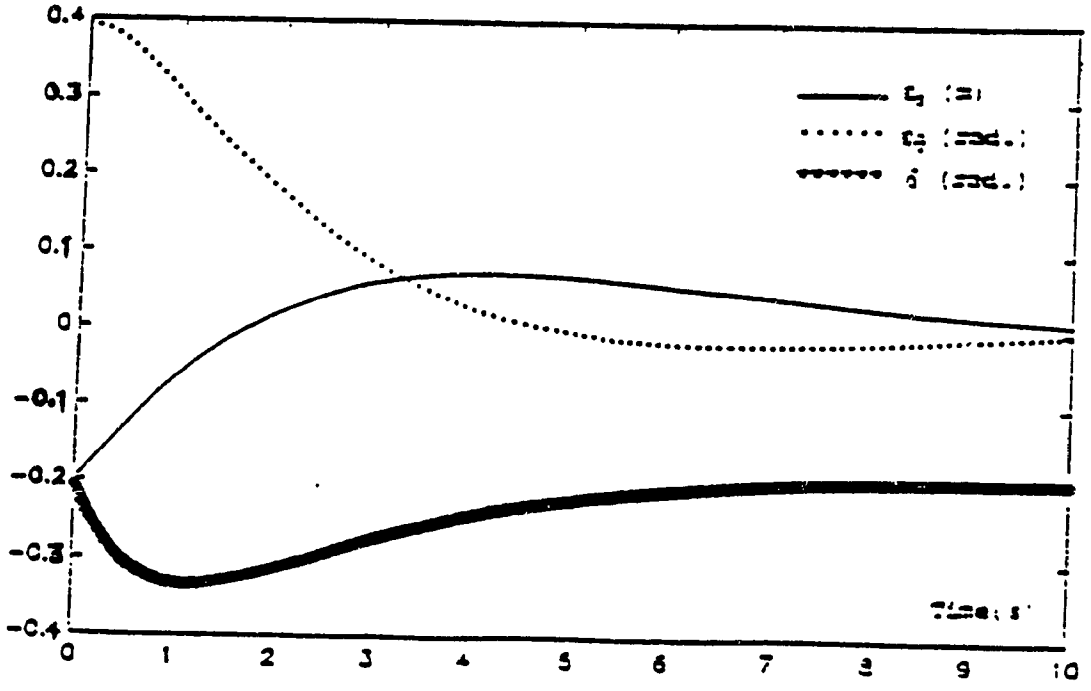

Fig. 7.16 Initial Offset =-0.2 m, Initial Orientation Error= π/8

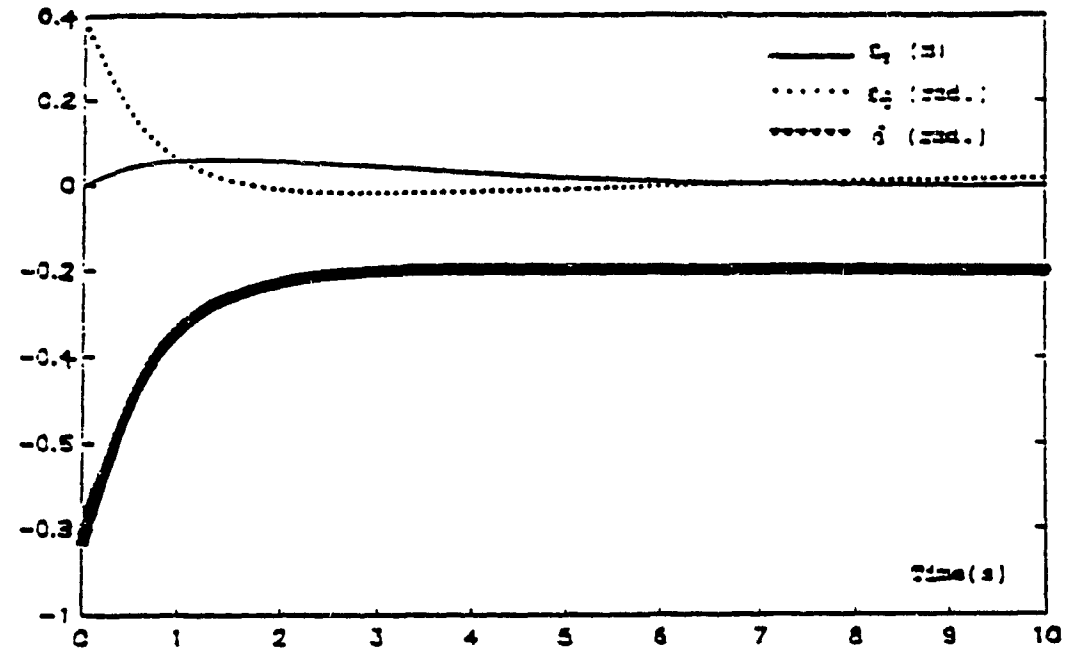

Fig. 7.17 Initial Offset =0. m, Initial Orientation Error= π/8 rad

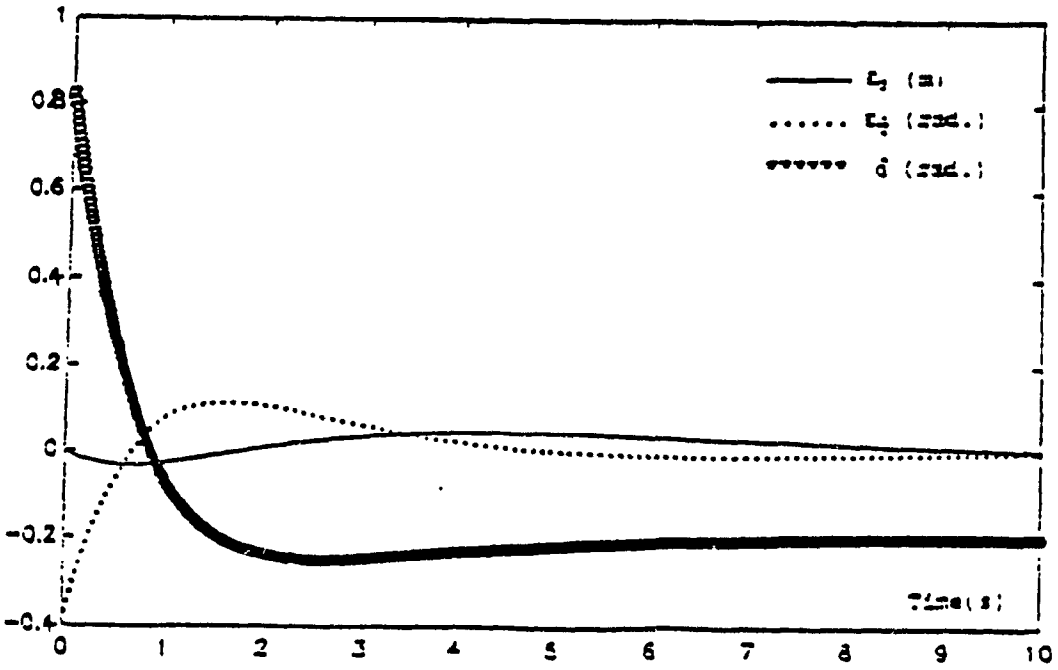

Fig. 7.18 Initial Offset =0.0 m, Initial Orientation Error= -π/8 rad

$$\delta_f = -3.1\varepsilon_d - 2.1\varepsilon_\theta - 0.8\varepsilon \tag{7.49}$$

The results of simulation for various initial conditions of ε_d and $\varepsilon\theta$ after the implementation of the control law (7.49) are illustrated in Figs.(7.11) to (7.18). It is seen that both errors go to zero, while the necessary steering angle (δ_f) will be kept after the errors are removed. Figs.(7.11) to (7.14) are for a straight line path and Figures (7.15) to (7.18) are for curved path.

7.4. Synthesis of a Controller for Vehicles with Two Independent Left and Right Traction Wheels

The steering action of the automated vehicles can also be achieved by controlling the differential velocities of the two side wheels. This section is devoted to the design of a controller for this class of vehicles. By using the kinematic equations relating the angular velocities of the two side wheels and position and orientation of the vehicle at each instant the problem is treated as a nonlinear multi input, multi output (MIMO) system. Analysis of steady state equations of the system leads us in finding the specific structure of the inputs (angular velocities of the two side wheels) in order to control the vehicle. The results of the simulations are also presented to show the performance of the controlled system.

7.4.1 Kinematic Equations

The schematic diagram of the vehicle is depicted in Fig. 7.19. The path-dependent coordinates are designated by P_x (tangent to the path) and P_y (normal to P_x), respectively. The positional error or offset, ε_d, is the distance between point C, the middle point between the two motorized wheels and the P_x-axis, and the orientational error, ε_θ, is the angle between the longitudinal axis of the vehicle at point C and the tangent to the path (P_x). In deriving the kinematic equations of motion, it is assumed that no slippage will occur in the wheels and they roll only. Referring to Fig. 7.19 the following relations (for straight line path) can be written:

$$V_u = \frac{r}{2}(\omega_L + \omega_R) \tag{7.50}$$

$$\psi = \frac{r}{2d}(\omega_L - \omega_R) \tag{7.51}$$

where ω_L and ω_R are the angular velocities of the right and left wheels respectively, V_u is the forward speed of the vehicle, r is the radius of the wheels, 2d is the wheel span and ψ is the yaw rate of the vehicle. Referring to Fig 7.20, for small orientational error the following relation holds between ε_d and ε_θ:

$$d\varepsilon_d \sim \varepsilon_\theta \, dl \tag{7.52}$$

which leads to

$$\varepsilon_\theta \sim \frac{d\varepsilon_d}{dt}\frac{dt}{dl} \sim \frac{\dot{\varepsilon}_d}{dl/dt} \sim \frac{\dot{\varepsilon}_d}{V_u} \tag{7.53}$$

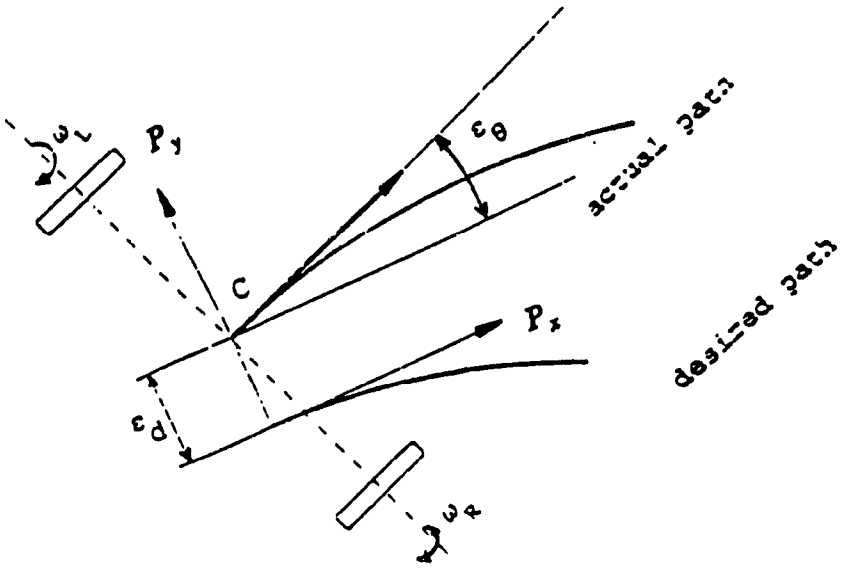

Fig. 7.19 Kinematic Configuration of the Vehicle

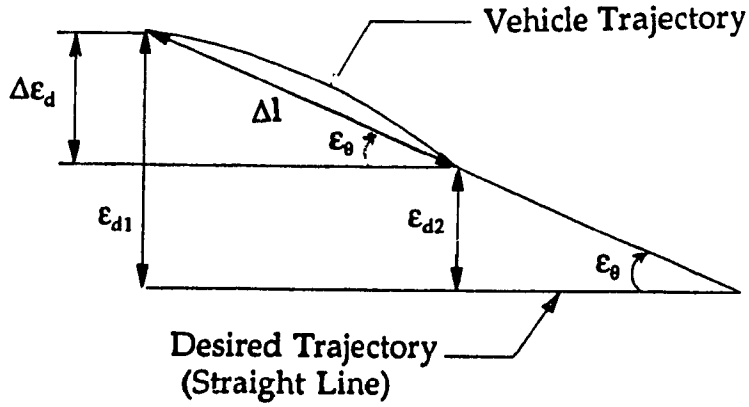

Fig. 7.20

or

$$\dot{e}_d \approx V_u e_\theta \tag{7.54}$$

It follows from Figs.(7.18-7.19) and also equation (7.51) that:

$$\dot{e}_\theta = \frac{r}{2d}(\omega_L - \omega_R) \tag{7.55}$$

The kinematic relations of the system can be written in the following state-space form in light of equations (7.50-7.51) and (7.54-7.55):

$$\dot{x}_1 = \frac{r}{2}(u_1 + u_2)x_2 \tag{7.56}$$

$$\dot{x}_2 = \frac{r}{2d}(u_1 - u_2) \tag{7.57}$$

where

$$[x]^T = [e_d \; e_\theta] \tag{7.58}$$

$$[u]^T = [\omega_L \quad \omega_R] \tag{7.59}$$

Equations (7.56) and (7.57) express the motion of a vehicle based on its kinematics, where the two inputs to the system are the angular velocities for the left and right wheels which must be properly determined based on the measured errors.

7.4.2 Controller Design

For the two inputs the following forms which imply linear feedback from the two errors are considered. The inclusion of K_3 in both equation implies that when the errors x_1 and x_2 are zero, both left and right wheels must have equal angular velocities corresponding to the forward velocity of the vehicle;

$$u_1 = K_1 x_1 + K_2 x_2 + K_3 \tag{7.60}$$

$$u_2 = K'_1 x_1 + K'_2 x_2 + K_3 \tag{7.61}$$

The closed loop equations after applying these inputs are in the form of:

$$\dot{x}_1 = c_1 x_1 x_2 + c_2 x_2^2 + c_3 x_2 \tag{7.62}$$

$$\dot{x}_2 = c_4 x_1 + c_5 x_2 \tag{7.63}$$

where

$$\begin{aligned} c_1 &= \frac{r}{2}(K_1 + K'_1) \\ c_2 &= \frac{r}{2}(K_2 + K'_2) \\ c_3 &= rK_3 \\ c_4 &= \frac{r}{2d}(K_1 - K'_1) \\ c_5 &= \frac{r}{2d}(K_2 - K'_2) \end{aligned} \tag{7.64}$$

If the steady state ($\dot{x}$= 0) of the system is considered, it follows from equations (7.62) and (7.63) that:

$$[x_2(c_1x_1+c_2x_2+c_3)]_{ss}=0 \tag{7.65}$$

$$[c_4x_1+c_5x_2]_{ss}=0 \tag{7.66}$$

Equations (7.65) and (7.66) imply that unless c_1 and c_2 are identically zero, this system has two sets of steady state values for x_1 and x_2, one set of which represents undesirable (nonzero) values for the states ε_d and ε_θ (in fact, this represents a case where the two errors remain constant at their initial values; it corresponds to $u_1 = u_2 = 0$, that is, the vehicle is not moving). For this reason c_1 and c_2 are set equal to zero in equation (7.64) and where applicable, thus:

$$c_1=c_2=0 \tag{7.67}$$

from which it follows that:

$$K_1=-K'_1 \tag{7.68}$$

and

$$K_2=-K'_2 \tag{7.69}$$

in light of equations (7.64). It then follows from equations (7.62),(7.63) and (7.67) that the differential equations of the controlled system in the state space form is:

$$\begin{bmatrix}\dot{x}_1\\ \dot{x}_2\end{bmatrix}=\begin{bmatrix}0 & c_3\\ c_4 & c_5\end{bmatrix}\begin{bmatrix}x_1\\ x_2\end{bmatrix} \tag{7.70}$$

Since c_3 is defined by the forward velocity of the vehicle (and is taken to be positive), the stability of the system depends on c_4 and c_5 which determine the closed-loop eigenvalues. By selecting a set of desired eigenvalues, thus, c_4 and c_5 are accordingly calculated; this in turn leads to the selection of the feedback coefficients K_1, K'_1, K_2 and K'_2 from equation (7.64).

It can be revealed from the expression for eigenvalues of the closed-loop plant matrix in equation (7.70), that is,

$$\lambda_{1,2} = \frac{1}{2}(c_5 \pm \sqrt{c^2_5 + 4c_3c_4}) \tag{7.71}$$

that both c_4 and c_5 must be negative.

7.4.3 Simulation Results

The results of the analysis and synthesis of a controller as outlined in previous section are used in a simulation study carried out based on the parameters of CONCIC II vehicle whose specifications are given in Appendix E. This simulation is based on the dynamics of motion, though the controller design is based on kinematics of motion only. In our study the feedback gain valued K_1 and K_2 in equations (7.60) and (7.61) have been rounded to integral values. These values are:

$$K_1 = -K'_1 = -4$$
$$K_2 = -K'_2 = -5 \qquad (7.72)$$

which for the given values of r and d correspond to:

$$c_4 = -1.15$$
$$c_5 = -1.44 \qquad (7.73)$$

The associated eigenvalues of the closed-loop matrix in equation (7.71) for a forward velocity of 0.4m/s are:

$$\lambda_1 = -0.96$$
$$\lambda_2 = -0.48 \qquad (7.74)$$

In the following figures namely Figs.(7.21-7.23) the behaviour of the controlled system for different initial conditions are illustrated. It is seen that for various initial conditions, the errors in position and orientation converges to zero in a stable manner.

7.5 Remarks

In derivations of the control laws introduced in this chapter (for tricycle model, front wheel steered vehicle), the dynamics of the steering system was assumed to be negligible meaning that at any instant, δ_f (command to steering system) is approximately equal to δ_{fw} (instantaneous front wheel steering angle) (see Fig. 7.20.a.). However, in reality some delays exist because of steering dynamics. From typical dynamic characteristics of the steering system (see Fig. 9.6) it appears that steering system can be approximated by a first order system. Block diagram of the controlled system (Fig. 7.20.a) suggests that by cascading a first order element in the form of $(\tau_c s + 1)$ to the controller (see Fig. 7.20.b), it is possible to compensate for the effects of steering dynamics by setting $(\tau_c = \tau)$. In

applying this proceedure, one should notice that because of the derivative term in ($\tau_c s$ +1), the effects of the unwanted noise may be amplified.

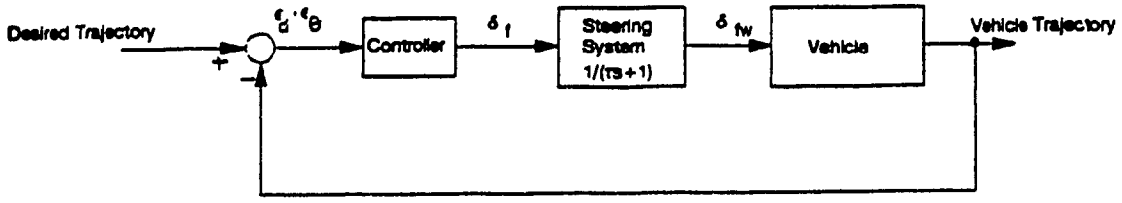

Fig. 7.20.a Block Diagram of the Uncompensated System

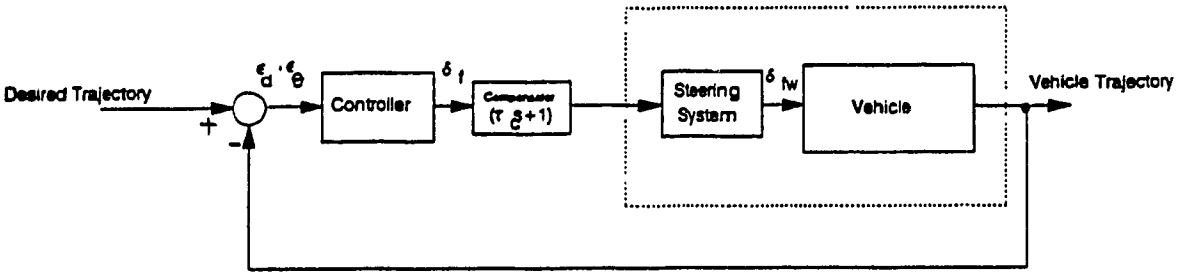

Fig. 7.20.b Block Diagram of the Compensated System

In order to further improve the performance of a vehicle in path following, other alternative ways can be thought. One possibility that is pursued and more elaborated in chapter 9 (in carrying experiments) is derived from the way a driver operates a vehicle. A driver always looks ahead and observes and predict the changes of the path beforehand. Accordingly he decides for the adjustments of the speed and the wheels steering [79]. The same idea can be adapted to enhance the path following performance of an automated vehicle. The information obtained can be fed to the system in a feedforward manner.

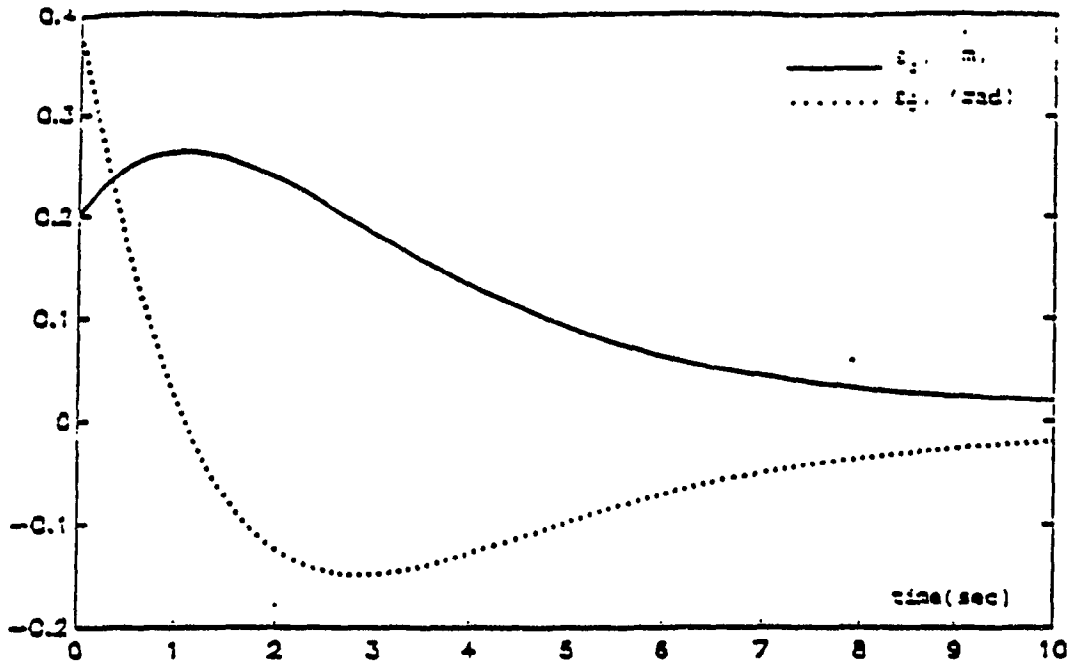

a: Variations of ε_d and ε_θ

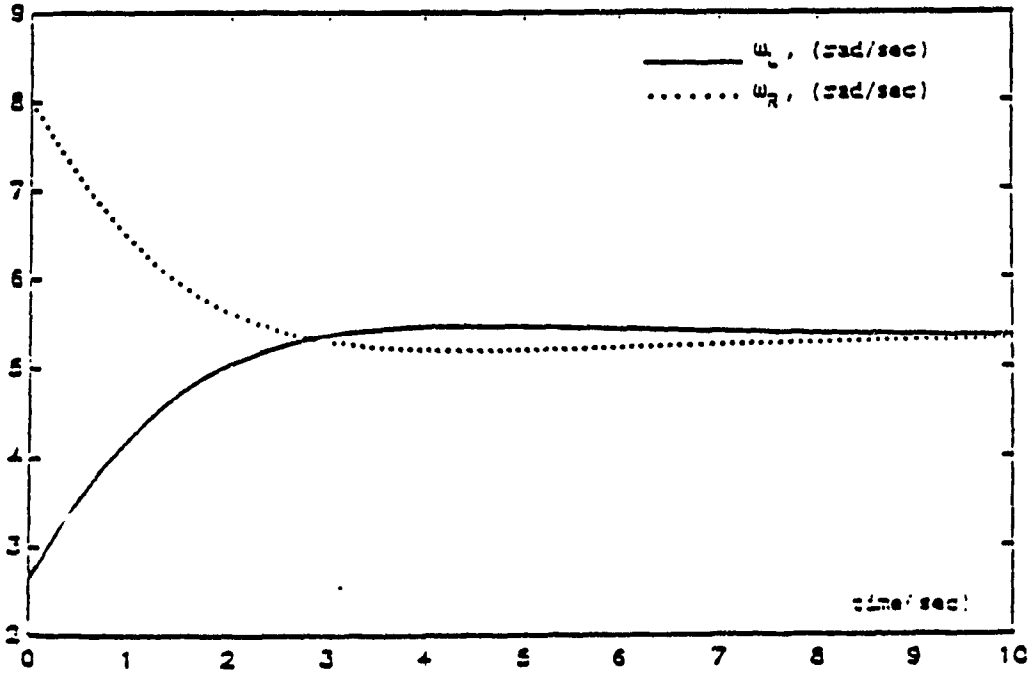

b: Variations of ω_L and ω_R

Fig. 7.21 initial Offset=0.20 m, Initial Orientation Error= $\pi/8$ rad

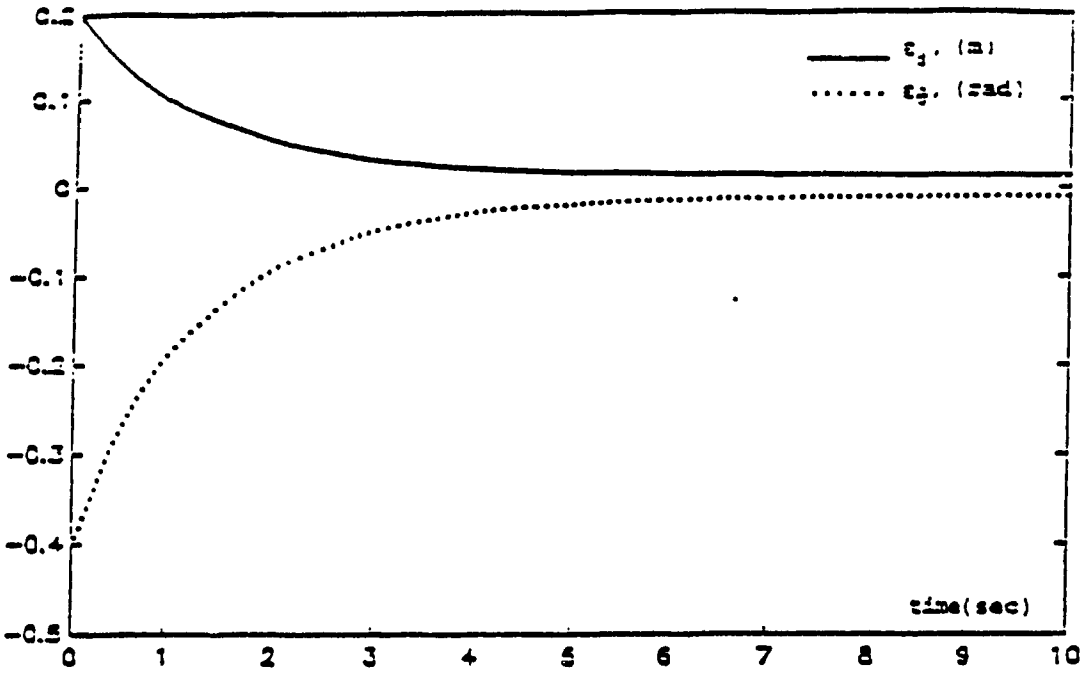

a: Variations of ε_d and ε_θ

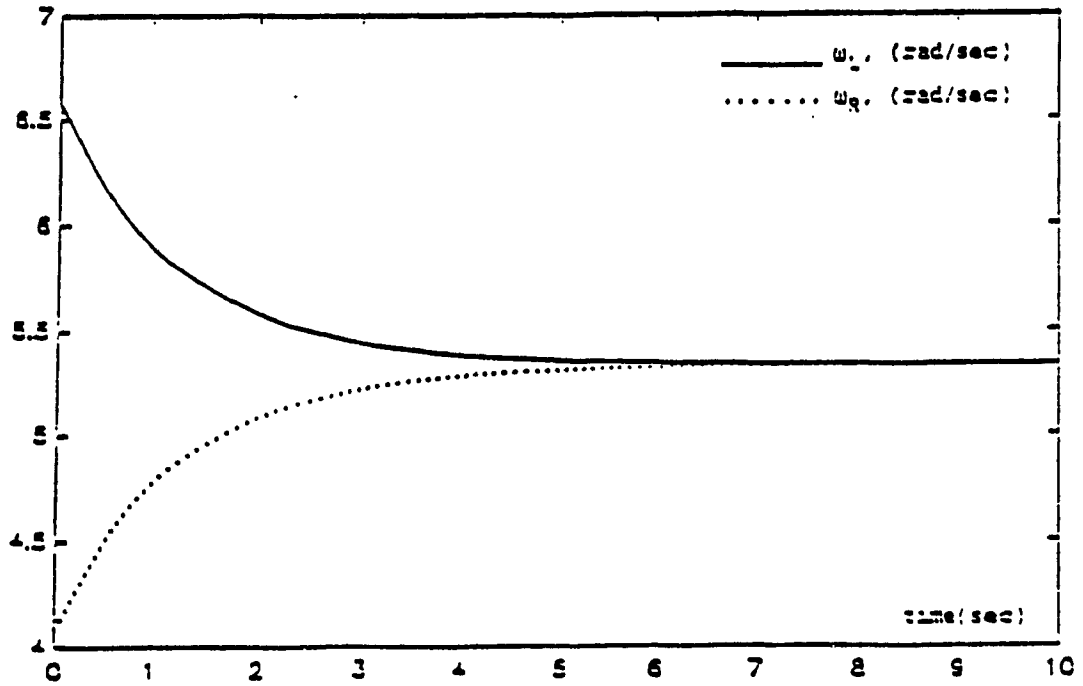

b: Variations of ω_L and ω_R

Fig. 7.22 initial Offset=0.20 m, Initial Orientation Error= -π/8 rad

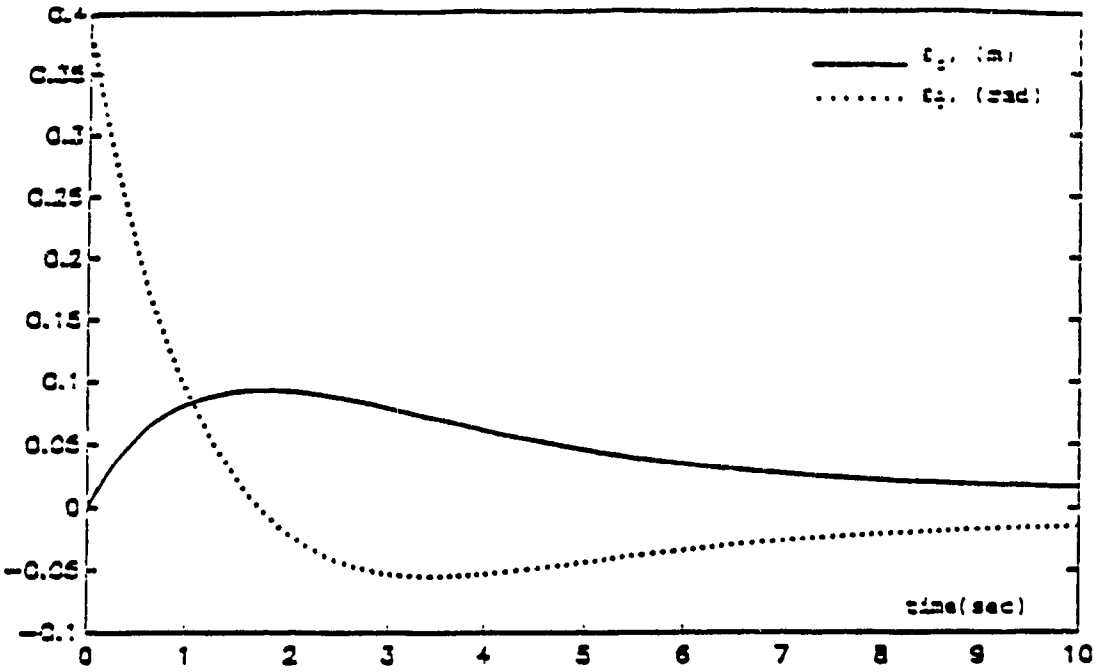

a: Variations of ε_d and ε_θ

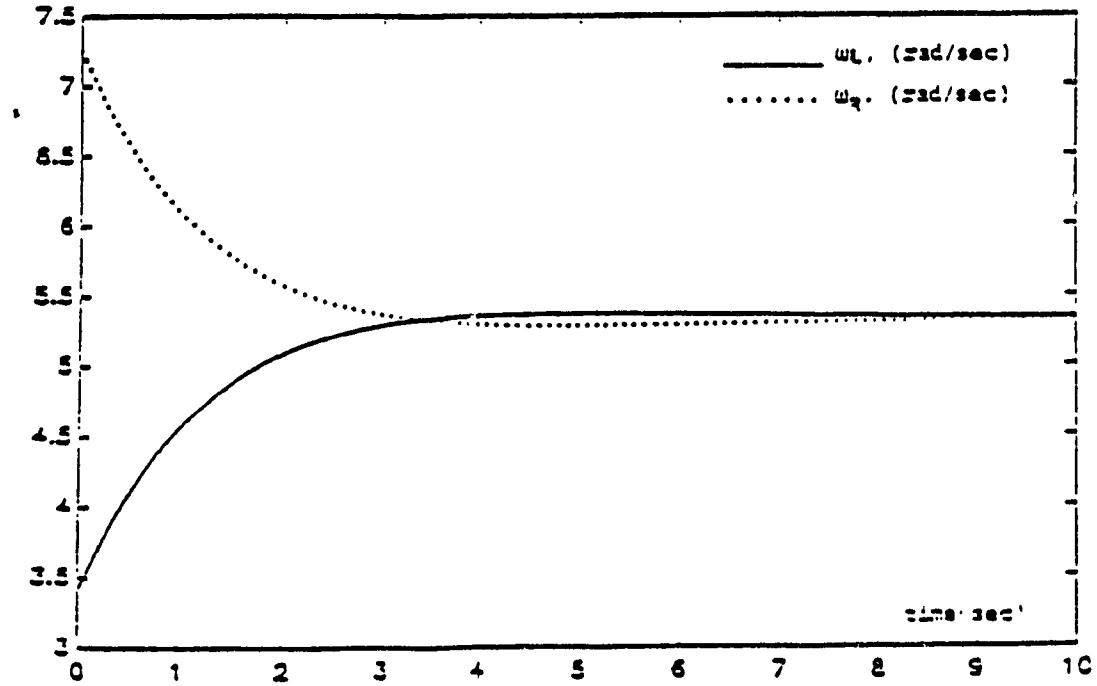

b: Variations of ω_L and ω_R

Fig. 7.23 initial Offset=0.0 m, Initial Orientation Error= $\pi/8$ rad

7.6 Summary

In this chapter, a number of control algorithm were proposed for the motion control of the common wheelbase configurations of automated vehicles. The models studied were tricycle model and differential drive. For the vehicles with front wheel steering systems, a nonlinear control policy was proposed by using the dynamic relations of the system. It was concluded that inclusion of a nonlinear term in the control structure improves the performance of the system in path following. However, the requirement of having the measurements of the vehicle yaw rate is a problem that needs to be investigated. Moreover, as the simulation results showed, implementing this controller needs a faster steering system that should be considered in their design.

Based on the optimal control theory, using the linearized dynamic model of the vehicle, an optimal controller was designed for path following of the vehicle. Since this controller was designed for straight line path, it could not remove the errors resulting from the changes in path curvature. Thus, an integral action was incorporated in the controller, which enhances the performance in lessening the steady-state error in curve tracking. The results of simulations for both straight line and curved paths were presented showing the satisfactory performance of the controlled system.

Another wheelbase configuration considered here was the class of differential drive vehicles with two independent side tractive wheels. By using the kinematic relations of the system, a control structure was proposed and a procedure for the adjustment of the controller's gain was presented. The performance of such a system under the proposed control law was investigated by simulation results.

CHAPTER 8

DEVELOPMENT OF CONCIC III PROTOTYPE VEHICLE

8.1 Introduction

CONCIC III is a prototype vehicle designed and built at Centre for Industrial Control (CIC) of Concordia University. This vehicle provides a suitable testbed for the analytical and experimental research in the area of automated vehicles. All the experimental results reported in this thesis are obtained by using CONCIC III. Due to its importance therefore, this chapter is devoted to description of the mechanical structure, comprising elements, various control units, etc. of CONCIC III. In this chapter, a general description of the architecture of this vehicle such as mechanical and hardware structure, power units, driving and steering units, motion control elements and the relevant interfacing cards, data acquisition system, arrangements of servo control units as well as software specifications and different software modules

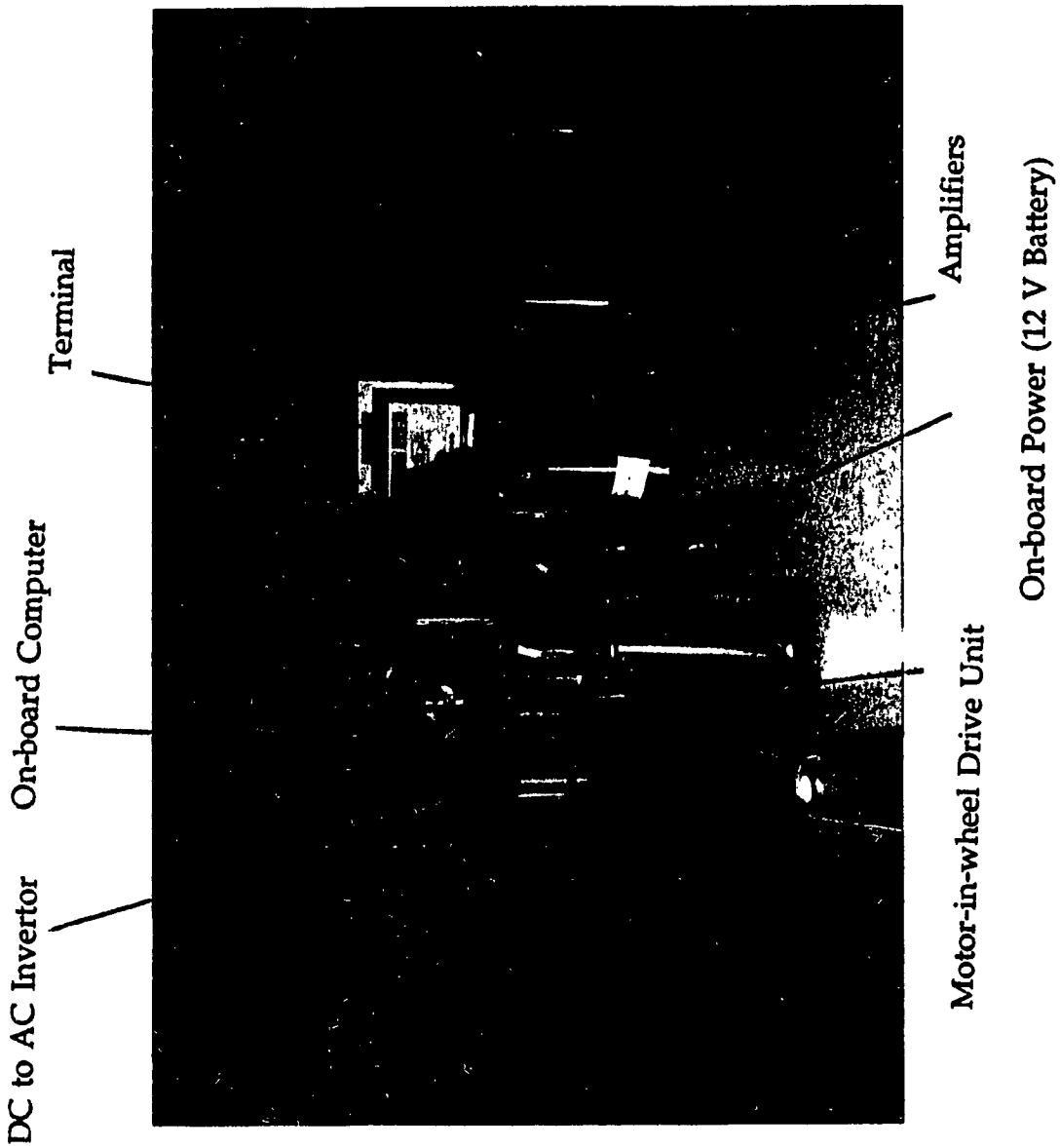

Fig. 8.1 Photograph of CONCIC III Prototype Vehicle

are provided. The details of the components are provide in Appendix F.[36,41].

8.2 Description of Mechanical Structure of CONCIC III

CONCIC III has a double steering wheelbase configuration with two sets of driving-steering units in the front and rear of the vehicle and two side casters for the purpose of stability of the vehicle. A photograph of CONCIC III is shown in Fig. 8.1. The size and frame shape of this vehicle (CONCIC III) is very similar to (CONCIC II)[36,41], however, the wheelbase configuration is different due to the purpose of the study. As it is seen in this figure, the body of the vehicle consists of two parts. The rear part provides space for carrying the load while the front part serves as a housing for the computer and data acquisition board. The frame of the vehicle consists of aluminium rods welded together. The structure of the vehicle consists of two parts at different levels: the lower level which consists of nine different compartments and upper level consists of just one part [36,41]. Schematic diagrams of the vehicle are shown in Figs.8.2(a-b). As it is shown in Fig. 8.2, lower level's compartments offer flexibility for different wheelbase configurations as desired. This is a unique feature of this vehicle and provides a variety of options in wheelbase configurations and according to the desired type of study, it can easily

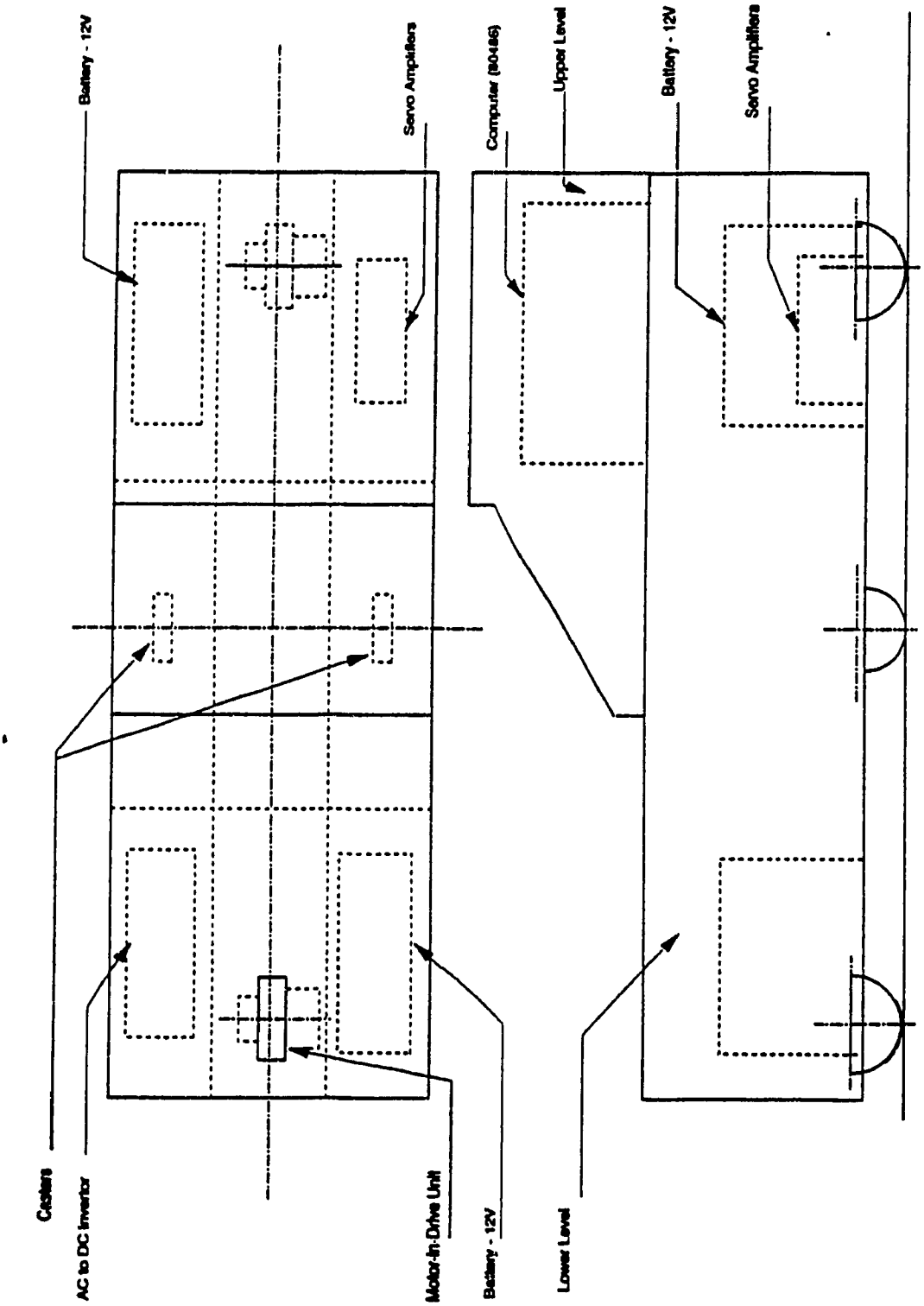

Fig. 8.2(a-b) Schematic Diagram of the Vehicle

be changed and switched from one option to another. Although in this thesis the vehicle has been used as a testbed for the vehicles with fore and aft steering systems with no redundancy, however, the other vehicle models such as differential drive with two side driving motors and one caster in the front (tricycle shape) or two casters in the front and the rear (diamond shape), tricycle models with the steering and driving motors in the front, double steering vehicle, various redundant structures, etc. can be achieved and studied by using this vehicle [41].

8.3 Driving and Steering Components

Each driving unit of CONCIC III has a driving motor geared to a solid rubber wheel and a steering motor with a ring type reduction gear all arrangements in one unit. This arrangement is suitable for the typical application due to its compact form which has the advantage of not having unnecessary mechanical components like chain, gears or belt to transfer power. A photograph of this arrangement is shown in Fig. 8.3. The motors (driving and steering) are permanent magnet (PM) motors whose characteristics are provided in Appendix B [36,41,125]. Both the driving and steering motors are equipped with shaft encoders to monitor the position/velocity (with the aid of LM628) of the wheels.

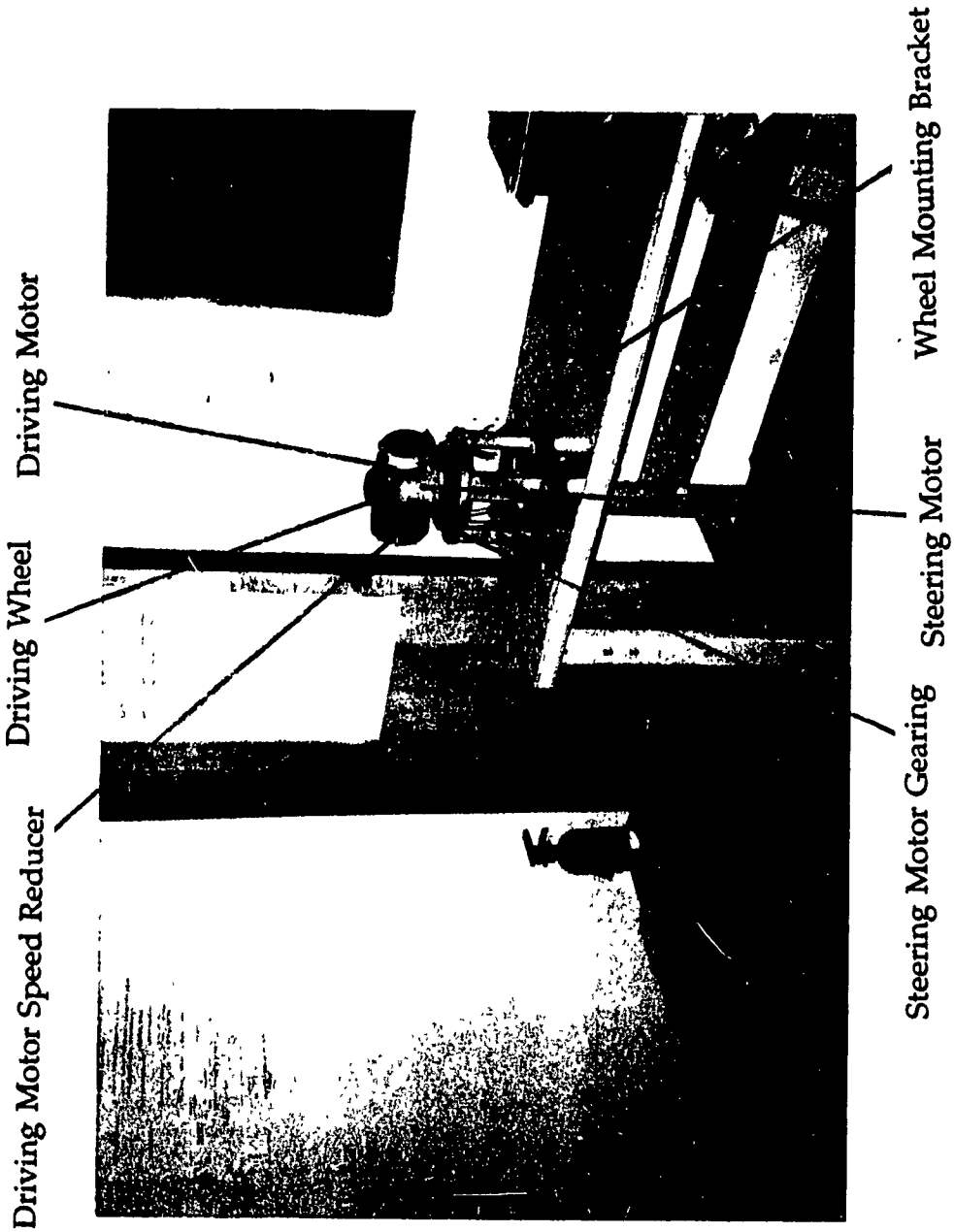

Fig. 8.3 Photograph of Driving-Steering Arrangement

8.4 Control Components

The on-board controller of CONCIC III is an INTEL-80486/DX50 micro-computer operating in MS DOS. Low level servo-control loops feature the National Semiconductor LM628 precision motion controller chip [36,41,126-127] and the pulse-width modulated amplifiers from Galil [128,41] operating in current mode as shown in Fig. 8.4. The motion controller features are: adjustable PID filter gains, good resolution for high accuracy in position and velocity and its easy interface with pc, direct connection of the encoder signals, etc.[41,126-127]. The components of the LM628 are shown in Fig. 8.5[41]. As it is shown in this figure, the motion controller is provided with a PID filter whose discrete time equations are:

$$u(n\delta t) = K_p\, e(n\delta t) + K_i \sum_{j=0}^{n} e(j\delta t) + K_d\, [e(k\delta t) - e\,(k-1)\delta t] \tag{8.1}$$

where u(n δt) is the digital command to the digital to analog convertor and is the command signal to the servo amplifiers. The terms K_p, K_i and K_d are the gains of the proportional, integral and derivative terms which are programmable

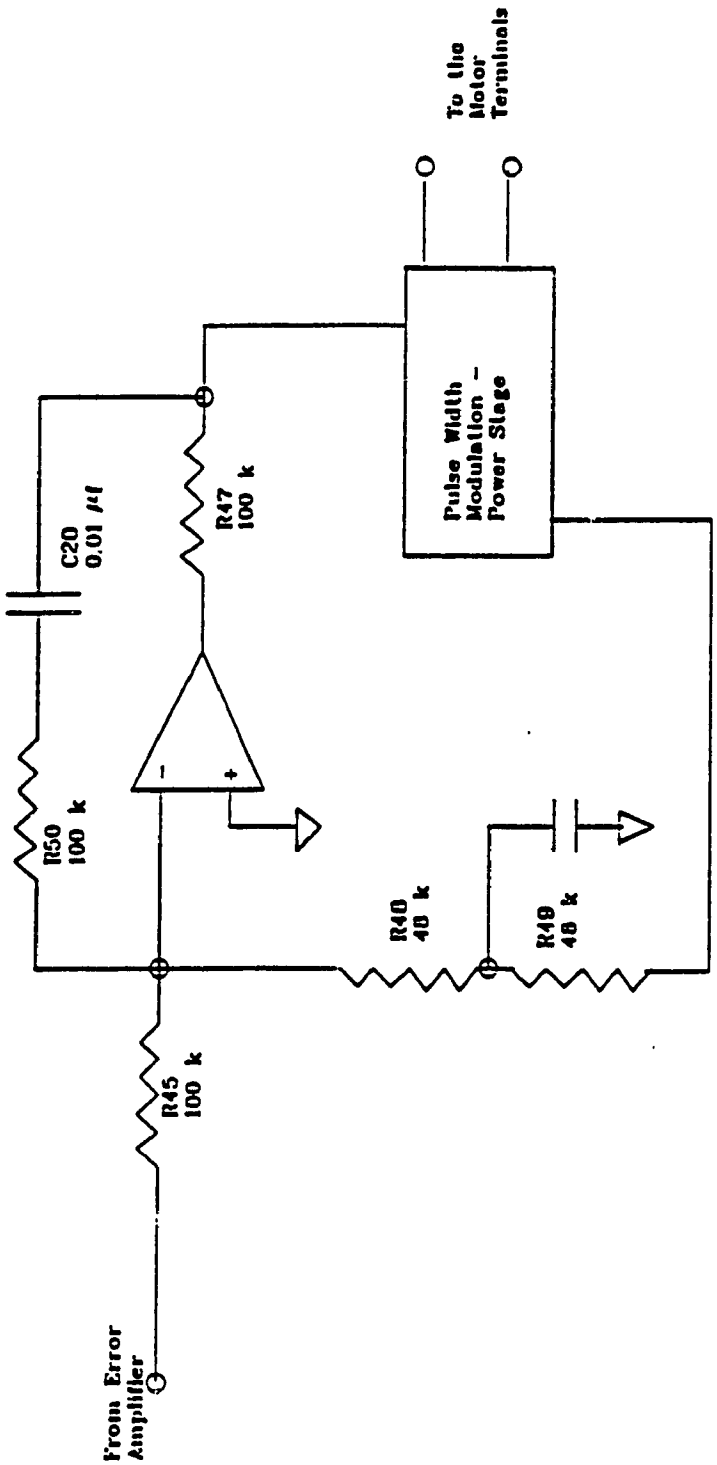

Fig. 8.4 Schematic of a Servo Amplifier in Current Mode [41]

and for every servoloop (driving (velocity mode) or steering (position mode)) they have to be properly tuned to get satisfactory performance. The chip accepts 5V TTL quadrature signals (A and B) and index pulse (I) from an incremental encoder. The above signals can be directly connected to the chip.
Because of the quadrature signal (see Fig. 8.6), the resolution of the counting is multiplied by four (4) as compared to the number of pulses per revolution of the encoder disk.

The motion controller has a trapezoidal trajectory generator (Fig. 8.7) which can be programmed by the user. All trajectory parameters are 32-bits values. Velocity and acceleration are positive values while position has a sign bit as well. The position and velocity values can be changed while the motion is executed but the acceleration can not be changed.

The code values of the position count that has to be loaded to the chip is [41,126-127]:

$$DP = SR * Desired\ \ Wheel\ \ Revolution * GR \qquad (8.2)$$

where DP is the desired position in encoder counts, SR is the system resolution which is equal to encoder resolution (* 4 if quadrature encoder is used) and GR

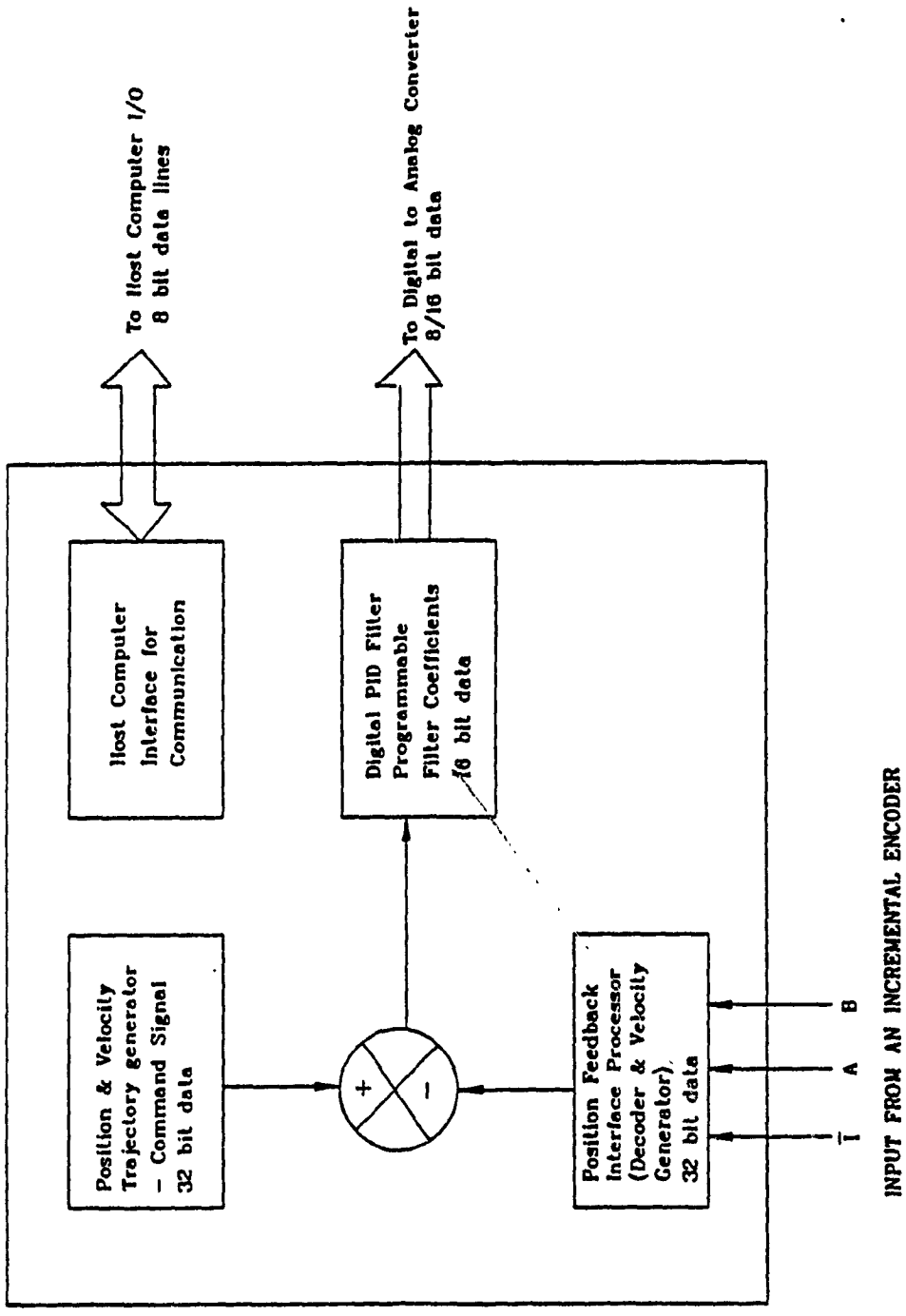

Fig. 8.5 Elements of the LM628 chip

(Courtesy of Rajagopalan[41])

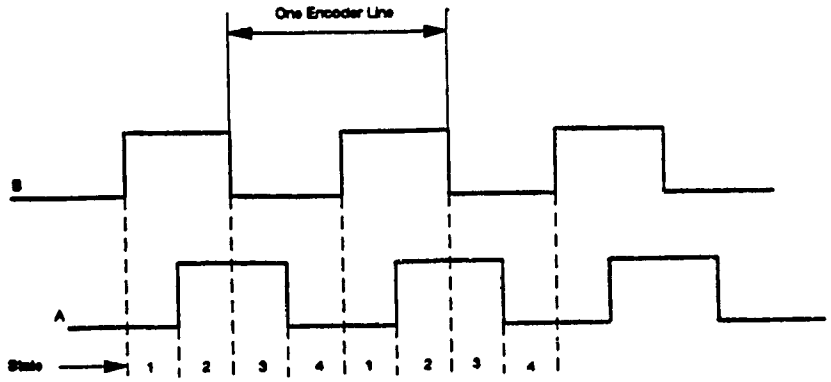

Fig. 8.6 Quadrature Signal Output of an Incremental Encoder

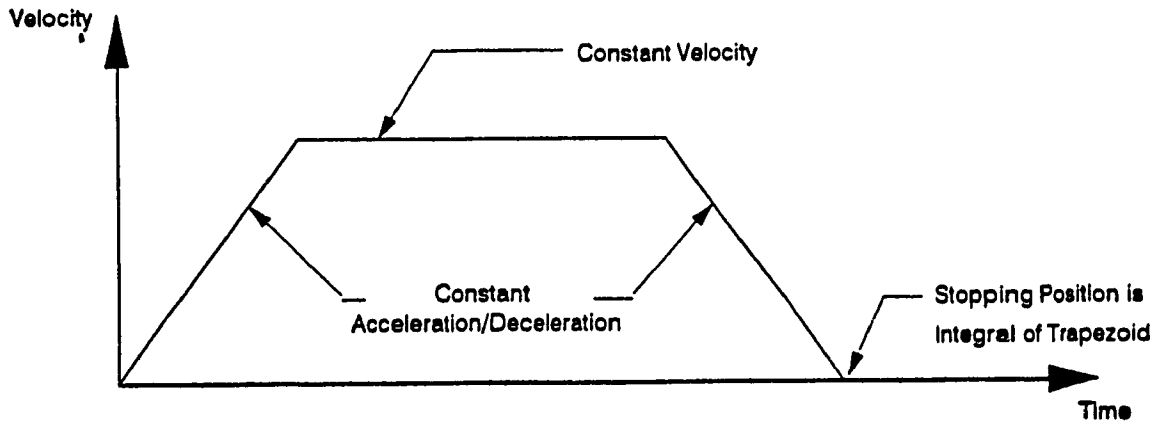

Fig. 8.7 LM628 Trajectory Generator Velocity Profile
(Courtesy of Rajagopalan[41])

is the gear ratio between the motor and the wheels. The encoder resolution for the driving and steering motors are 1024 and 256 counts per encoder revolution respectively and therefore, the System Resolution (SR) are 4096 and 1024 counts per encoder revolution for driving and steering motors respectively. The coded value of the velocity V(coded) is given by:

$$V(coded) = SR * \delta t * CF * GR * Desired\ Wheel\ rpm * 65536 \quad (8.3)$$

where δt is the sampling time of the chip (341 μs for 6MHz clock), CF is the conversion factor from minutes to seconds, (65536) is to adjust for the fractional part of the velocity data after conversion to counts per sample. The acceleration (coded) is computed from:

$$A(coded) = SR * \delta t * \delta t * Desired\ Acceleration * GR \quad (8.3)$$

More explanations regarding the layout of the interfacing board, operation, functions, commands, etc. of the LM chip as well as more technical details of the amplifier are provided in Appendix F [126-127,41-42].

8.5 Power and Data-Acquisition System

The power system of CONCIC III provides power (by using a dc to ac

invertor) for the host computer and the servo amplifiers. The power is derived from two 12 Volts dc batteries rated at 75 Amp hrs. There are provisions to charge the batteries whenever required and also push botton are provided for power on/off of the motor, computer and monitor.

An on-board data acquisition system and timer have been designed and implemented in the vehicle to monitor the motor current and the torques as well as the angular velocities of the motors. The information are employed in driving the simulation of the various dynamic models and control algorithms used for path following of the vehicle. The conditioning circuitries are also provided to filter out the noise that may be present in the analog signals. The signals are converted to digital by using a 12-bits analog to digital convertor (ADC). The timer 8254 is programmed to generate the interrupts (interrupt 3 of the host computer is used) at the desired sampling time.

More explanations regarding the layout of the power system and data acquisition system can be found in Appendix F.

8.6 System Software

The system software of CONCIC III is modular such that any further enhancement is possible. The codes are developed in Borland TC compiler. The

system software which consists of several header files containing the parameters of the vehicle, the major supervisory program and more than 30 subfunctions called by the main or the other subfunctions. Besides the above subfunctions, there are some other functions that are developed for the purpose of simulating the motion of the vehicle by using the dynamic models and animation of the resulting motion.

8.7 Summary

In this chapter, a general description of the architecture of CONCIC III was given. The mechanical structure, driving and steering units, elements of the motion controllers as well as software specifications, power units and data acquisition system were explained. Specifications of the control components and low level servo control loops as well as the components of feedback loop were described.

CHAPTER 9

CONTROL OF CONCIC III PROTOTYPE VEHICLE EXPERIMENTAL RESULTS

The focus of this chapter is directed toward the experimental investigations of dynamic models and various control algorithms using CONCIC III vehicle whose structures and components were explained in the previous chapter. A nonlinear dynamic model is developed and its linearized version is also obtained. The latter has been used to design an optimal controller, for path following of the vehicle, that minimizes a quadratic measure of performance consisting of the integral of the errors (errors in position and orientation of the vehicle) and the inputs (steering angles of the front and rear). The controller has been implemented on the vehicle and its performance is studied through experimentations. The result of trajectory following of the vehicle obtained from simulation of the dynamic model is compared with the actual motion. This provides a basis for investigating both the accuracy of the model as well as the effectiveness of the controller. The linear model is compared with the original

nonlinear model and the validity of the assumptions made during the process of linearization are investigated. The experimental results are reported for different initial conditions, various paths and under some severe disturbances to show the performance of the controller. In addition, the controller is further improved by making advantage of the on line data obtained during the vehicle motion. In this regard, the control structure is revised by adding a feedforward action in its structure. A simple estimation scheme is used that approximately identifies the future motion of the vehicle from on-line collected data.

Since the design of the controller is based on the reduced order linear model, which is obtained by assuming the forward speed of the vehicle to be constant, a constant gain controller is unable to respond properly to the changes in forward speed. Therefore, a variable gain controller is designed which can adapt itself to such changes.

In the following section, development of a nonlinear dynamic model is described for this vehicle with fore-and-aft steering systems.

9.1 Nonlinear Dynamic Model of CONCIC III

For the vehicle under consideration (CONCIC III), the roll number is 0.15, which is considered to be low. Hence the 2-DOF model is quite sufficient. The

approach followed toward development of the dynamic models (both nonlinear and linear) is the same as in chapter 4. Therefore, the details of derivations are not explained here.

Fig. 9.1 shows schematically the free-body diagram of the vehicle, indicating the spatial arrangements of the 2 steered wheels (in the fore-and-aft position) and the 2 non-steered casters (left and right). U and W are the longitudinal and lateral axes (body axes). Equating force components in the two directions:

$$m(\dot{V}_u - V_w\Omega) = F_{Rf2}\cos\delta_{fw} - F_{Rf1}\sin\delta_{fw} + F_{Rr2}\cos\delta_{rw} - F_{Rr1}\sin\delta_{rw} - F_{cr}\cos\gamma_r - F_{cl}\cos\gamma_l \tag{9.1}$$

$$m(\dot{V}_w + V_u\Omega) = F_{Rf2}\sin\delta_{fw} + F_{Rf1}\cos\delta_{fw} + F_{Rr2}\sin\delta_{rw} + F_{Rr1}\cos\delta_{rw} - F_{cr}\sin\gamma_r - F_{cl}\sin\gamma_r \tag{9.2}$$

where V_u and V_w are the forward and lateral velocities of the vehicle (in its own frame) and Ω is the yaw rate of the vehicle about the vertical axis, m is the mass of the vehicle, F_{Rf1}, F_{Rf2}, F_{Rr1}, F_{Rr2} the reaction forces of the front and rear wheels, F_{cl}, F_{cr} the forces on the left and right casters, γ_l and γ_r the left and right caster

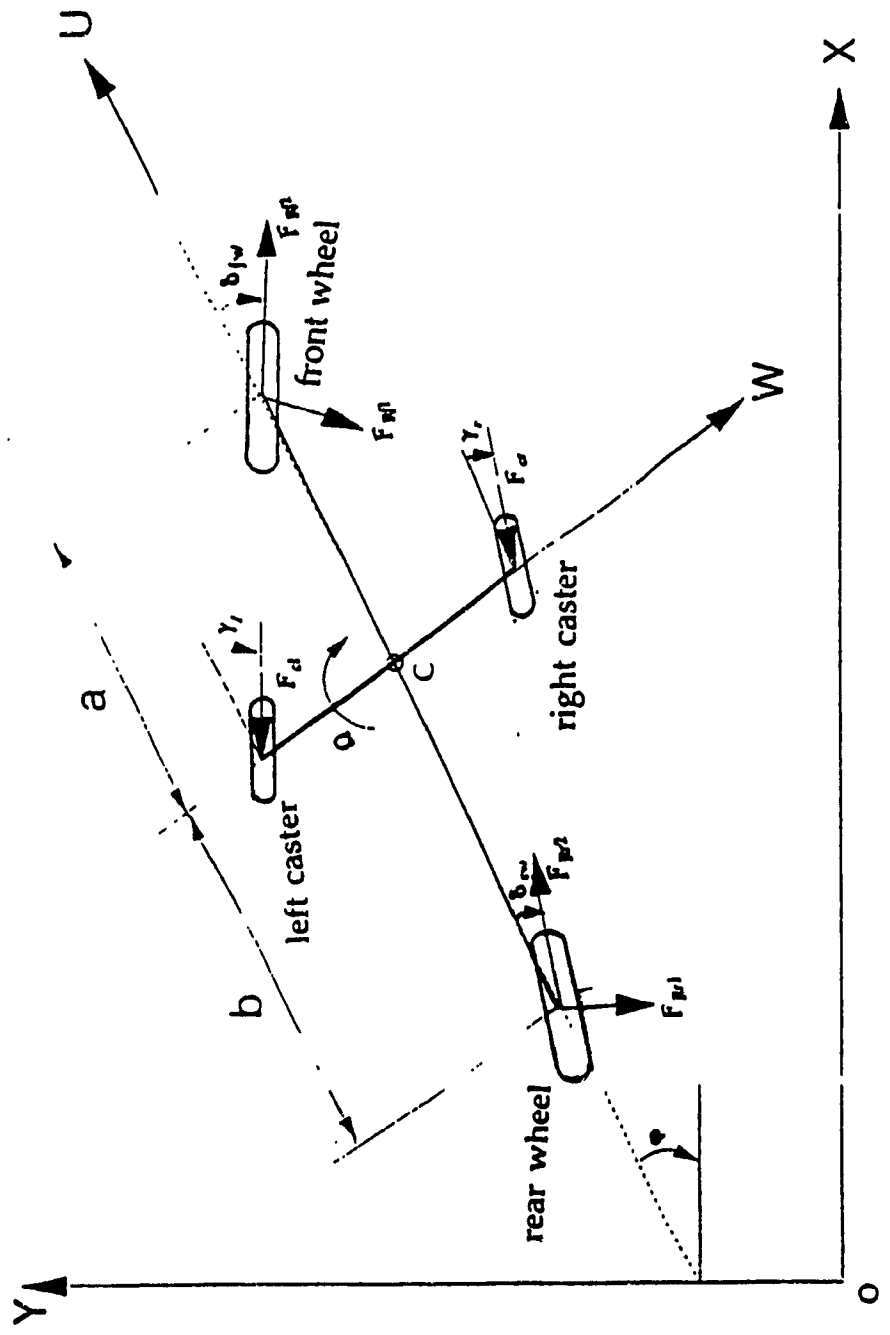

Fig.9.1 Freebody Diagram of the Vehicle

angles, and δ_{fw} and δ_{rw} the instantaneous steering angles of the front and rear wheels respectively.

Similarly, equating moments about the centre of mass of the vehicle gives:

$$I_z\dot{\Omega} = a(F_{Rf2}\sin\delta_{fw} + F_{Rf1}\cos\delta_{fw}) - b(F_{Rr2}\sin\delta_{rw} + F_{Rr1}\cos\delta_{rw}) - c(F_{cl}\cos\gamma_l - F_{cr}\cos\gamma) \quad (9.3)$$

I_z is the mass moment of the vehicle about a vertical axis through the centre of mass C (perpendicular to U-W) , and a and b the distance between the front and rear wheels to the centre of mass (Fig 9.1). The difference between equations (9.1) to (9.3) with the similar ones in chapter 4 is the inclusion of the effect of casters. The expressions for the forces and moments acting on the wheels as well as the equations are the same as in chapter 4 (see Fig.4.3) and they will not be repeated here. Also, development of the linear model and the assumptions involved are the same as in chapter 4.

9.2 Implementation of the Optimal Controller

The linear dynamic model of the vehicle can be represented in state space format (including error equations) as:

$$\dot{x} = Ax + Bu \quad (9.4)$$

where

$$x^T=[\epsilon_d \;\; V_w \;\; \Omega \;\; \epsilon_\theta] \tag{9.5}$$

$$u^T=[\delta_f \;\; \delta_r] \tag{9.6}$$

and with the parameters of the vehicle (for a constant forward speed of 0.5 m/sec) given in Appendix B, A and B are:

$$A=\begin{bmatrix} 0 & 1 & 0 & 0.5 \\ 0 & -88.9 & 2.6 & 0 \\ 0 & 28.8 & -104.6 & 0 \\ 0 & 0 & 1 & 0 \end{bmatrix} \tag{9.7}$$

and

$$B=\begin{bmatrix} 0 & 0 \\ 22.2 & -22.2 \\ 65.7 & 80.1 \\ 0 & 0 \end{bmatrix} \tag{9.8}$$

Typical values of the "velocity constant" and "yaw number" for this vehicle are -88.9 and 1.05 (for V_U=0.5 m/s) showing that the poles (open loop) associated with lateral and yaw velocities are close to each other (since yaw number is close to unity) and far from imaginary axis due to large value of velocity constant. Therefore, the system can be decoupled into two fast and slow subsystems where the slow modes corresponds to resulting errors namely position and orientation

errors of the vehicle.

The eigenvalues of the open loop plant matrix A are:

$$\lambda_{1,4}=0.0,0.0$$
$$\lambda_{2,3}=-89,\ -105 \tag{9.9}$$

and with the choice of matrix P (transformation matrix similar to equation (7.31)) as:

$$P=\begin{bmatrix} 2.0 & 0.0225 & -0.0002 & 0 \\ 0 & 0 & -0.0095 & 0 \\ 0 & -0.0112 & 0.0004 & 0 \\ 0 & 0 & 0.0095 & 1 \end{bmatrix} \tag{9.10}$$

whose columns are the eigenvectors of A, the slow subsystem obtained from this transformation is in the form of:

$$\dot{z}_{1,4}=\begin{bmatrix} 0 & 1 \\ 0 & 0 \end{bmatrix} z_{1,4}+\begin{bmatrix} 0.49 & 0.52 \\ 0.63 & -0.76 \end{bmatrix}\begin{bmatrix} \delta_f \\ \delta_r \end{bmatrix} \tag{9.11}$$

With the choice of Q and R matrices as:

$$Q=\begin{bmatrix}6 & 10\\ 10 & 17\end{bmatrix}\ ,\ R=\begin{bmatrix}1 & 0\\ 0 & 3\end{bmatrix} \tag{9.12}$$

the gain matrix (K) resulting from the solution of Ricatti equations (similar to equation (7.38)) is:

$$K=\begin{bmatrix}3.4 & 2.6\\ 2.6 & 2.3\end{bmatrix} \tag{9.13}$$

and the following control law is obtained:

$$\begin{bmatrix}\delta_f\\ \delta_r\end{bmatrix}=\begin{bmatrix}2.3 & 1.7\\ 0.8 & 0.9\end{bmatrix}\begin{bmatrix}\epsilon_d\\ \epsilon_\theta\end{bmatrix} \tag{9.14}$$

With this control law, the eigenvalues of the slow subsystem (closed-loop system) are at (-0.32 and -0.87). The closed-loop poles of the original model corresponding to the fast mode are at (-88.2 and -104.6) as compared to (-89 and -105); this suggests that the eigenvalues of the fast mode subsystem are not sensitive to this order reduction.

9.3 Experimental Results

The path to be followed by the vehicle can be specified in various ways, including real-time path generation using binary camera and tape, free ranging CCD camera, ultrasonic arrays, and others. The objectives of this experimental study is to investigate the performance of the optimal controller through experimentation, validations of the dynamic models (both nonlinear and linear models) and their comparison as well as verification of the assumptions made in their derivations and finally further possible improvements on the controller. The technique used to identify the path or the errors is not the concern of this experimental investigation. For the purpose of this study, "dead reckoning control" is used which is adequate to study the above issues; however, one should notice that this scheme (dead reckoning) suffers from accumulated error. The information about the path profile is stored in the memory of the on-board computer as a data file, containing the coordinates of the knot points. The cubic spline technique is employed to link the knot points by a smooth curve, as in robotic control [129,130].

The block diagram of the controlled system is shown in Fig. 9.2. As it is shown in this figure, the resulting errors, namely ε_d and ε_θ, are used by the optimal controller to generate the command signals to the steering motors of the front and rear wheels and the angular velocities of the front and rear wheels are calculated accordingly. The posture of the vehicle is calculated in real time according to the data obtained from the encoders of the steering and driving

motors. The new position and orientation of the vehicle are fed back and compared with the desired trajectory and accordingly, the new control signals are generated. Performance of the vehicle is tested for various initial conditions, different trajectories and under disturbances. Samples of the results are presented here. Figs.(9.3.a-9.3.f; 9.3.f inclusive) and (9.4.a-9.4.d; 9.4.d inclusive) show the results for straight line trajectory when the initial offset and orientation errors are (0.3,0.0) and (-0.3,0.5), respectively. Figs.(9.3.a-9.3.b) and (9.4.a-9.4.b) show the variations of the errors with time. It is seen that in both cases the initial errors converge to zero in a stable manner. Control action was applied after the vehicle reached a desired speed (0.5 m/s) as observed from Figs.(9.3.e-9.3.f). As well, while the steering angles of the front and rear wheels are relatively large at the beginning (due to large values of initial errors), they decay to zero as the errors are diminished (Figs.9.3.c-d & 9.4.c-d).

As an example of path following of the vehicle, Fig. 9.5.a shows a plot of the desired path juxtapositioned with the actual path covered by the vehicle, the control signals being generated on-line from a given data file of knot points. It is seen that the strict application of this control law (equation 9.14) results in some accumulated errors in the path of the vehicle, although by and large the vehicle does follow the desired path quite accurately. It should be pointed out that there is no external independent means of determining the displacement and orientation errors of the vehicle at any time. The time series of the control signals

are recorded and later used as driving inputs of numerical dynamic simulation of the CONCIC III. The result of the simulated path compares well with the actual path (see Fig. 9.5.b) indicating that the dynamic formulation and the values of the pertinent parameters that are included in the model are valid.

Also included are Figs.(9.5.c-9.5.n; 9.5.n inclusive) the time histories of the other variables corresponding to the above trajectory as follows: Fig 9.5.c & 9.5.d -- steering angle, front and rear; Fig 9.5.e & 9.5.f -- angular speed, front and rear; Fig 9.5.g & 9.5.h -- instantaneous slip angles of the front and rear wheels; Fig 9.5.i & 9.5.j -instantaneous forward velocity and lateral velocity of vehicle; Fig 9.5.k & 9.5.l -- instantaneous yaw rate and vehicle orientation; Fig 9.5.m & 9.5.n -- instantaneous steering angles. All recordings are sampled at 100 Hz. It can be appreciated (see Fig 9.5.c to 9.5.f) that the servo control follows the command signals very well, after an initial period of transient errors. It is also noticed that for larger command (angles), the actual angles delayed more from the command.

Figs.9.5.g and 9.5.h, illustrating the instantaneous slip angle of the front and rear wheels, confirm that the assumption invoked in the dynamic model (that slip angle not exceeding 4° in magnitude) is not violated during the test run. Comparing Fig. 9.5.c with 9.5.g (and Fig. 9.5.d with 9.5.h) it is observed that during the transition period the slip angle increases to a maximum, while maintaining a low value at other times.

It is observed that the lateral velocity and the yaw rate (Fig 9.5.j-9.5.k) attain their maximum at a time (approximately 3.8 s) when the desired trajectory features a relatively sharp curvature. As a result, a larger steering angle is required to follow the path.

It is observed that at the beginning of every updated command, the current of the steering motors reach a peak value, during which time there is little motion of the motor (dead zone). The current then drops rapidly as the motion resumes (see Figs.9.5.m-9.5.n). This nonlinear phenomenon (so called stick-slip or hunting) can be attributed to the stiffness and inertia properties of the wheels and their interaction with the contact surface. During the course of experimentation, it was observed that at zero velocity, the dead zone is more pronounced. Typical result is shown in Fig. 9.6.

9.4 Comparisons of the Nonlinear and Linear Models

Noting that the linear model is a simplified approximation of the nonlinear model (based on the assumption as stated), it is useful to check for its accuracy as well as the assumptions involved. With the same sampling frequency (100 Hz), the time series of the control signals are recorded and are used as the inputs to the linear dynamic model after the vehicle has reached the desired speed (0.5 m/s). Fig. 9.7.a shows the resulting trajectory of the two models. It is seen that

the linear model is quite acceptable to represent the more complex nonlinear model. Comparison of the trajectories obtained from the nonlinear and linear models (see Figs.9.7.a) and the actual trajectory (see Fig.9.5.a (measured path)) reveals that the nonlinear model is closer to the path followed by the vehicle. Also included are the set of Figs.(9.7.b-9.7.d) illustrating the comparison of time histories of other variables for linear and nonlinear models corresponding to the above trajectory. These are recorded as follows: Fig 9.7.b & 9.7.c – instantaneous slip angles of the front and rear wheels; Fig 9.7.d &9.7.e – instantaneous lateral velocity and yaw rate of vehicle and Fig 9.7.f -- vehicle orientation. Referring to Figs.9.7.b-9.7.c, it is seen that the resulting slip angles of the front and rear wheels while having the same dynamic pattern as the nonlinear model, are well below four (4) degrees as it was the assumption in the derivations of the linear model. As well, from Figs.9.7.d-9.7.e, it is seen that the other variables such as lateral velocity and yaw rate obtained from the two models are also compatible.

The performance of the system is tested for different trajectories. Typical results are shown in Figs.(9.8.a-9.8.f; 9.8.f inclusive). The desired trajectory and the actual trajectory ("reconstructed path", whose derivation are explained in Appendix G) are shown in Fig. 9.8.a. It is seen that strict application of the optimal controller results in undershoot as well as a steady state error . By noting that in derivation of the optimal controller, the trajectory was assumed to be a straight line which suggest that this controller may not compensate for the errors

produced due to path curvature. Therefore some minor modifications are necessary to achieve a better performance (for straight line trajectory, as it was observed from the results (Figs.9.3.a-b & 9.4.a-b), the errors both in position and orientation are totally removed). Fig. 9.8.b illustrates the path following of the vehicle relative to desired trajectory which provides a better view for both relative position and orientation. It is seen that the vehicle by and large follows the trajectory with a proper orientation. Also presented are the variations of steering angles of the front and rear wheels (Fig. 9.8.c-d) showing larger steering angles as required for more steering action at sharper parts of the trajectory. The results are obtained for constant forward speed of the vehicle (0.5 m/s) which was assumed in all derivations of the optimal controller.

The control structure was further revised and a feedforward action was introduced in the control structure (refer to the remarks in chapter 7). A simple estimation scheme was used to find the future position of the vehicle based on its current position. This was performed by assuming that the vehicle approximately moves forward with the same angle as that of the tangent to the desired trajectory. The estimation was employed in real time based on the data collected during motion. As a result, the future errors were estimated and they were used to revise the original optimal controller. As well, an integral action was introduced to remove the resulting steady state errors. The performance of the system for path following of the same trajectory under the same condition is

shown in Fig. 9.9.a and its posture relative to the desired path is illustrated in Fig. 9.9.b. The estimated path is also represented in Fig. 9.9.a showing improvement in performance of the vehicle as well as relative accuracy of the employed estimation technique. Also presented are Figs.9.9.c-d showing the required steering angles of the front and rear wheels. Fig. 9.9.e illustrates the followed trajectory of the centre of mass of the vehicle measured from the floor and its comparison with the reconstructed path (obtained from the on-line data obtained from the encoders of the front and rear steering and driving motors). It is observed that as the vehicle moves forward, while following the desired trajectory, it suffers from accumulated error due to the dead-reckoning technique used in trajectory generation. It should be noticed that no external sensor is used to update the errors.

An example of path following of the vehicle for another trajectory is shown in Fig. 9.10.a with the corresponding posture of the vehicle and the desired trajectory (Fig. 9.10.b). It is seen that the vehicle is able to follow the trajectory successfully without considerable error. The forward speed of the vehicle throughout the motion was kept the same as in derivation of the optimal controller (0.5 m/s). Also presented are the required steering angles of the front and rear wheels (Figs.9.10.e-f) according to path curvature.

9.5 Performance under Disturbances

There are some disturbances introduced in the system during the motion of a vehicle. The examples of disturbances are the irregularity in the surface of ground (rough or smooth), the condition of the surface (wet, dry, etc.), tire condition (nonuniformity), variations in payload, etc. Such disturbances certainly affect the performance of the vehicle and therefore, it is desirable to see the performance of the system under existence of a disturbance that causes the changes in motion. For instance, during the motion the vehicle may slip because of sudden change in the surface condition or application of any external force. The performance of the system under this condition are presented in Figs.(9.11.a-9.11.b). As it is shown in Figs.9.11.a-b, at approximately 8.4 seconds suddenly the vehicle is intentionally drifted from its original path by giving it a side push. It is seen that the controller is able to compensate for this type of changes and after a transient period, the vehicle is on the desired path again. Also, presented in Figs.(9.11.c-9.11.d) are the variations of the front and rear wheel steering angles. As it is illustrated in the figures, at the time 8.4 seconds, the steering angles experience a sudden change required to compensate for the error and to bring back the vehicle to the desired trajectory.

9.6 Variable Gain Controller

In derivation of the linear model, it was assumed that the forward speed of the vehicle is kept constant throughout the motion. This assumption was made

in order to obtain a less complex model of the vehicle that helps in obtaining the control law. However, it is desirable to change the speed of the vehicle according to the path curvature, such that for sharper curves, the speed be reduced to prevent the slippage while for smoother trajectories it can go at higher speeds. Therefore, it is necessary to develop a scheme for this speed regulation as well as adjustment of the gains of the control law.

Consider a vehicle negotiating a curve (on a flat surface) with a forward speed of (V_u); if the frictional forces developed in the contact region of the tires and the ground are large enough to overcome the centrifugal force, the vehicle is able to move without any slippage; otherwise, it starts loosing the track. This criteria is employed as a basis for changing the speed. The following relations can be written between the components of frictional forces of the front and rear wheels and the centrifugal force:

$$M(\frac{V_u^2}{\rho}) = C_o(F_{cf} + F_{cr}) \tag{9.15}$$

where M and V_u are the mass and forward speed of the vehicle, ρ is the radius of the curve, C_0 is a coefficient for safety (less than one), F_{cf} and F_{cr} are the frictional forces of the front and rear wheels respectively, and are proportional to coefficient of friction and normal load of the tires.

Control gains are obtained from experimental data collected from the motion of the vehicle by running it at different speeds (within its speed range of operation) and accordingly finding suitable gains for a satisfactory performance on the floor. The results obtained are illustrated in Figs.(9.12-9.13). Although the variations of the gains with speed appear to be linear (approximately), this result may not be generalized for other systems. In that case, a type of curve fitting may be required. As a result, the following relations can be written between the gains and the speed:

$$\begin{aligned} K_1 &= 0.71 V_U + 1.95 \\ K_2 &= 0.36 V_U + 0.62 \\ G_1 &= 0.14 V_U + 1.13 \\ G_2 &= 0.11 V_U + 0.64 \end{aligned} \tag{9.16}$$

where

$$K = \begin{bmatrix} K_1 & G_1 \\ K_2 & G_2 \end{bmatrix} \tag{9.17}$$

corresponds to gains of the controller in control law (9.14).

The block diagram of the controlled system with feedforward and integral action as well as the variable gain optimal controller is shown in Fig.9.14. As it is shown, the data obtained from path curvature is used to adjust the speed as well as the gains of the controller according to equations (9.15) and (9.16) respectively. Also, the future position of the vehicle is estimated from its current position. The estimated error (obtained in real time) is used for further

adjustment of the steering angles.

The results of path following of the vehicle are shown in Figs.(9.15.a-h; 9.15.h inclusive). It is seen that the vehicle is following the path quite satisfactory. As an example, the corresponding speed of the rear wheel is also shown in Fig. 9.15.b. It is seen that as the vehicle is going through sharper curves, the speed is reduced while it speeds up for smoother segments of the desired trajectory. Variations of the steering angles of the front and rear wheels and the gains are also shown (Fig. 9.15.c-h; 9.15.h inclusive) which confirm the compatibility of the steering angles and the gains.

9.7 Remarks

As it was noticed in this chapter, the effects of steering dynamics was neglected in the formulation of the optimal controller. In this section, it is tried to investigate the effects of steering dynamics of the front and rear wheels on the performance of the controlled system. Typical step response of the steering system (see Fig. 9.6) suggests that it can be represented by (approximately) a first order system as (dynamic characteristics of the front and rear wheel steerings are quite similar) :

$$\begin{aligned} \dot{\delta}_{fw} &= -5.0\ (\delta_{fw} - \delta_f) \\ \dot{\delta}_{rw} &= -5.0\ (\delta_{rw} - \delta_r) \end{aligned} \tag{9.18}$$

where δ_{fw}, δ_{rw} are the instantaneous steering angles of the front and rear wheels and δ_f, δ_r are the control commands to the steering system, respectively. By substituting for (z_1, z_4) in equation (9.11) in terms of ε_d, ε_θ (similar to equation 7.42) and also using control law (9.14) and equation (9.18), the new state space representation of the controlled system (closed loop system) is obtained that takes

steering dynamics. The eigenvalues of the controlled system (steering dynamic included) are:

$$\lambda_{1,4} = (-0.98 \quad -0.27, \quad -3.7, \quad -5.2) \tag{9.19}$$

It is seen that the system is stable (as observed during the course of experimentation). Also, the dominancy of the poles are not greatly affected (compare the pairs (-0.98, -0.27) with (-0.87, -0.32) (see end of section 9.2) which are the eigenvalues of the closed loop system with and without steering dynamic effects, respectively). This result is valid just for the system under consideration (CONCIC III). If the time constant of the steering system is large, then the problem can be treated as explained in chapter 7 (see section 7.5).

9.8 Summary

In this chapter, a nonlinear dynamic model was developed to represent the motion of CONCIC III vehicle. The linearized version of this model was employed in design of an optimal controller for path tracking of the vehicle. This controller minimizes a quadratic measure of performance consisting of the integral of the errors (position and orientation) and the inputs (front and rear steering angles). The performance of the controller was investigated for various initial conditions for straight line trajectories and it was shown that by employing the optimal control law, the vehicle is able to correct its position and orientation in a stable manner. The accuracy of the models were verified by inputting the real time data acquired during the motion of the vehicle in driving the dynamic models. From the analytical results obtained from the solution of the nonlinear dynamic equations and those obtained from the actual motion followed by the vehicle, it appears that the model is quite accurate. As well, the assumptions made in derivation of the models (like the values of slip angles) were checked

and it was shown that they are not violated under the test conditions. A detailed comparison was made between the two models, namely nonlinear and linear model. From the results, it appears that the linear model is a good approximation of the nonlinear model under the conditions and the assumptions made for its derivation. The performance of the vehicle was tested for curved trajectories and it appeared that although by and large the vehicle is able to negotiate the curves within its physical limitations, however, for sharper curves it experiences overshoots (undershoots) and also some steady state error. These difficulties are overcome by adding a feedforward (to reduce the overshoots) and integral (to compensate for steady state error) action in the control structure. In order to implement the scheme (for feedforward action), a simple algorithm was adapted in real time to estimate the future motion of the vehicle from its current position from the data collected. The revised controller was tested for various trajectories and satisfactory performance of the vehicle in path following was observed. As well, the actual path of the vehicle measured from the floor was compared with the reconstructed path obtained from the encoder readings during the motion of the vehicle. The system was suffering from accumulative error due to dead reckoning technique employed for its trajectory generation. To improve the motion of the vehicle, a scheme was developed to adjust the speed of the vehicle as a function of curvature of the desired trajectory. By noting that one of the assumptions made in deriving the optimal control law was that the forward speed of the vehicle is kept constant, it is expected that the gains of the controller should be changed as a function of the speed. This problem is overcome by properly adjusting the values of the gains to get a satisfactory performance of the vehicle. It was observed that the variations of the gains with speed are quite linear with different slopes within the speed range of operation of the vehicle. However, this linear property may not be generalized for other systems and more study is needed. The satisfactory performance of the vehicle under variable speed control was experimentally investigated and the results were presented.

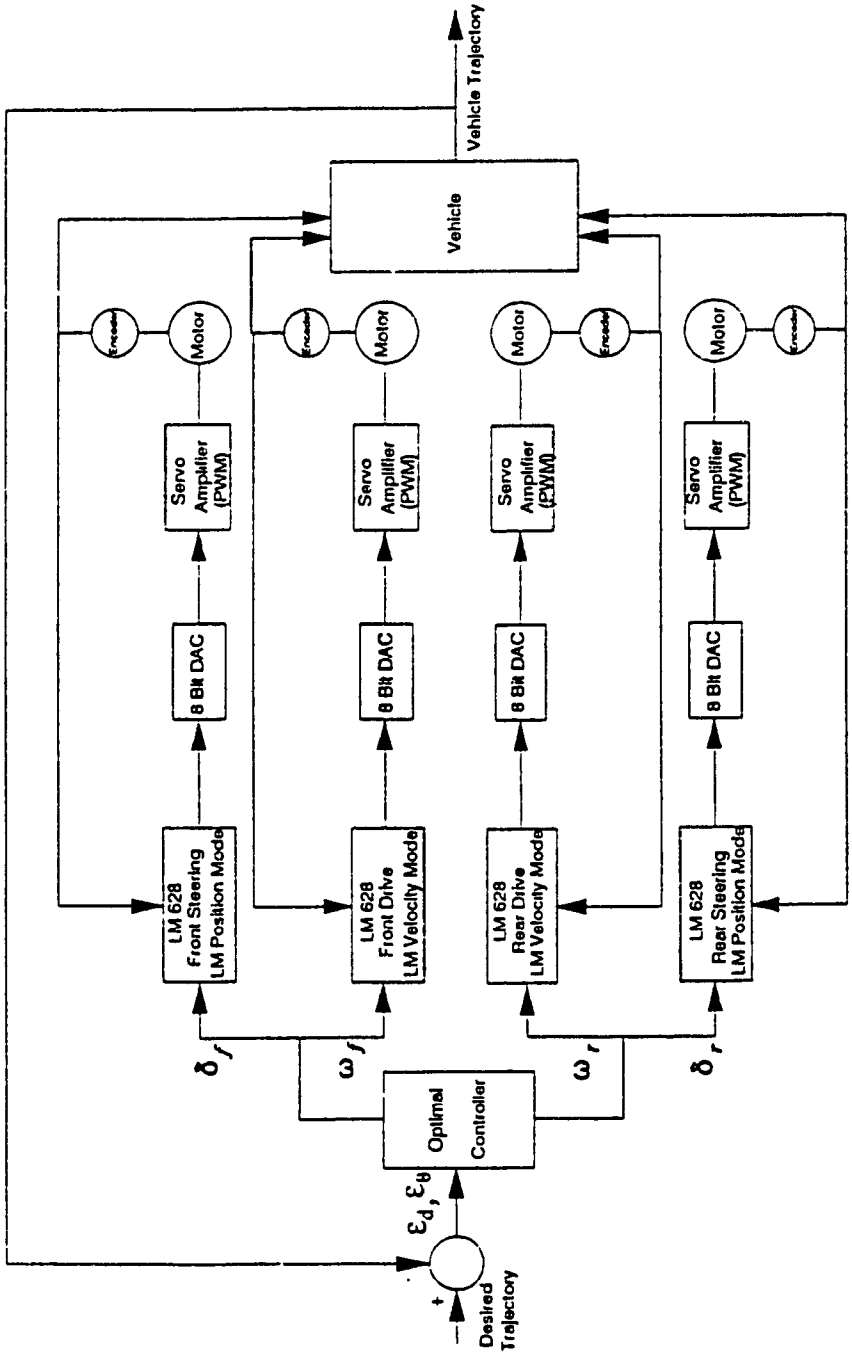

Fig.9. 2. Block Diagram of the Controlled System.

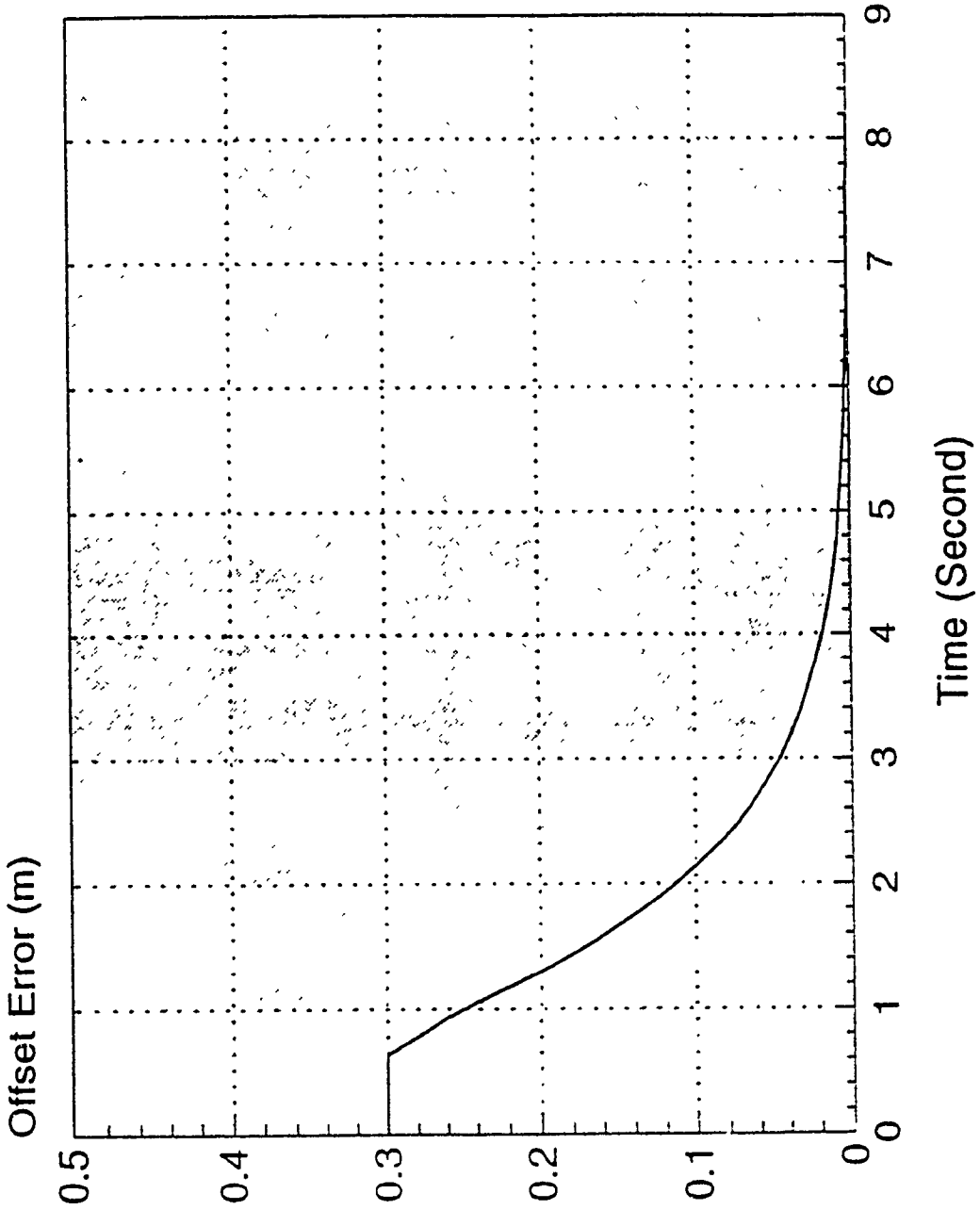

Fig.9.3.a Variations of Offset Error

Initial Conditions: ε_d=0.3 (m), ε_θ=0.0 (rad).

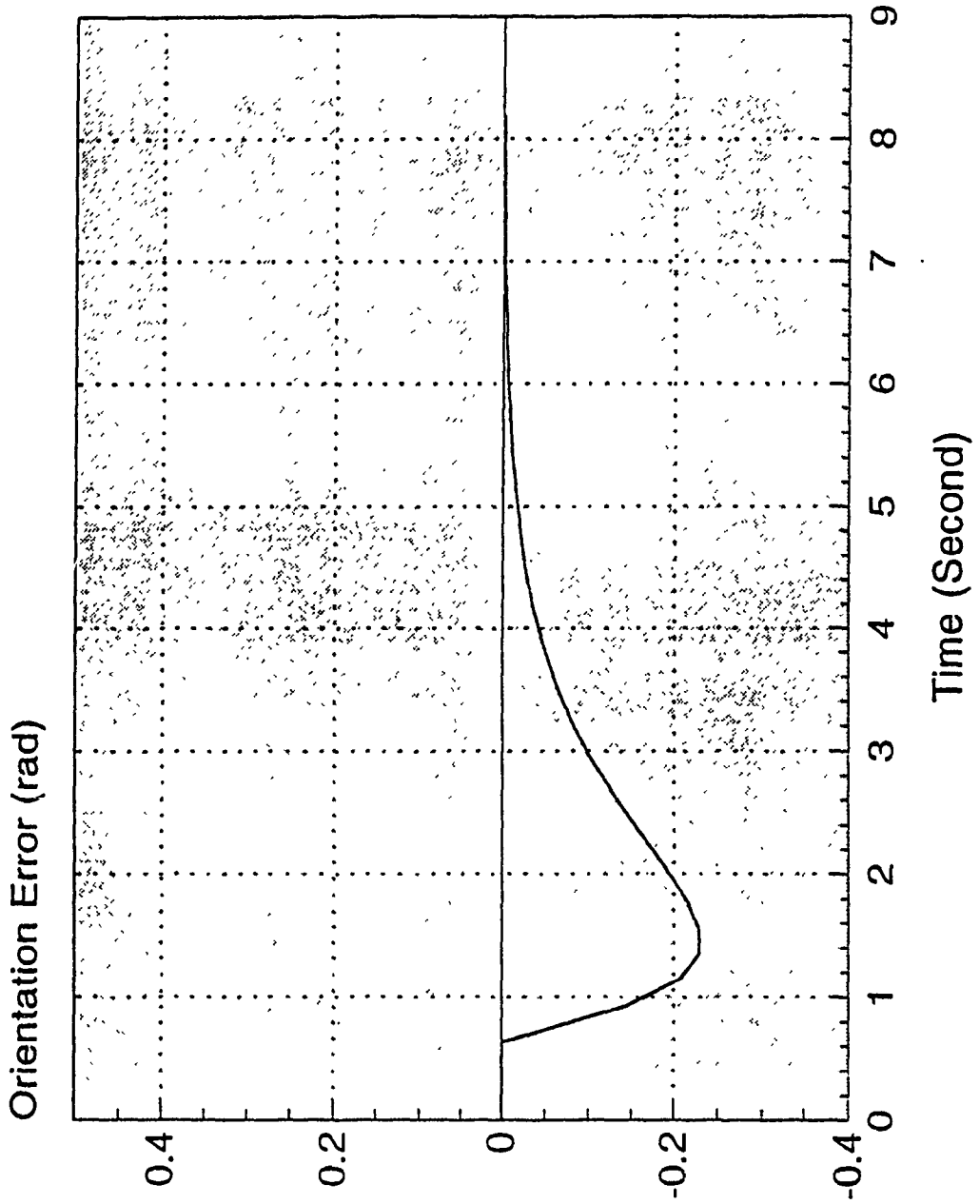

Fig.9.3.b Variations of Orientation Error

Initial Conditions: ε_d=0.3 (m), ε_θ=0.0 (rad)

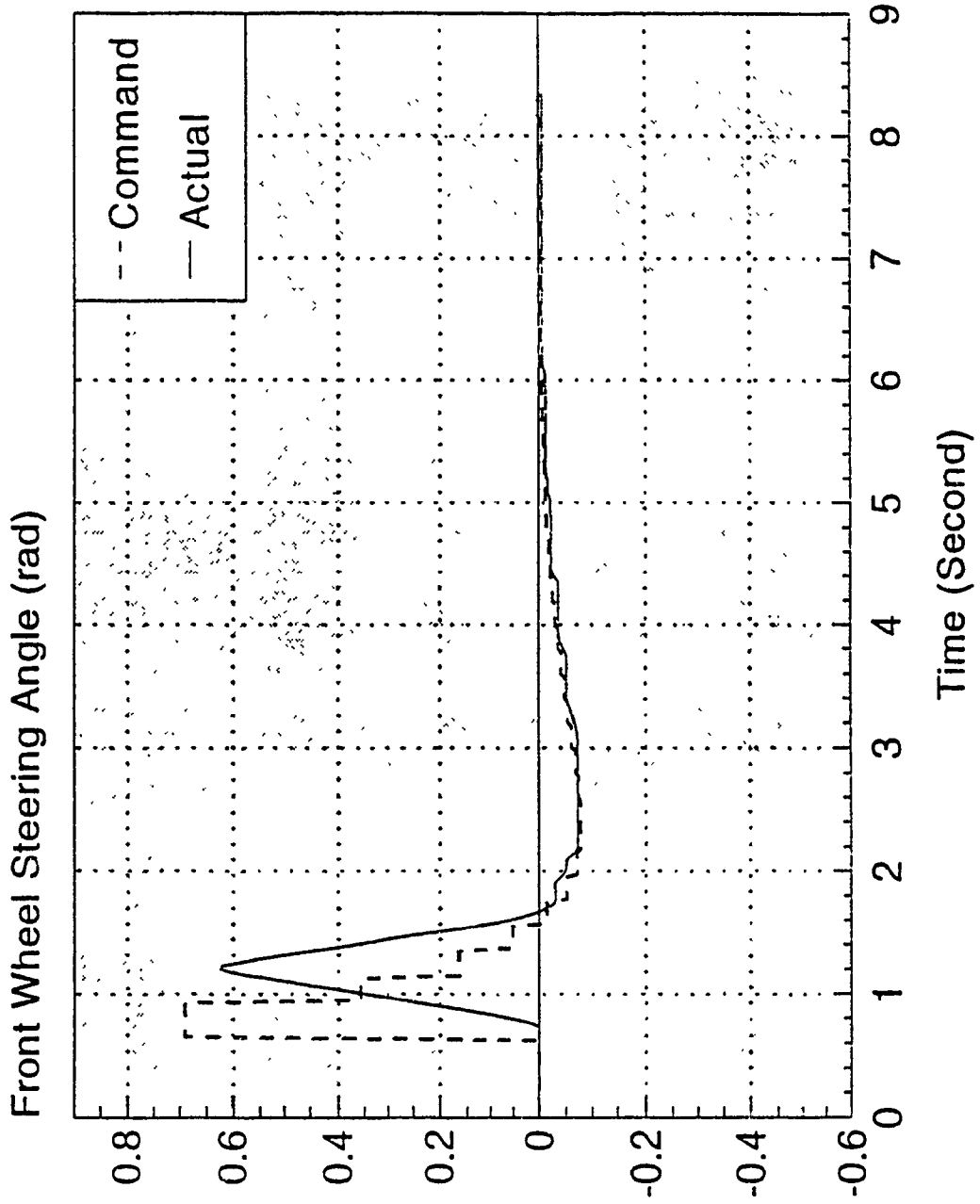

Fig.9.3.c Variations of Front Wheel Steering Angle

Initial Conditions: ε_d=0.3 (m), ε_θ=0.0 (rad)

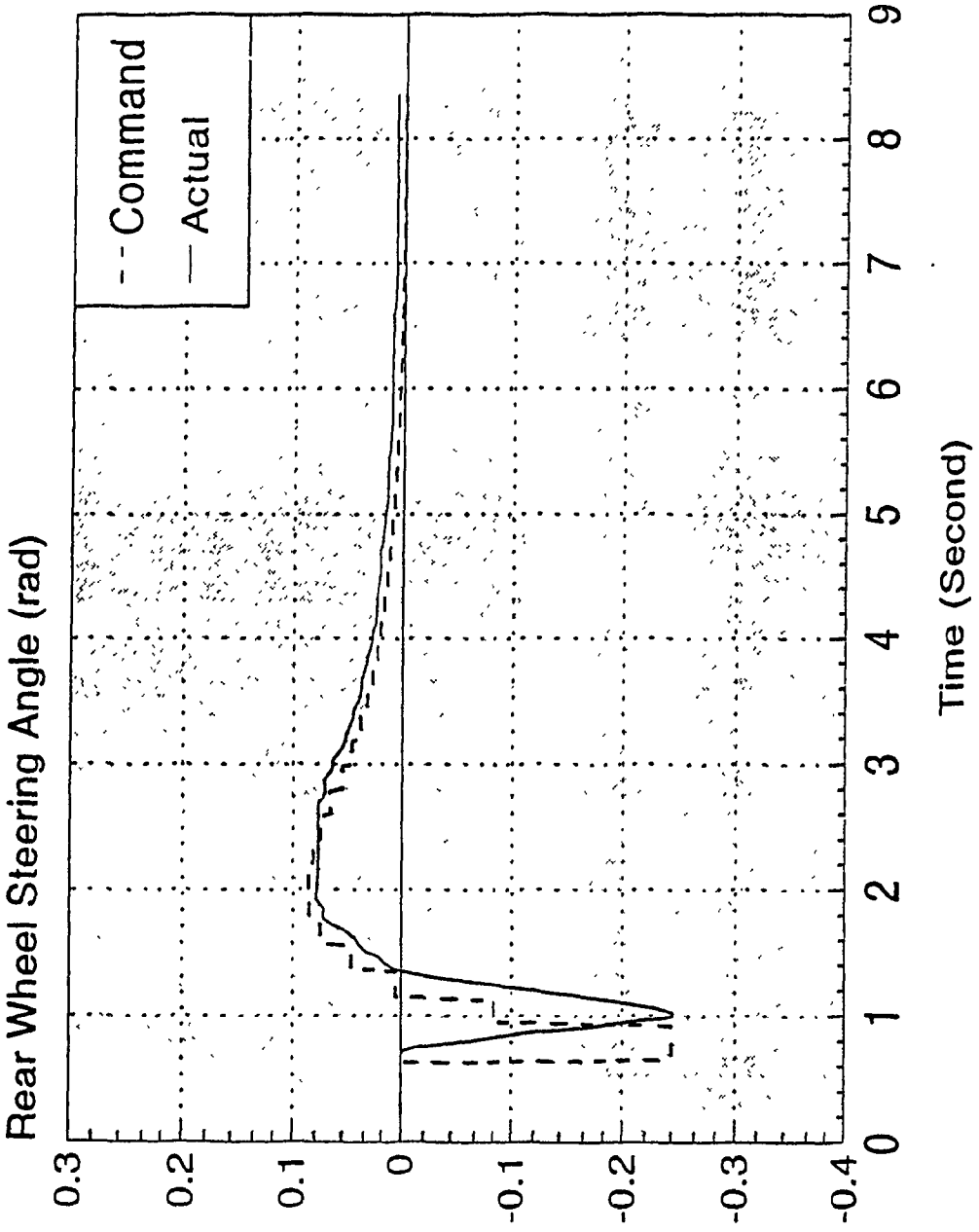

Fig.9.3.d Variations of Rear Wheel Steering Angle

Initial Conditions: ε_d=0.3 (m), ε_θ=0.0 (rad)

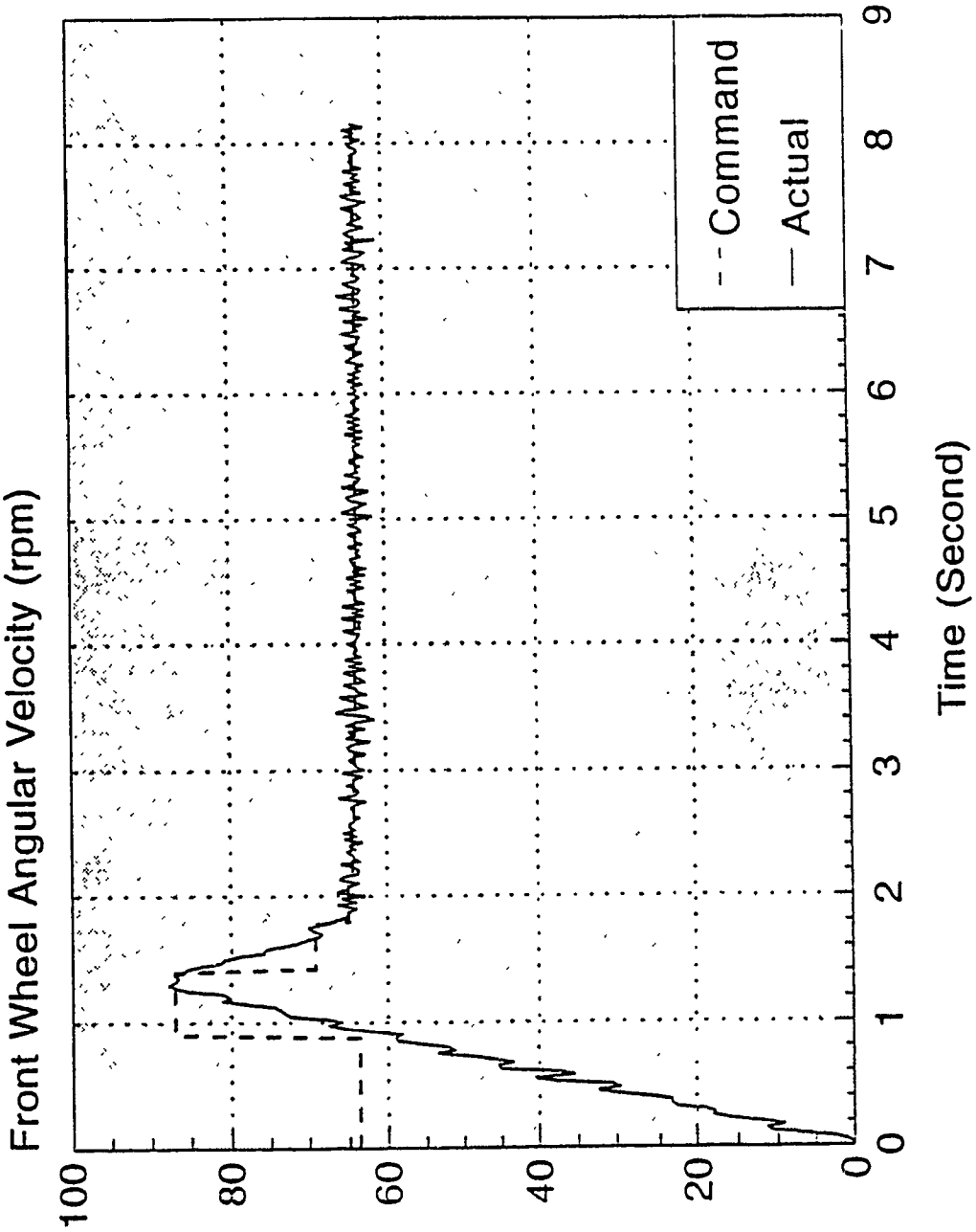

Fig.9.3.e Variations of Front Wheel Angular Velocity

Initial Conditions: ε_d=0.3 (m), ε_θ=0.0 (rad)

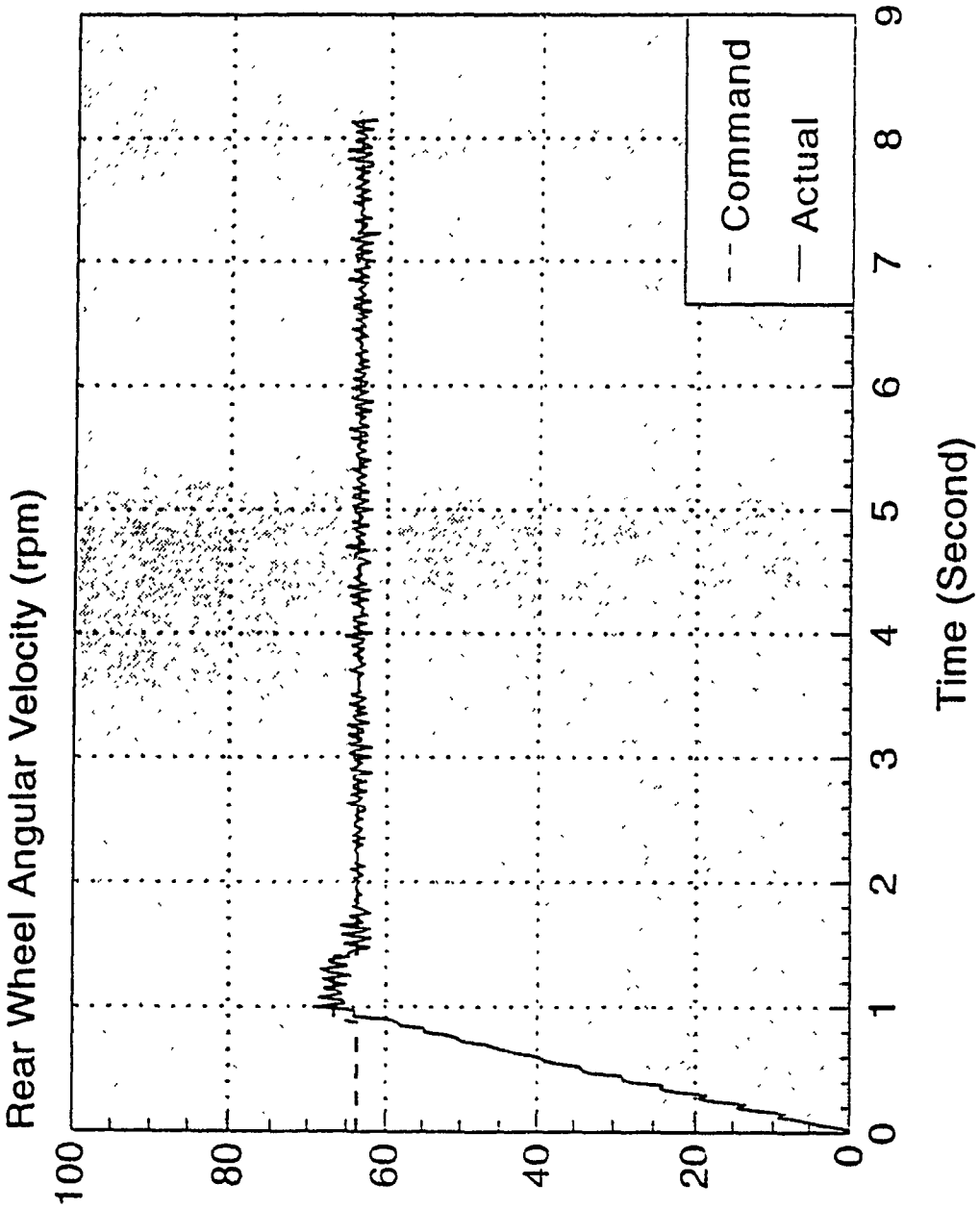

Fig.9.3.f Variation of Rear Wheel Angular Velocity

Initial Conditions: ε_d=0.3 (m), ε_0=0.0 (rad)

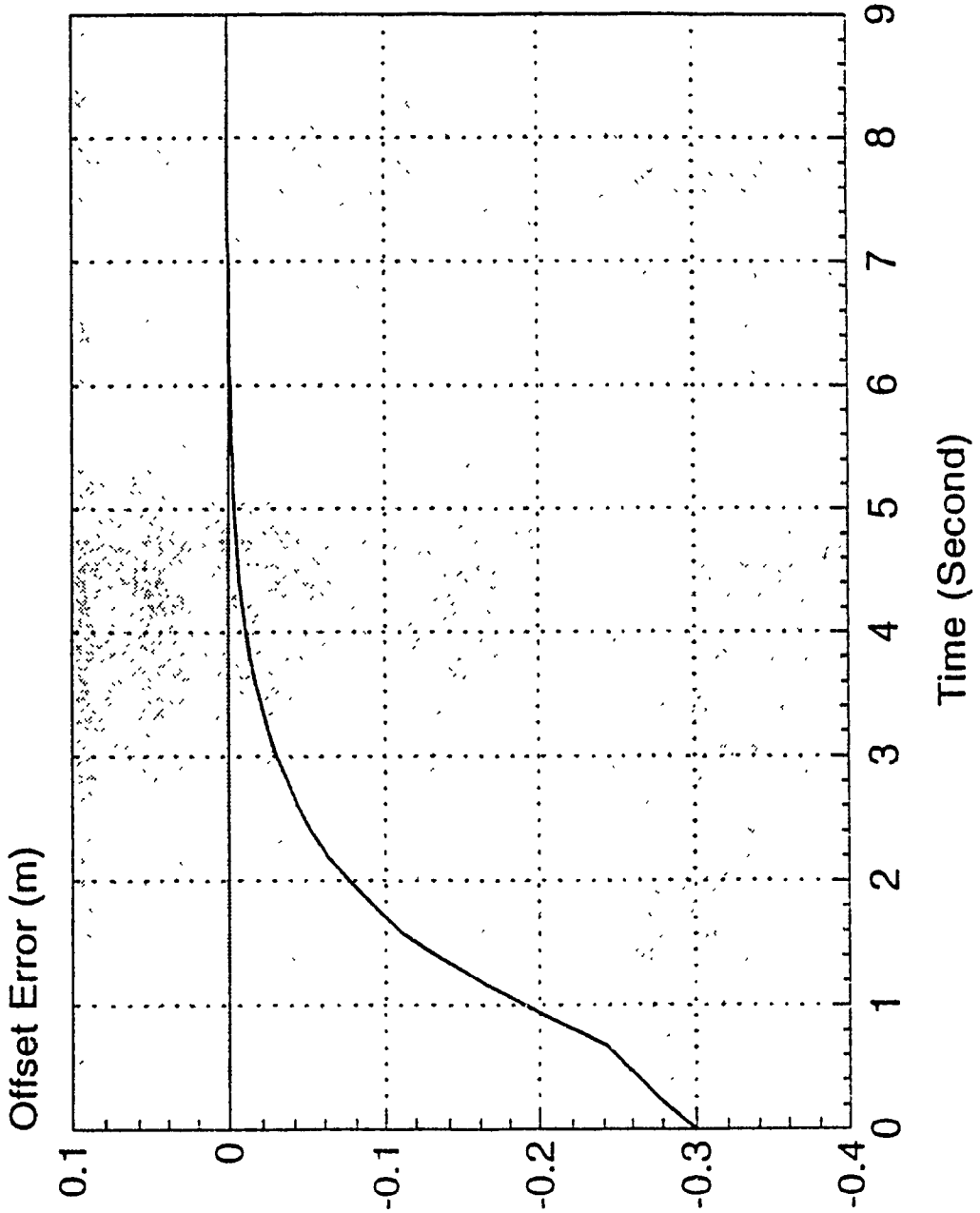

Fig.9.4.a Variations of Offset Error

Initial Conditions: ε_d=-0.3 (m), ε_θ=0.524 (rad)

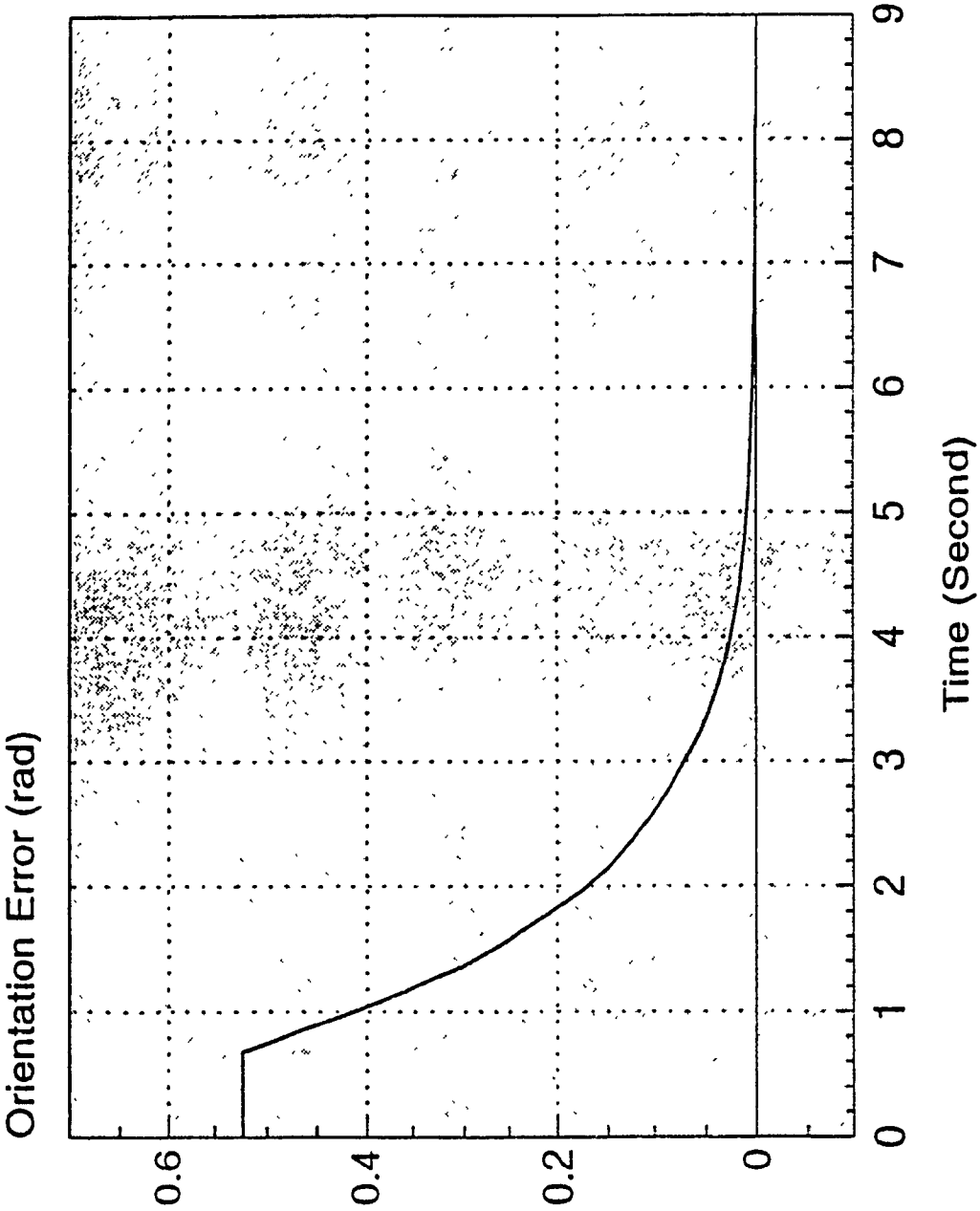

Fig.9.4.b Variations of Orientation Error

Initial Conditions: ε_d=-0.3 (m), ε_θ=0.524 (rad)

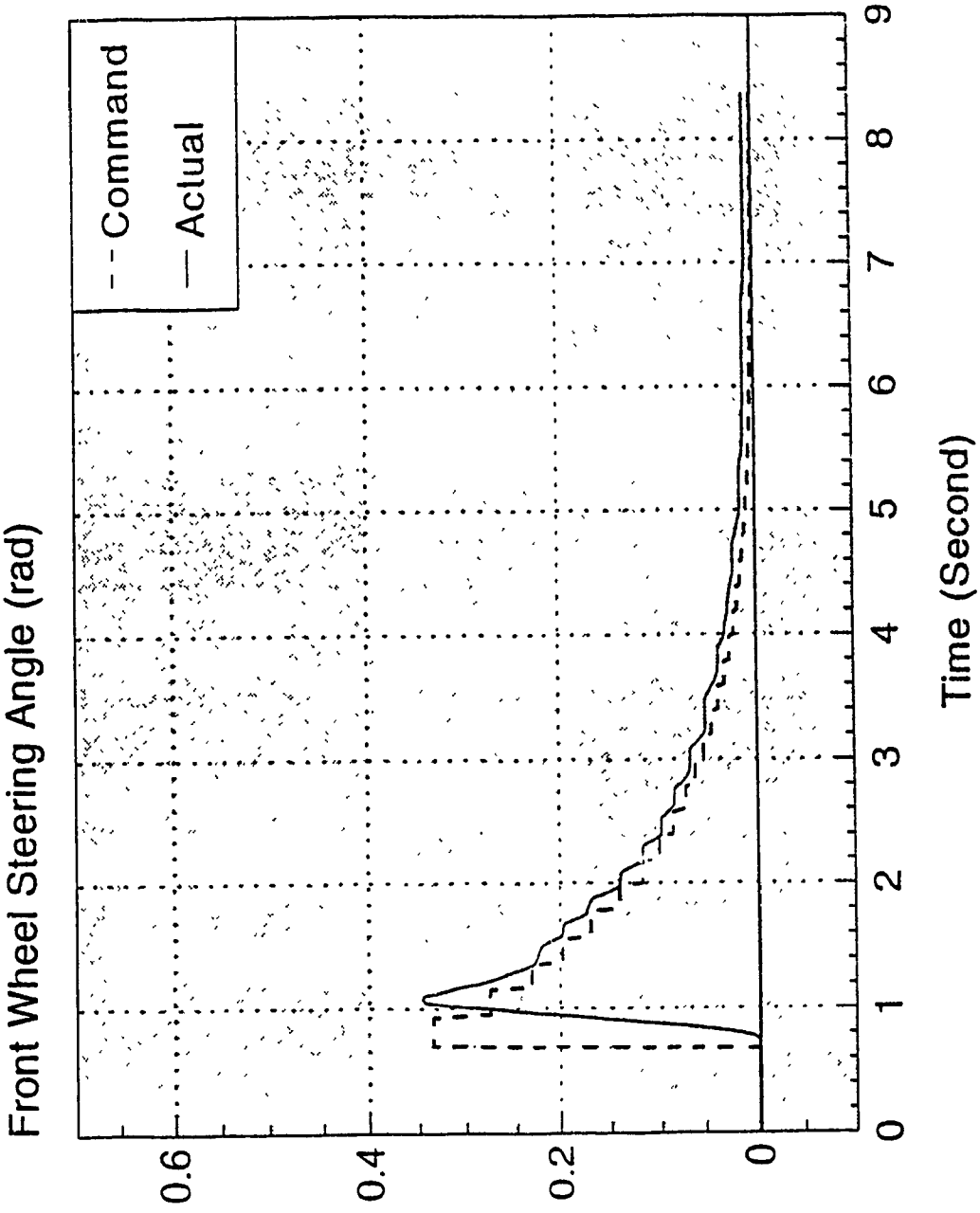

Fig.9.4.c Variations of Front Wheel Steering Angle

Initial Conditions: ε_d=-0.3 (m), ε_θ=0.524 (rad)

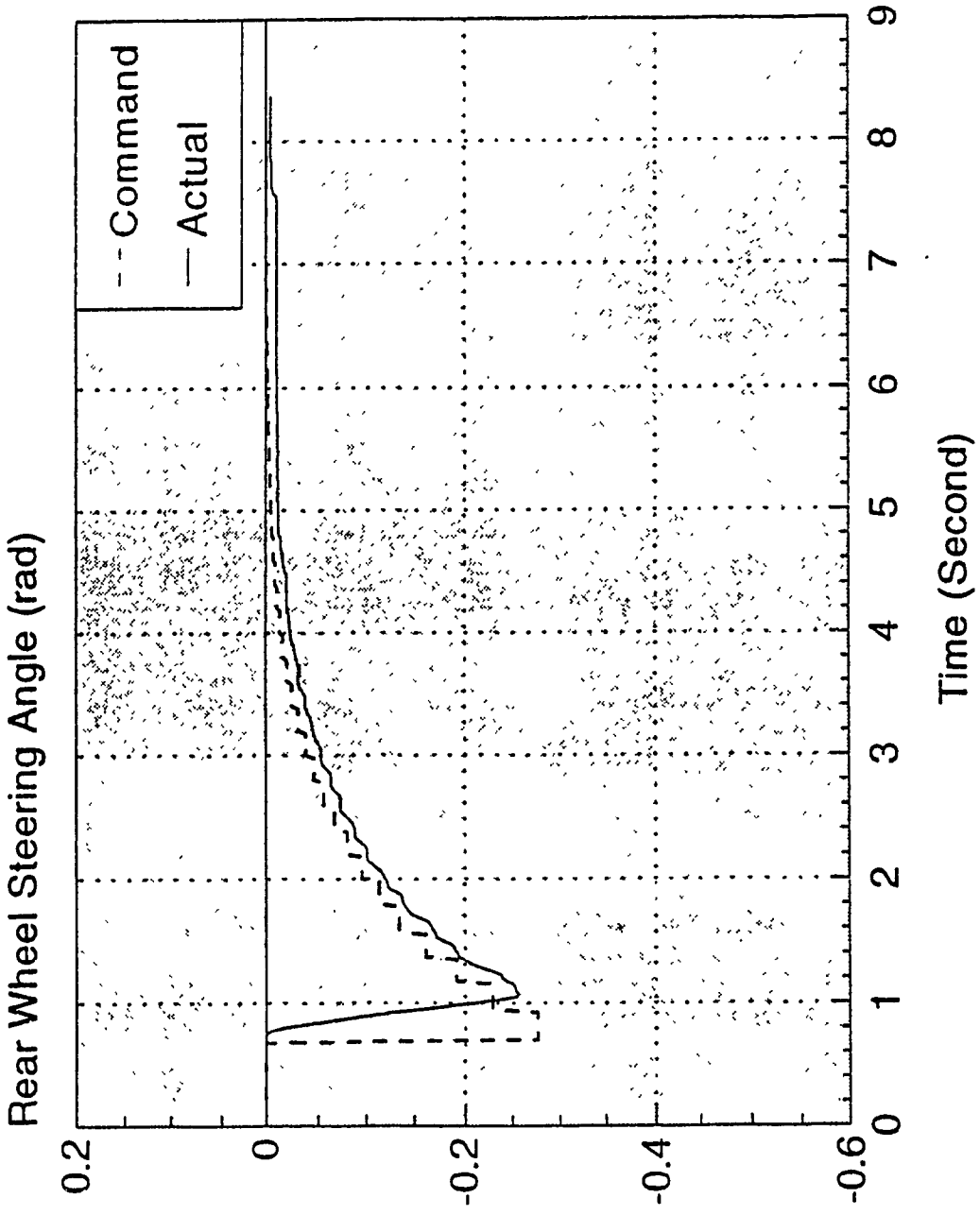

Fig.9.4.d Variations of Rear Wheel Steering Angle

Initial Conditions: ε_d=-0.3 (m), ε_θ=0.524 (rad)

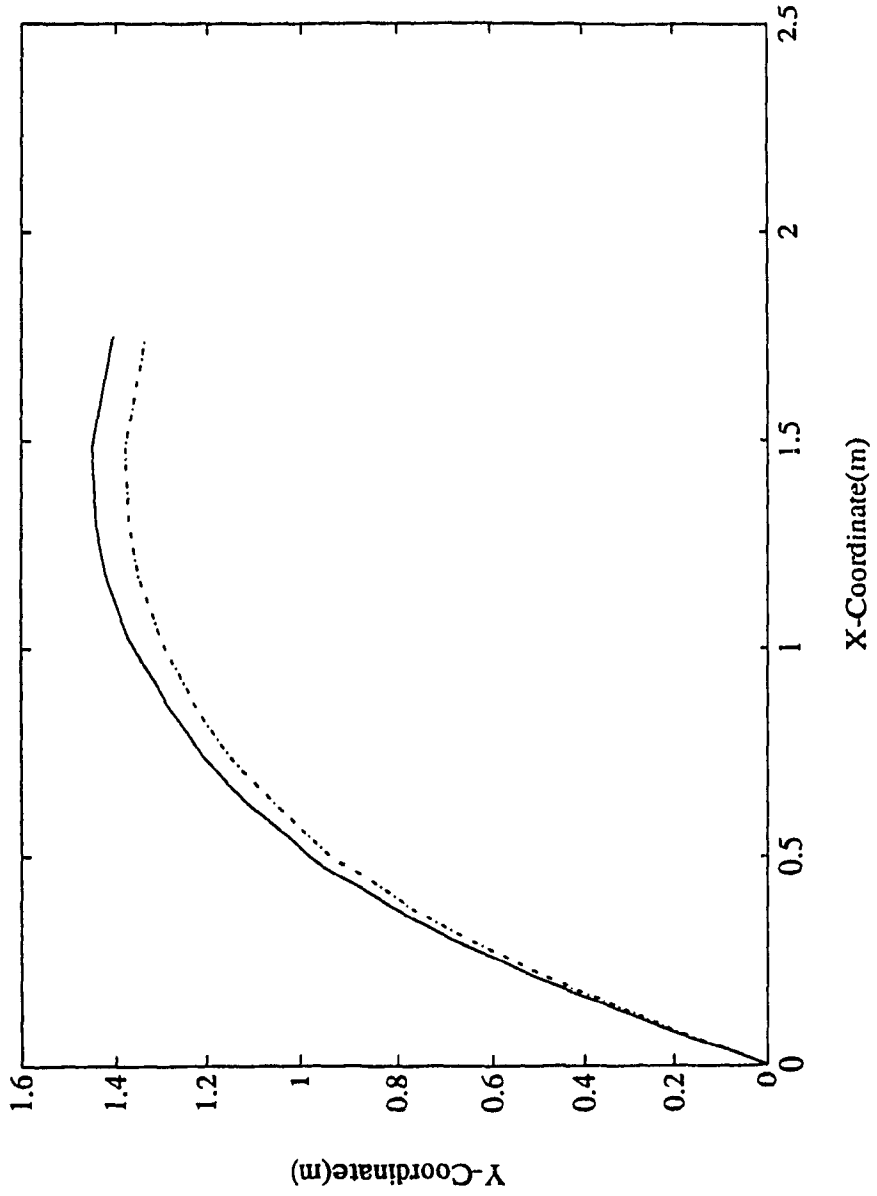

Fig. 9.5.a Desired Path (_._._) and Actual Path (____) (Measured)

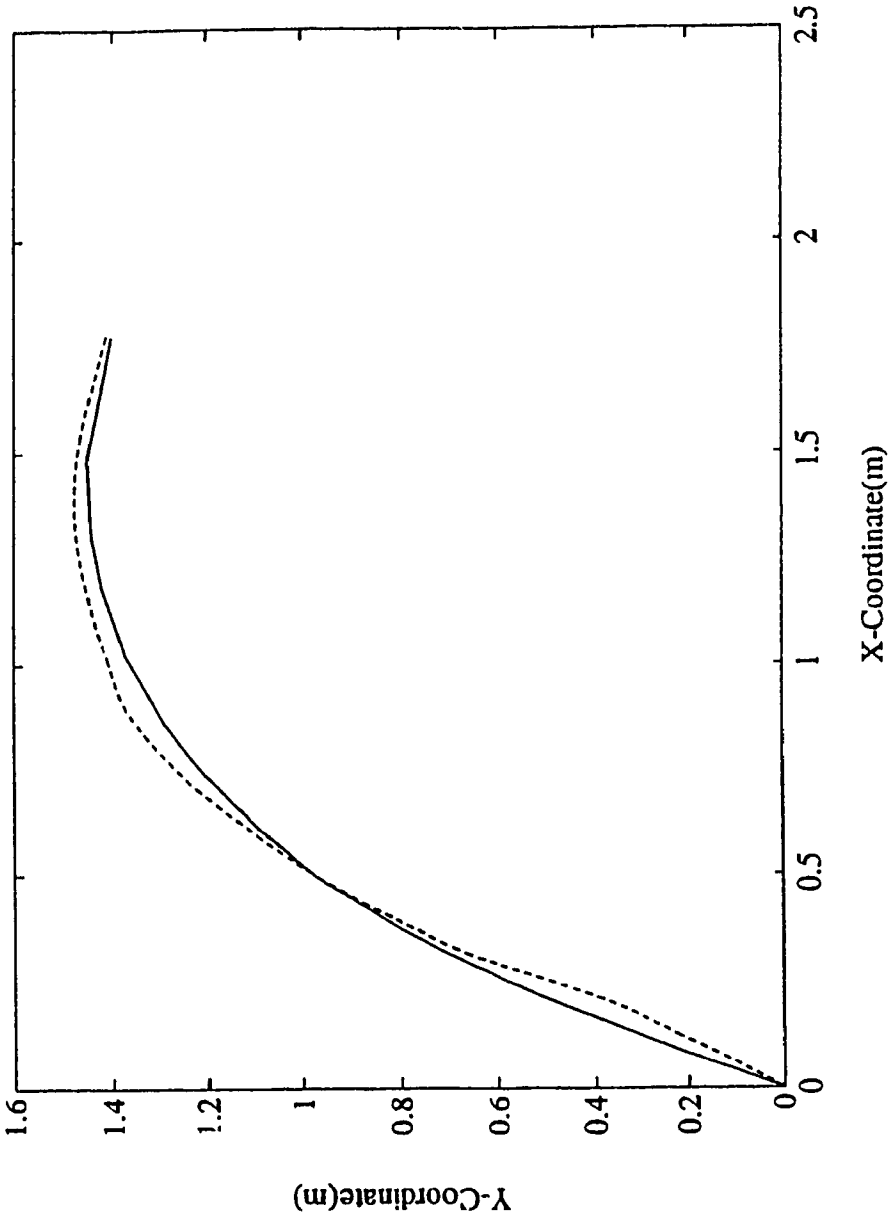

Fig. 9.5.b Actual Path (____) (Measured) and the Path Obtained from Dynamic Model (_ _ _)

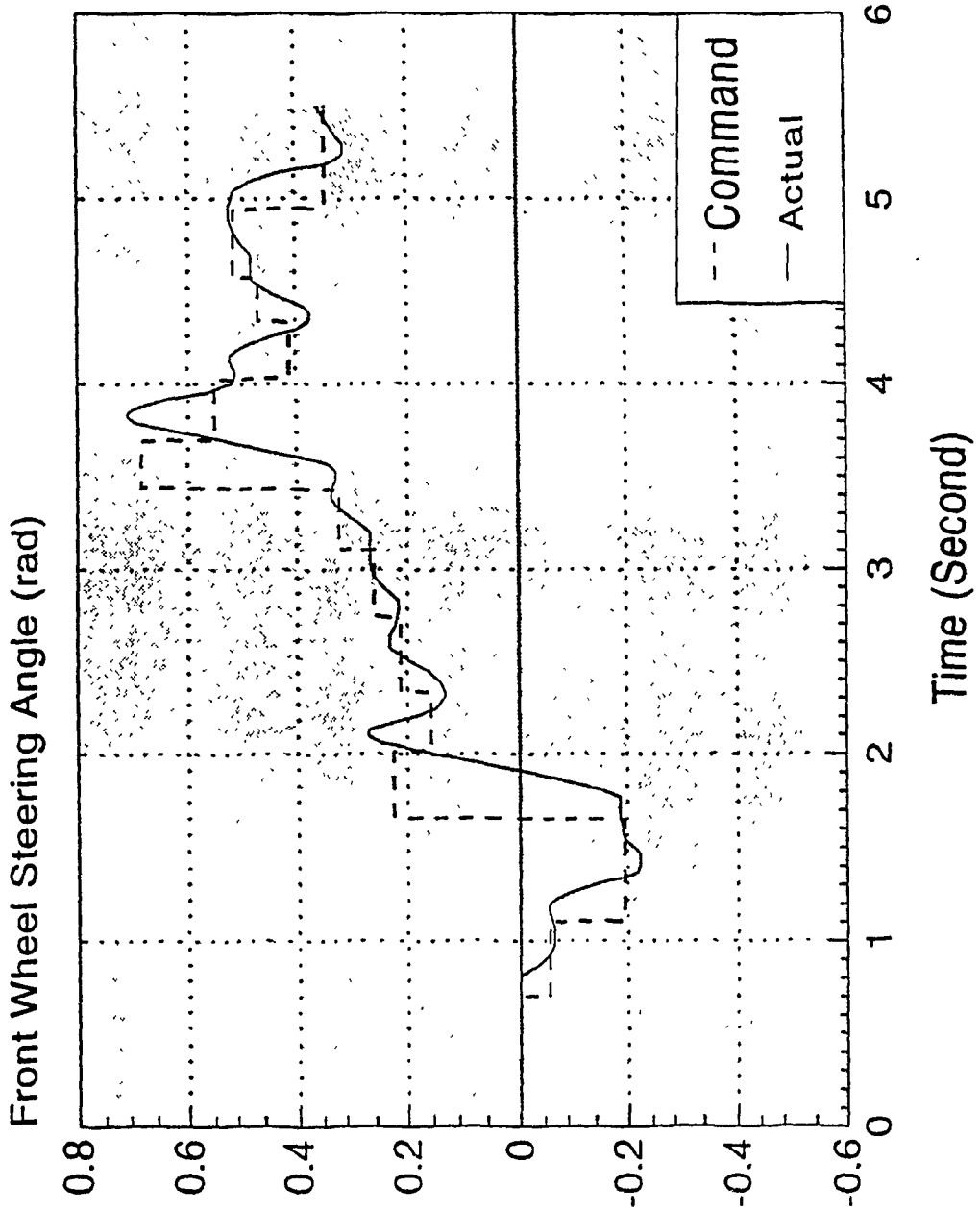

Fig. 9.5.c Variation of Front Wheel Steering Angle

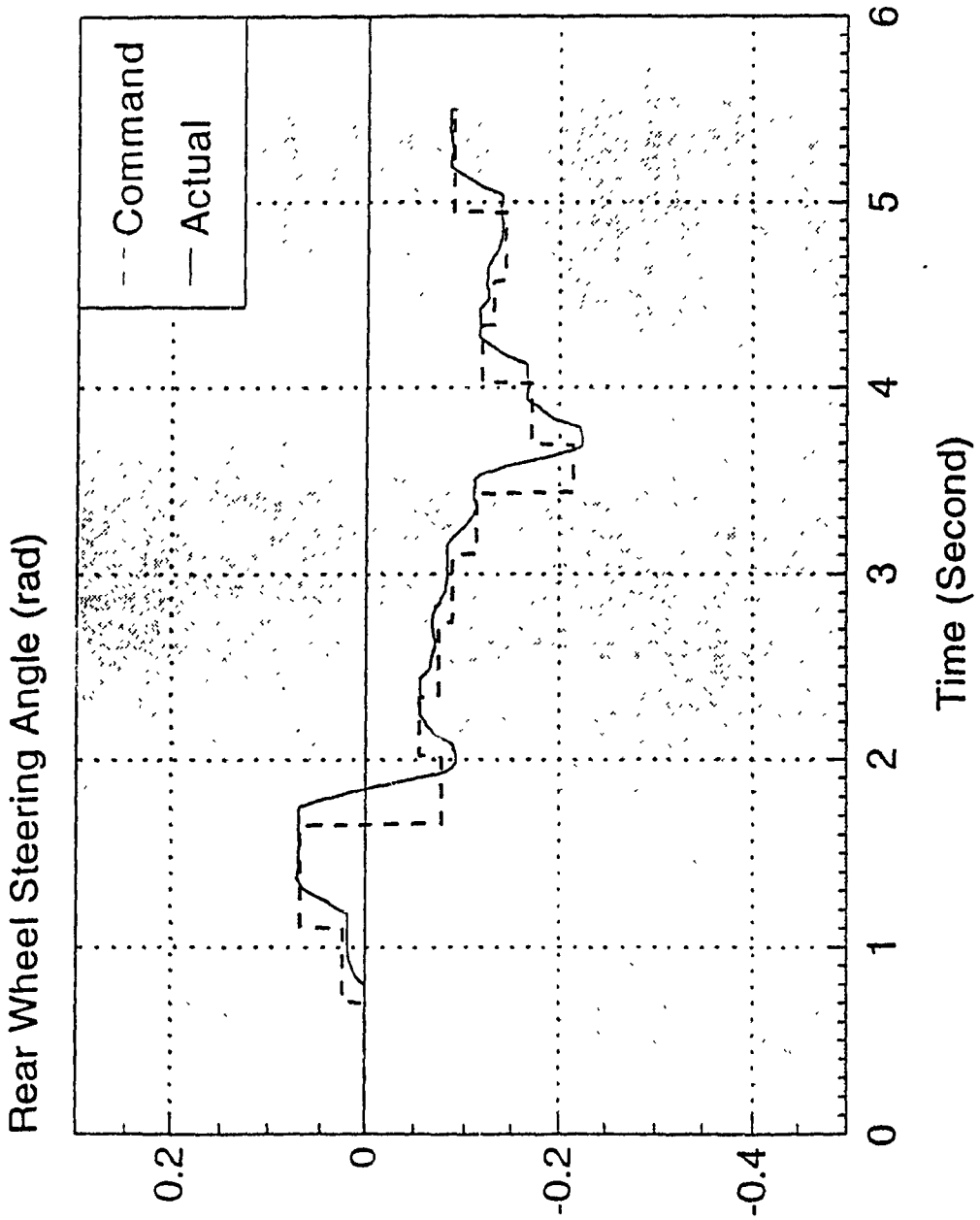

Fig. 9.5.d Variation of Rear Wheel Steering Angle

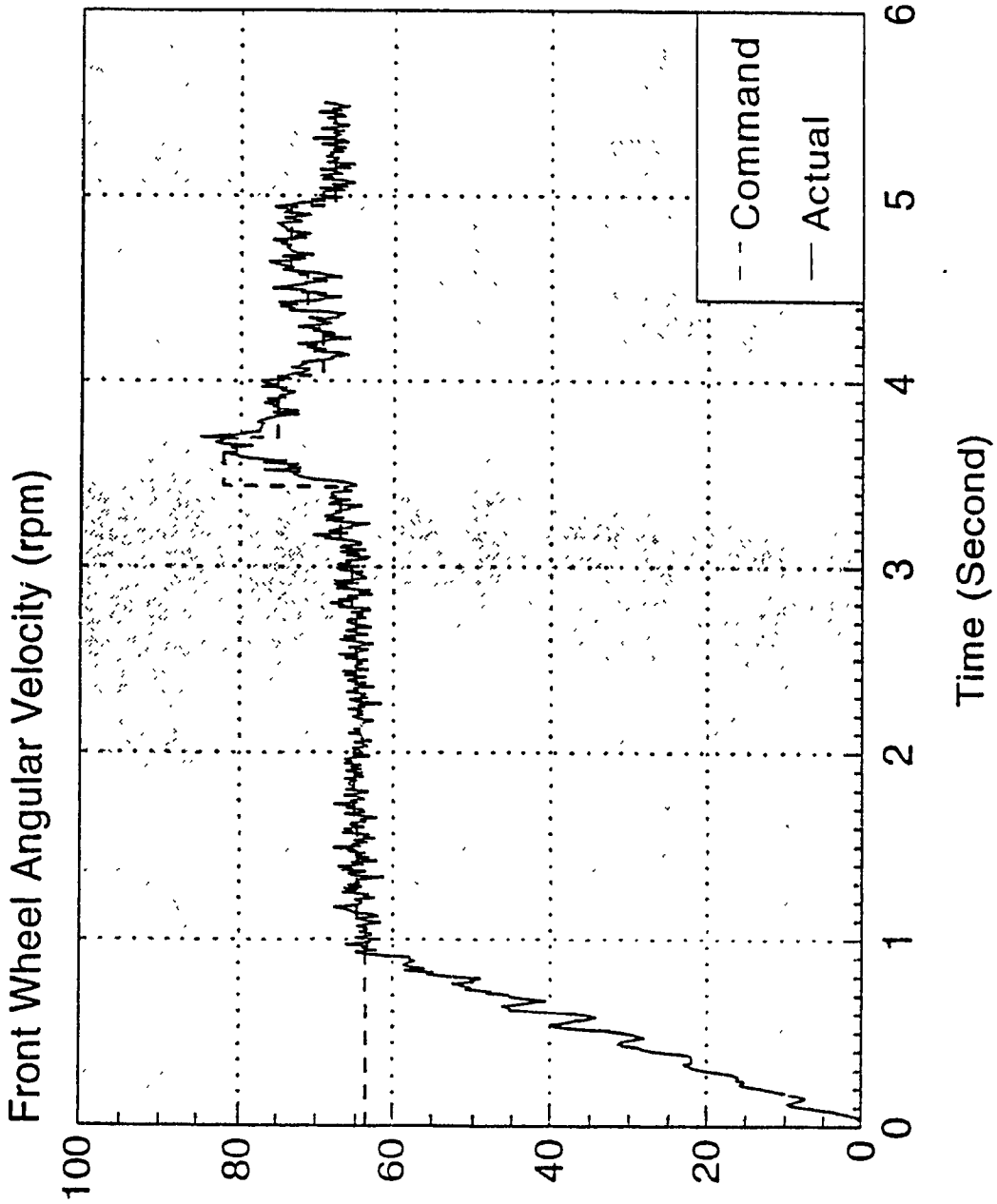

Fig. 9.5.e Variation of Angular Velocity of the Front Wheel

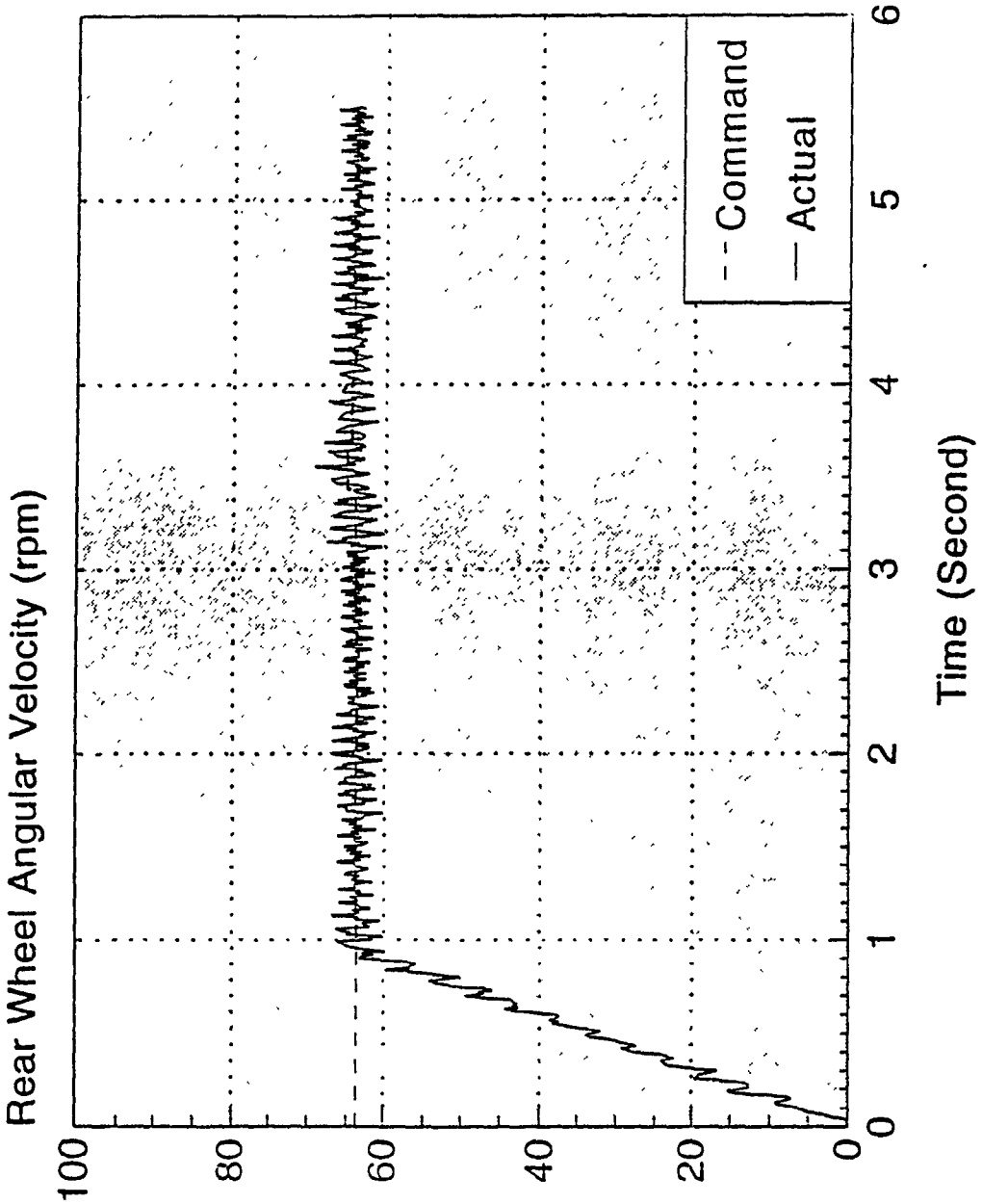

Fig. 9.5.f Variation of Angular Velocity of the Rear Wheel

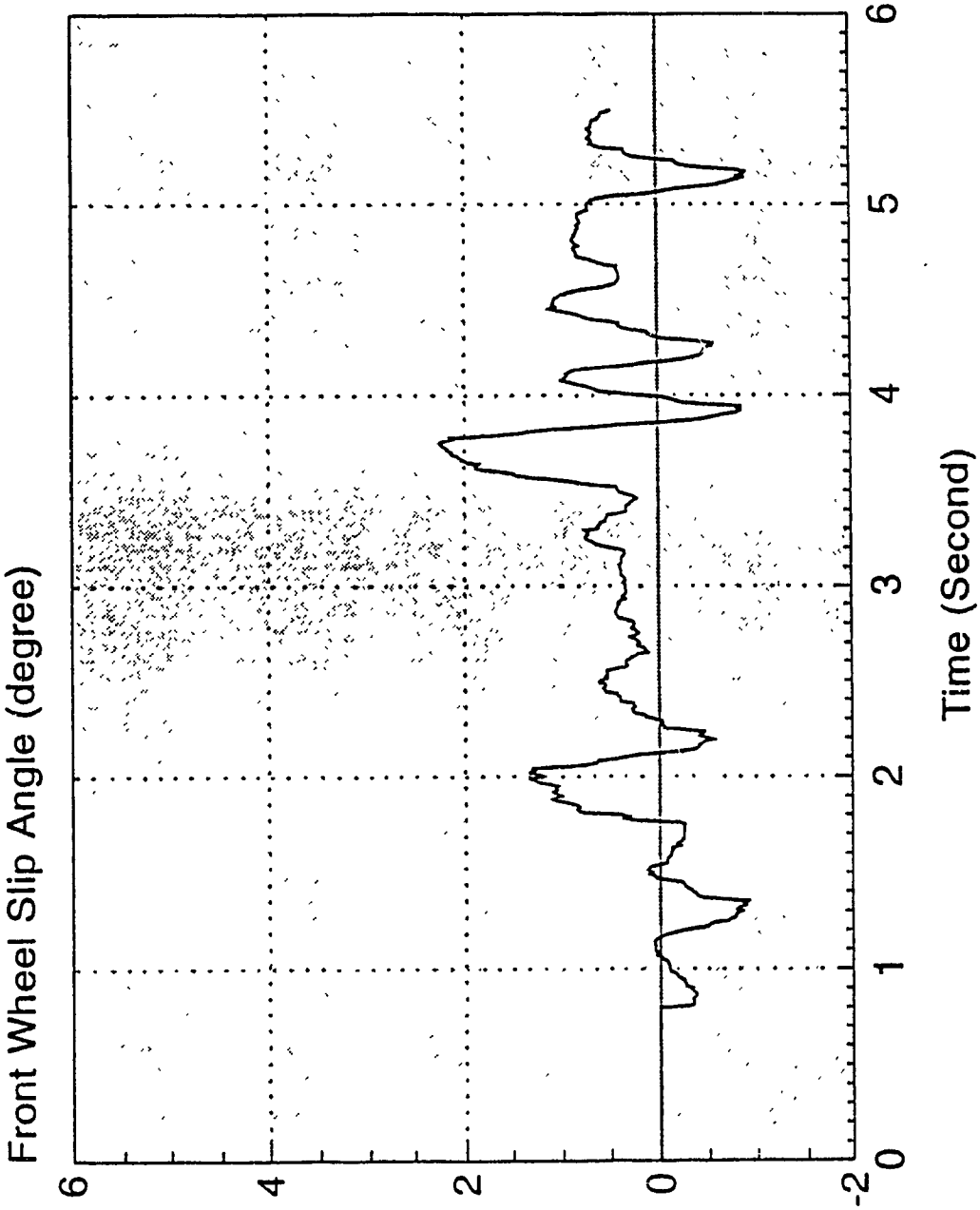

Fig. 9.5.g Variation of Front Wheel Slip Angle

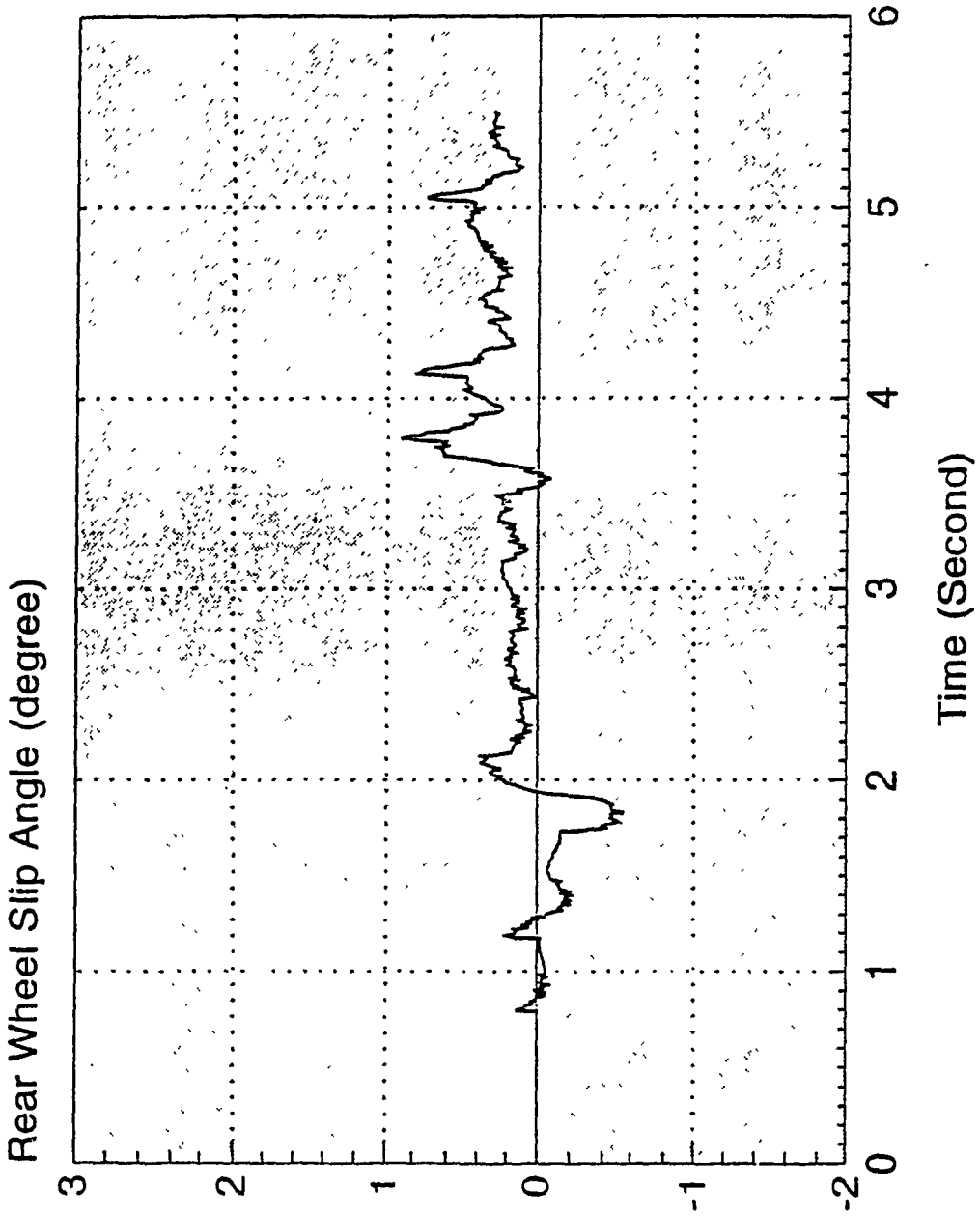

Fig. 9.5.h Variation of Rear Wheel Slip Angle

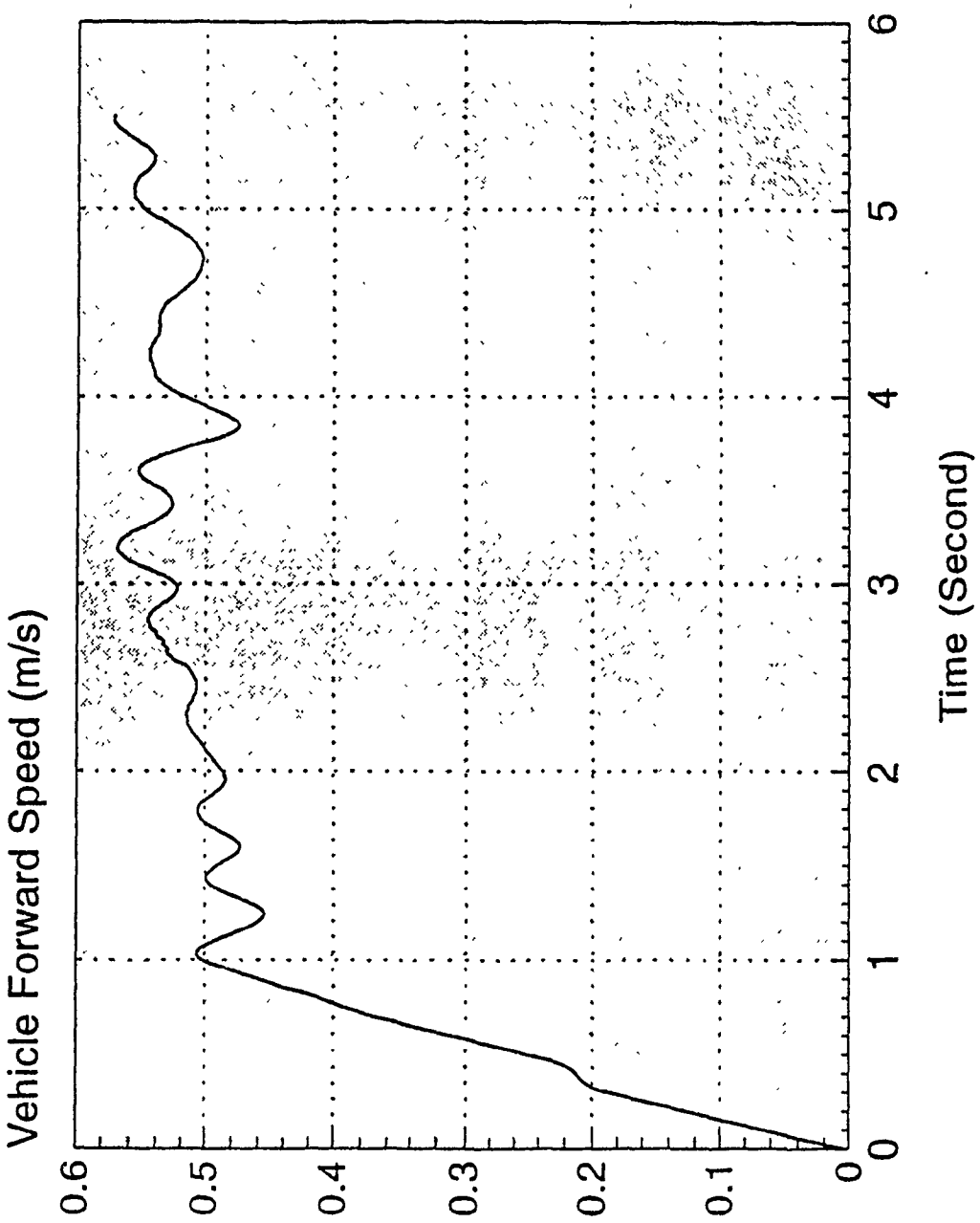

Fig. 9.5.i Variation of Forward Speed of the Vehicle

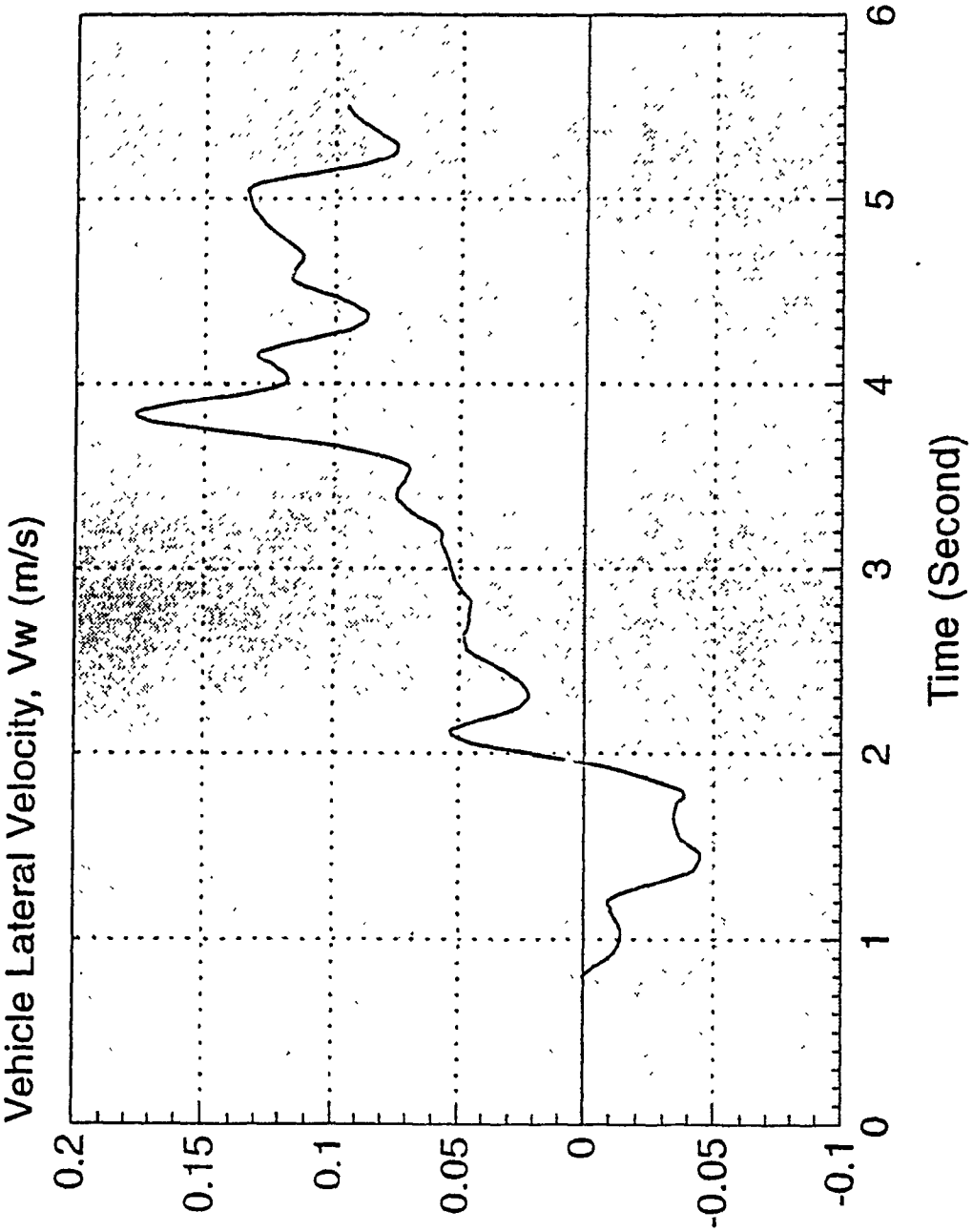

Fig. 9.5.j Variation of Lateral Velocity of the Vehicle

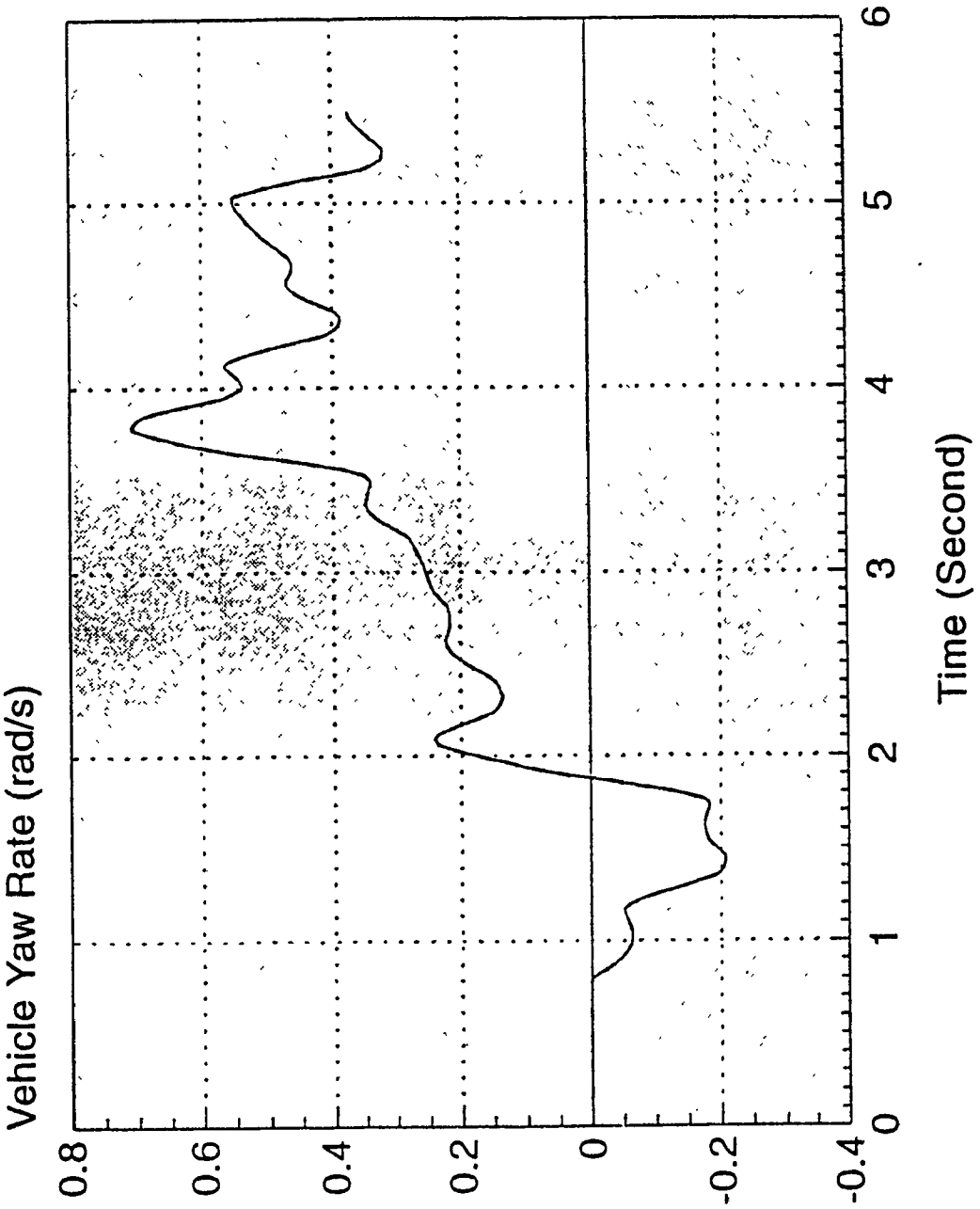

Fig. 9.5.k Variation of Yaw Rate of the Vehicle

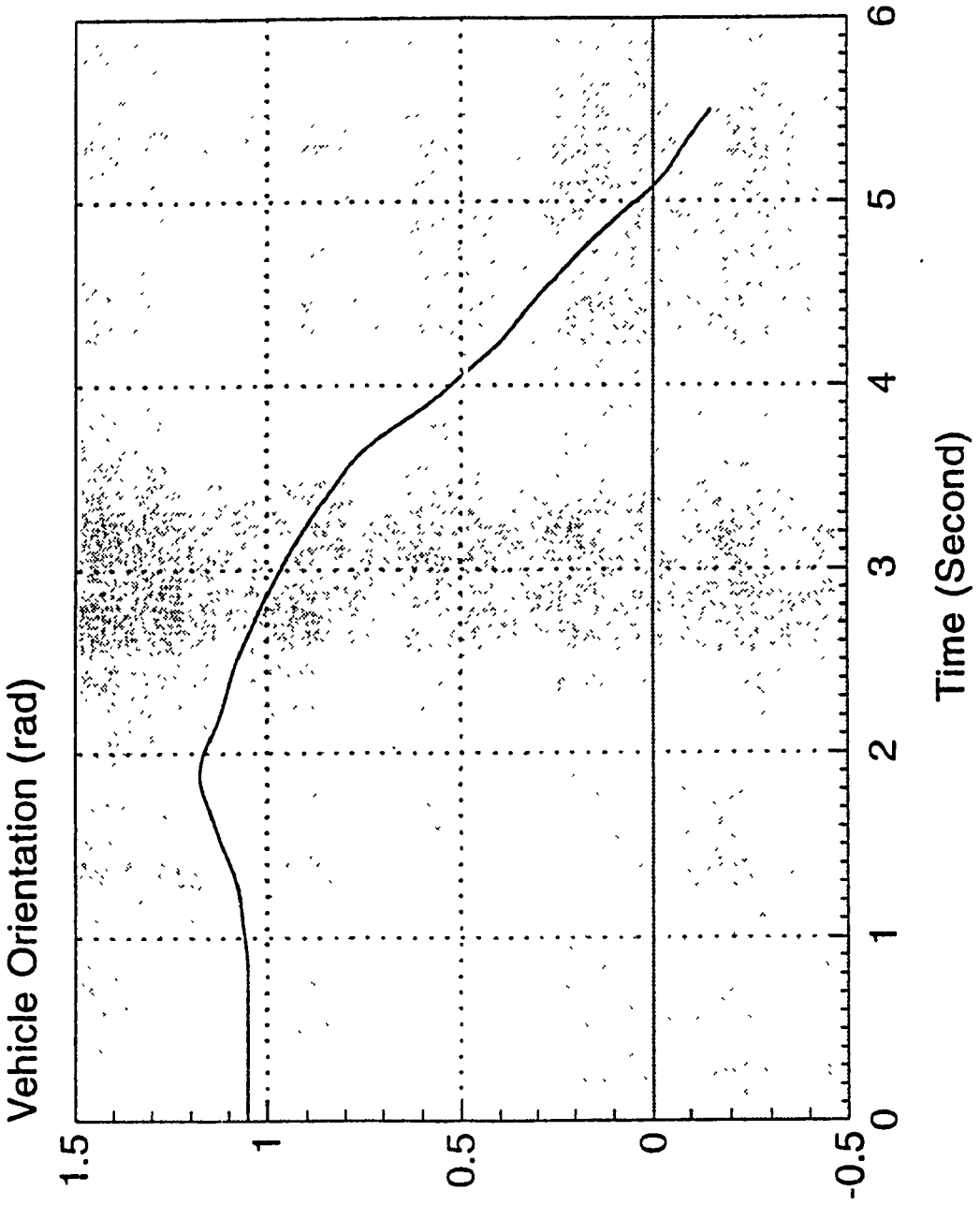

Fig. 9.5.1 Variation of Vehicle Orientation

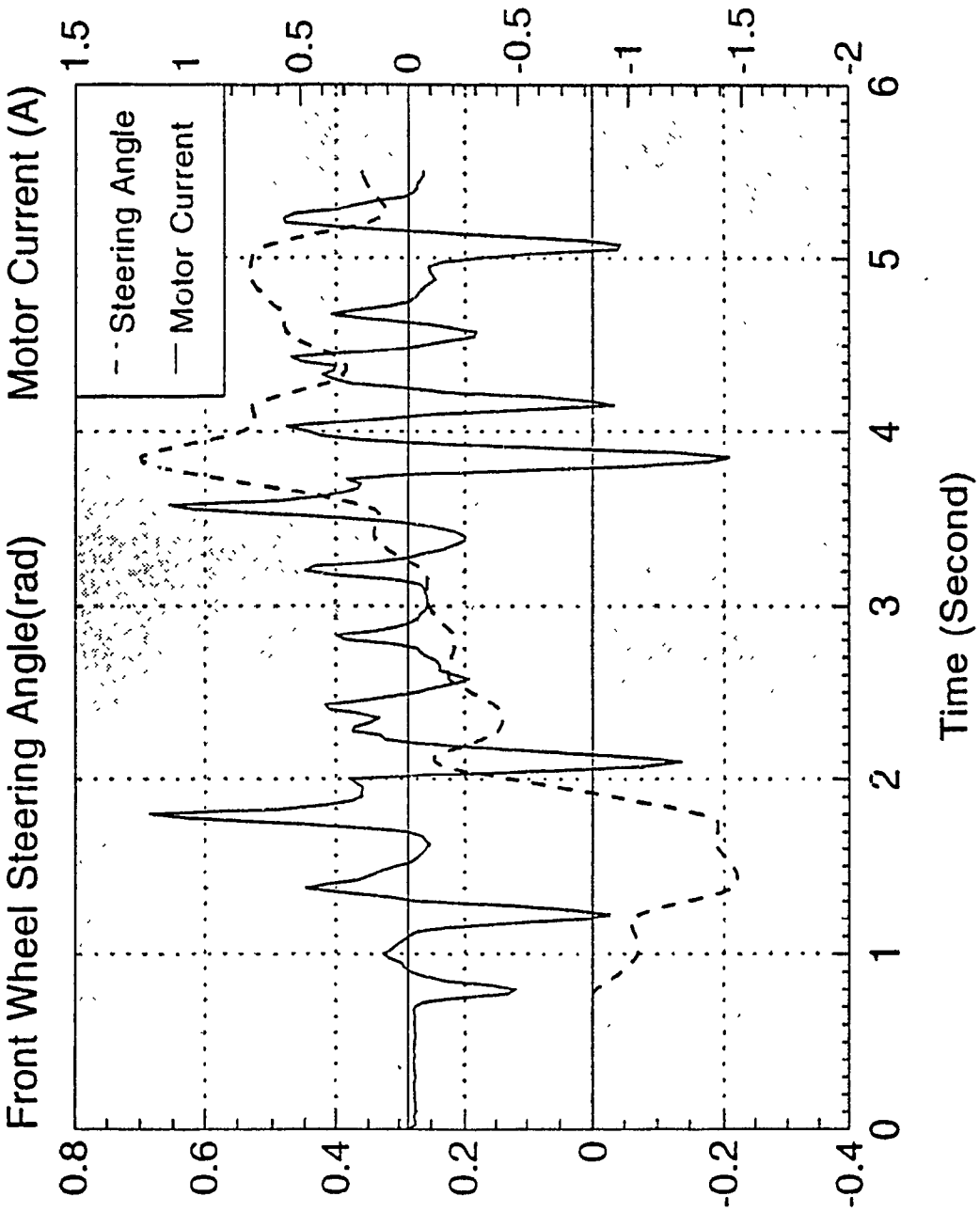

Fig. 9.5.m Variation of Front Wheel Steering Angle and Motor Current

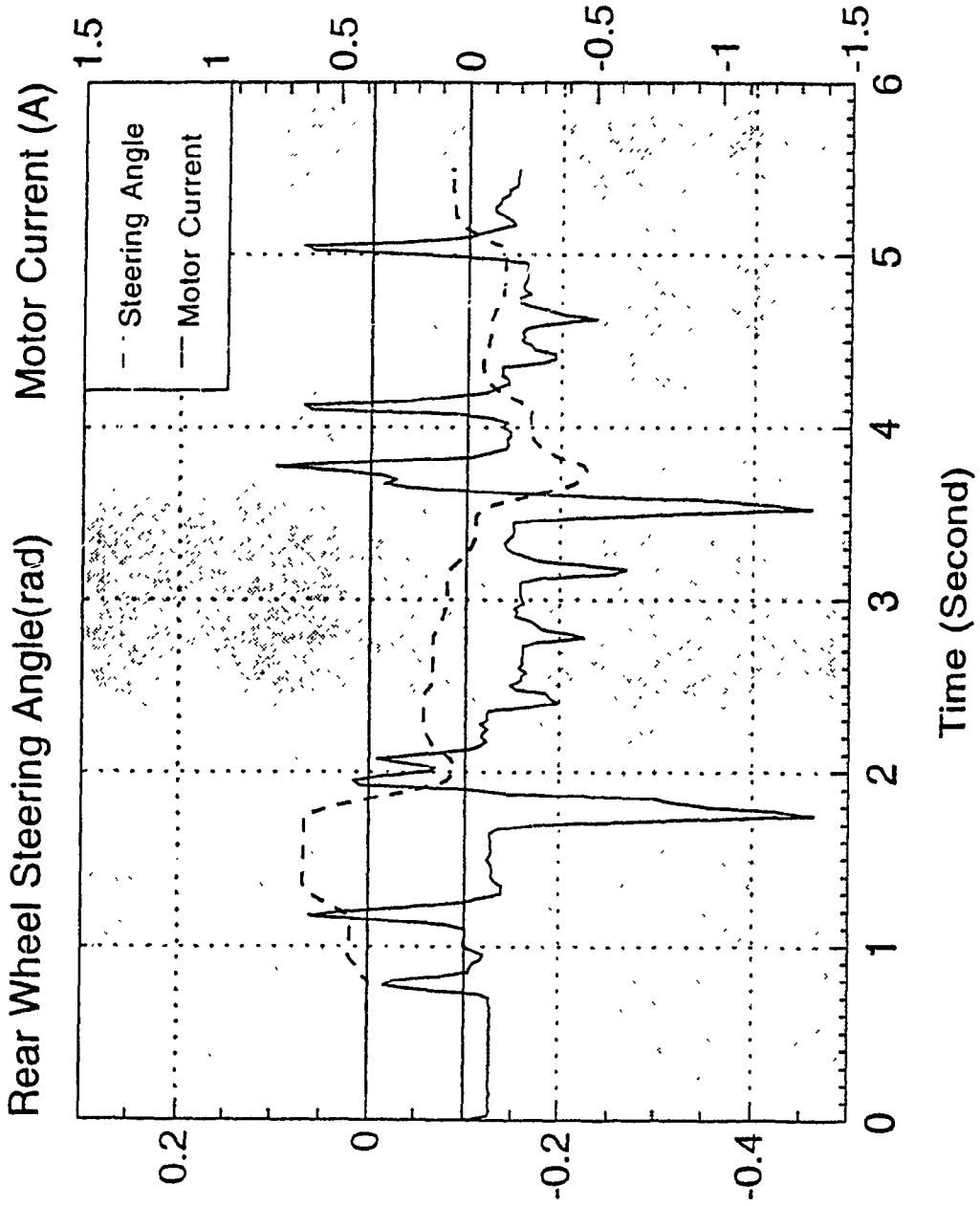

Fig. 9.5.n Variation of Rear Wheel Steering Angle and Motor Current

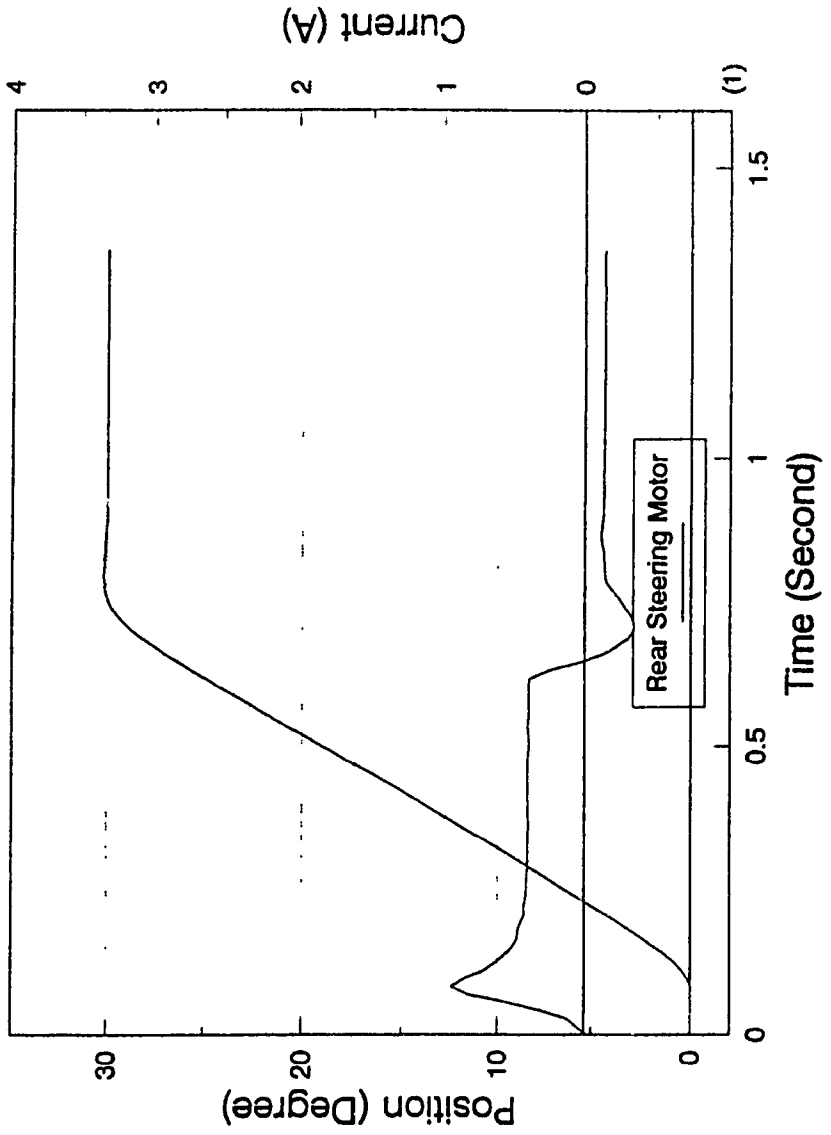

Fig. 9.6 Variation of Rear Wheel Steering Angle and Motor Current (Zero Speed)

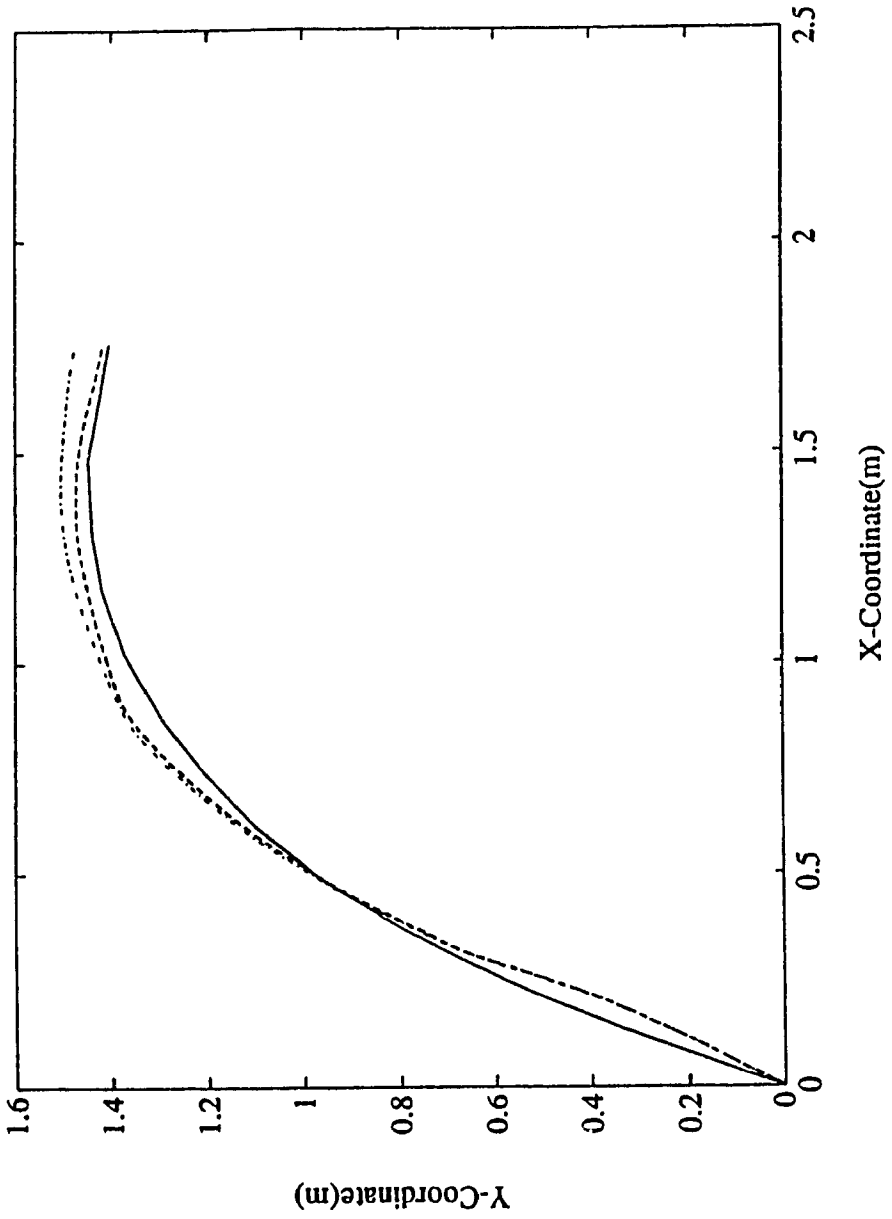

Fig. 9.7.a Comparison of the Trajectories for Actual (Measured_____),

Linear (_._._) and Nonlinear Models (------)

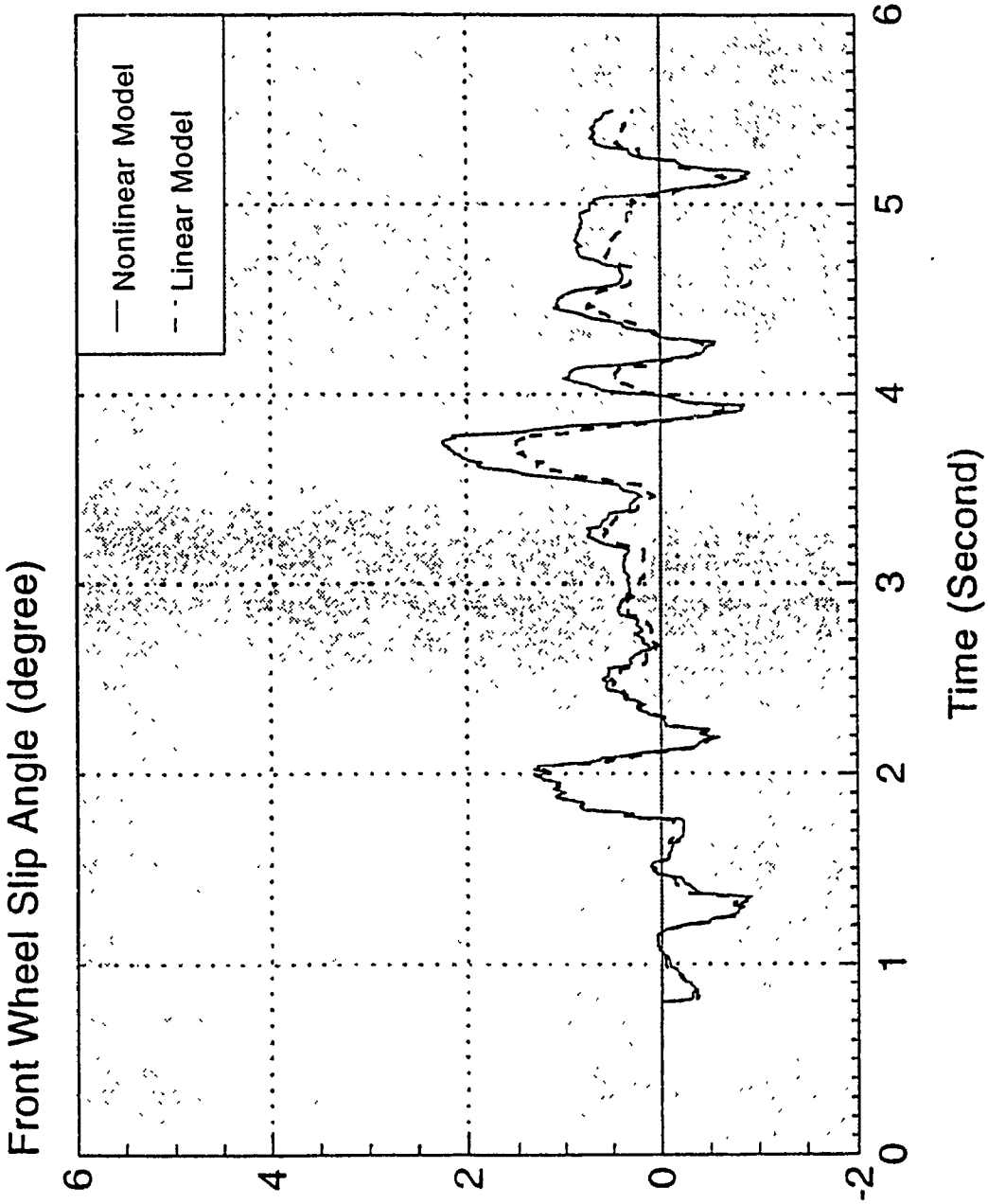

Fig.9.7.b Comparison of Slip Angles of the Front Wheel

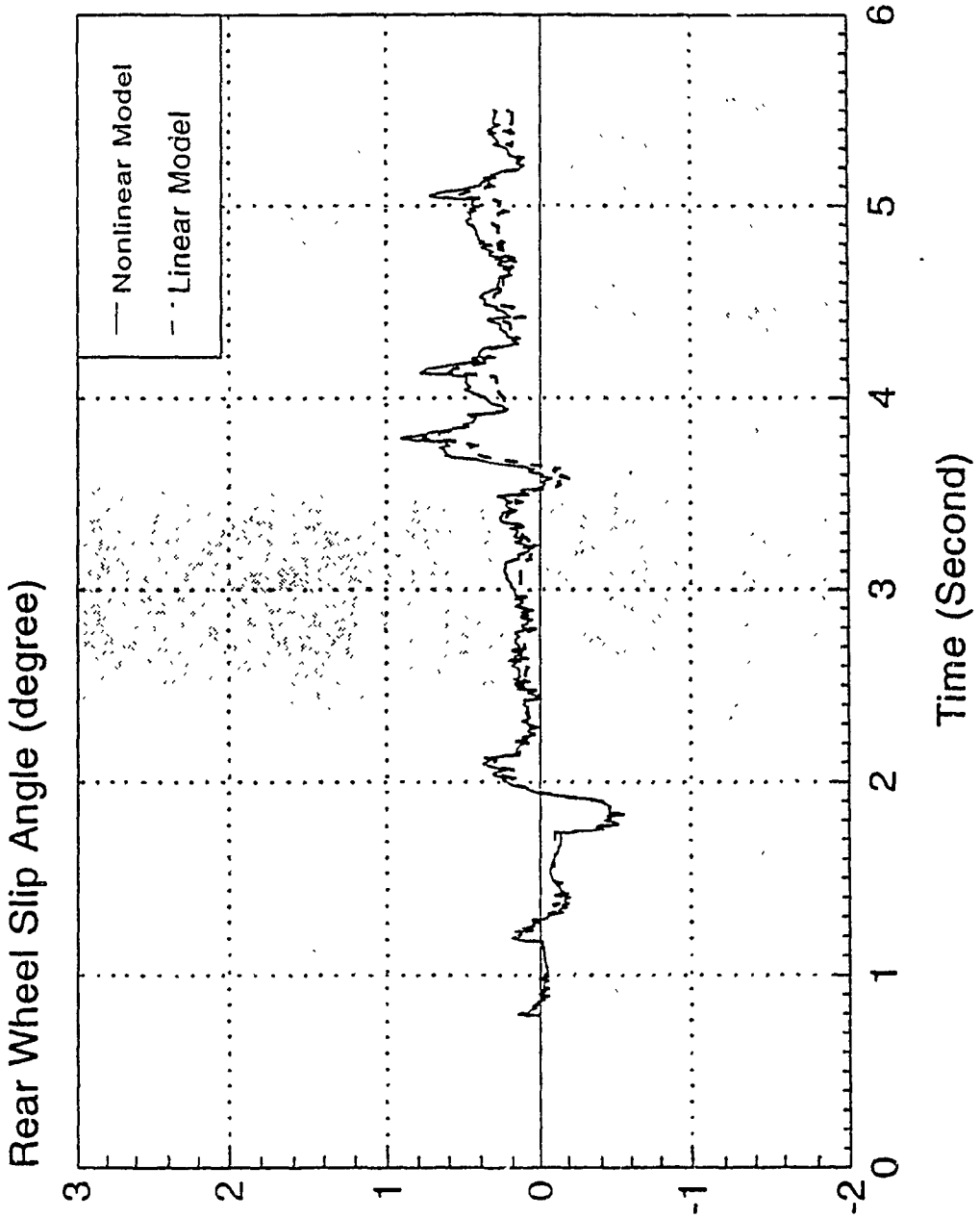

Fig.9.7.c Comparison of Slip Angles of the Rear Wheel

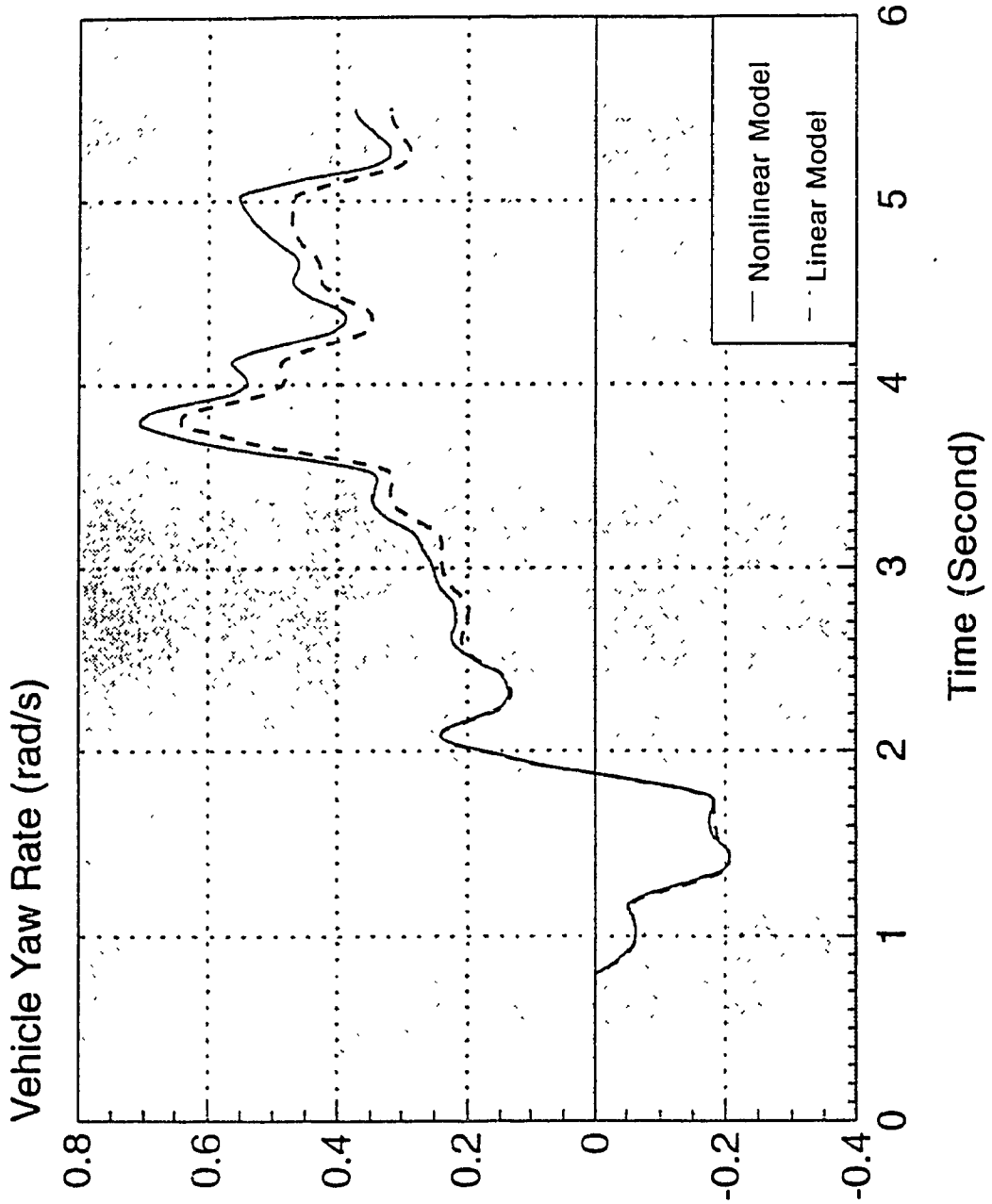

Fig.9.7.d Comparison of the Yaw Rate of the Vehicle

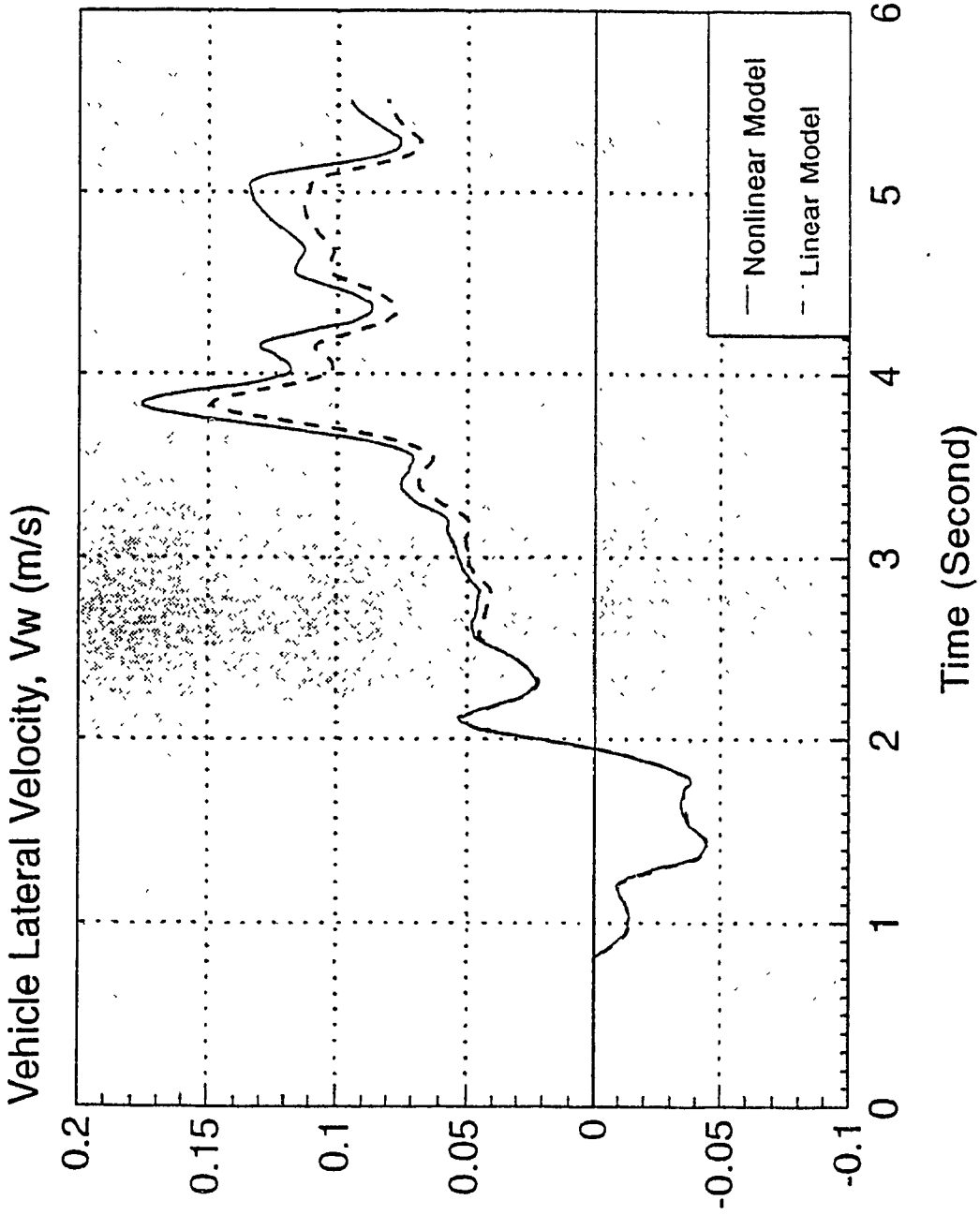

Fig.9.7.e Comparison of the Lateral Velocity of the Vehicle

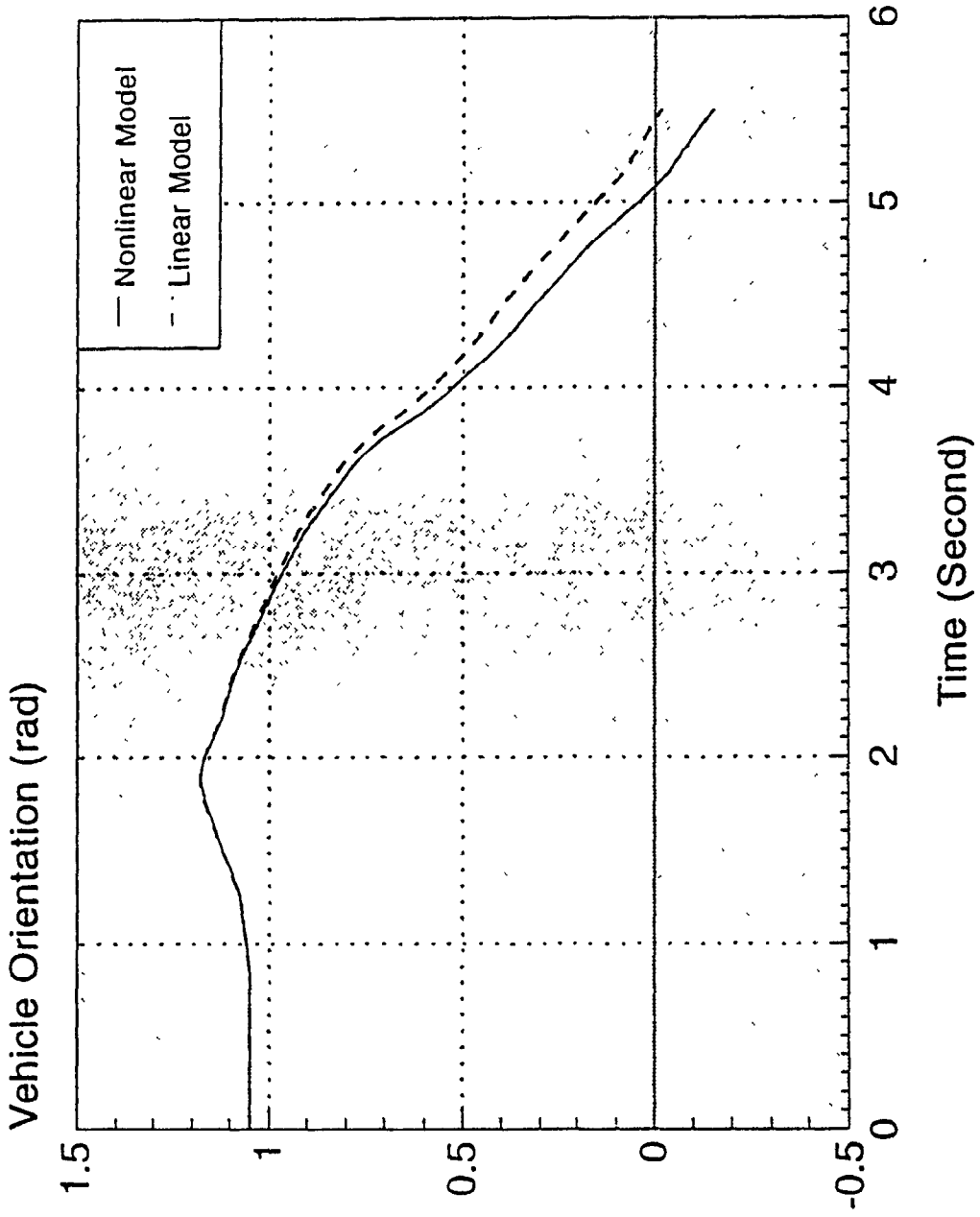

Fig.9.7.f Comparison of Vehicle Orientation

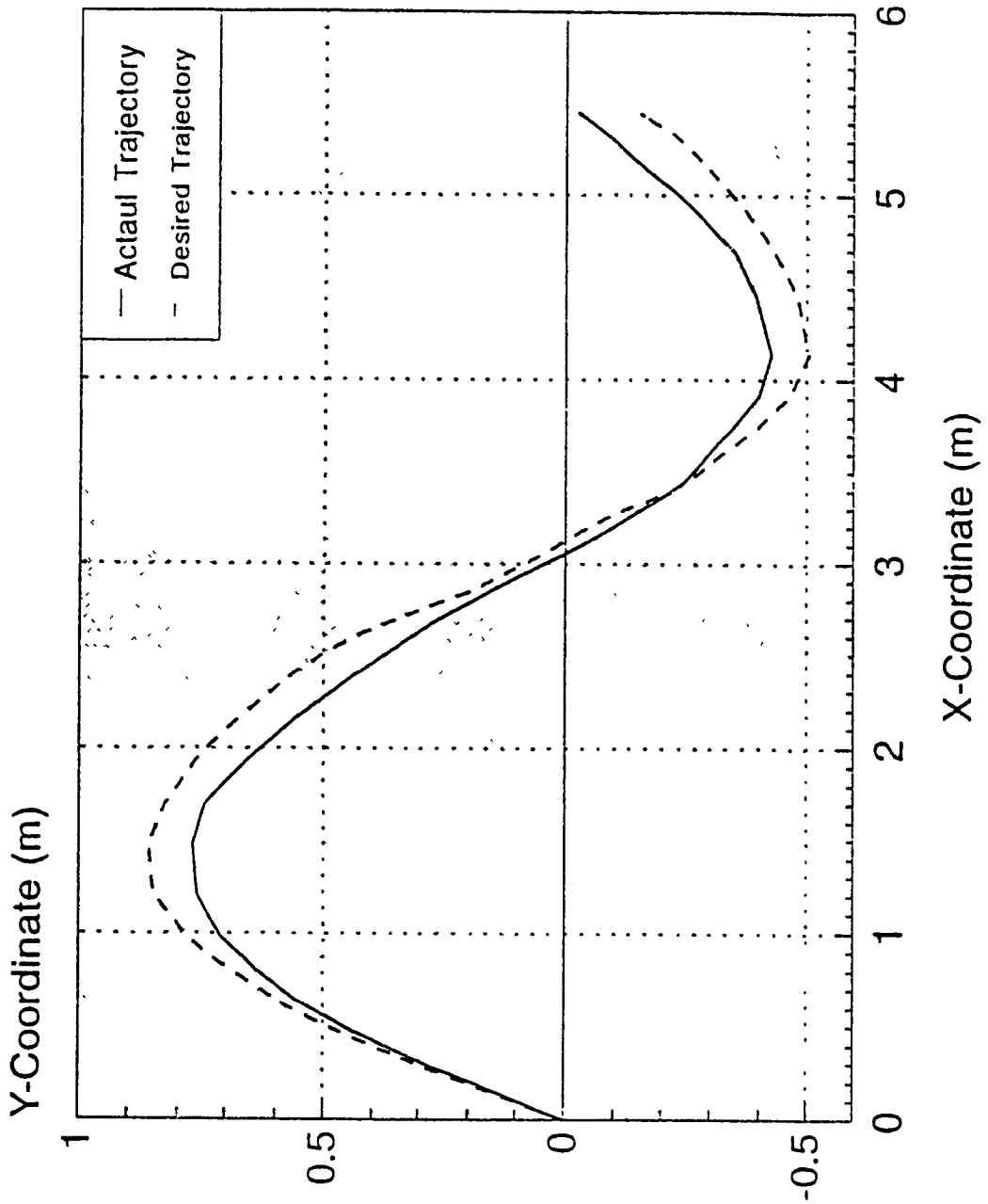

Fig.9.8.a Path Following of the Vehicle

(Actual Trajectory (Reconstructed Path) and Desired Trajectory)

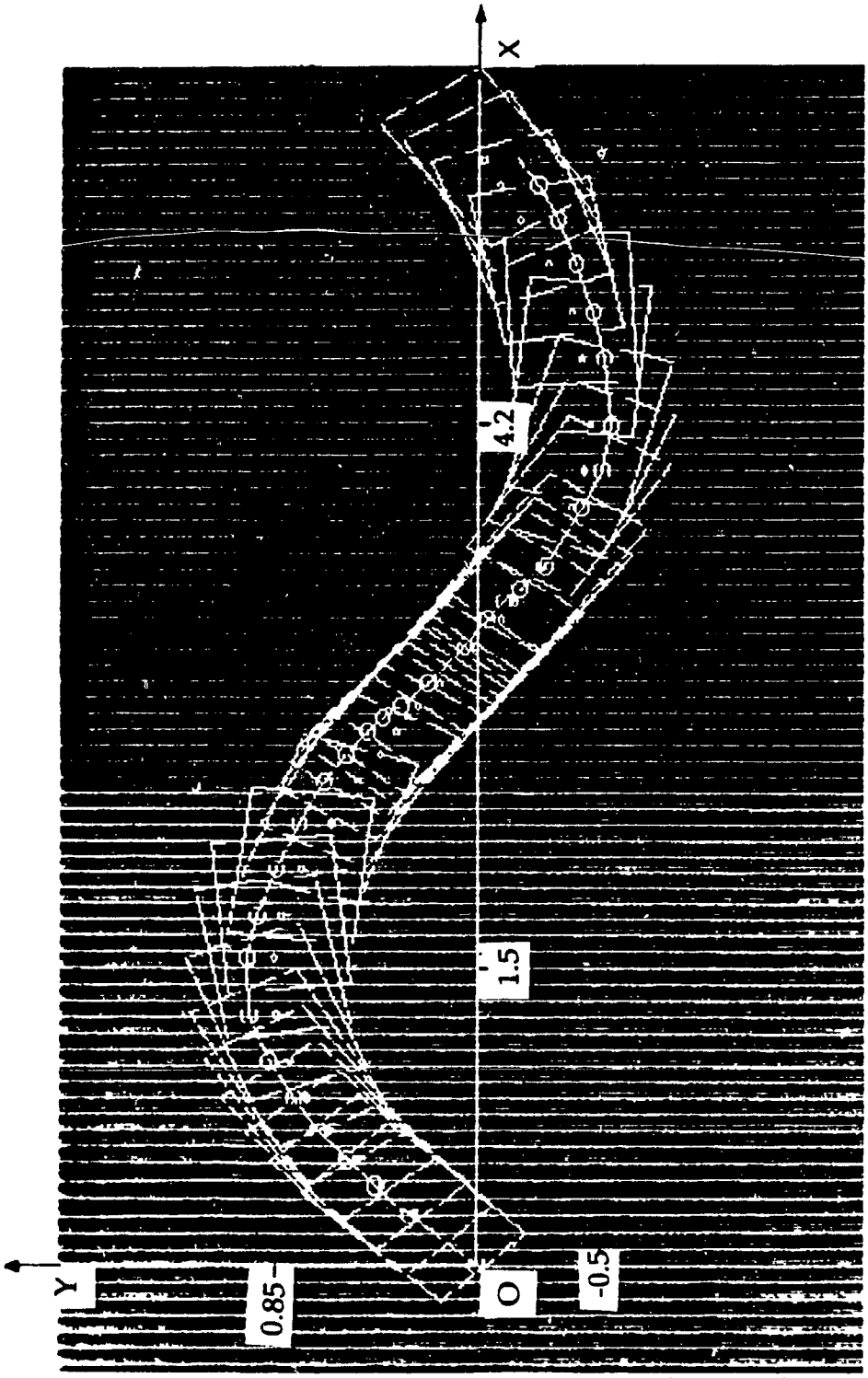

Fig. 9.8.b Position and Orientation of the Vehicle During Motion.

("o" is the Centre of Mass (Vehicle), "O" is the Desired Path)

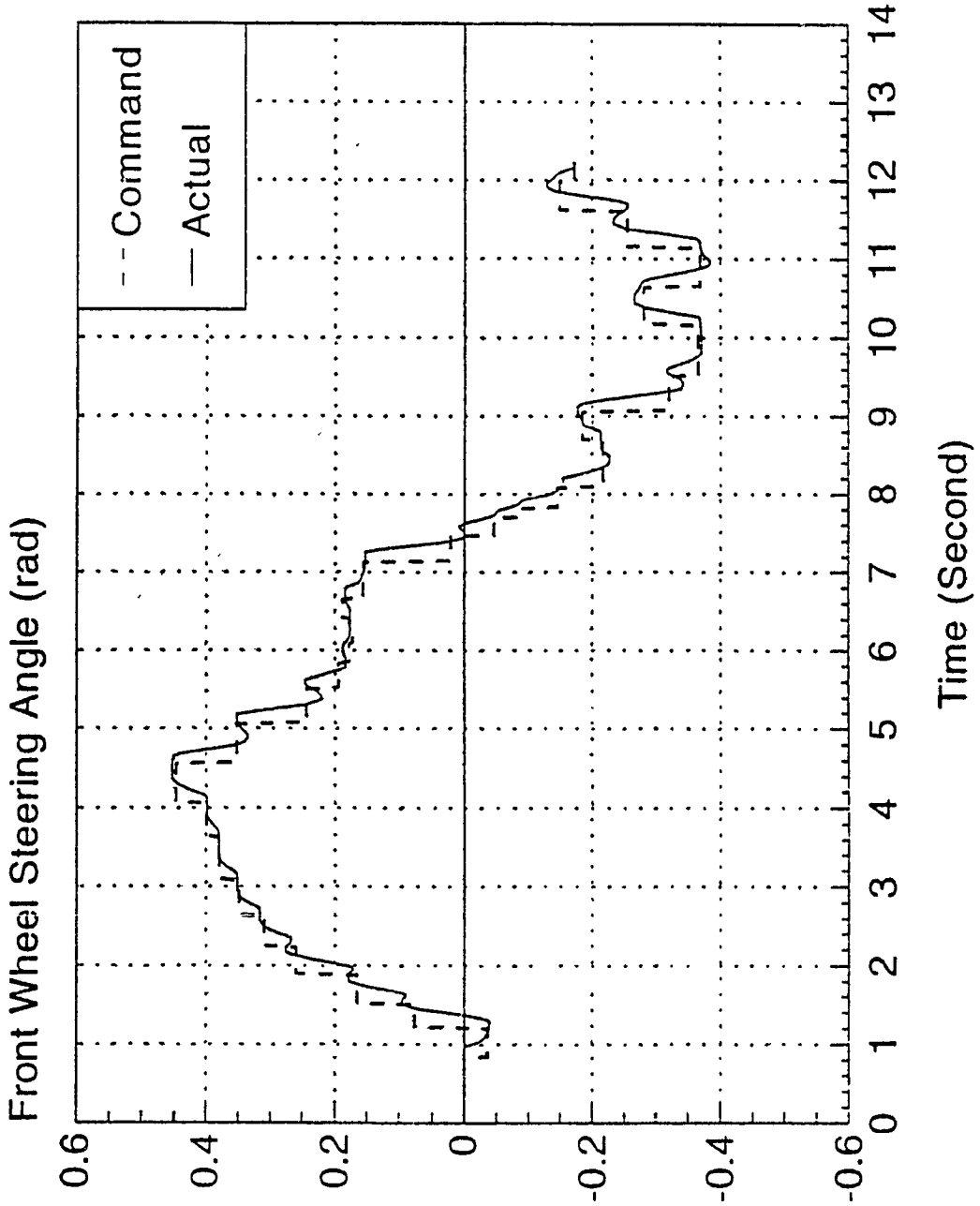

Fig.9.8.c Variation of Front Wheel Steering Angle

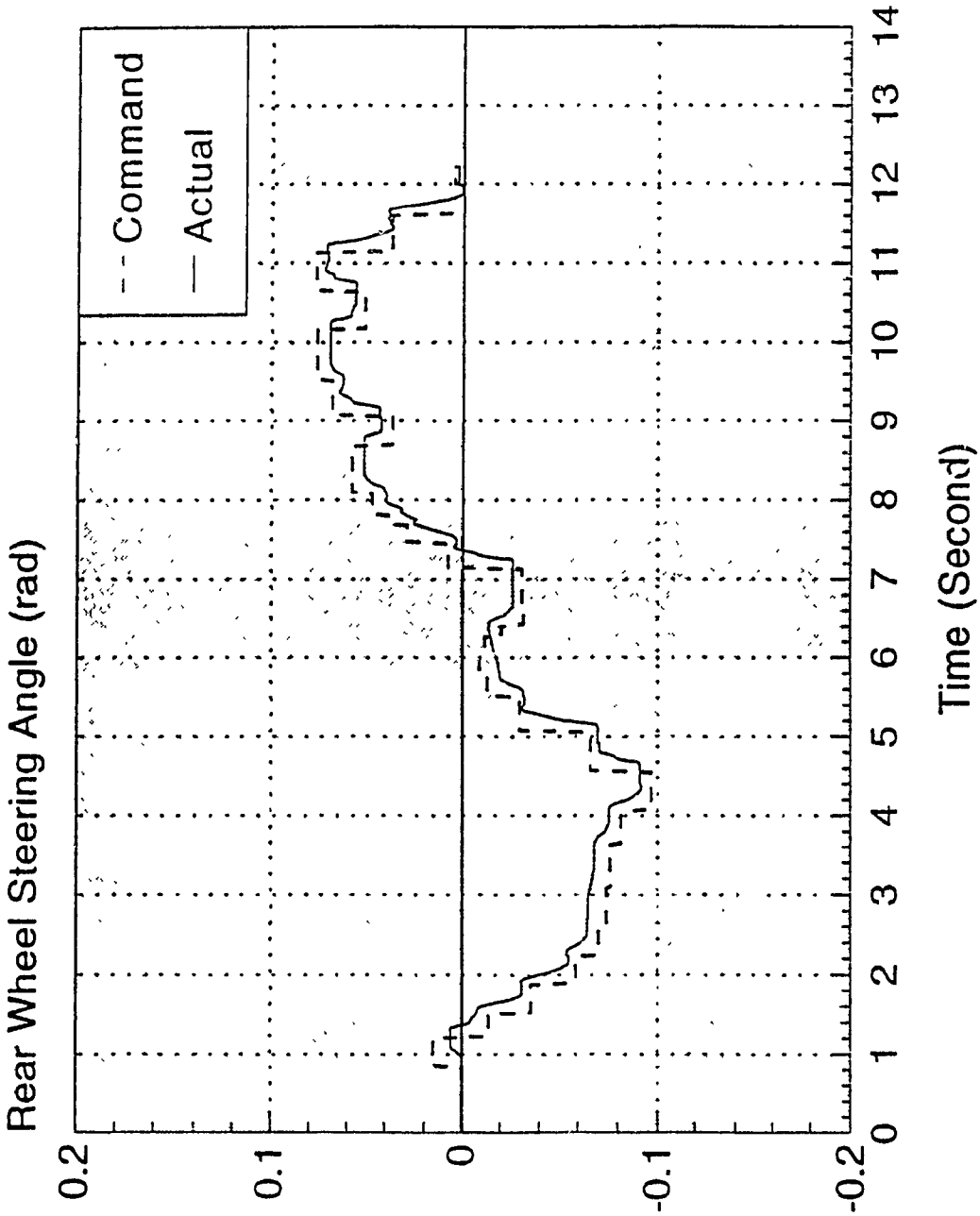

Fig.9.8.d Variation of Rear Wheel Steering Angle

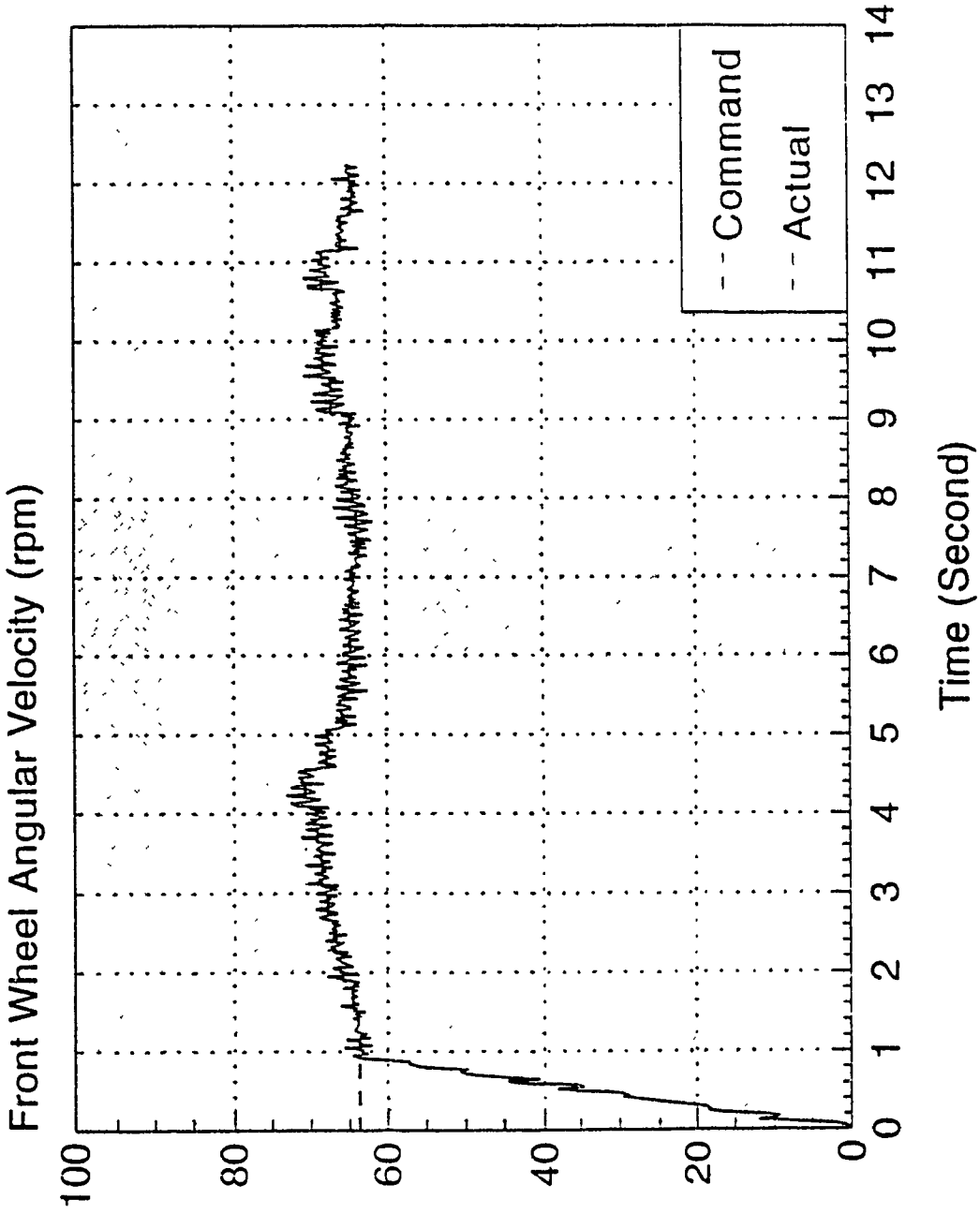

Fig.9.8.e Variation of Angular Velocity of the Front Wheel

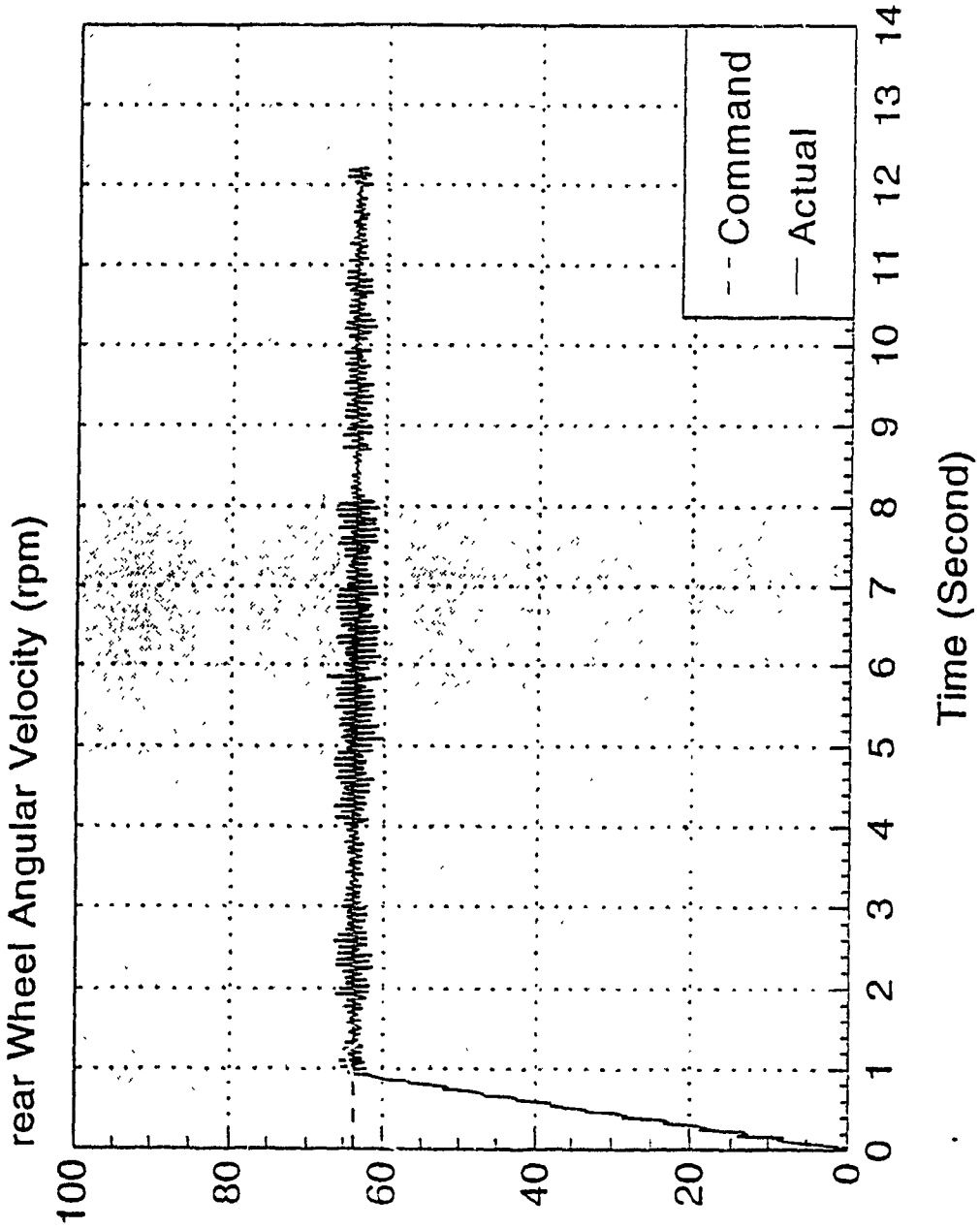

Fig.9.8.f Variation of Rear Wheel Angular Velocity

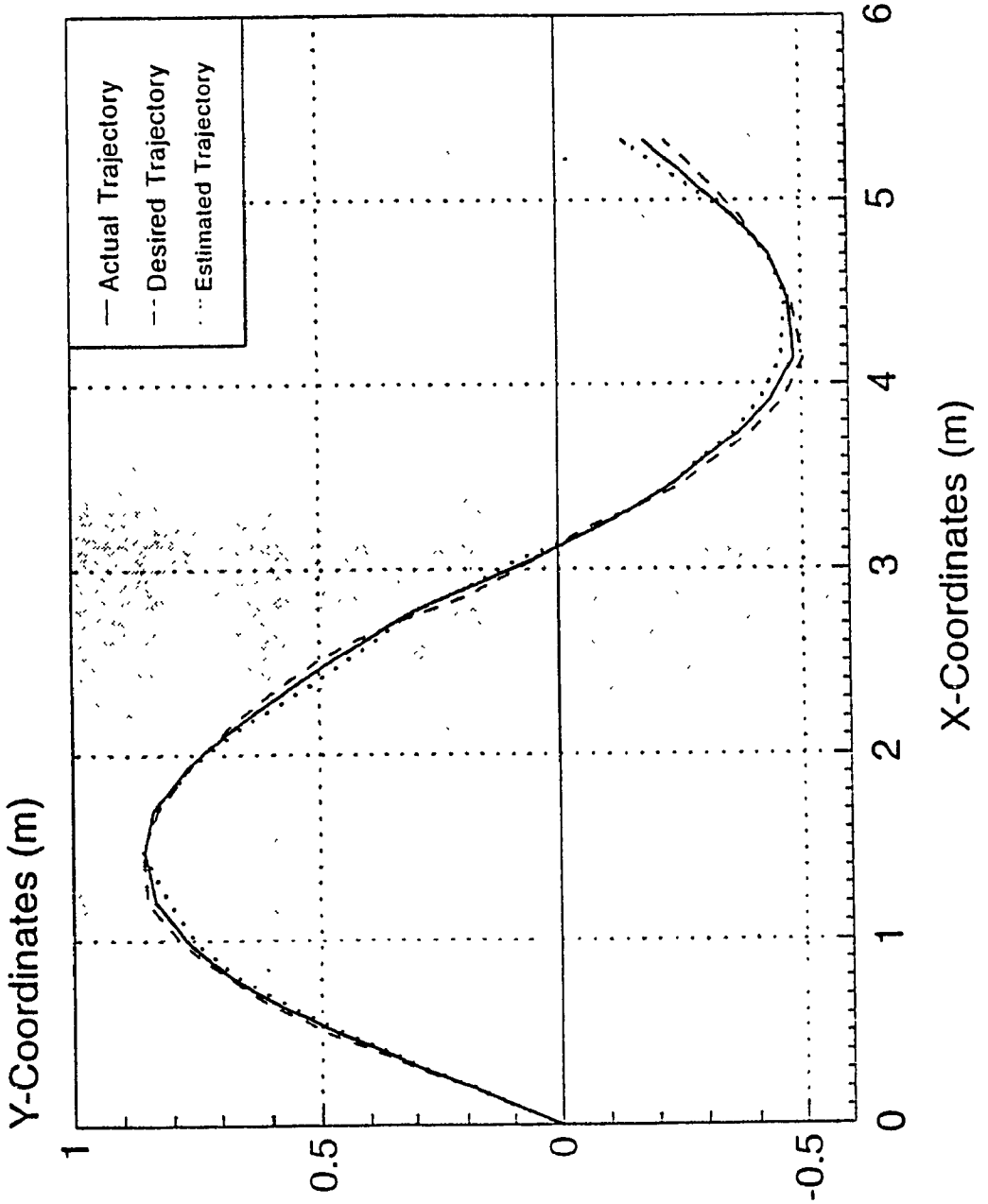

Fig.9.9.a Path Following of the Vehicle

(Actual Path (Reconstructed), Desired Trajectory and Estimated Path)

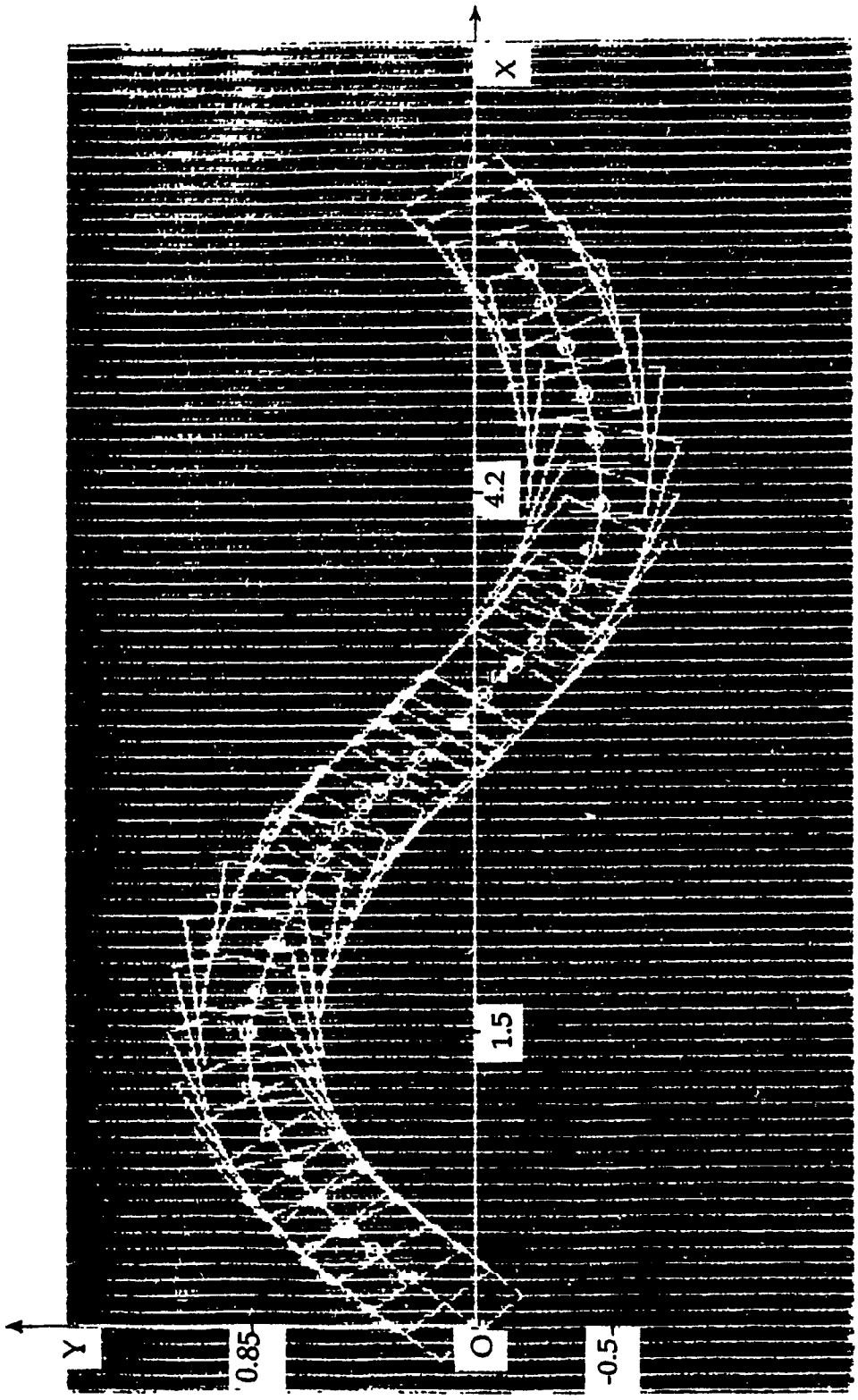

Fig.9.9.b Relative Posture of the Vehicle and Desired Trajectory

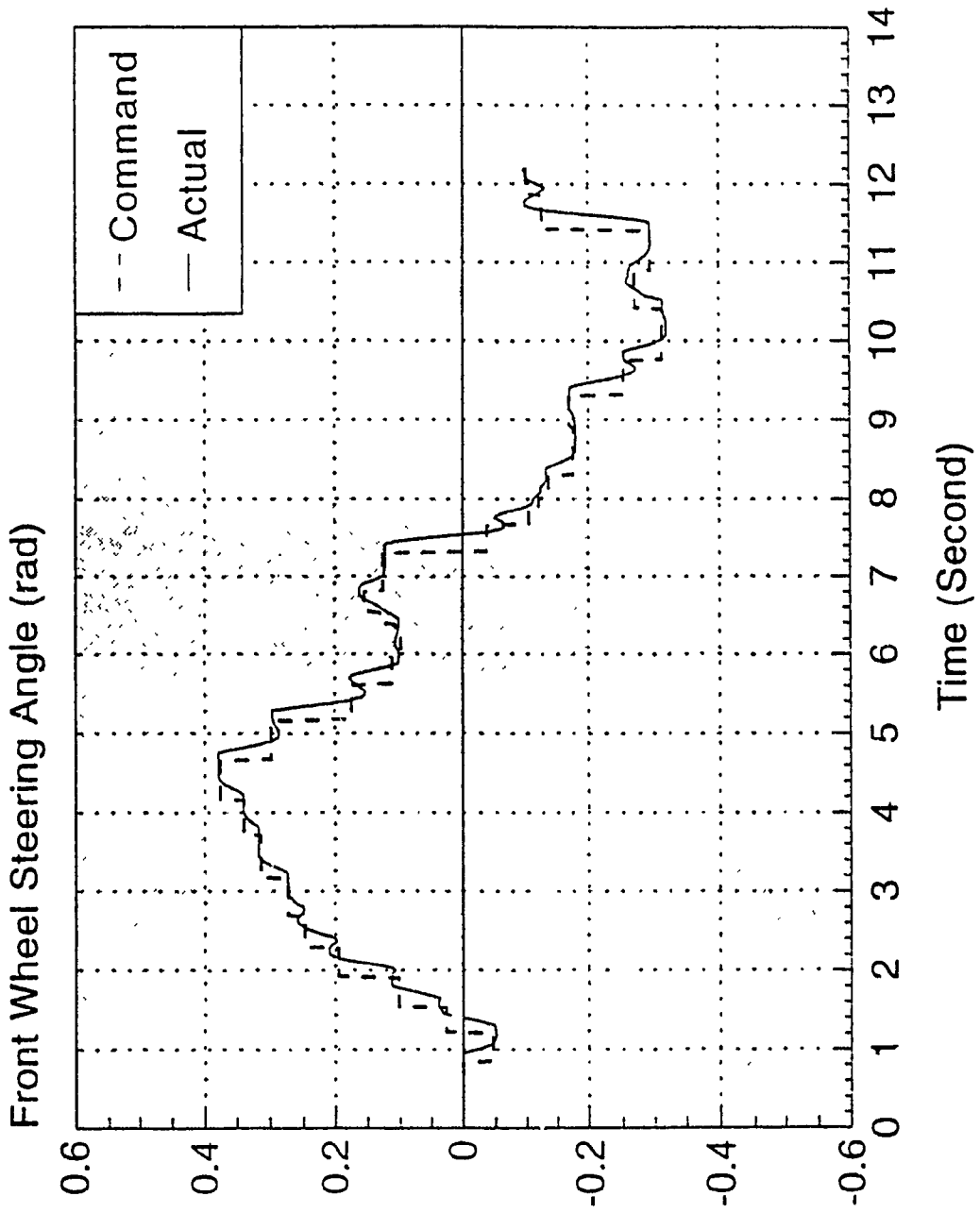

Fig.9.9.c Variation of Front Wheel Steering Angle

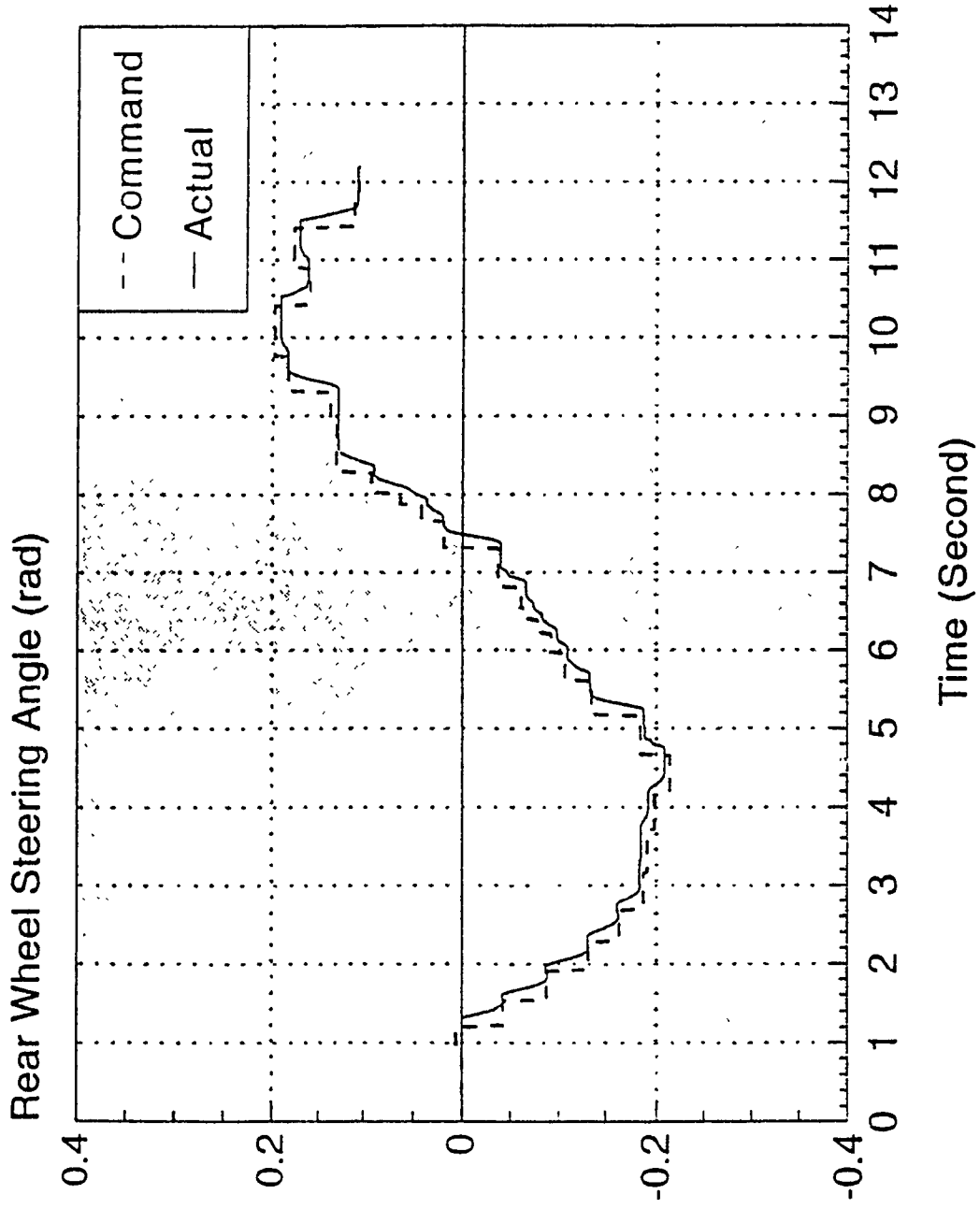

Fig.9.9.d Variation of Rear Wheel Steering Angle

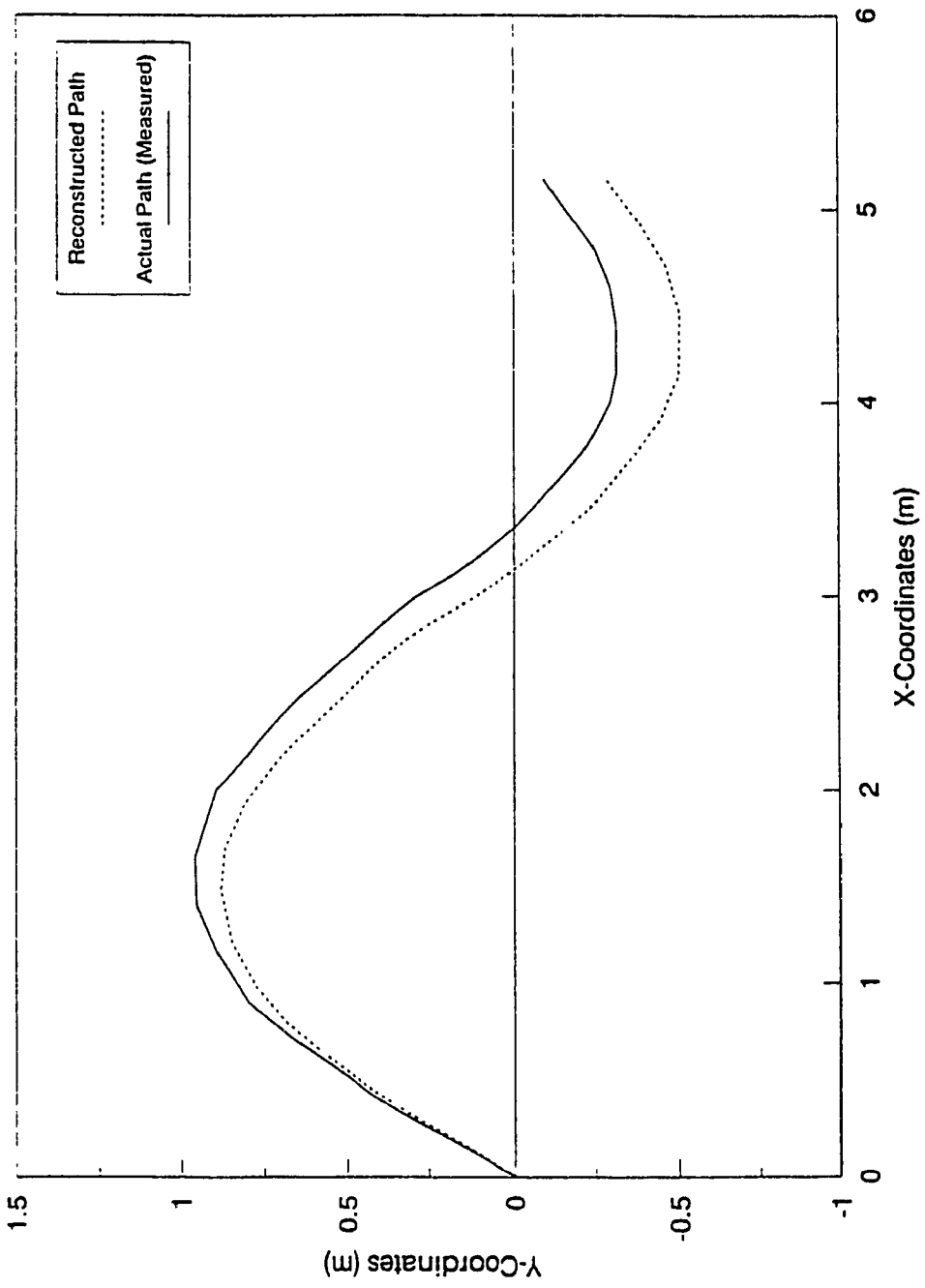

Fig.9.9.e Comparison of the Actual Path (measured from the floor) and Reconstructed Path

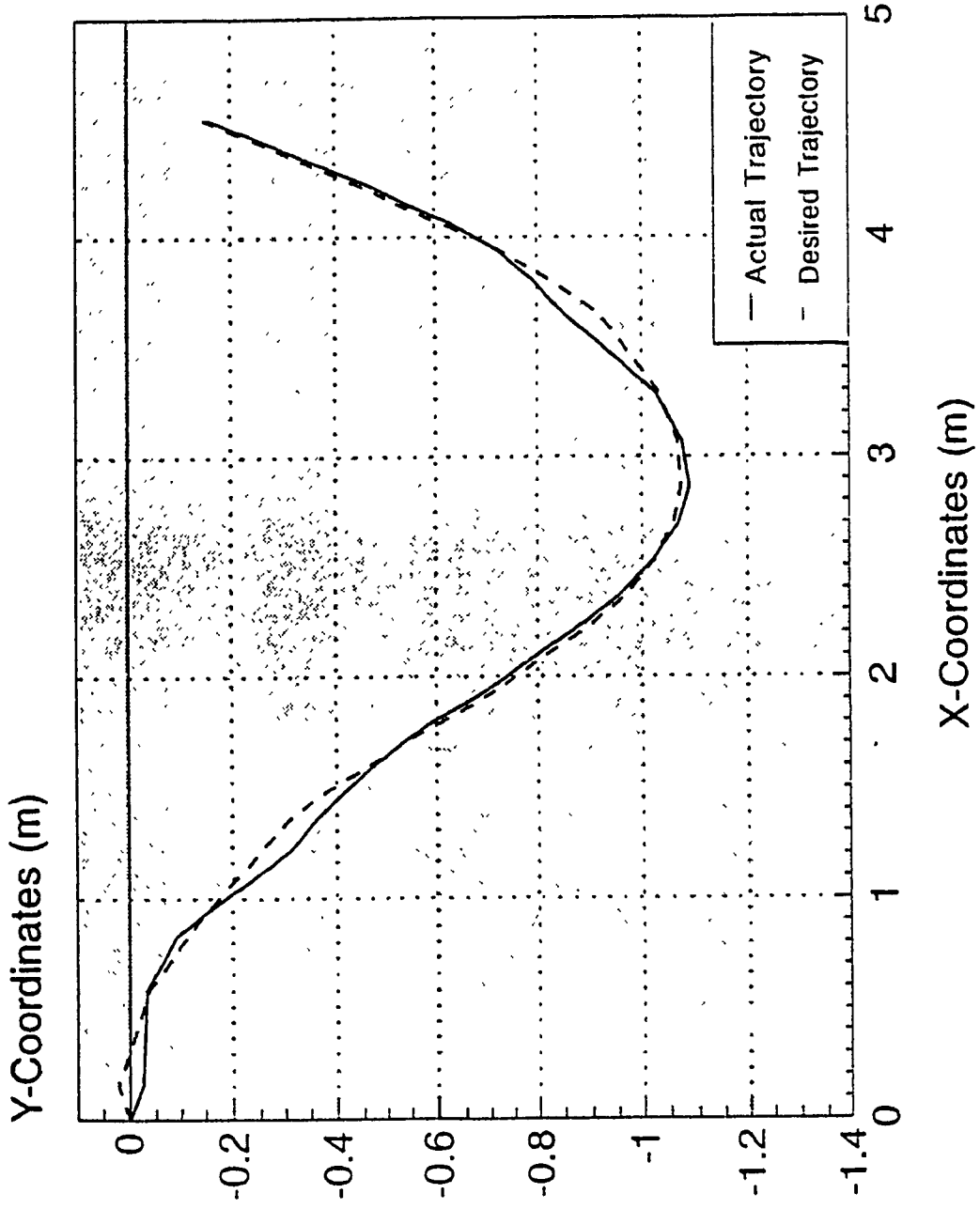

Fig.9.10.a Path Following of the Vehicle for Another Trajectory

(Comparison of the Actual Path (Reconstructed) and Desired Trajectory)

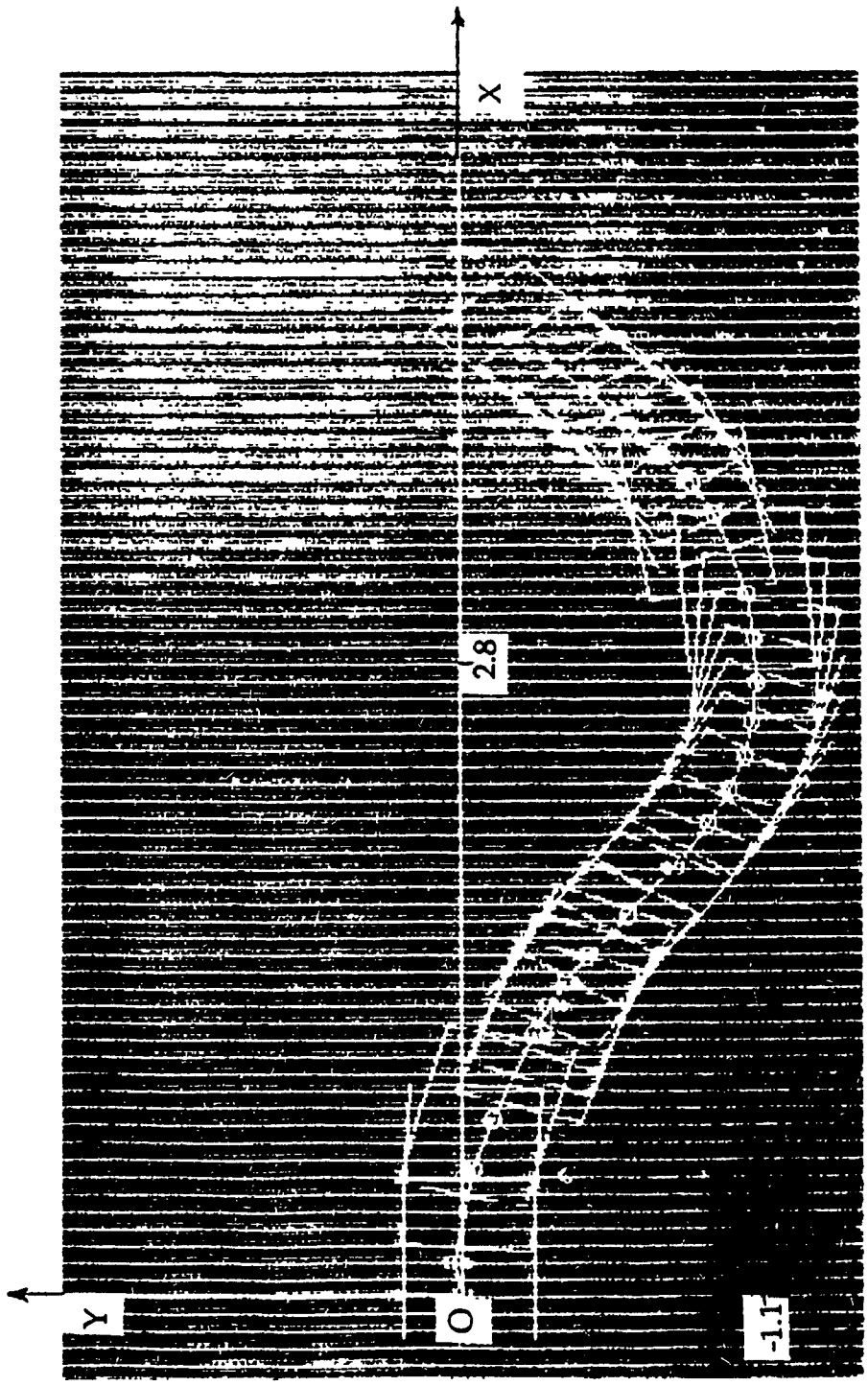

Fig.9.10.b Relative Posture of the Vehicle and the Desired Trajectory

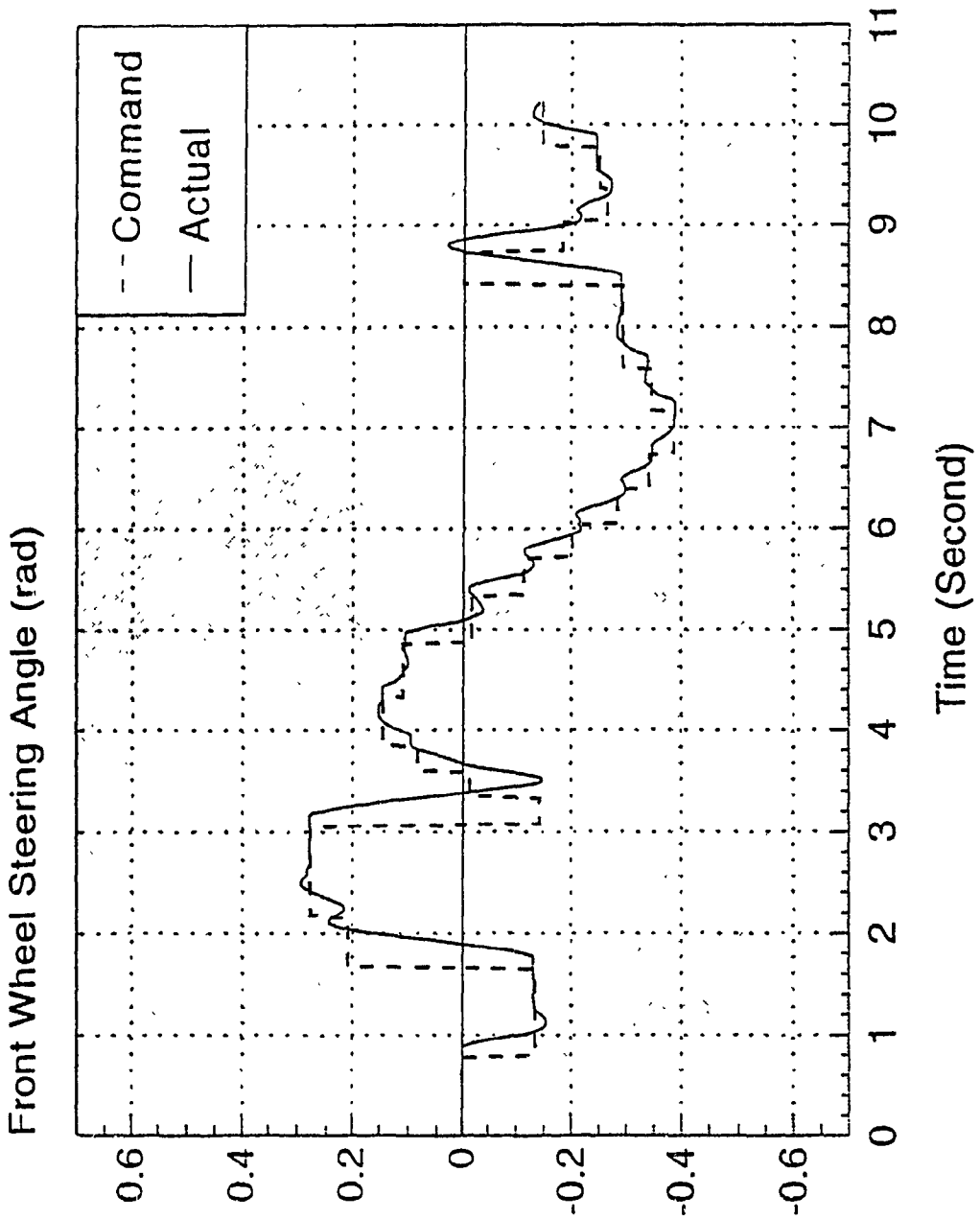

Fig.9.10.c Steering Angle of the Front Wheel

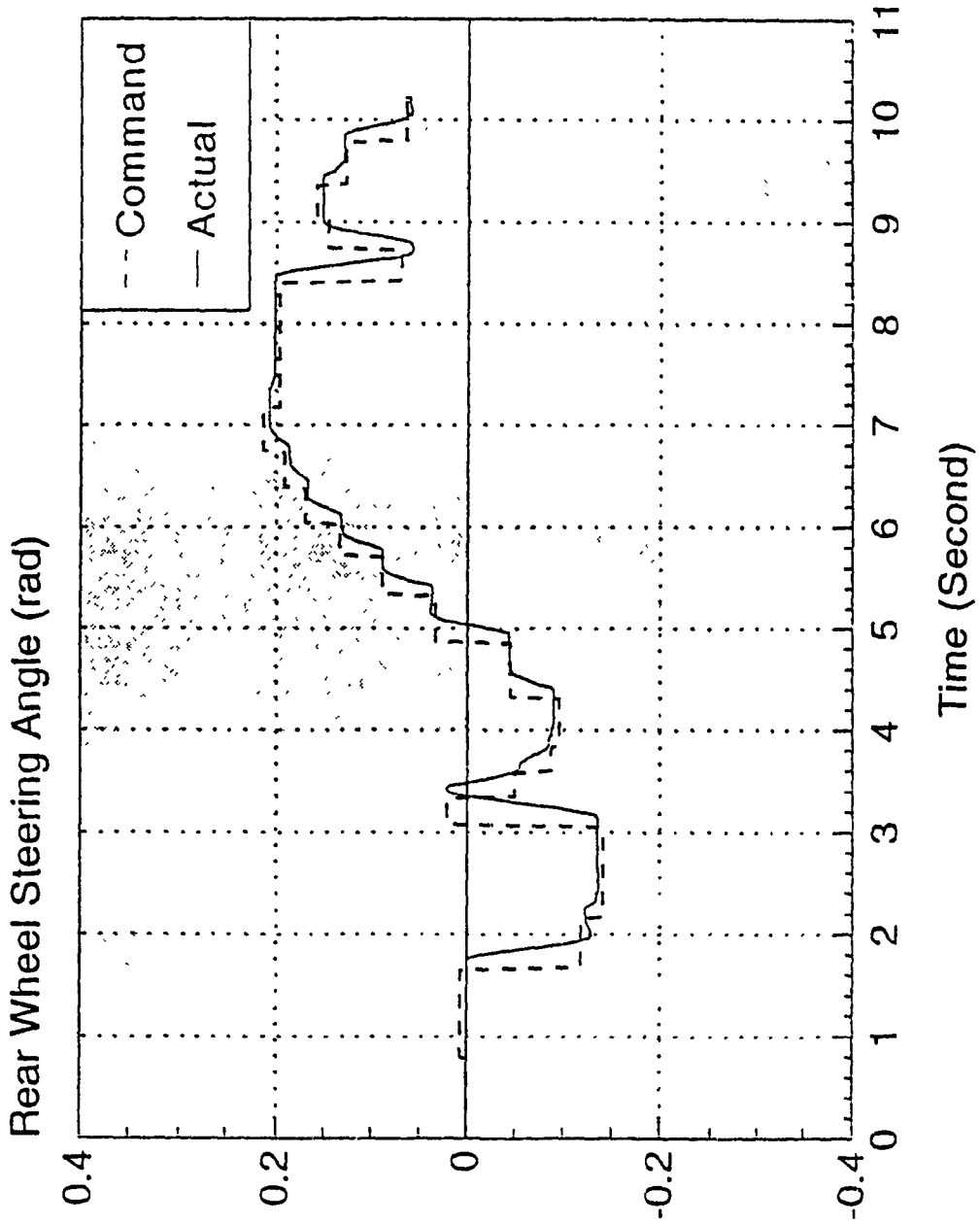

Fig.9.10.d Variation of Rear Wheel Steering Angle

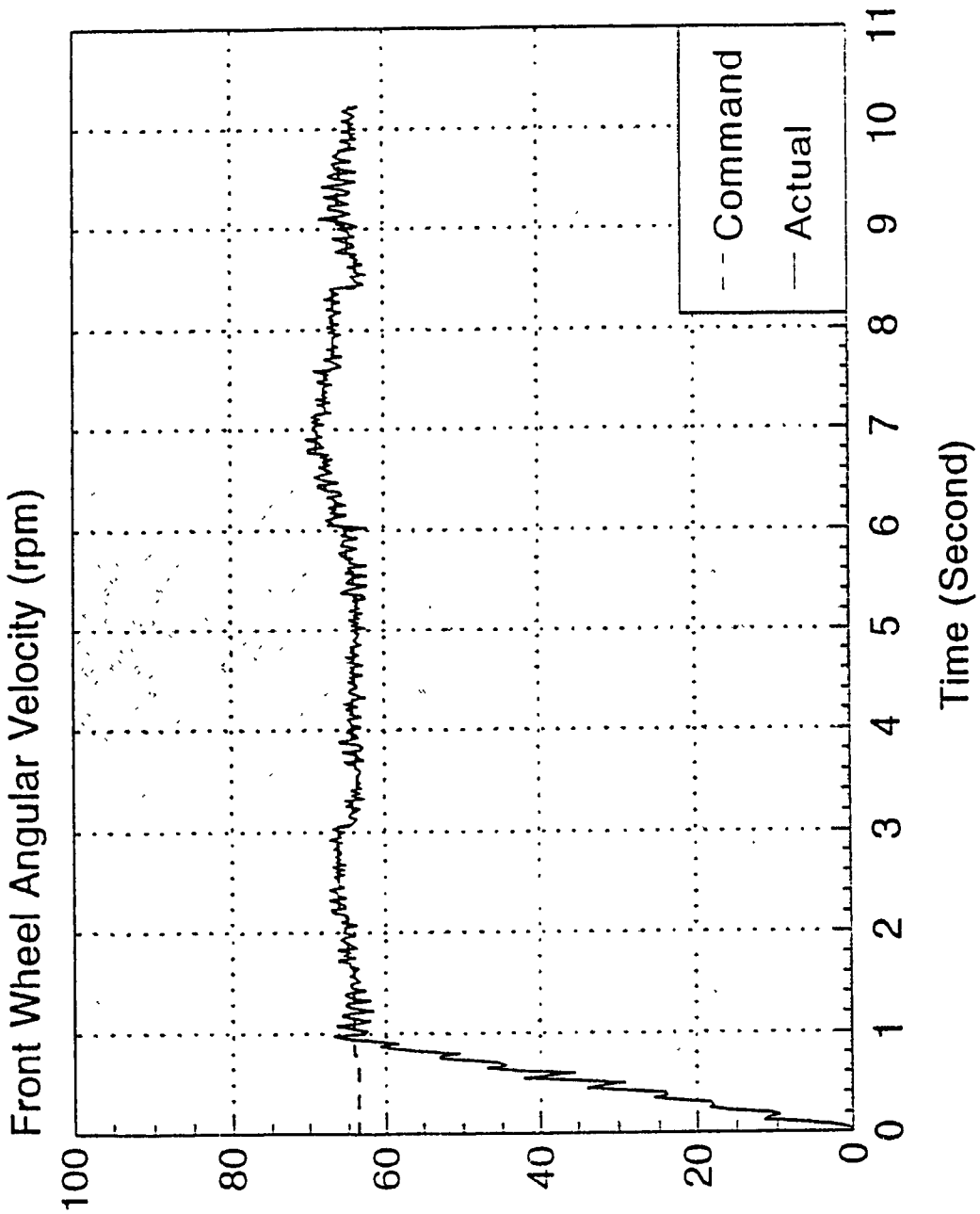

Fig.9.10.e Variation of Front Wheel Angular Velocity

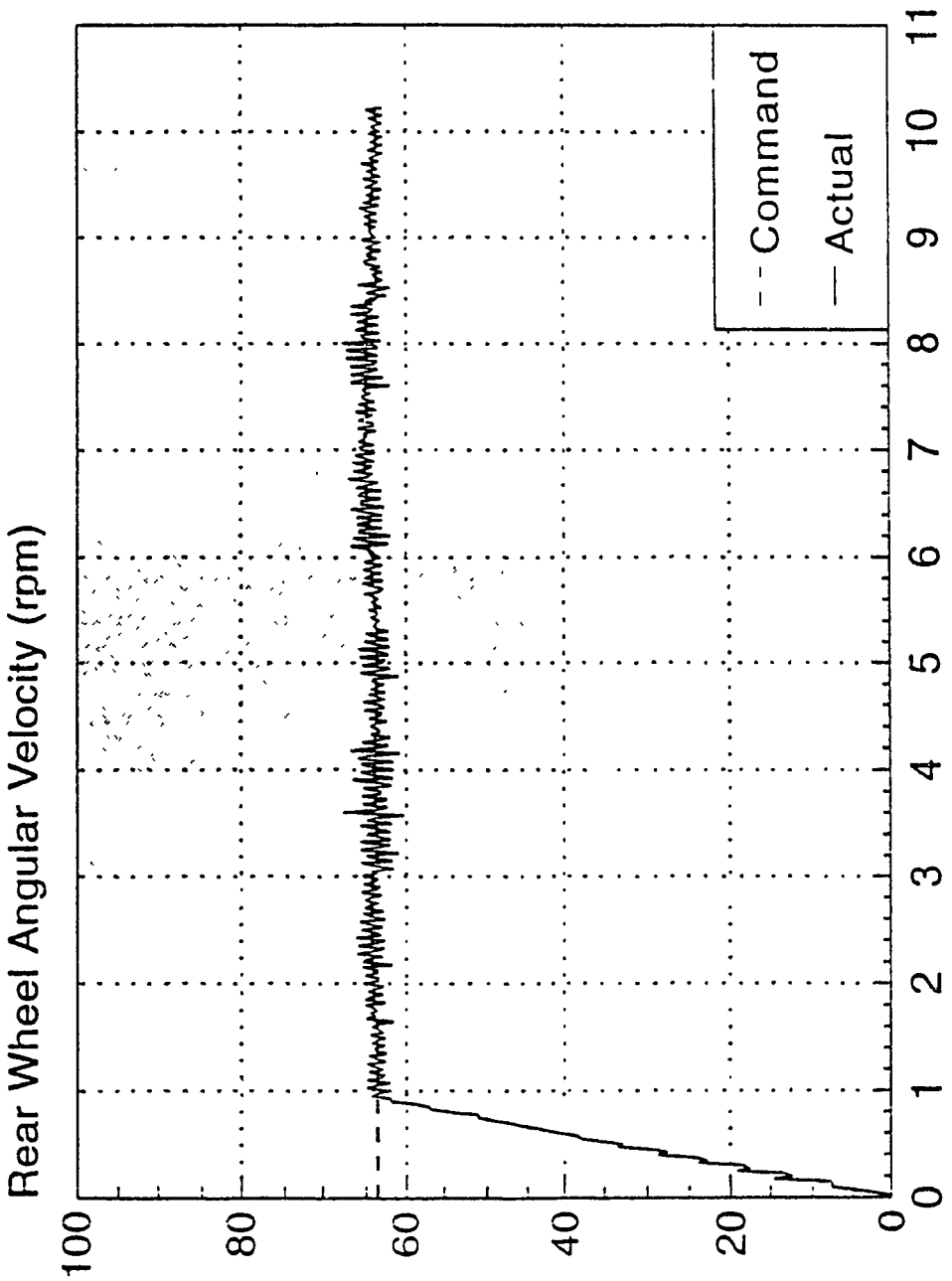

Fig.9.10.f Variation of Rear Wheel Angular Velocity

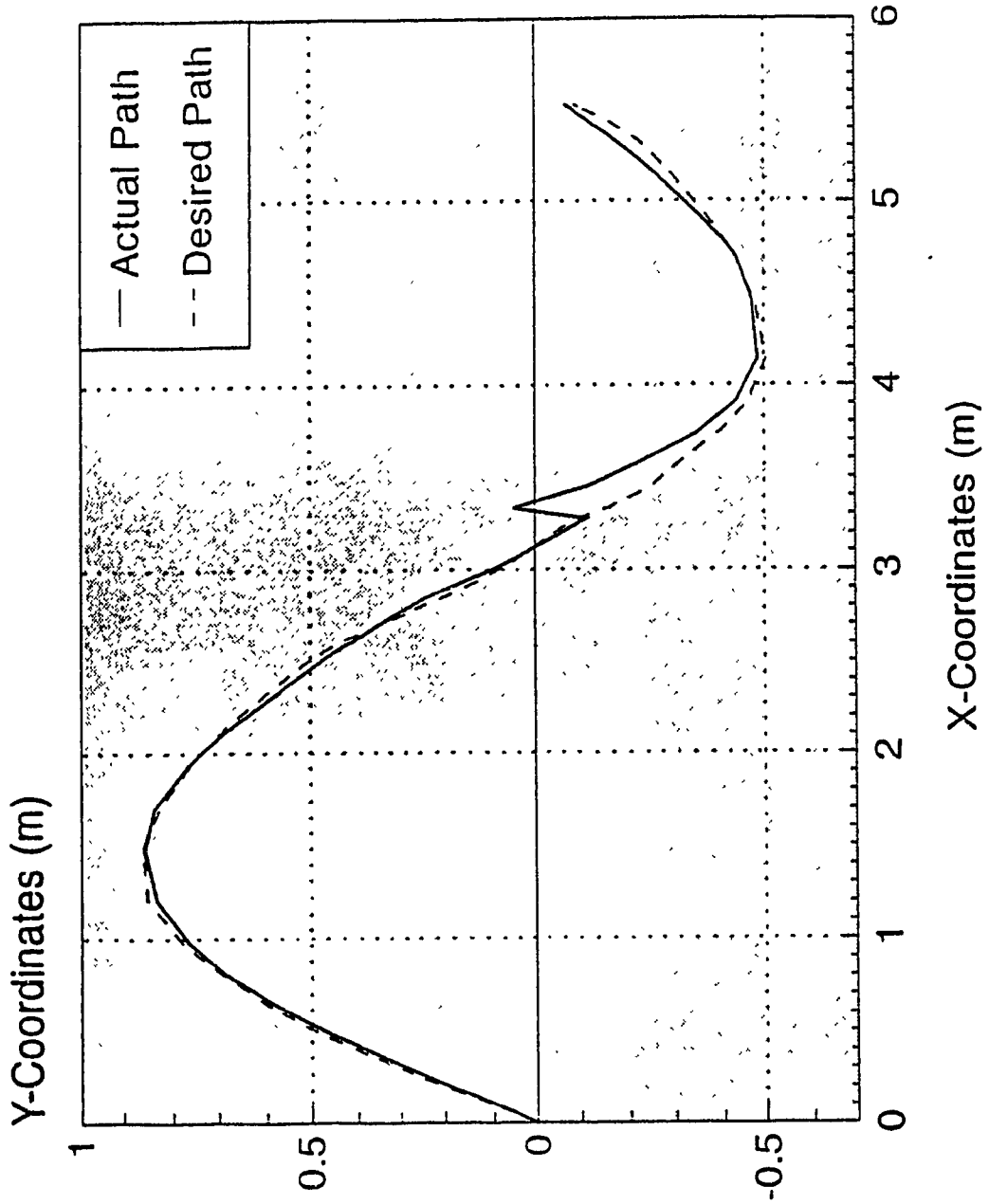

Fig.9.11.a Path Following of the Vehicle Under Disturbance

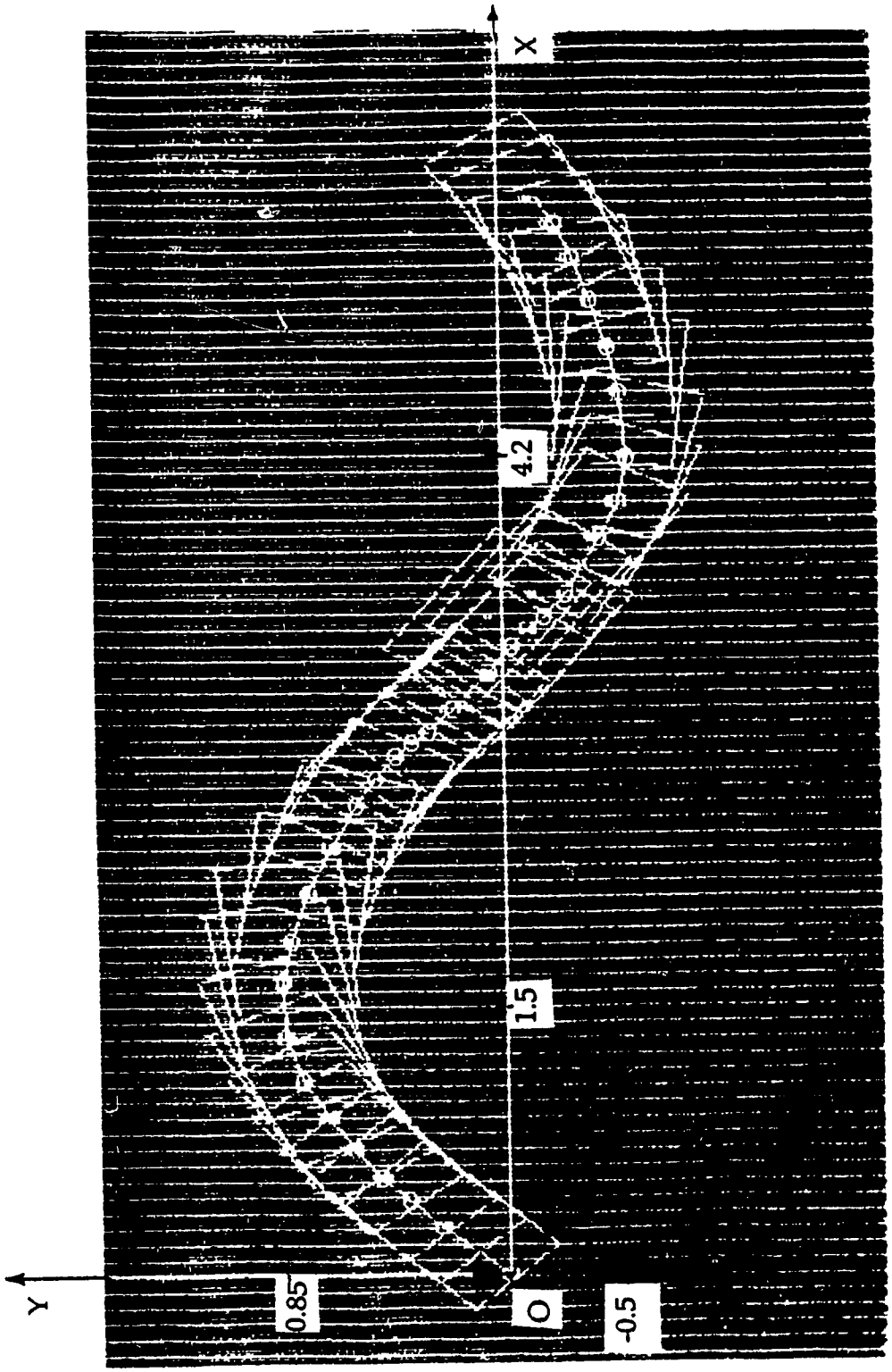

Fig.9.11.b Relative Posture of the Vehicle and the Desired Path

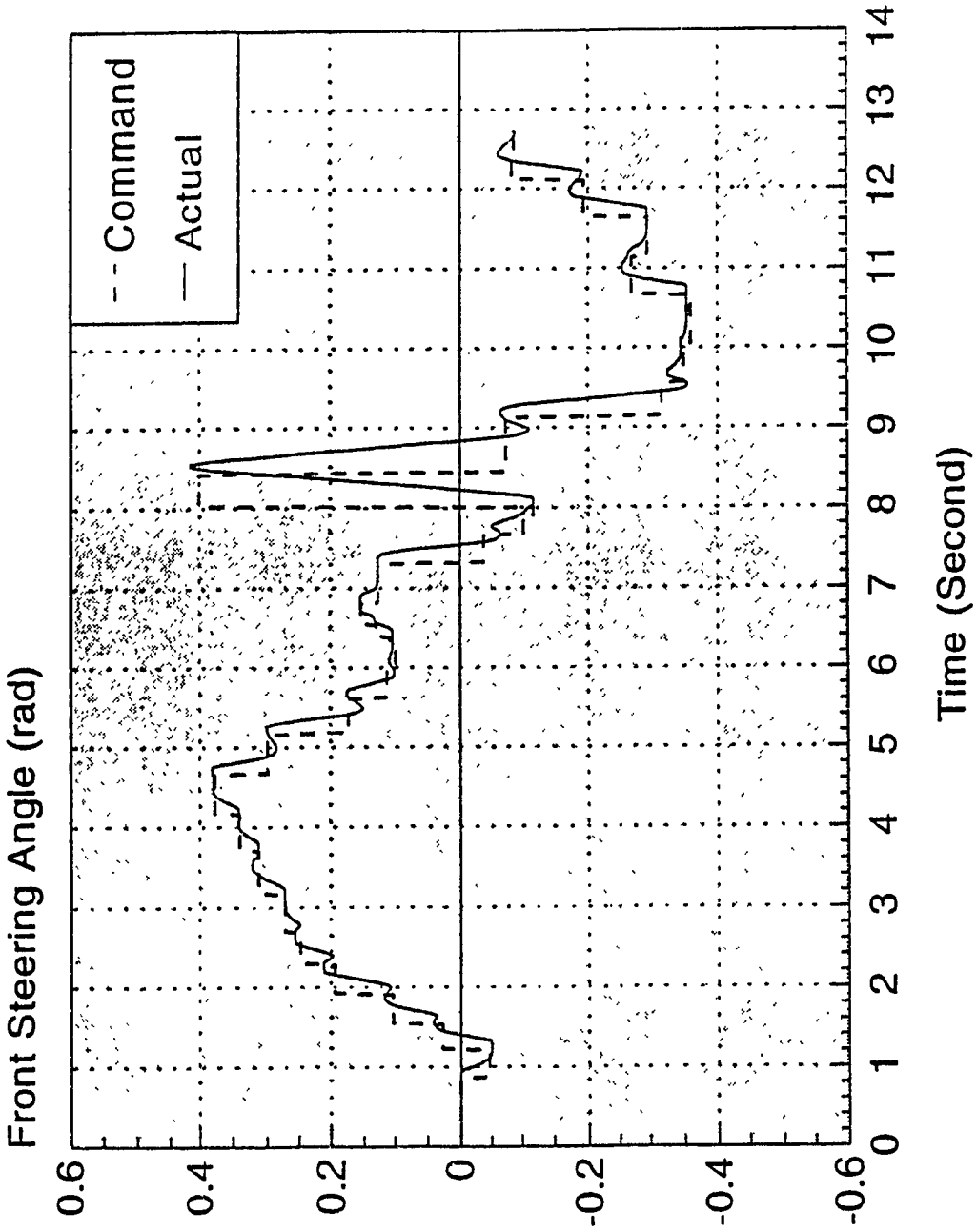

9.11.c Front Wheel Steering Angle Under the

Effect of External Disturbances

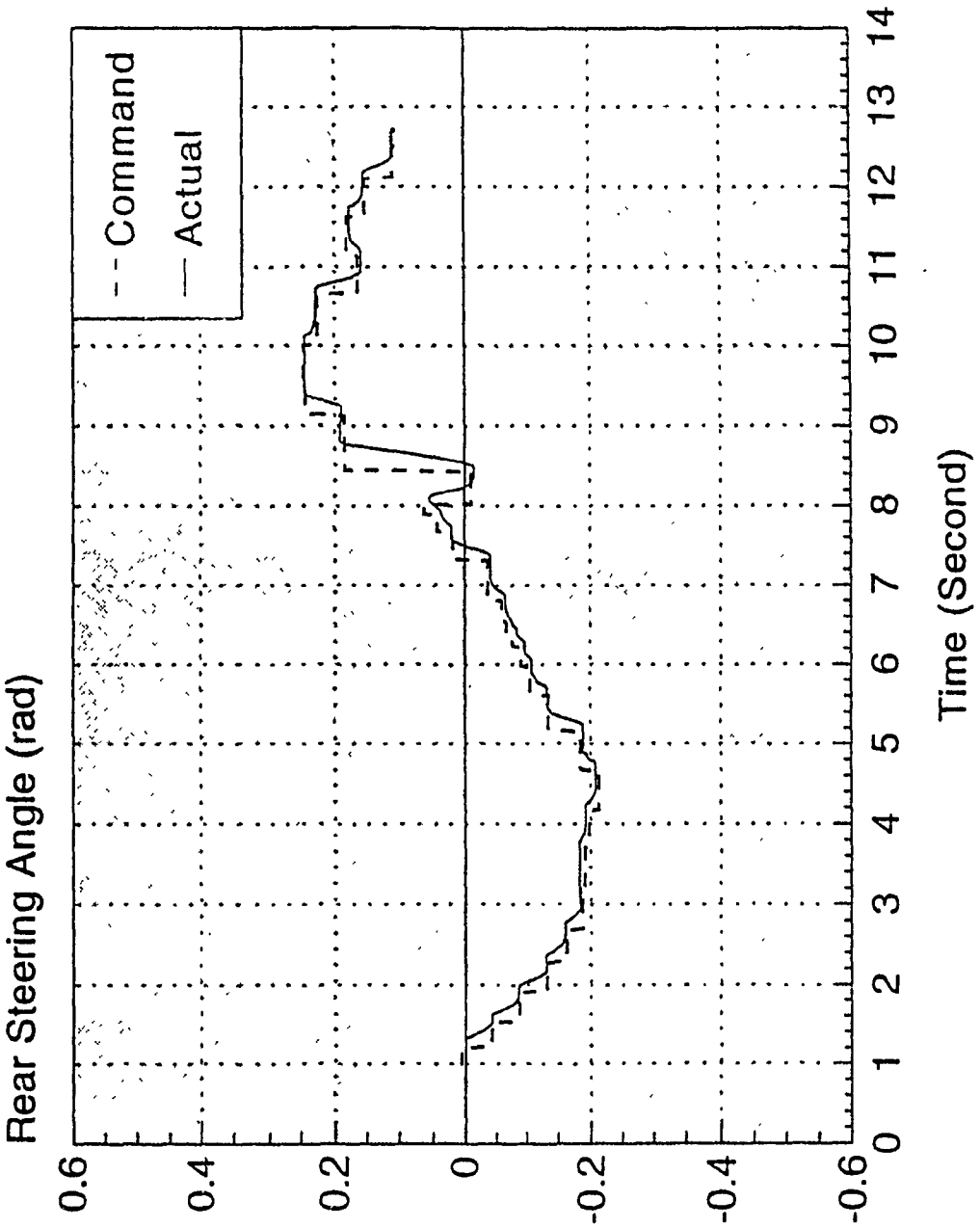

Fig.9.11.d Variation of Rear Wheel Steering Angle

Under the Effect of External Disturbances

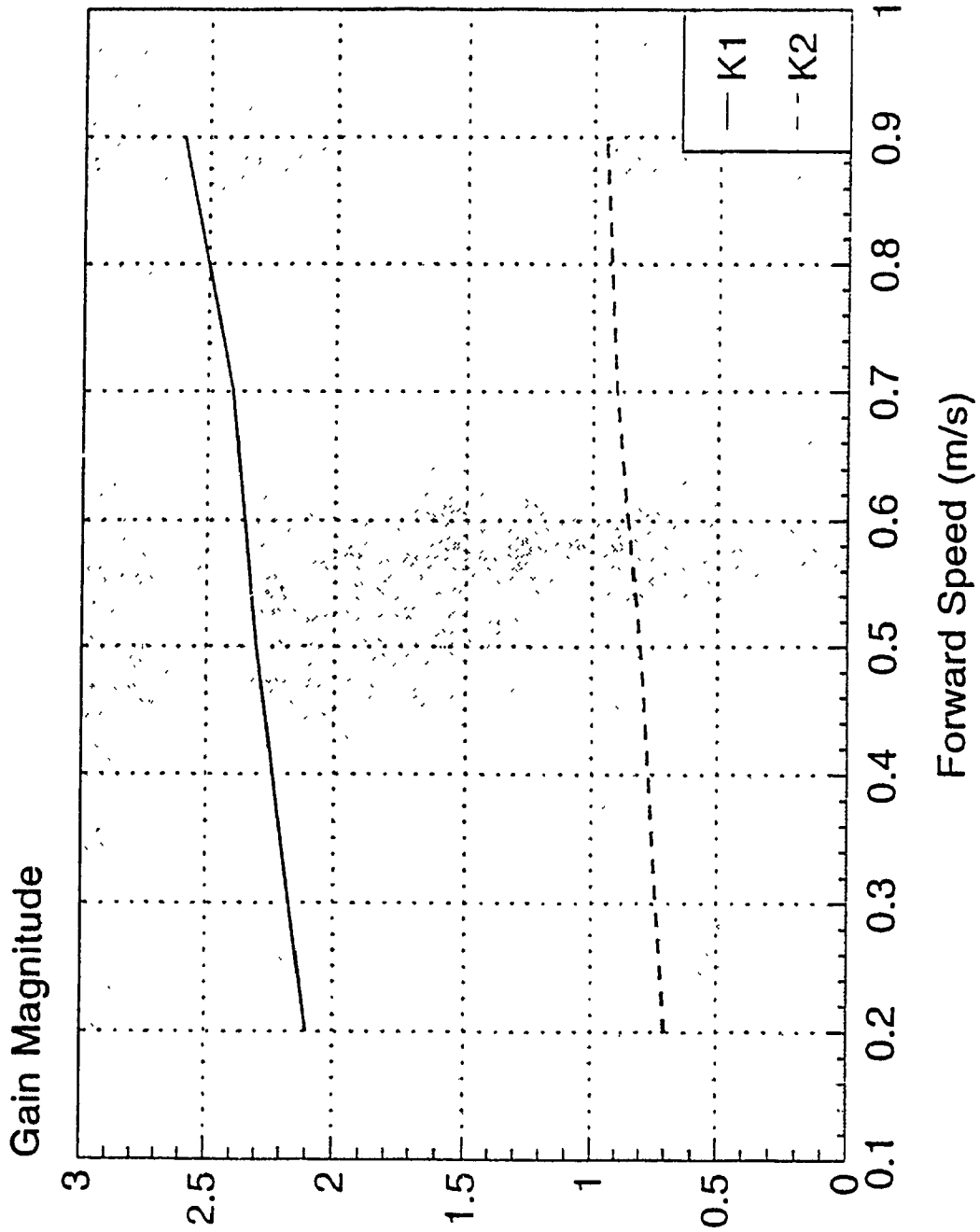

Fig.9.12 Variations of K_1 and K_2 as a Function of the Speed.

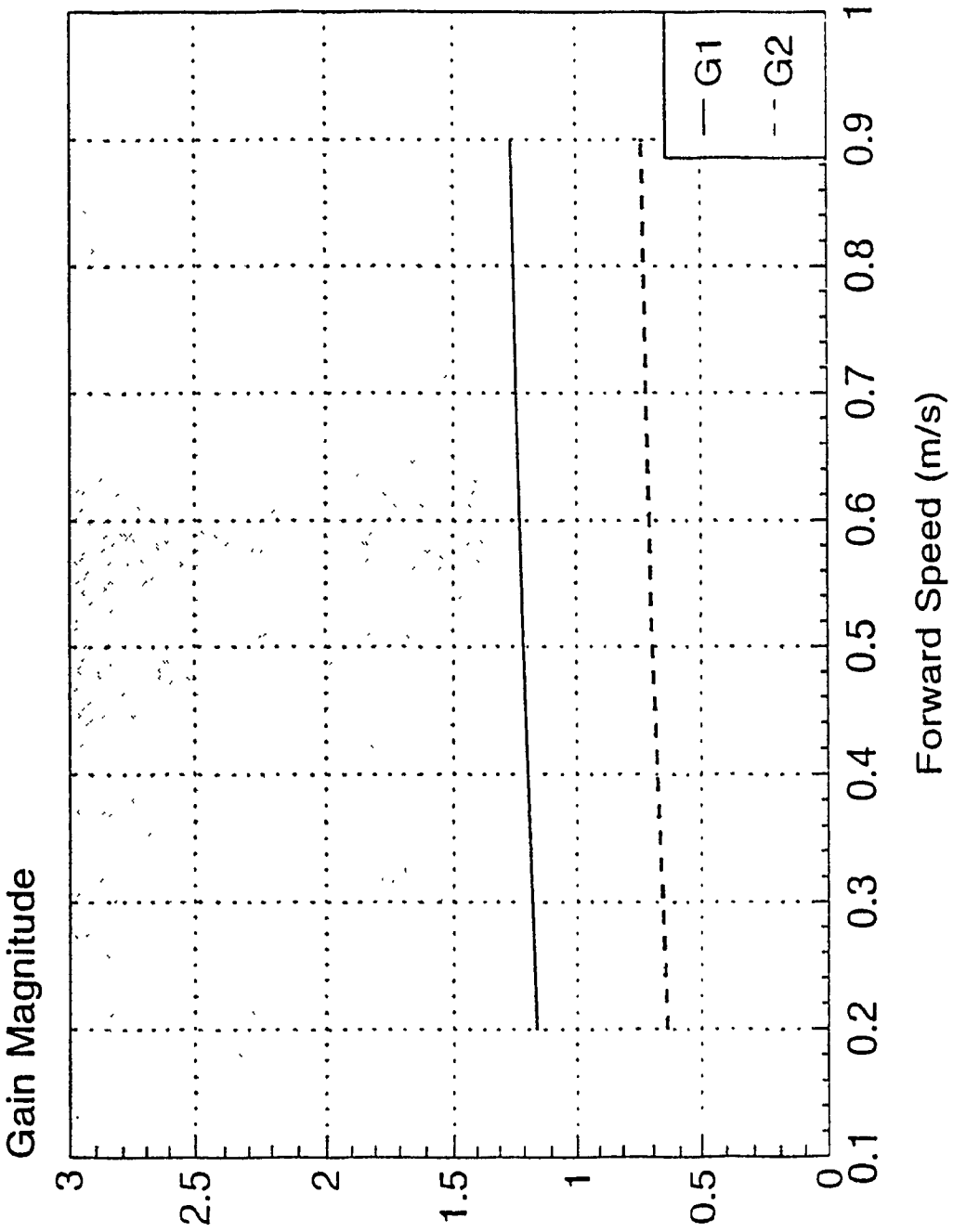

Fig.9.13 Variations of G_1 and G_2 as a Function of Speed

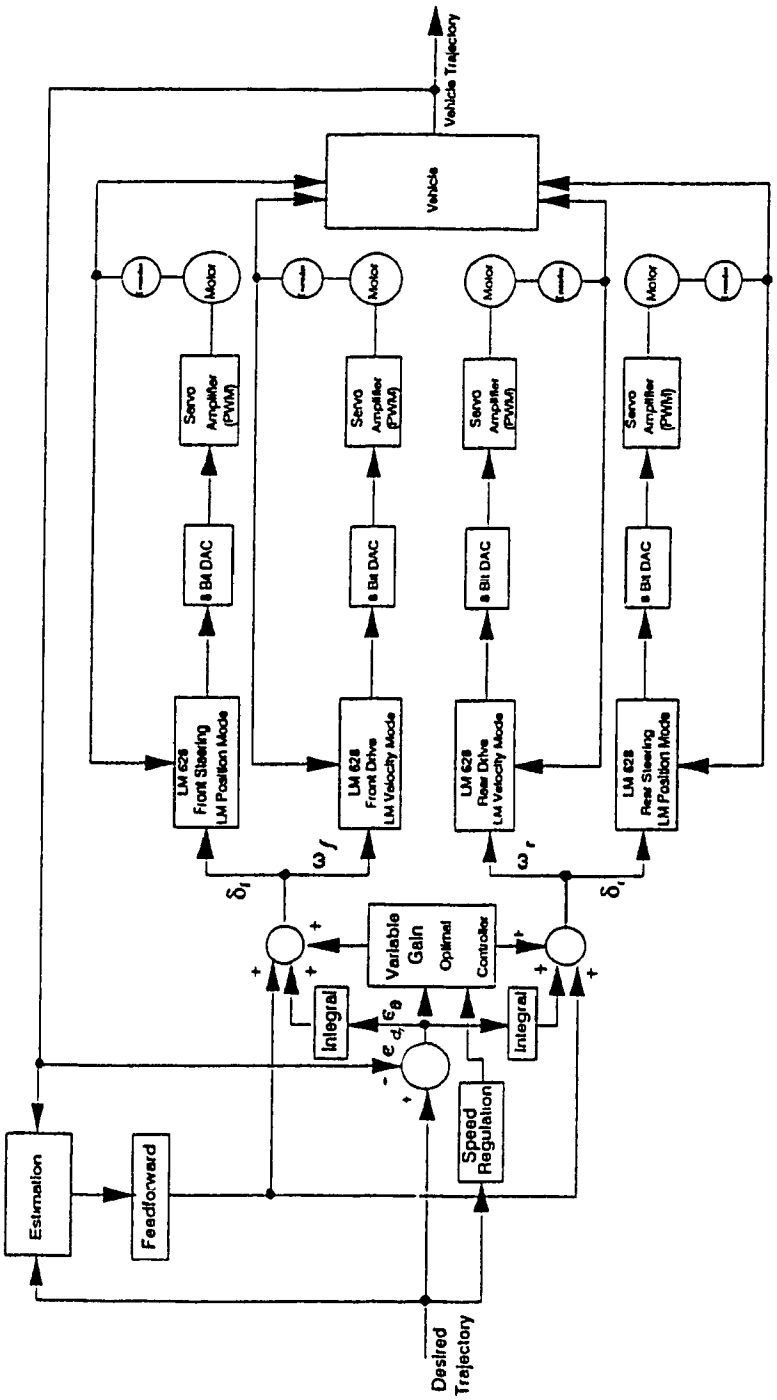

Fig. 9.14 Complete Block Diagram of the Controlled System

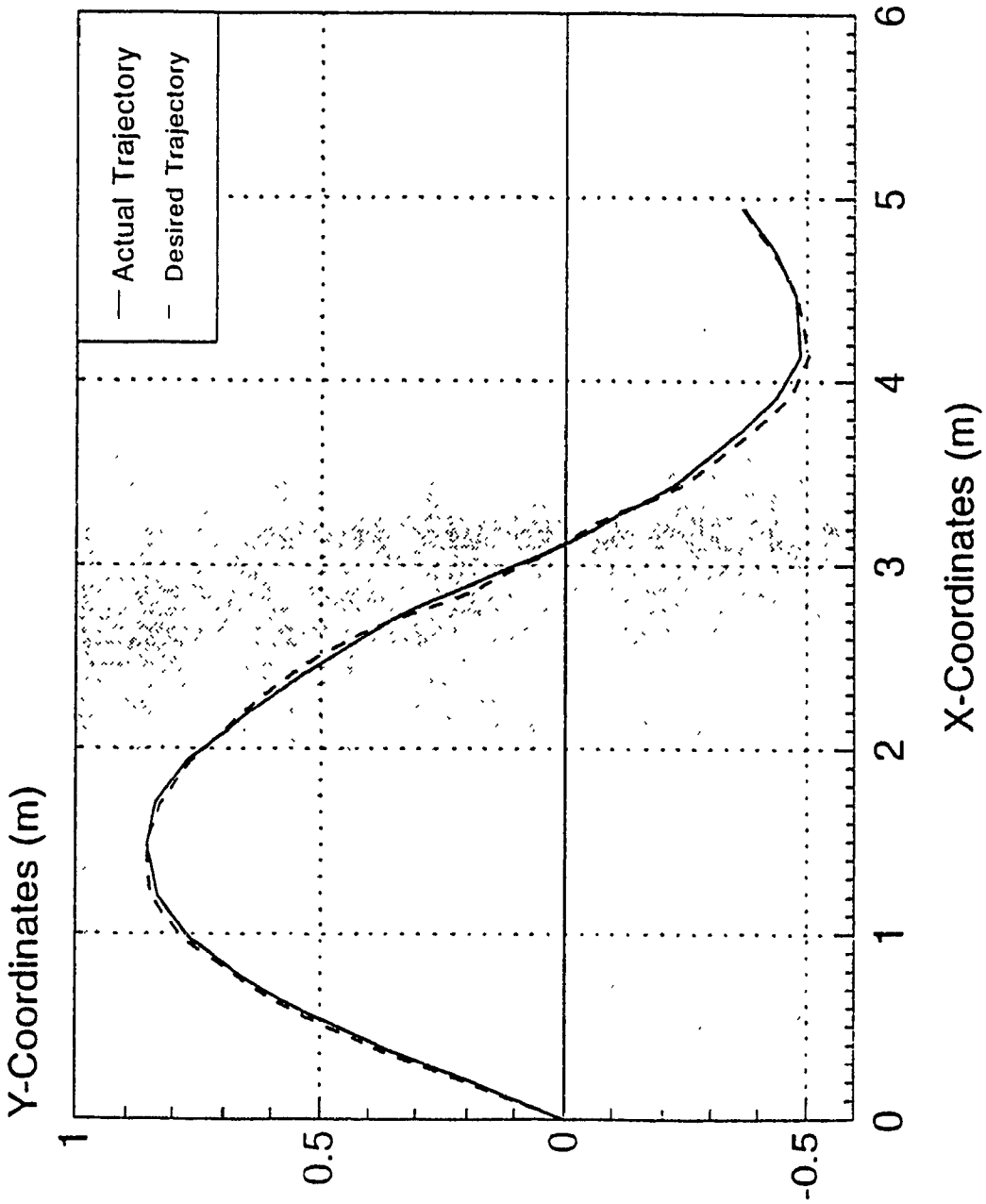

Fig. 9.15.a Path Following of the Vehicle with Adjustable Speed

Actual Path (Reconstructed Path) and Desired Path

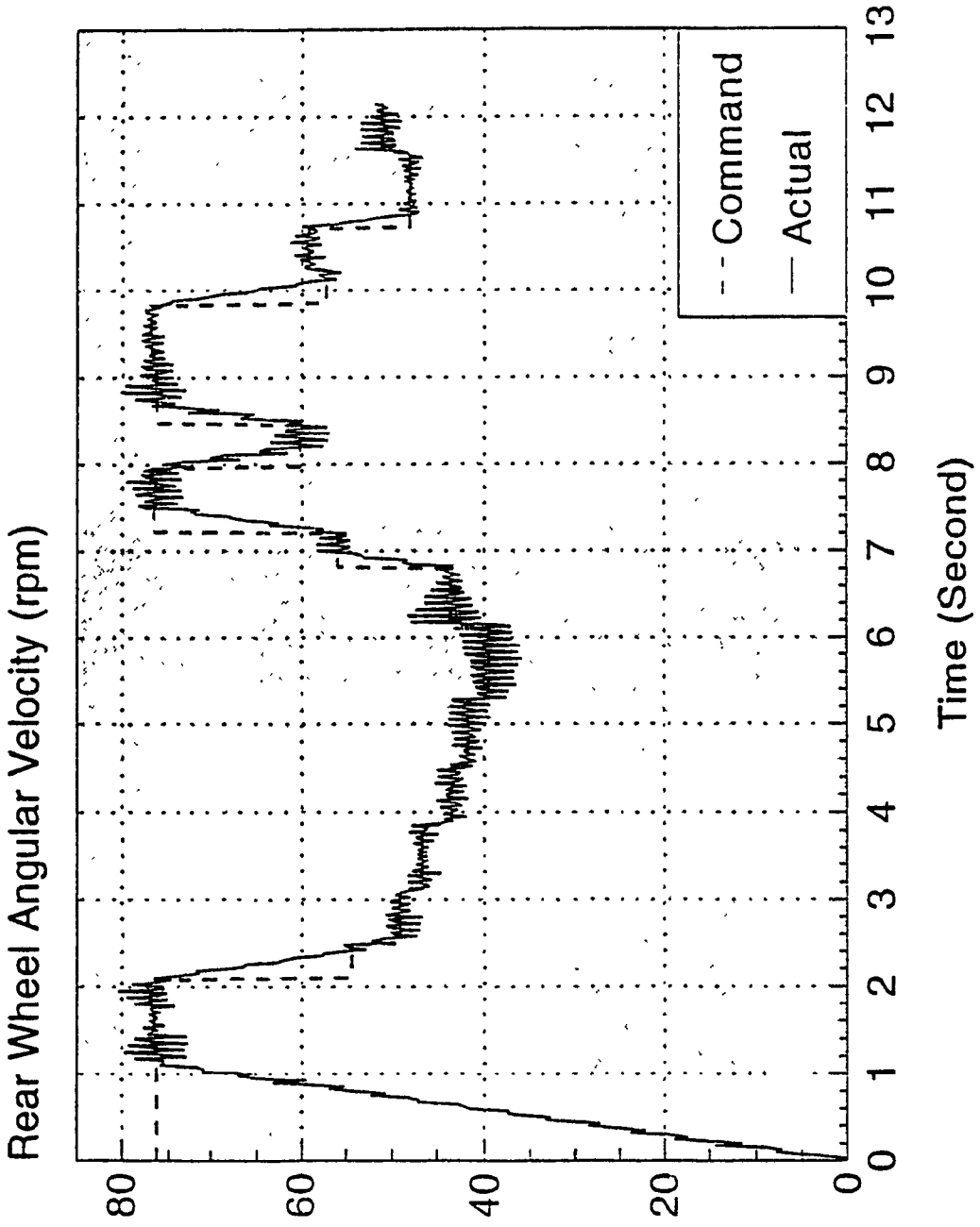

Fig. 9.15.b Angular Velocity of the Rear Wheel

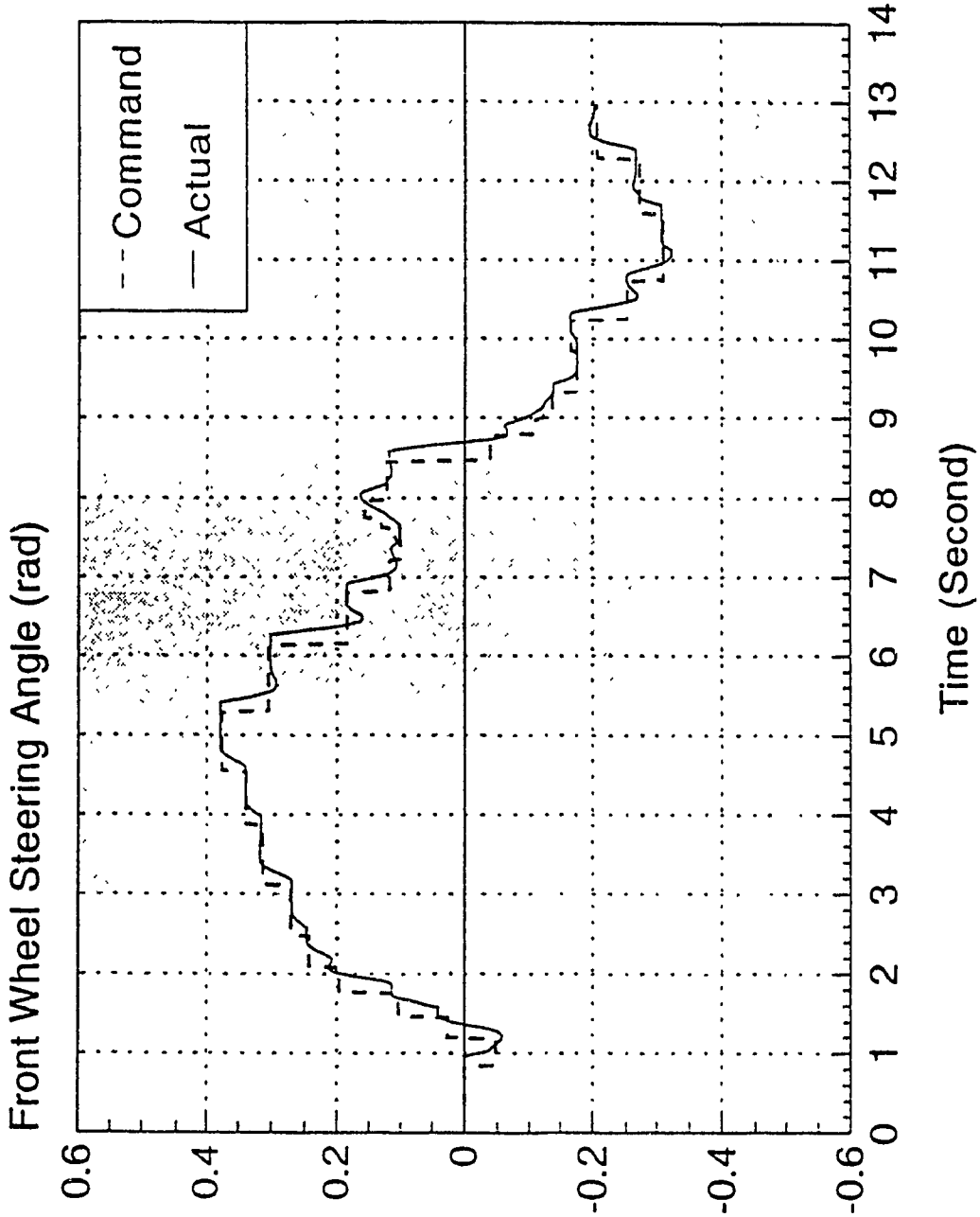

Fig. 9.15.c Variation of Front Wheel Steering Angle

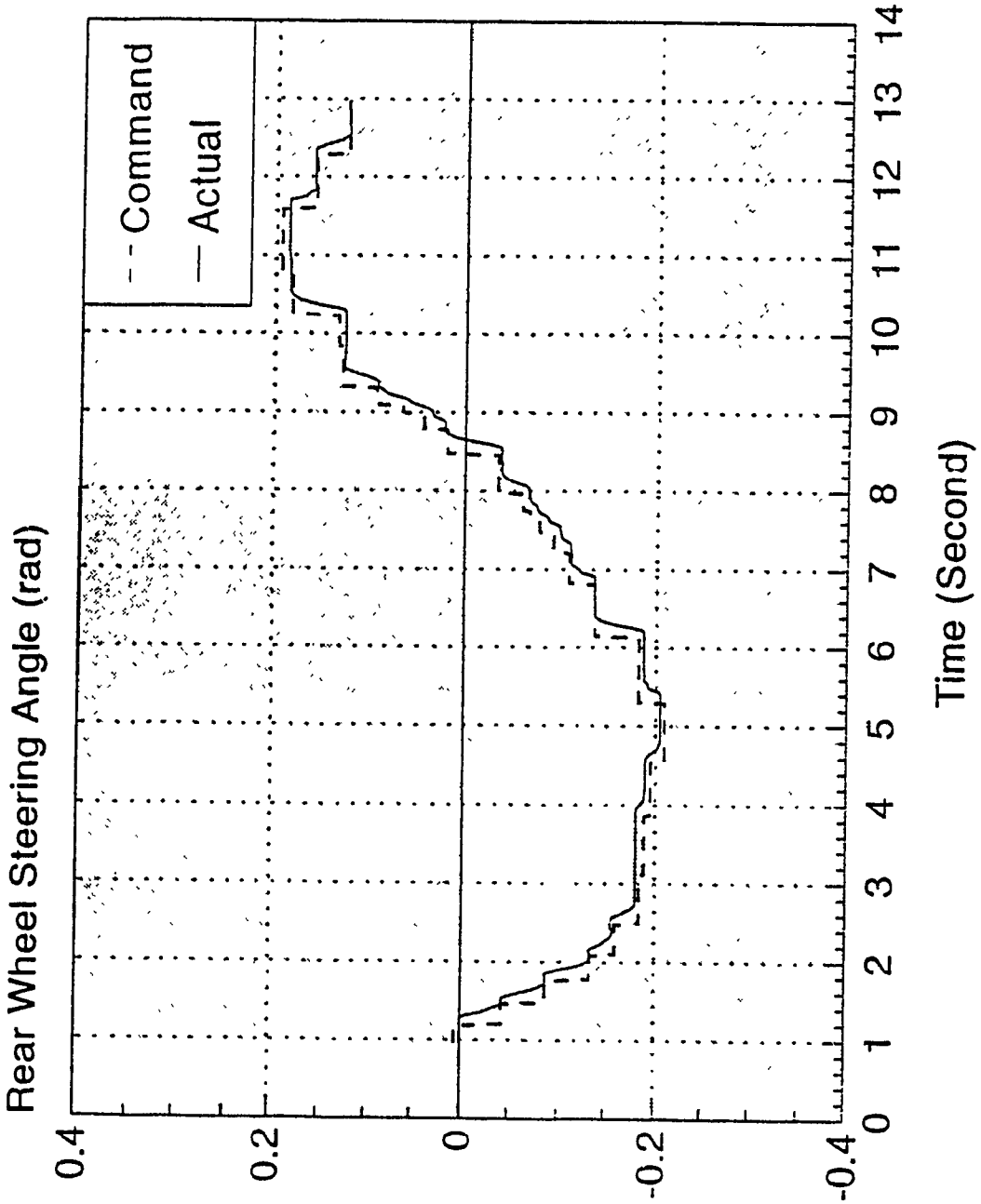

Fig. 9.15.d Variation of Rear Wheel Steering Angle

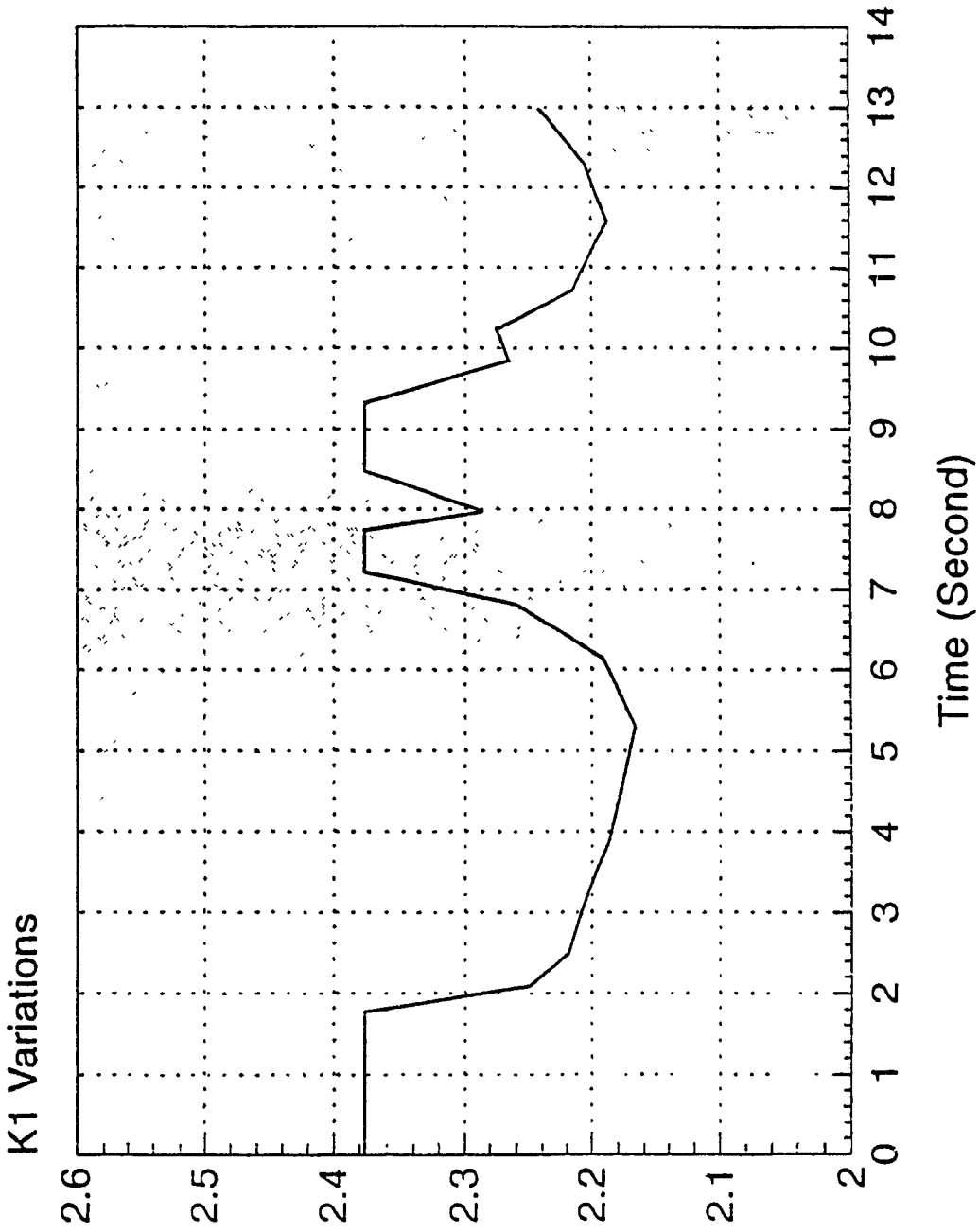

Fig. 9.15.e Variation of K_1 with Time

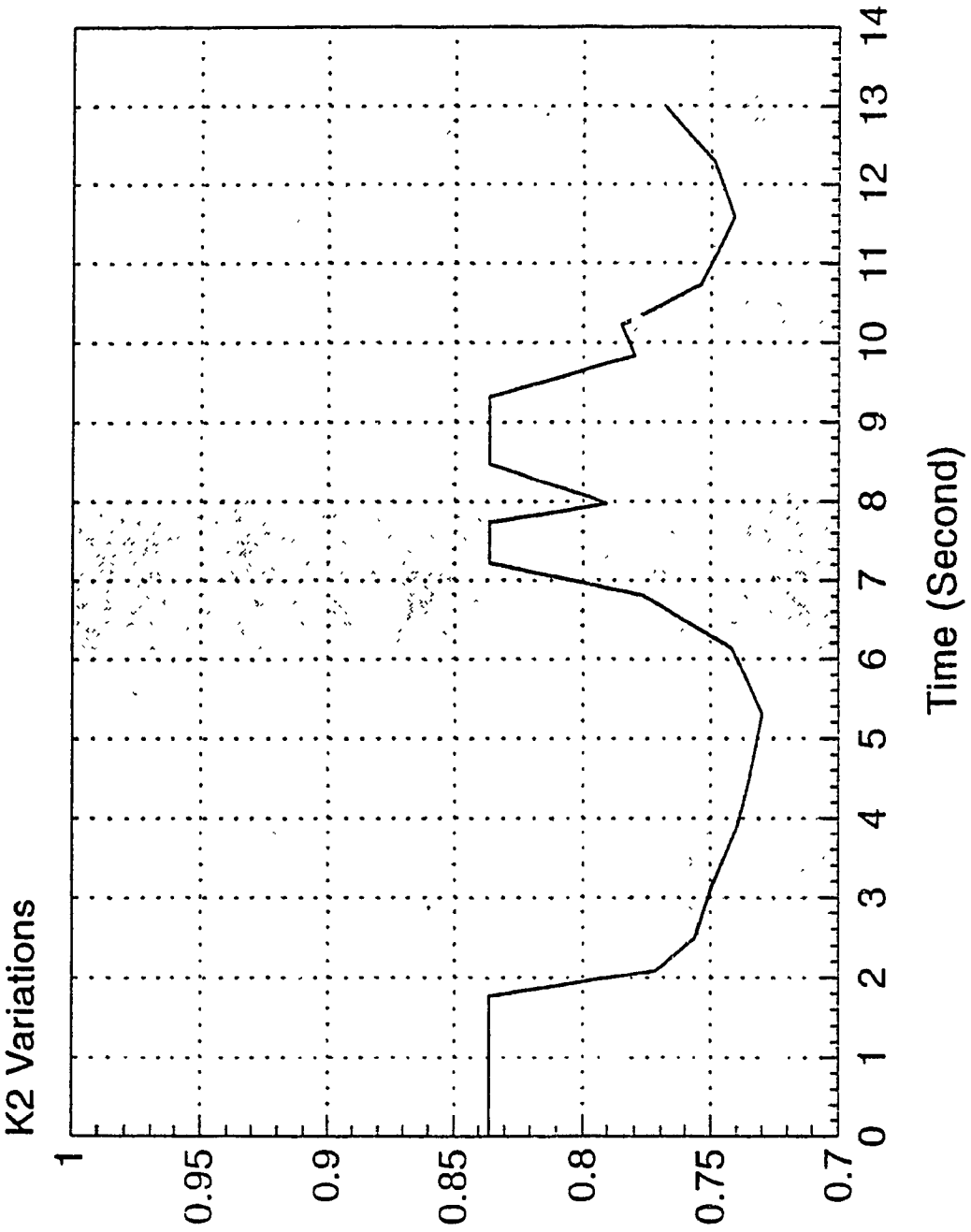

Fig. 9.15.f Variation of K_2 with Time

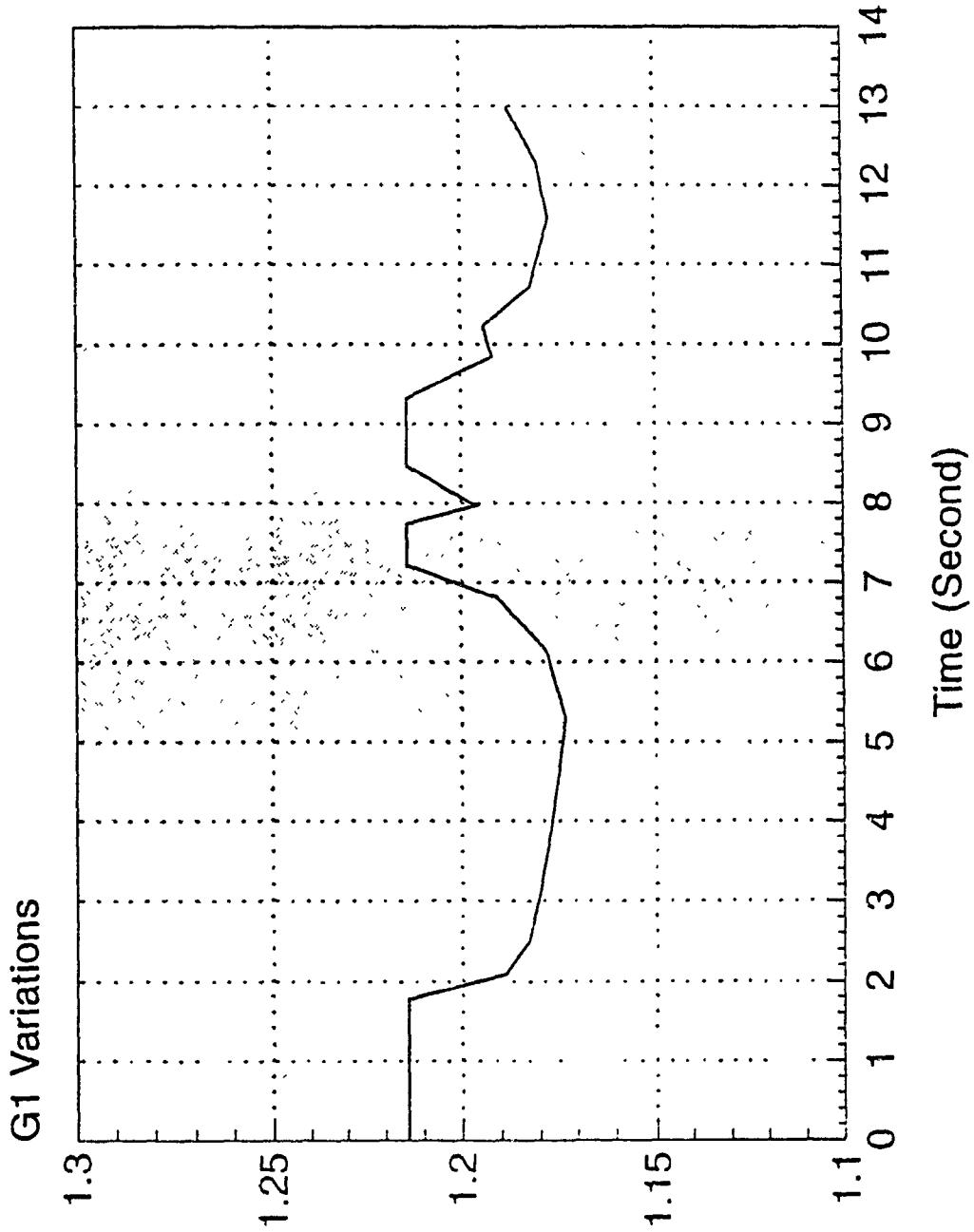

Fig. 9.15.g Variation of G_1 with Time

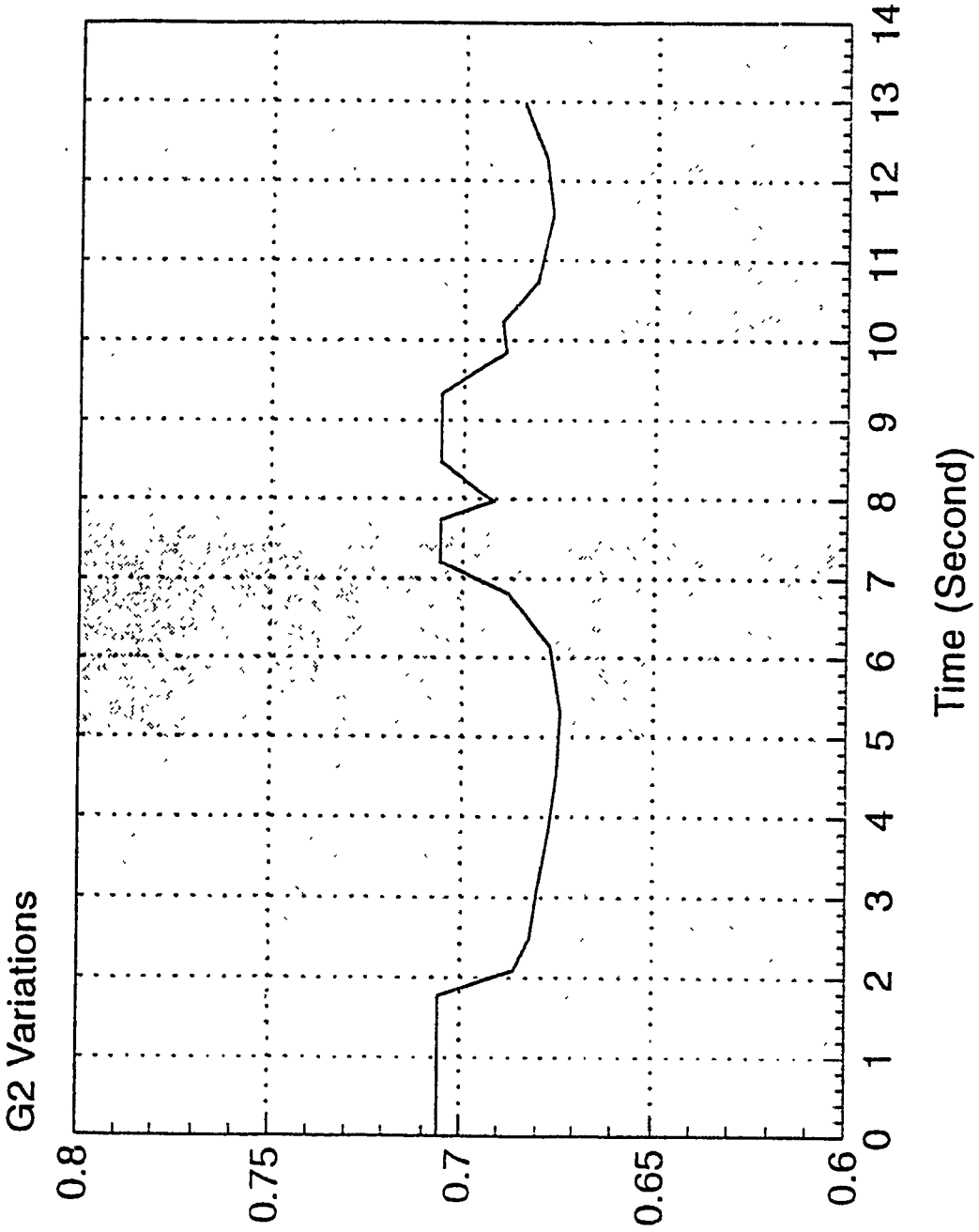

Fig. 9.15.h Variation of G_2 with Time

CHAPTER 10

CONCLUSIONS AND RECOMMENDATIONS FOR FUTURE WORK

10.1 Introduction

Path tracking control of automated vehicles has been the principal subject of this thesis. The theoretical results have been accomplished by experimentation on a real size prototype. In this regard, CONCIC III vehicle was built at the Centre for Industrial Control (CIC) of Concordia University and all the experimentations were accomplished by using this vehicle.

The purpose of this chapter is to summarize and discuss the overall results obtained from all theoretical studies and the experimental work. The various dynamic models that can be used in the motion study of these vehicles are briefly

explained and their advantages and disadvantages are mentioned. The characteristics of dynamics of these systems are described. The methods that can be used to identify their dynamic properties are summarized and the respective importance of the physical parameters of these vehicles that affect their dynamic behaviour are pointed out. A number of control strategies developed for different wheelbase configurations are discussed. Finally, the results of experimental studies on a vehicle with front and rear steering regarding validations of different dynamic models as well as implementations of various control policies are summarized.

10.2 Characterization of Dynamics of Automated Vehicles

Various dynamic models were studied to represent the motion of a vehicle. The equations of motion were developed by using the freebody diagram of a vehicle and taking into account the nonholonomic constraints, necessary for nonslipping motion of the vehicle, the inertia properties of the vehicle's body and the wheels, stiffness properties of the tire and their rolling resistance. For control applications the nonlinear equations are further simplified in order to enable one to get closed-form solutions. The linearized models are obtained by making certain assumptions and using some trigonometric approximations. While the linear equations retain the important dynamic properties of a system, they simplify any further analytical study. As well, they can be represented in the

state space format, which is a preferred choice for controller design and simulation purposes.

Two linear models are considered in this thesis: 3-DOF model, that takes into account yaw, lateral and roll motions of a vehicle and 2-DOF model that considers only the yaw and lateral motion corresponding to plane motion of a vehicle. The roll motion is coupled to the lateral and yaw motions as it is observed from the equations of motion. How strong this coupling is, how closely the two models are compatible and the effect of the parameters of the vehicle involved in this interaction, all are specified by a dimensionless number called "roll number". In this work, it is shown that the dimensionless "roll number" can be employed in deciding when to use each of the above models. For a system whose roll number is small, the 3-DOF model is effectively reduced to a 2-DOF model as a result of pole-zero cancellation. By checking this number for any vehicle one can avoid the complexities associated with the studies of steering controller design, directional response, directional stability as well as structural design if the simpler model would suffice.

Another issue studied in this thesis is the investigation on the importance of transient responses of yaw and lateral velocities and their relevant effects on plane motion of a vehicle. In this regard, two other entities called "velocity constant" and "yaw number" are introduced. These entities are functions of the

parameters of a vehicle and characterize its transient behaviour in plane motion. They can effectively be utilized in deciding when to use a dynamic model or a simpler model based on kinematics, to represent the motion of the vehicle. Design of the optimal control for path following of the prototype vehicle CONCIC III is an example of effective use of the above quantities.

A parametric study is carried out in chapter 6 by employing sensitivity theory as a tool to investigate the effects of various parameters of a vehicle on its dynamic behaviour. The linear three degrees of freedom (3-DOF) dynamic model was employed for this purpose. For a particular vehicle (CONCIC III) whose roll number is small (0.15) it is shown that generally speaking, those vehicle parameters which directly are related to roll motion, like sprung mass (M_s), roll moment of inertia (I_u), roll damping (D_p), etc. do not have a significant contribution to the yaw and lateral motions. This supports the properties of "roll number" which states that for small roll number, the effect of roll motion can be neglected. From the results, it was shown that the geometric-kinematic parameters are the most influential on the motion of a vehicle. Among them, it was shown that the forward speed is the most significant parameter affecting the motion of the vehicle with yaw rate being the most sensitive mode. This result also supports the properties of "velocity constant" and "yaw number" entities where in their expressions, the forward speed is the dominant parameter. Furthermore, it was shown that the transient response of a vehicle is mostly

affected by its inertia parameters.

10.3 Various Control Algorithms for Automated Vehicles

There are two measurable errors produced during the plane motion of a vehicle, namely offset (the positional error, the distance from the vehicle mass centre to the line tangent to the path at the point nearest to the mass centre) error and orientation error (the angle between the vehicle longitudinal axis and the line tangent to the path). The function of a controller is to generate necessary command signals such that, by proper steering action the vehicle follows the desired path. The steering action can be achieved in various ways such as controlling the angular velocities of the side wheels or steering of wheel.

In this thesis, for tricycle model vehicles with steering wheel in the front, a nonlinear control strategy is developed and its performance is compared with previous proposed algorithms. Simulation demonstrates improvement in path tracking of a vehicle (approximately 25 percent less overshoots).

The linear dynamic model representing the motion of vehicles with tricycle wheelbase configurations (front wheel steering system), is employed in design of an optimal controller for path following of the vehicle. It is shown that the

system can be decoupled into two fast and slow subsystems and in the controller design, the slow subsystem is employed. In design of the controller, a quadratic measure of performance consisting of the integral of the errors (errors in position and orientation of the vehicle) and the inputs (front and rear steering angles) are minimized. This controller is unable to compensate for the errors produced due to path curvature. This is due to the original assumption made in design of the controller (in design of the controller, it was assumed that the desired path is a straight line not a curved trajectory). Thus, an integral action is incorporated in the controller, to enhance the performance of the vehicle in curve tracking.

Another class of vehicles considered in this thesis is the vehicles with two independent side tractive wheels. For these vehicles, a controller is designed that employs a linear feedback of the position and orientation errors as command to control the velocities of the side wheels. The performance of the controlled system in path tracking is shown by simulations results.

10.4 Experimental Results

In order to carry out experimental studies regarding the verification of dynamic modelling and control of automated vehicles, the prototype vehicle CONCIC III was designed and developed at Centre for Industrial Control (CIC) of Concordia University. This vehicle is equipped with front and rear

steering/driving wheels which offer flexibility in wheelbase configurations and can effectively be employed for experimental studies of the issues relevant to path tracking of automated vehicles.

Some of the experimental results carried out by using CONCIC III are reported in this thesis. The results of nonlinear dynamic modelling of automated vehicles developed in the previous chapters is implemented to this vehicle. The optimal controller designed based on the linear model was employed to path tracking control of the vehicle. The performance of the optimal controller is investigated for various initial conditions in following a straight line. The experimental results show that the controller performs satisfactory. From the comparison of the analytical results obtained from the solution of the nonlinear dynamic equations and those obtained from actual motion followed by the vehicle, it was observed that the model is quite accurate. As well, the assumptions made in derivation of the model are checked and it is shown that they are not violated during the motion. A detailed comparison is made between the two models (linear and nonlinear) as well as the verification of the assumptions made in its derivation. From the results, it was shown that the linear model is a good approximation of the nonlinear model under the conditions and the assumptions made for its derivation.

The performance of the vehicle for curved trajectories indicates that

although by and large, the vehicle is able to negotiate the curves within its physical limitations, however, for sharper curves, it experiences overshoots or undershoots and some steady state error. The experimental results show that by adding a feedforward predictive action (to reduce the oscillations) the performance of the vehicle in path tracking is improved. A simple algorithm is developed to estimate in real time the future motion of the vehicle from its current position. From the experimental data collected during the motion of the vehicle and its comparison with the trajectory followed by centre of mass (measured from the floor), it is revealed that the system is suffering from accumulated error due to dead reckoning technique employed for trajectory generation. This is quiet significant for longer distances. The other sources of errors are misalignment of the wheels and the controller errors.

The gains of the controller are further adjusted as a function of forward speed of the vehicle since in all derivations of the controller, the speed was assumed to be constant. A scheme is developed and implemented to adjust the speed of the vehicle according to path curvature such that the speed is reduced for sharper curves and increased for the trajectories with less curvature.

10.5 Recommendations for Future Work

The following topics stem from the studies carried out and reported in this

thesis. They are recommended for future research.

1. In developments of control laws such as the optimal control law, the reduced order model was employed for different wheelbase configurations. This may not be the case for those vehicles whose "velocity constants" are small. As a result, the controller should be designed for the nonreduced model. In principle, the approach to the solution of control problem remains the same.

2. In forming the performance index for the optimal control synthesis one may include the effects of other states, like lateral velocity or yaw rate (which requires their measurements). This is particularly necessary for passenger vehicle. It seems to be feasible to calculate the approximate values of these states directly from the real time data obtained during the motion. This can be achieved by noting that the rate of change of offset error with respect to time is directly related to lateral velocity and similarly, the rate of change of orientation error is proportional to yaw rate of the vehicle. The other option is to design an observer to generate the states in real time which requires more computing power. The new form of performance index has the advantage of controlling the lateral acceleration or yaw rate which enhance the passenger comfort as well as improvement in vehicle motion. In addition, it is possible to include the rate of change of steering angle in the performance index to take into account the limitations of steering dynamics.

3. From the analytical results obtained in this thesis, it was noticed that in the case of low "velocity constant", the modes associated with dynamics of the vehicle (what was called as fast modes) become important. Therefore, there exists a critical speed at which the fast and slow modes have equal real part. More investigations are required to study the properties of this speed. As well, this property may be useful in adjusting the gains of the controlled system.

4. Although in this thesis, the variable gain controller was obtained by using the experimental data, it is also interesting to find the analytical solution for this problem.

5. Design and implementation of other control techniques can be considered as a part of future study. For instance, another control algorithm that can be studied for these vehicles is a proportional controller such that the rear steering wheel is steered proportional to the front wheel. In this regard, some preliminary investigation is done and the work is underway. More research can be carried out in development and implementation of other control techniques such as fuzzy control and neural network control.

6. The technique of navigation used in this thesis is dead reckoning and as the results show, although this method was adequate for the type of study carried out in this thesis, it cannot be implemented for the vehicles moving at higher

speeds and longer distances. Therefore, some check points are necessary such that the vehicle can update its position and orientation.

7. The redundant systems are not addressed in this thesis. However, control of redundant vehicles itself is another area of research for which, so far, very little has been done. By redundancy is meant when two or more independent powered wheels are employed like four (independent) wheel drive.

8. Throughout this study, it was assumed that the vehicle moves without any slippage. However, certain techniques should be developed to measure the amount of slippage of the wheels or predict it before happening. In this regard, it is possible to use an extra idler wheel; so from the relative position or velocity of the wheels one can predict slippage and measure the amount of slippage.

REFERENCES

1. Hollier, R.H., Automated Guided Vehicle Systems, IFS Publications Ltd, Bedford, England, 1987.

2. Dooling, D., "Transportation", IEEE Spectrum, Jan. 1993, pp. 68-69.

3. Hammond, G. : "Automated Guided Vehicle Systems (AGVs) at Work", IFS Publications Ltd, Bedford, England, 1986.

4. Cox, I.J. and G.T. Wilfong, Autonomous Robot Vehicles, Springer_Verlag, New York, U.S.A, 1990.

5. Singh, S. and P. Keller, "Obstacle Detection for High Speed Autonomous Navigation", Proc. of the IEEE Int. Conf. on Robotics and Automation, Vol. 3, pp. 2798-2806, Sacramento, California, 1991.

6. Steer, B. and M. Larcomb, "A Goal Seeking and Obstacle Avoiding Algorithm for Autonomous Mobile Robots" Proc. of the IEEE Int. Conf. on Robotics and Automation, 1991, Sacramento, California, Vol. 2, pp. 1518-1530,.

7. Adams, M.D. and P.J. Probert, "Mobile Robot Motion Planning - Stability, Convergence and Control", IEEE/RSJ Int. Workshop on Intel. Robots and Sytems'91 (IROS'91), Osaka, Japan, 1991, pp. 1019-1025.

8. Steer, B., "Trajectory Planning for a Mobile Robot", Int. J. of Robotics Research, Vol.8, No. 5, 1989, pp. 3-14.

9. Wilfong, G.T., "Motion Planning for an Autonomous Vehicle", Proc. of the IEEE Int. J. of Robotics and Automation, pp. 529-533, Philadelphia, 1988.

10. Cox, I.J., "Blanche: Position Estimation for an Autonomous Robot Vehicle", Proc. of the IEEE/Rsj Int. Workshop on Robots and Systems (IORS), pp. 423-439, 1989.

11. Moravec, H.P., "The Stanford Cart and the CMU Rover", Proc. of the IEEE, Vol. 71, No. 7, pp. 872-884, 1983.

12. Fujii, S., Yoshimoto, K., Ohtsuki, H., Matsomoto, H. and K. Yamada, "Computer Control of a Locomotive Robot with Visual Feedback", Proc. 11th Int. Symp. on Industrial Robots, 1981, Tokyo, pp. 219-226.

13. Thompson, A.M., "The Navigation System of the JPL Robot", Proc. Fifth Int. Joint Conf. on Artificial Intel., 1977, Cambridge, Massachusetts, pp. 749-757.

14. Wickens, A.H., "Dynamics of Actively Guided Vehicles", Vehicle System Dynamics, Vol. 20, 1991, pp. 219-242.

15. Jullier, M., Marc, L. and H. Place, "A Guidance System for a Mobile Robot", 13th ISIR/Robots 7 Conf., Chicago, pp. 13-58, 1983.

16. Tsumura, T., Fujiwara, N., Shirakawa, T. and M. Hashimoto, "An Experimental System for Automatic Guidance of Roboted Vehicle Following the Route Stored in Memory", Proc. 11th Symp. on Industrial Robots, 1981, Tokyo, pp. 187-193.

17. Hongo, T., Arakawa, H., Sugimotop, G., Tange, K. and Y. Yamamoto, "An Automatic Guidance System of a Self-Controlled Vehicle", IEEE Trans. on Industrial Electronics, Vol.IE-34, No.1, pp. 5-10.

18. Fujiwara, K., Kawashima, Y., Kato, H. and M. Watanabe, "Development of Guideless Robot Vehicle", Proc. 11th Int. Symp. on Industrial Robots, Tokyo, 1981, pp. 195-202.

19. Iijima, J., Yuta, S. and Y. Kanayama, "Elementary Functions of a Self Contained Robot 'Yamabico 3.1'", Proc. 11th Int. Symp. Industrial Robots, Tokyo, 1981, pp. 211-218.

20. Nelson, W.L. and I.J. Cox, "Local Path Control for an Automatic Vehicle", Proc. of the IEEE Int. J. of Robotics and Automation, pp. 1504-1510, Philadelphia, 1988.

21. Kanayama, Y., Kimura, Y., Miyazaki, F. and T. Noguchi, "A Stable Tracking Control Method for an Autonomous Mobile Robot", Proc. of the IEEE Conf. on Robotics and Automation, Cincinnati, Ohio, pp. 384-390, 1990.

22. Kanayama, Y., Nilpour, A. and C. Leim, "A Locomotion Control Method for Autonomous Vehicles", Proc. IEEE Conf. on Rob. and Automation, Vol. 2, pp. 1315-1317, 1988.

23. Kanayama, Y. and S. Yuta, "Vehicle Path Specification by a Sequence of Straight Lines", IEEE J. of Robotica and Automation, Vol. 4, No.3, pp. 265-276.

24. Canudas de Wit, C. and R. Roskam, "Path Following of a 2-DOF Wheeled Mobile Robot Under Path and Input Torque Constraints", IEEE Int. Conf. on Robotics and Automation, 1991, Sacramento, California, pp. 1142-1147.

25. Nisonger, R.L. and D.N. Wormley, "Dynamic Performance of Automated Guideway Transit Vehicles with Dual-Axle Steering", IEEE Tran. on Vehicular Tech., Vol. VT-28, No. 1, 1979, pp. 88-94.

26. Bronstein, J. and Y. Koren, "Motion Control Analysis of a Mobile Robot", ASME J. of Dynamic Systems, Measurement and Control, Vol.109, pp.73-79, 1987.

27. Larcomb, M.H.E., "Tracking Stability of Wire Guided Vehicles", Proc. 1st Int. Conf. on Automated Guided Vehicle Systems, Stratford-upon-Avon, UK, June 1981, pp. 137-144.

28. Helferty, J.J. and Biswas, H., "Neuromorphic Control of Robotic Manipulators", Proc. IEEE Conf. on Rob. and Automation, Sacramento, California, Vol. 3, pp. 2436-2441, 1991.

29. Bulsari, A.B. and H. Saxen, "A Feedforward Neural Network for System Identification of a Chemical Process", J. of Syst. Eng., No. 1, 1991.

30. Choi, G.S., "Neural Network Based Control of Two Axis Positioning Table", Research Report, Dept. Mech. Eng., Berkeley, 1989.

31. Chen, F.C., "Back-Propagation Neural Network for Nonlinear Self-Tuning Adaptive Control", IEEE Cont. Syst. Magazine, 1990, Vol. 10, No. 3, pp. 63-72.

32. Ishikawa, S., "A Method of Indoor Mobile Robot Navigation by Using Fuzzy Control", IEEE/RSJ Int. Workshop on Intel. Robots and Sytems'91 (IROS'91), Osaka, Japan, 1991, pp. 1013-1019.

33. Cheng, R.M.H., Xiao, J.W. and LeQuoc, S., "Neuromorphic Controller for AGV Steering", Proc. of the IEEE Int. Conf. on Robotics and Automation, Vol. 3, pp. 2057-2062, Nice, France, 1992.

34. Cheng, R.M.H., Huang, M. and T.S. Sankar, "Dynamic Modelling and Simulation of an AGV (The CONCIC II Vehicle)", IFToMM Congress, Prague, Czechoslovakia, Aug.1991.

35. Cheng, R.M.H. and M. Huang, "A Study of Control Strategy of an AGV System Using the Simulation of the Dynamic Model", IASTED Int. Symposium, Robotics and Manufacturing, Santa Barbara, Nov.13-15, 1990.

36. Huang, M., "Dynamic Modelling and Simulation of an AGV (CONCIC II)", Master Thesis, Concordia University, Montreal, Canada, March 1991.

37. Rajagopalan, R. and R.M.H. Cheng, "Guidance and Control of Automated Guided Vehicles Using Binary Camera Vision", SME Transactions on Robotics Research, Vol.II, Sept. 1992.

38. Rajagopalan, R., Chang, R.M.H. and S. Lequoc, "A Guidance Control Scheme Employing Knowledge-base for AGV Navigation", The American Control Conf., Illinois, June 1992.

39. Rajagopalan, R., Cheng, R.M.H. and S. Lequoc, "A Guidance Control Scheme for Accurate Track Following of AGVs", The IEEE Int. Conf. on Robotics and Automation, Nice, May 1992, pp. 188-194.

40. Rajagopalan, R. and R.M.H. Cheng, "Binary Camera Vision for AGV Navigation", Fourth World Conference on Robotics Research, RI of the SME, Pittsburg, Sept. 1991.

41. Rajagopalan, R., "Guidance Control for Automated Guided Vehicles Employing Binary Camera Vision", Ph.D. Thesis, Concordia University, Montreal, Canada, September 1991.

42. Cheng, R.M.H. and R. Rajagopalan, "System Architecture of an Automated Guided Vehicle (AGV)", 4th Int. Conf. on CAD/CAM Robots & Factories of the Future, New Delhi, India, 1989.

43. Cheng, R.M.H. and R. Rajagopalan, "Kinematics of an Automated Guided Vehicle with an Inclined Steering Column", ASME Int. Computer in Engineering Conf., San Francisco, California, Aug. 1988.

44. Cheng, R.M.H. and R. Rajagopalan, "Kinematics of an Automated Guided Vehicle with an Inclined Steering Column and an Offset Distance- Criterion for Existence of Inverse Kinematic Solution", Journal of Robotic Systems, Vol.9 (8), Dec.1992.

45. Muir, P.F. and C.P. Neuman, "Kinematic Modelling of Automated Guided Vehicles", Technical Report No. CMU-RI-TR-86-12, The Robotic Institute, Carnegie-Mellon University, PA, 1986.

46. Muir, P.F. and C.P. Neuman, "Kinematic Modelling of Wheeled Mobile Robots", J. of Robotic Systems, Vol. 4, No. 2, 1987a, pp. 281-340.

47. Muir, P.F. and C.P. Neuman, "Kinematic Modelling for Feedback Control of an Omnidirectional Mobile Robot", IEEE Int. Conf. on Robotics and Automation, 1987, pp. 1772-1778.

48. Agullo, J., Cardona, S. and J. Vivancos, "Kinematics of Vehicles With Directional Sliding Wheels", Mechanics and Machine Theory, Vol. 22, No.4, pp. 295-301, 1987.

49. Alexander, J.C. and J.H. Maddock, "On the Kinematics of Wheeled Mobile Robots", The Int. J. of Robotics Research, Vol. 8, NO. 5, pp. 15-27, 1989.

50. Feng, D. and B.H. Krogh, "Dynamic Steering Control of Conventionally-Steered Mobile Robots", Proc. of the IEEE Int. Conf. on Robotics and Automation, Vol. 1, pp. 390-395, Cincinnati, Ohio, 1990.

51. Murray, R.M. and S.S. Sastry, "Steering Nonholonomic Systems Using Sinosoids", Proc. of the 29th Conf. on Dec. and Cont., Hawaii, 1990, pp. 2097-2101.

52. Samson, C. and K. Abit-Abderrahim, "Feedback Control of a Nonholonomic Wheeled Cart in Cartesian Space", IEEE Int. Conf. on Robotics and Automation, 1991, Sacramento, California, pp. 1136-1141.

53. Saha, S.K. and J. Angeles, "Kinematics and Dynamics of a Three-Wheeled 2-DOF AGV", Proc. of the IEEE Int. Conf. on Robotics and Automation, Vol. 3, pp. 1572-1577, Scottsdale, Arizona, 1989.

54. D'Andrea-Novel, B.G., Bastin, G. and G. Camion, "Modelling and Control of Nonholonomic Wheeled Mobile Robots", Proc. of the IEEE Int. Conf. on Robotics and Automation, Vol. 2, pp. 1130-1135, Sacramento, California, 1991.

55. Gillespie, T.D.,Fundamentals of Vehicle Dynamics, Society of Automotive Engineers, Inc., PA, U.S.A.

56. Wong, J.Y., Theory of Ground Vehicles, John Wiley & Son, New York, 1978.

57. Shladover, S.E., Wormley, D.N., Richardson, H.H. and R. Fish, "Steering Controller Design for Automated Guideway Transit Vehicles", ASME J. of Dyn. Sys. Measurement and Control, Vol. 100, 1978, pp. 1-8.

58. Cormier, W.H. and R.E. Fenton, "On the Steering of Automated Vehicles -- A Velocity Adaptive Controller", IEEE Trans. on Vehicular Tech., Vol. VT-29, No. 4, 1980, pp. 375-385.

59. Cheng, R.M.H. and M.G. Mehrabi, "Dynamic Modelling of Wheeled Mobile Robots and Automated Transit Vehicles Using Dimensionless 'Roll Number'", The 1st IEEE Conf. on Control Applications, 1992, Dayton, Ohio, pp.160-167.

60. Hemami, A., Mehrabi, M.G. and R.M.H. Cheng, "A New Control Strategy for Tracking in Mobile Robots and AGV's", IEEE Int. Conference on Robotics and Automation, 1990, Cincinnati, pp. 1122-1127.

61. Hemami, A., Mehrabi, M.G. and R.M.H. Cheng, "Synthesis of an Optimal Control Law for Path Tracking in Mobile Robots and Automated Guided Vehicles", AUTOMATICA, 1992, Vol. 28, No. 2, pp.383-387.

62. Hemami, A. Mehrabi, M.G. and R.M.H. Cheng, "Optimal Control of Path Tracking in Mobile Robots and Automated Guided Vehicles", Proc. of Fourth World Conference on Robotic Research, Pittsburgh, PA, Sept. 17-19, 1990.

63. Mehrabi, M.G., Hemami, A. and R.M.H. Cheng, "Analysis of Steering Control in Vehicles with Two Independent Left and Right Traction Wheels", '91 ICAR, Pisa, Italy, June 19-21, 1991.

64. Mehrabi, M.G., Cheng, R.M.H., and A. Hemami, "Control of a Wheeled Mobile Robot with Double Steering", IEEE/RSJ Int. Workshop on Intel. Robots and Sytems'91 (IROS'91), 1991, Osaka, Japan, pp. 806-810.

65. Mehrabi, M.G., Cheng, R.M.H. and A.Hemami, "Dynamic Modelling and Control of Wheeled Mobile Robots: Theory and Experiments", The 2nd IEEE Conf. on Control Applications, 1993, Vencouver, B.C.

66. Mehrabi, M.G., "Sensitivity Study of Wheeled Mobile Robots and Automated Guided Vehicles", Internal Report, Centre for Industrial Control, Concordia University, CIC No-0047, July 1991.

67. Mehrabi, M.G. and R.M.H. Cheng, "Sensitivity Study of Wheeled Mobile Robots and Automated Transit Vehicles", Int. Conf. on Engineering Applications of Mechanics, 1992, Tehran, pp. 298-305.

68. Mehrabi, M.G., Cheng, R.M.H and A. Hemami, "Tracking Stability and Control of Wheeled Mobile Robots and Automated Transit Vehicles", CSME Forum, 1992, Montreal, Canada, pp.424-429.

69. Verma, M.K., and T.D. Gillespie,"Roll Dynamics of Commercial Vehicles", Vehicle System Dynamics, Vol.9, 1980, pp 1-17.

70. El-Gindy, M. and L. Ilosrai, "Computer Simulation Study on Vehicle's Directional Response in Some Sever Manoeuvres. Part 1: Rapid Lane Change Manoeuvres", Int. J. of Veh. Design, Vol. 4, No. 4, 1983, pp. 386-401.

71. Whitehead, J.C., "Rear Wheel Steering Dynamics Compared to Front Steering", ASME J. of Dyn. Sys. Measurement and Control, Vol. 112, 1990, pp. 88-93.

72. Whitehead, J.C., "A Prototype Steering Weave Stabilizer for Automobiles", ASME J. of Dyn. Sys. Measurement and Control, Vol. 113, 1991, pp. 138-142.

73. Metz, D. and D. William, "Near Time-optimal Control of Racing Vehicles", Automatica, Int. J. of IFAC, 1989, pp. 841-857.

74. Hatwal, H. and E.C. Mikulcik, "Some Inverse Solutions to an Automobile Path-Tracking Problem with the Input of Steering and Brakes", Veh. Syst. Design, Vol. 15, 1986, pp. 61-71.

75. Tousi, S., Bajaj, A.K. and W. Soedel, "On the Stability of a Flexible Vehicle Controlled by a Human Pilot", Veh. Sys. Dynamics, Vol. 17, 1988, pp. 37-56.

76. Nalecz, A.G., "Influence of Vehicle and Road Way Factors on the Dynamics of Trippled Rollover", Int. J. of Veh. Design, Vol. 10, No. 3, 1989, pp. 331-345.

77. Nalecz, A.G. and A.C. Bindamin, "Analysis of Dynamic Response of Four Wheel Steering Vehicles at High Speed", Int. J. of Veh. Design, Vol. 9, No. 2, 1988, pp. 179-202.

78. Noguchi, H., "An Analysis of Vehicle Behaviour in a Cross Wind", Int. J. of Vehicle Design, Special Issue on Vehicle Safety, 1986, pp. 304-317.

79. Legouis, T., Laneville, A., Bourassa, P. and G. Payre, "Vehicle/pilot System Analysis: A New Approach Using Optimal Control with Delay", Vehicle System Dynamics, Vol. 16, 1987, pp. 279-295.

80. Motsumoto, N. and M. Tomizuka, "Vehicle Lateral Velocity and Yaw Rate Control with Two Independent Control Inputs", ASME J. of Dyn. Sys. Meas. and Control, Vol. 114, 1992, pp. 606-613.

81. Furukawa, Y., Yuhara, N., Sano, S., Takeda, H. and Y. Mutsuhita, "A Review of Four-Wheel Steering Studies from the View Point of Vehicle Dynamics and Control", Veh. Syst. Design, Vol.18, 1984, pp.151-186.

82. Nagai, M. and M. Ohki, "Theoretical Study on Active Four-Wheel-Steering System by Virtual Vehicle Model Following Control", Int. J. Vehicle Design, Vol. 10, No. 1, 1989, pp. 16-33.

83. Dugoff, H. and B.J. Brown, "Measurement of Tire Shear Forces", Paper No. 700092, SAE Transactions, 1970, pp. 316-324.

84. Dugoff, H. and B.J. Brown, "An Analysis of Tire Traction Properties and Their Influence on Vehicle Dynamic Performance", Paper No. 700377, SAE Transactions, 1970, pp. 1219-1243.

85. Sakai, H., "Theoretical and Experimental Studies on the Dynamic properties of tires :Part 1-4", Int. J. Veh. Design, Vol.2, No. 1, 1981, pp. 78-110.

86. Maalej, A.Y., Guenther, D.A. and J.R. Ellis, "Experimental Development of Tyre Forces and Moments Models", Int. J. Veh. Design, Vol. 10, 1989, No.1, pp. 34-51.

87. Ellis, J.R., Vehicle Dynamics, Business Books, London, 1969.

88. Collins, R.L. and Wong, J.P., "A Comparison of Tire Influence on Vehicle Handling", Proc. of the Int. Conf. on Vehicle Syst. Dynamics, 1975, pp. 176-184.

89. Radt, H.S. and W.F. Milikan, "Non-dimensionalizing Tire Data for Vehicle Simulation", Road Vehicle Handling, Inst. of Mech. Eng., Conf. Publication, 1983, pp. 229-240.

90. Cheng, R.M.H., Coubert, Y., Surpaceanu, Favreau, P. and A. Fahim, "Investigation of an Automated Guided Vehicle (AGV) Driven by Camera Vision", Proc. of the Int. Conf. on Intelligent Autonomous Systems, pp. 162-167, Amsterdam, Netherlands, 1986.

91. Cyril, X., Cheng, R.M.H. and Sankar, T.S., "On the Dynamics of AGVs", Proc. of the 4th Int. Conf. on CAD/CAM, Robotics and Factories of the Future, Vol. 2, pp. 264-273, India, 1989.

92. Barraquand, J. and J.C. Latombe, "Nonholonomic Multibody Mobile Robots: Controllability and Motion Planning in the Presence of an Obstacle", Proc. of the IEEE Int. Conf. on Robotics and Automation, Vol. 3, pp. 2328-2336, Sacramento, California, 1991.

93. Steer, B., "A Unified Homing and Obstacle Avoiding Algorithm for Autonomous Mobile Robots", IEEE/RSJ Int. Workshop on Intel. Robots and Sytems'91 (IROS'91), Osaka, Japan, 1991, pp. 1007-1013.

94. Liu, Y.H. and S. Arimoto, "Proposal of Tangent Graph and Extended Tangent Graph for Path Planning of Mobile Robots", Proc. of the IEEE Int. Conf. on Robotics and Automation, Vol. 1, pp. 312-318, Sacramento, California, 1991.

95. Vasseur, H.A., Oin, F.G. and J.R. Taylor, "Navigation of a Car-like Mobile Robot using a Decomposition of the Environment in Convex Cell", Proc. of the IEEE Int. Conf. on Robotics and Automation, Vol. 2, pp. 1496-1503, Sacramento, California, 1991.

96. Fenton, R.E., Melocik, G.C. and K.W. Olson, "On the Steering of Automated Vehicles: Theory and Experiments", IEEE Trans. on Auto. Control, Vol. AC-21, No. 3, 1976, pp. 306-315.

97. Blazevic, P., Delaplace, S., Fontaine, J.G. and J. Robit, "Mobile Robot Using Ultrasonic Sensors: Case Study of a Degraded Mode", Robotica, Vol. 9, 1991, pp. 365-170.

98. Miller, G.L. and E.R. Wagner, "An Optical Rangefinder for Autonomous Robot Cart Navigation", Proc. of the IEEE Robotics and Automation, Vol. RA-3, No.3, pp. 239-248, Raleigh, North Carolina, 1987.

99. Takeno, J., Shin, Y., Nishiyama, S., Mizugui, N. and K. Sorimoti, "Realization of a 3D Vision Mobile Robot That can Avoid Collision with Moving Obstacles", Proc. of the IEEE Int. Conf. on Robotics and Automation, Vol. 3, pp. 2010-2026, Sacramento, California, 1991.

100. Nakeno, E., Koyochi, N., Agori, Y. and S. Hirroka, "Sensor System of a Guideless Autonomous Vehicle in a Flexible Manufacturing System", Proc. of the 15th Int. Symp. on Ind. Robots, pp. 305-312, 1985.

101. Lee, A.Y., "Design of Stability Augmentation Systems for Automotive Vehicles", ASME J. of Dyn. Sys. Measurement and Control, Vol. 112, 1990, pp. 489-495.

102. Miyawakin, I., Ishiguro, H. and S. Tsuji, "Active Observation Along Circular Path by Vision-Guided Mobile Robot", IEEE/RSJ Int. Workshop on Intel. Robots and Sytems'91 (IROS'91), Osaka, Japan, 1991, pp. 891-817.

103. Grattinger, T.J. and B.H. Krogh, "Evaluation and Time Scaling of Trajectories for Wheeled Mobile Robots", ASME J. of Dyn. Sys. Measurement and Control, Vol .111, 1990, pp. 222-231.

104. Beranard, J. and M. Pickelmann, "An inverse Linear Model of a Vehicle", Vehicle System Dynamics, Vol. 15, 1986, pp, 180-186.

105. Kwak, Y.K., and C.C. Smith, "An Active and Passive Steering Controller Study of Rubber-Tired Automated Guideway Transit Vehicles", ASME Tran. on Dyn. Syst. Meas. and Contr., Vol. 102, Sept.1980, pp 168-173.

106. Rakheja, S., Lecture Notes on Vehicle Dynamics, Dept. of Mech. Eng., Concordia University, 1991.

107. Pacejka, H.B. and R.S. Sharp, "Shear Force Development by Pneumatic Tires in Steady-State Conditions: A Review of Modelling Aspects", Veh. Syst. Dynamics, Vol. 20, 1991, pp. 121-176.

108. Pacejka, H.B., "Tire Factors and Vehicle Handling", Int. J. of Veh. Design, Vol. 1, No. 1, 1979, pp. 1-23.

109. Pacejka, H.B., "Tire Factors and Front Wheel Vibrations", Int. J. of Veh. Design, Vol. 1, No. 2, 1979, pp. 97-119.

110. Pacejka, H.B., "In-plane and Out-of-plane Dynamics of Pneumatic Tires", Veh. Syst. Design, Vol. 10, 1981, pp. 221-251.

111. Gim, G. and P. Nikravesh, "An Analytical Model of Pneumatic Tires for Vehicle Dynamic Simulation. Part 3: Validation Against Experimental Data", Int. J. of Veh. Design, Vol. 12, No. 2, pp. 217-227.

112. Maple V Language Reference Manual, Springer-Verlag, New York.

113. Cruz, J.B. and W.R. Perkins,"A New Approach to the Sensitivity Problem in Multivariable Feedback System Design", IEEE Trans. Aut. Contr. Vol. 9, pp. 216-223, July 1964.

114. Kokotovic, P.V., Heller, J., and P. Sannuti,"Sensitivity Comparison of Optimal Controls", Int. J. Contr. Vol.9, pp 111-117, Jan.1969.

115. Kreindler, E.,"Closed_Loop Sensitivity Reduction of Linear Optimal Control Systems", IEEE Tran. Aut. Cont., Vol.13, pp 254-262, June 1968.

116. Holtzman, J.M., and S. Horing,"The Sensitivity of Terminal Conditions of Optimal Control Systems to Parameter Variations", IEEE Tran. Auto. Cont., Vol.10, pp 420-426, 1965.

117. Frank, P.M., Introduction to System Sensitivity Theory, Academic Press, New York, 1978.

118. Farahat, S., "Application of Sensitivity Analysis to Parameter Changes in Nonlinear Control Systems", Master Thesis, Dept. of Mech. Eng., Concordia University, July 1987.

119. Vilenius, M.J., "The Application of Sensitivity Analysis to Electrohydraulic Position Control Servos", ASME Journal of Dyn. Syst. Meas. and Cont., Vol.105, June 1983, pp 77-82.

120. Daniel, A.R., Lee, Y.B. and M.K. Pal,"Nonlinear Power System Optimization Using Dynamic Sensitivity Analysis", Proc. of IEE, Vol. 123, No. 4, April 1976, pp. 365-370.

121. Dorato, P.,"On Sensitivity in Optimal Control Systems", IEEE Trans. Aut. Contr., Vol.8, pp. 256-257, July 1963.

122. Cruz, J.B., System Sensitivity Analysis, Dowden Hutchinson and Ross, Stroudsburg, Pennsylvaina, 1973.

123. Radanovic, L., Sensitivity Methods in Control Theory, Pergamon Press Ltd., 1966, London, UK.

124. Athans, M. and P.L. Falb, Optimal Control, McGraw-Hill, New York, 1966.

125. Data Sheets on Motor-in-Wheel Drive Units, Schabmuler Elektromotoren, Feldkirchen, West Germany and NDC Automation, Charlotte, North Carolina.

126. The LM628 Precision Motion Controller Chip Data Sheets, The National Semiconductor, U.S.A, 1988.

127. Dale, D., "LM628/LM629 User Guide", Application Note No. 806, National Semiconductor, August 1990.

128. PWM Servo Amplifiers Users and Operating Manual, Galil Motion Control, California, U.S.A, 1988.

129. Kabra, S., "The Development and Analysis of an Integrated Workcell Controller for Multiple Robot Synchronization", Master Thesis, Concordia University, Dept. of Mech. Eng., 1992.

130. Gerald, C. and P.O. Wheatly ,Applied Numerical Analysis, Addison-Wesly, California, U.S.A, 1989.

131. Whittaker, E.T. ,Analytical Dynamics, Dover Publications, New York, 1944.

132. Rosenberg, R.M. ,Analytical Dynamics, Plenum Press, New York, 1977.

APPENDIX-A

Derivation of Transfer Functions

Starting with dynamic equations of the system

$$M(\dot{v}_w + v_u\Omega) + M_s h\ddot{q} = F_f + F_r \tag{A-1}$$

$$I_z\dot{\Omega} = aF_f - bF_r \tag{A-2}$$

$$I_u\ddot{q} + M_s h(\dot{v}_w + v_u\Omega) = -D_p\dot{q} + (M_s gh - K_p)q \tag{A-3}$$

$$\dot{q} = p \tag{A-4}$$

Writing equation (A-4) in frequency domain and substituting the resulting equation into (A-3) we get:

$$q(s) = \frac{[-M_s hsv_w(s) - M_s hv_u\Omega(s)]}{F(s)} \tag{A-5}$$

where

$$F(s) = s^2 I_u + D_p s + (K_p - M_s gh) \tag{A-6}$$

substituting for β_f and β_r from their definitions into equations (5.1-5.4) and combining them with equations (A-2) we get:

$$\omega(S)[SI_z+\frac{(a^2C_f+b^2C_r)}{v_u}]+(\frac{aC_f-bC_r}{v_u})v_w(S)-aC_f\delta_f(S)-bC_r\delta_r(S) \quad \text{(A-7)}$$

substituting the expressions for F_f and F_r in equation (A-1) we get:

$$\Omega(s)[Mv_u+(\frac{aC_f-bC_r}{v_u}+[sM+(\frac{C_f+C_r}{v_u})]v_w(s)+s^2M_shq(s)-C_f\delta_f+C_r\delta_r \quad \text{(A-8)}$$

Solving equations (A-7) and (A-8) for $v_w(s)$ and $\Omega(s)$ (outputs) in terms of δ_f and δ_r (inputs), the following four transfer functions can be obtaind as:

$$T_1(s)=\frac{\Omega(s)}{\delta_f(s)}=\frac{Z_1(s)}{P_s(s)} \qquad \text{(A-9)}$$
$$T_2(s)=\frac{\Omega(s)}{\delta_r(s)}=\frac{Z_2(s)}{P_s(s)}$$

$$T_3(s)=\frac{v_w(s)}{\delta_f(s)}=\frac{Z_3(s)}{P_s(s)} \qquad \text{(A-10)}$$
$$T_4(s)=\frac{v_w(s)}{\delta_r(s)}=\frac{Z_4(s)}{P_s(s)}$$

where $T_{i(i=1,4)}(s)$ are the transfer functions, $Z_{i(i=1,4)}(s)$ the numerator polynomials (zeros) and $P_s(s)$ the characteristics polynomial (poles) of the system for different

input-output pairs.

In the above equations, the expressions for $Z_{i(i=1,4)}(s)$ are as follows:

$$Z_1(s) = v_u C_f[-aMv_u s + (aC_f - bC_r)F(s) - a(C_f + C_r)F(s) + Z_{11}(s)] \quad \text{(A-11)}$$

$$Z_2(s) = v_u C_r[bMv_u s + (aC_f - bC_r)F(s) + b(C_f + C_r)F(s) + Z_{21}(s)] \quad \text{(A-12)}$$

$$Z_3(s) = v_u C_f[v_u I_z s F(s) + (a^2 C_f + b^2 C_r)F(s) - a(aC_f - bC_r)F(s) + Z_{31}(s)] \quad \text{(A-13)}$$

$$Z_4(s) = v_u C_r[v_u I_z s F(s) + (a^2 C_f + b^2 C_r)F(s) + b(aC_f - bC_r)F(s) + Z_{31}(s)] \quad \text{(A-14)}$$

where Z_{11}, Z_{21}, Z_{31}, Z_{41} after rearranging the terms are obtained as:

$$Z_{11}(s) = -av_u [(I_u M - M_s^2 h^2)s^3 + Ms[D_p s + (K_p - M_s gh)]] \quad \text{(A-15)}$$

$$Z_{21}(s) = bv_u[(I_u M - M_s^2 h^2)s^3 + Ms[D_p s + (K_p - M_s g h)]] \quad \text{(A-16)}$$

$$Z_{31}(s) = -av_u^2[(I_u M - M_s^2 h^2)s^2 + MD_p s + M(K_p - M_s g h)] \quad \text{(A-17)}$$

$$Z_{41}(s) = bv_u^2[(I_u M - M_s^2 h^2)s^2 + MD_p s + M(K_p - M_s g h)] \quad \text{(A-18)}$$

Furtheremore, the characteristic polynomial of the system ($P_s(s)$) is obtained as:

$$\begin{aligned} P_s(S) = F(S) \; [\; & M(aC_f - bC_r)v_u^2 - (C_f + C_r)I_z v_u S \\ & + (aC_f - bC_r)^2 - M(a^2 C_f + b^2 C_r)v_u S \\ & - I_z M v_u^2 S^2 - (C_f + C_r)(a^2 C_f + b^2 C_r) \;] \\ & + M_s^2 h^2 v_u \; P_{s1}(S) \end{aligned} \quad \text{(A-19)}$$

where $P_{s1}(s)$ is given by:

$$P_{s1}(S) = [\; I_z v_u S^2 + (a^2 C_f + b^2 C_r)S - (aC_f - bC_r)v_u \;] \quad \text{(A-20)}$$

Rearranging the terms in equation (A-19) we get:

$$\begin{aligned} P_s(s) = F(s)[\; & -Mv_u[\; I_z v_u s^2 + (a^2 C_f + b^2 C_r)s - (aC_f - bC_r)v_u \;] \\ & + (aC_f - bC_r)^2 - (C_f + C_r)(a^2 C_f + b^2 C_r) - (C_f + C_r)I_z v_u S \;] \\ & + M_s^2 h^2 v_u s^2 P_{s1}(s) \end{aligned} \quad \text{(A-21)}$$

or

$$P_s(s) = v_u P_{s1}(s)[\ -MF(s) + M_s^2 h^2 s^2\ ] - F(s)[\ -(aC_f - bC_r)^2 + (C_f + C_r) I_z v_u s + (C_f + C_r)(a^2 C_f + b^2 C_r)\ ] \quad \text{(A-22)}$$

Substituting the expression of F(s) from equation (A-6) into the first term of equation (A-22) we get:

$$P_s(s) = -v_u P_{s1}(s)\ [\ (I_u M - M_s^2 h^2) s^2 + M[D_p s + (K_p - M_s g h)\ ] - F(s)\ [\ -(aC_f - bC_r)^2 + (C_f + C_r) I_z v_u s + (C_f + C_r)(a^2 C_f + b^2 C_r)\ ] \quad \text{(A-23)}$$

Substituting for M_s equal to zero in equations (A.1) and (A.2) and solving for $V_u(s)$ and $\Omega(s)$, the characteristic equation of the 2-DOF model are obtained as:

$$P'(s) = I_z M v_u^2 s^2 + [I_z v_u (C_f + C_r) + M v_u (a^2 C_f + b^2 C_r)] s + [(C_f + C_r)(a^2 C_f + b^2 C_r) - (bC_r - aC_f)(bC_r - aC_f - M v_u^2)] \quad \text{(A.24)}$$

APPENDIX-B
PARAMETERS OF CONCIC III VEHICLE

a	Distance of c.g. to the front wheel axis (0.32 m)
b	Distance of c.g. to the rear wheel axis (0.39 m)
I_z	Yaw moment of inertia (14.6 kg m^2)
I_u	Roll moment of inertia (6.0 kg m^2)
M	Mass of the vehicle (124.5 kg)
J_w	Wheel moment of inertia (0.0025 Kg m2)
m_w	Mass of the Wheel (9.5 kg)
r_w	Wheel radius (0.075 m)
2d	Wheel span (0.52 m)
C_f	Cornering stiffness of the front wheel (4000 N/rad)
C_r	Cornering stiffness of the rear wheel (4000 N/rad)
f_r	Rolling resistance of the wheel (0.023 N/N)

Table B.1 Physical Parameters of CONCIC III

Mechanical Time Constant	0.088 s
Electrical Time Constant	0.0078 s
Motor Torque Constant	0.114 Nm/A
Mechanical Damping Coefficient	0.0228 Kg-m^2/s
Rotor Inertia	0.002 Kg.m2

Table B.2 Parameters of Driving Motor

Stall Torque	18.0 Nm
Electrical Time Constant	0.00378 s
Motor Torque Constant	3.0 Nm/A
No Load Speed	45 rpm

Table B.3 Parameters of Steering Motor

APPENDIX-C

VEHICLE PARAMETERS
(EXAMPLES OF OVERSTEER AND UNDERSTEER VEHICLES)

The parameters of the vehicle used in the examples in chapter 5 are [82,106]:

Distance of c.g. to the front wheel axis (a)	(1.1 m)
Distance of c.g. to the rear wheel axis (b)	(1.3 m)
Yaw moment of inertia (I_z)	(1800 kg m^2)
Mass of the vehicle (M)	(1200 kg)
Cornering stiffness of the front wheel (C_f)	(68 KN/rad)
Cornering stiffness of the rear wheel (C_r)	(58 KN/rad)

and:

Distance of c.g. to the front wheel axis (a)	(1.4 m)
Distance of c.g. to the rear wheel axis (b)	(1.0 m)
Yaw moment of inertia (I_z)	(1000 kg m^2)
Mass of the vehicle (M)	(1000 kg)
Cornering stiffness of the front wheel (C_f)	(60 KN/rad)
Cornering stiffness of the rear wheel (C_r)	(60 KN/rad)

APPENDIX-D

DERIVATIONS OF MATRICES OF DRIVING FUNCTIONS

The states space representation of the system is:

$$\dot{x} = Ax + Bu \tag{D.1}$$

where

$$x^T = [V_w \quad \Omega \quad p \quad q \quad \delta_f \quad \delta_r] \tag{D.2}$$

is the state vector and

$$u^T = [\ \delta_{f_0} \quad \delta_{r_0}\ ] \tag{D.3}$$

is the input vector. Matrix A is:

$$\begin{bmatrix}
\frac{-I_u(C_f+C_r)}{I_s V_u} & \frac{I_u(bC_r-aC_f)}{I_s V_u} - V_u & \frac{M_s h D_p}{I_s} & \frac{-M_s h(M_s gh-K_p)}{I_s} & \frac{I_u C_f}{I_s} & \frac{I_u C_r}{I_s} \\
\frac{(bC_f-aC_r)}{I_z V_u} & \frac{(-a^2C_f-b^2C_r)}{I_z V_u} & 0 & 0 & \frac{aC_f}{I_z} & \frac{-bC_r}{I_z} \\
\frac{M_s h(C_f+C_r)}{I_s V_u} & \frac{-M_s h(bC_r-aC_f)}{I_s V_u} & \frac{-MD_p}{I_s} & \frac{M(M_s gh-K_p)}{I_s} & \frac{-M_s hC_f}{I_s} & \frac{-M_s hC_f}{I_s} \\
0 & 0 & 1 & 0 & 0 & 0 \\
0 & 0 & 0 & 0 & -T_{sf} & 0 \\
0 & 0 & 0 & 0 & 0 & -T_{sr}
\end{bmatrix} \tag{D.4}$$

The parameters of the vehicle are classified in vectors of mass and inertia parameters

$$\alpha_1^T = [M \quad M_s \quad I_z \quad I_u] \tag{D.5}$$

vector of stiffness and damping coefficients

$$\alpha_2^T = [C_f \quad C_r \quad K_p \quad D_p] \tag{D.6}$$

and geometric and kinematic parameter vector

$$\alpha_3^T = [a \quad b \quad h \quad V_u] \tag{D.7}$$

The partial derivatives of matrix A with respect to various elements of the above vectors (like M, M_s, ...) are obtained in order to solve the trajectory sensitivity equations

For mass (M), the nonzero elements of the matrix ($\frac{\partial A}{\partial M}$) are:

$$ma_{11} = \frac{I_u^2 V_u (C_f + C_r)}{[(I_u M - M_s^2 h^2) V_u]^2}]$$

$$ma_{12} = \frac{-I_u^2 V_u (bC_r - aC_f)}{[(I_u M - M_s^2 h^2) V_u]^2}$$

$$ma_{13} = \frac{-I_u M_s h D_p}{(I_u M - M_s^2 h^2)^2}$$

$$ma_{14} = \frac{I_u M_s h (M_s g h - K_p)}{(I_u M - M_s^2 h^2)^2}$$

$$ma_{15} = \frac{-I_u^2 C_f}{(I_u M - M_S^2 h^2)^2}$$

$$ma_{16} = \frac{-I_u^2 C_r}{(I_u M - M_s^2 h^2)}$$

$$ma_{21} = \frac{-(bC_r - aC_f)l_{eq}^2}{I_z^2 V_u}$$

$$ma_{22} = \frac{(a^2C_f + b^2C_r)}{I_z^2 V_u}$$

$$ma_{25} = \frac{-a\ C_f\ l_{eq}^2}{I_z^2}$$

$$ma_{26} = \frac{bC_r l_{eq}^2}{I_z^2}$$

$$ma_{31} = \frac{-I_u V_u M_s h(C_f + C_r)}{[(I_u M - M_s^2 h^2)V_u]^2}]$$

$$ma_{32} = \frac{I_u M_s h(bC_r - aC_f)}{[(I_u M - M_s^2 h^2)V_u]^2}$$

$$ma_{33} = \frac{-D_p(I_u M - M_s^2 h^2) + I_u M D_p}{(I_u M - M_s^2 h^2)^2}$$

$$ma_{34} = \frac{-(M_s\ g\ h - K_p)\ M_s^2 h^2}{(I_u M - M_s^2 h^2)^2}$$

$$ma_{35} = \frac{I_u\ M_s\ h\ C_f}{(I_u M - M_s^2 h^2)^2}$$

$$ma_{36} = \frac{I_u\ M_s\ h\ C_r}{(I_u M - M_s^2 h^2)^2} \qquad \text{(D.8)}$$

By noting that yaw moment of inertia of the vehicle (I_z) is a function of mass (M) which is not explicitly shown in matrix A, in the above derivations it is assumed that (I_z) and (M) are (approximately) related by: $\mathbf{I_z = M\ l_{eq}^2}$.

Similarly, for M_s the nonzero elements of the matrix ($\frac{\partial A}{\partial M_s}$) are :

$$msa_{11} = \frac{-(C_f+C_r)(2I_u-M_s h_{eq}^2)M_s h^2}{(I_u M-M_s^2 h^2)^2 V_u}$$

$$msa_{12} = \frac{M_s h^2(bC_r-aC_f)(2I_u-M_s h_{eq}^2)}{(I_u M-M_s^2 h^2)V_u}$$

$$msa_{13} = \frac{hD_p\,[\,I_s-M_s\,(m\,h_{eq}^2-\,2\,M_s h^2)]}{(I_u M-M_s^2 h^2)^2}$$

$$msa_{14} = \frac{h[I_s(\,K_p-2M_s\,gh)+M_s\,(M_s gh-K_p)(Mh_{eq}^2-2M_s h^2)]}{(I_u M-M_s^2 h^2)^2}$$

$$msa_{15} = \frac{C_f\,M_s\,h^2\,(2\,I_u-\,M_s\,h_{eq})}{(I_u M-M_s^2 h^2)^2}$$

$$msa_{16} = \frac{C_r\,M_s\,h^2\,(2\,I_u-\,M_s\,h_{eq}^2)}{(I_u M-M_s^2 h^2)^2}$$

where I_u and M_s are assumed to be related by: $I_u = M_s\,h_{eq}^2$.

$$msa_{31} = \frac{h(C_f+C_r)[I_s-M_s(Mh_{eq}^2-2M_s h^2)]h^2}{(I_u M-M_s^2 h^2)^2 V_u}$$

$$msa_{32} = \frac{-h(bC_r-aC_f)[I_s-M_s(Mh_{eq}^2-2M_s h^2)]}{(I_u M-M_s^2 h^2)^2 V_u}$$

$$msa_{33} = \frac{MD_p(Mh_{eq}^2-2M_s h^2)]}{(I_x M-M_s^2 h^2)^2}$$

$$msa_{34} = \frac{M[ghI_s+(K_p-M_s gh)(Mh_{eq}^2-2M_s h^2)]}{(I_u M-M_s^2 h^2)^2}$$

$$msa_{35} = \frac{-h\,C_f[I_s-M_s(Mh_{eq}^2-2M_s h^2)]}{(I_u M-M_s^2 h^2)^2}$$

$$msa_{36} = \frac{-hC_r[I_s-M_s(Mh_{eq}^2-2M_s h^2)]}{(I_u M-M_s^2 h^2)^2}$$

(D.9)

For I_z, the nonzero elements of matrix ($\frac{\partial A}{\partial I_z}$) are:

$$iza_{21}=\frac{-V_u(bC_r-aC_f)}{I_zV_u^2}$$
$$iza_{22}=\frac{V_u(a^2C_f+b^2C_r}{I_zV_u^2)}$$
$$iza_{25}=\frac{-aC_f}{I_z^2} \qquad \textbf{(D.10)}$$
$$iza_{26}=\frac{b\ C_r}{I_z^2}$$

For I_u, the nonzero elements of the matrix ($\frac{\partial A}{\partial I_x}$) are :

$$iua_{11}=\frac{V_u(C_f+C_r)M_s^2h^2}{[(I_uM-M_s^2h^2)V_u]^2}$$
$$iua_{12}=\frac{V_u(bC_r-aC_f)M_s^2h^2}{[(I_uM-M_s^2h^2)V_u]^2}$$
$$iua_{13}=\frac{-M\ M_s\ hD_p}{(\ I_u\ M\ -M_s^2\ h^2)}$$
$$iua_{14}=\frac{MM_sh(M_sgh-K_p)}{(I_uM-M_s^2h^2)^2}$$
$$iua_{15}=\frac{-M_s^2h^2C_f}{(I_uM-M_S^2h^2)^2}$$
$$iua_{16}=\frac{-M_s^2h^2C_r}{(I_uM-M_s^2h^2)}$$

$$iua_{31} = \frac{-MM_s hV_u(C_f+C_r)}{[(I_u M-M_s^2 h^2)V_u]^2}$$

$$iua32 = \frac{-MM_s hV_u(bC_r-aC_f)}{[(I_u M-M_s^2 h^2)V_u]^2}$$

$$iua_{33} = \frac{M^2 D_p}{(I_u M - M_s^2 h^2)^2}$$

$$iua_{34} = \frac{M^2(M_s gh-K_p)}{(I_u M-M_s^2 h^2)^2}$$

$$iua_{35} = \frac{M \quad M_s \quad h \quad C_f}{(I_u M-M_s^2 h^2)^2}$$

$$iua_{36} = \frac{-M \quad M_s \quad h \quad C_r}{(I_u M-M_s^2 h^2)^2}$$

(D.11)

For C_f, the nonzero elements of matrix ($\frac{\partial A}{\partial C_f}$) are:

$$
\begin{aligned}
cfa_{11} &= \frac{-I_u}{[(I_u M - M_s^2 h^2) V_u]} \\
cfa_{12} &= \frac{-aI_u}{[(I_u M - M_s^2 h^2) V_u]^2} \\
cfa_{15} &= \frac{I_u}{(I_u M - M_s^2 h^2)} \\
cfa_{21} &= \frac{-a}{I_z V_u} \\
cfa_{22} &= \frac{-a^2}{I_z V_u} \\
cfa_{25} &= \frac{a}{I_z} \\
cfa_{31} &= \frac{M_s h}{(I_u M - M_s^2 h^2) V_u} \\
cfa_{32} &= \frac{aM_s h}{(I_u M - M_s^2 h^2) V_u} \\
cfa_{35} &= \frac{-M_s h}{(I_u M - M_s^2 h^2)}
\end{aligned}
\qquad \textbf{(D.12)}
$$

For C_r, the nonzero elements of matrix ($\frac{\partial A}{\partial C_r}$) are:

$$
\begin{aligned}
cra_{11} &= \frac{-I_u}{[(I_u M - M_s^2 h^2) V_u]} \\
cra_{12} &= \frac{bI_u}{[(I_u M - M_s^2 h^2) V_u]^2} \\
cra_{16} &= \frac{I_u}{(I_u M - M_s^2 h^2)} \\
cra_{21} &= \frac{b}{I_z V_u} \\
cra_{22} &= \frac{-b^2}{I_z V_u} \\
cra_{26} &= \frac{-b}{I_z} \\
cra_{31} &= \frac{M_s h}{(I_u M - M_s^2 h^2) V_u} \\
cra_{32} &= \frac{-bM_s h}{(I_u M - M_s^2 h^2) V_u} \\
cra_{36} &= \frac{-M_s h}{(I_u M - M_s^2 h^2)}
\end{aligned}
\qquad \text{(D.13)}
$$

For K_p, the nonzero elements of matrix ($\frac{\partial A}{\partial K_p}$) are:

$$kpa_{14} = \frac{M_s h}{(I_u M - M_s^2 h^2)}$$
$$kpa_{35} = \frac{-M}{(I_u M - M_s^2 h^2)} \qquad \textbf{(D.14)}$$

For D_p, the nonzero elements of matrix ($\frac{\partial A}{\partial D_p}$) are:

$$dpa_{13} = \frac{M_s h}{(I_u M - M_s^2 h^2)}$$
$$dpa_{33} = \frac{-M}{(I_u M - M_s^2 h^2)} \qquad \textbf{(D.15)}$$

For a, the nonzero elements of matrix ($\frac{\partial A}{\partial a}$) are:

$$
\begin{aligned}
aa_{12} &= \frac{-I_u C_f}{(I_u M - M_s^2 h^2) V_u} \\
aa_{21} &= \frac{-C_f}{I_z V_u} \\
aa_{22} &= \frac{-2a\ C_f}{I_z V_u} \\
aa_{25} &= \frac{C_f}{I_z} \\
aa_{32} &= \frac{M_s h C_f}{(I_u M - M_s^2 h^2) V_u}
\end{aligned}
\qquad \textbf{(D.16)}
$$

For b, the nonzero elements of matrix ($\frac{\partial A}{\partial b}$) are:

$$
\begin{aligned}
ba_{12} &= \frac{I_u C_r}{(I_u M - M_s^2 h^2) V_u} \\
ba_{21} &= \frac{C_r}{I_z V_u} \\
ba_{22} &= \frac{-2bC_r}{I_z\ V_u} \\
ba_{26} &= \frac{-C_r}{I_z} \\
ba_{32} &= \frac{-M_s h C_r}{(I_u M - M_s^2 h^2) V_u}
\end{aligned}
\qquad \textbf{(D.17)}
$$

For h, the nonzero elements of matrix ($\frac{\partial A}{\partial h}$) are:

$$ha_{11}=\frac{-2\,M_s^2\,h\,I_u\,V_u\,(\,C_f+C_r\,)}{[(\,I_u\,M-M_s^2h^2)V_u]^2}$$

$$ha_{12}=\frac{2\,V_u\,I_u\,M_s^2\,h(\,b\,C_r-a\,C_f\,)}{[(I_uM-M_s^2h^2)V_u]^2}$$

$$ha_{13}=\frac{M_s\,D_p(\quad I_u\,M+\,M_s^2\,h^2\quad)}{(\,I_u\,M\,-M_s^2\,h^2)}$$

$$ha_{14}=\frac{-[M(M_sgh-K_p)+M_s^2gh](I_uM-M_s^2h^2)-2M_s^3h^2(M_sgh-K_p)}{(I_uM-M_s^2h^2)^2}$$

$$ha_{15}=\frac{2\quad M_s^2\quad I_x\quad h\quad C_f}{(\quad I_u\quad M-\quad M_S^2\quad h^2\quad)^2}$$

$$ha_{16}=\frac{2\quad M_s^2\quad h\quad I_u\quad C_r}{(\quad I_u\quad M\quad -\quad M_s^2\quad h^2\quad)}$$

$$ha_{31}=\frac{M_sV_u(C_f+\,C_r\,)(\,I_u\,M+\,M_s^2h^2\,)}{[(I_uM-M_s^2h^2)V_u]^2}$$

$$ha_{32}=\frac{-M_sV_u\,(\,bC_r-aC_f\,)(\,I_u\,M+\,M_s^2\,h^2)}{[(I_uM-M_s^2h^2)V_u]^2}$$

$$ha_{33}=\frac{-2M_s^2\,\,M\,h\,D_p}{(\,I_u\quad M-\,M_s^2h^2)^2}$$

$$ha_{34}=\frac{MM_s[g(I_uM-M_s^2h^2)+2M_sh(M_sgh-K_p)]}{(I_uM-M_s^2h^2)^2}$$

$$ha_{35}=\frac{-M_s\,C_f(\,I_u\,\,M\,+\,\,M_s^2\,\,h\,)}{(I_uM-M_S^2h^2)^2}$$

$$ha_{36}=\frac{-M_s\,C_r(\,I_u\,\,M\,+\,\,M_s^2\,h^2\,)}{(I_uM-M_s^2h^2)^2}$$

(D.18)

For V_u, the nonzero elements of the matrix ($\frac{\partial A}{\partial V_u}$) are :

$$
\begin{aligned}
vua_{11} &= \frac{I_u(I_uM-M_s^2h^2)(C_f+C_r)}{[(I_uM-M_s^2h^2)V_u]^2} \\
vua_{12} &= \frac{-I_u(I_uM-M_s^2h^2)(bC_r-aC_f)}{[(I_uM-M_s^2h^2)V_u]^2} - 1 \\
vua_{21} &= \frac{-I_z(bC_r-aC_f)}{I_z^2V_u^2} \\
vua_{22} &= \frac{I_z(a^2C_f+b^2\ C_r)}{I_z^2V_u^2} \\
vua_{31} &= \frac{-M_s\ h(\ I_u\ M-M_s^2h^2)(C_f+C_r)}{[(\ I_u\ M\ -M_s^2\ h^2)V_u]^2} \\
vua_{32} &= \frac{M_s\ h(I_uM-M_s^2h^2)(bC_r-aC_f)}{[(I_uM-M_s^2h^2)V_u]^2}
\end{aligned}
\qquad \text{(D.19)}
$$

APPENDIX-E
PARAMETERS OF CONCIC II VEHICLE

VEHICLE	
total mass	$m = 124.4$ (kg)
moment of inertia	$I_z = 14.6$ (kg.m^2)
wheel base	$k = 0.39$ (m)
wheel span	$l = 0.26$ (m)
distance between pivot point and camera	$l_c = 0.3$ (m)
MOTOR-WHEEL UNIT	
mass	$m_d = 9.5$ (kg)
moment of inertia (refer to motor shaft)	$J = 0.0025$ (kg.m^2)
gear ratio	$n = 9.9$
radius of the wheel	$r_d = 0.075$ (m)
static friction of motor	$T_f = 0$ (N.m)
viscous damping factor	$D = 0.0001$ (N.m.s/rad.)
torque constant	$k_t = 0.114$ (N.m/A)
voltage constant	$k_e = 0.163$ (Volt.s/m)
resistance of motor	$R = 0.602$ ( )
inductance of motor	$L = 0.0047$ (H)
coeffecient of rolling friction	$k_1 = 0.007$; $k_2 = 0.01$ (s/m)
CASTER	
mass of caster	$m_c = 2.4$ (kg)
polar moment of inertia	$I_c = 0.001$ (kg.m^2)
offset	$d = 0.04$ (m)
coeffecient of rolling friction	$k_{c1} = 0.007$; $k_{c2} = 0.01$ (s/m)
coeffecient of side friction	$k_n = 0.01$
SERVO LOOP	
gain of DAC	$k_{dac} = 0.073$
gains of PID filter	$k_p = 225$; $k_i = 100$; $k_d = 50$
integral limit of PID filter	± 30

Table E.1 Paratmeters of CONCIC II [36,41]

(Courtesy of Huang [36])

APPENDIX-F

DESCRIPTIONS OF COMPONENTS OF SERVO-CONTROLLERS, DATA ACQUISITION AND POWER SYSTEM

The LM628 motion controllers are employed at the lower level control loops. Their components, operation and a brief explanation of the commands are explained in this appendix [41,126-127]. Fig. F.1 [41] shows the pinout of the chip. D0-D7(pins 4-11) are the bi-directional data lines connected to data bus of the host computer and are used to read/write data or write commands to the chip. Pins 1,2 and 3 are the encoder lines I, A and B respectively. Pins 12 and 16 are the Chip Select (CS) and Port Select (PS) that perform the reading and write operations. Pins 26 and 27 are the system clock (CLK) and RESET input pins; the latter initialize the chip internal registers. The chip accepts 5V TTL quadrature signals from the incremental encoder and it is possible to read the position and velocity from the encoder counts. The latter is computed by using the time interval of pulses. The LM628 chip has a velocity profile generator in the from of trapezoidal function with acceleration, constant velocity and deceleration period. The velocity and position can be changed during the execution of the motion but acceleration can

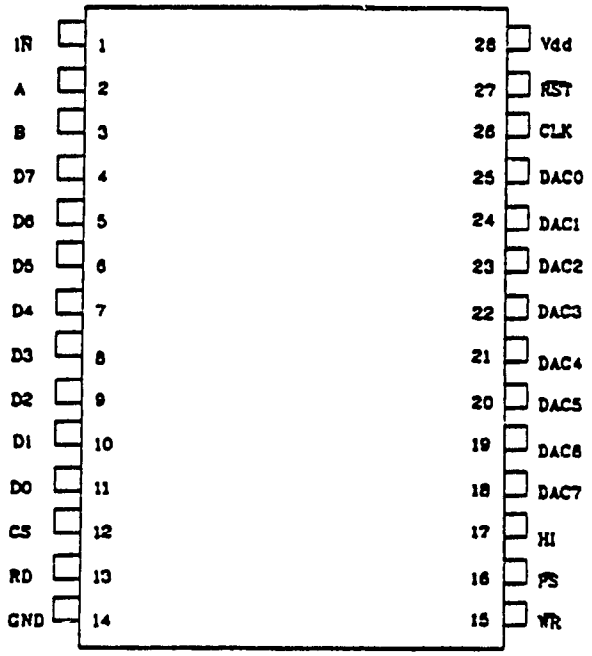

Fig. F.1 Pin Layout of the LM628 Motion Controller

(Courtesy of Rajagopalan[41])

not be changed. Commands are written to the chip by the host computer by using Input/Output ports. Before writing (commands and data) or reading data to the chips, it is necessary to check the busy bit in the status byte of the chip whose maximum duration is 100 μs. The details of timing diagrams of the command byte write, status byte read and data read/write operations can be found in [41,126-127].

The LM628 has a set of commands to perform various functions such as initialization commands, filter, trajectory and interrupt control commands (the latter has not been used here) and data reporting commands, as shown in Table F.1 with their corresponding data values.

There are four initialization commands performed by the chip, namely RFSET (to initialize the chip's internal registers), set the output ports to PORT8 or PORT12 (depending upon the type of DAC) and DEFINE HOME (to provide an absolute zero position). The hexadecimal values of these commands are 00 Hex, 05 Hex, 06 Hex and 02 Hex respectively. The PID filter commands are: load filter parameters (1E Hex) and update filter (04 Hex). Table F.2 shows the filter control word bit allocation[41,126-127]. The Proportional (P) and Integral (I) terms of the filter have a sampling time of $2048/f_{CLK}$ where f_{CLK} is the operating frequency of the LM628 (in our case, the sampling time is 341 μs corresponding

Type	Description	Hex Value	Data Bytes
Initialize	Reset LM628	00	0
Initialize	8 bit output	05	0
Initialize	12 bit output	06	0
Initialize	Define home	02	0
Filter	Load filter para.	1E	2 to 10
Filter	Update filter	04	0
Trajectory	Load trajectory	1F	2 to 14
Trajectory	Start motion	01	0
Interrupt	Set index pos.	03	0
Report	Read status byte	None	2
Report	Read signal regs.	0C	2
Report	Read index pos.	09	4
Report	Read desired pos.	08	4
Report	Read real pos.	0A	4
Report	Read desired vel.	07	4
Report	Read real vel.	0B	2
Report	Read int. sum.	0D	2

Table F.1 LM628 Command Summary

(Courtesy of Rajagopalan[41])

Bit Position	Function
Bit 15	Derivative sampling interval bit 7
Bit 14	Derivative sampling interval bit 6
Bit 13	Derivative sampling interval bit 5
Bit 12	Derivative sampling interval bit 4
Bit 11	Derivative sampling interval bit 3
Bit 10	Derivative sampling interval bit 2
Bit 9	Derivative sampling interval bit 1
Bit 8	Derivative sampling interval bit 0
Bit 7	Not used
Bit 6	Not used
Bit 5	Not used
Bit 4	Not used
Bit 3	Loading Kp (Proportional) data
Bit 2	Loading Ki (Integral) data
Bit 1	Loading Kd (Derivative) data
Bit 0	Loading Il (Integral limit) data

Table F.2 Filter Control Word Bit Allocation

Bit Position								Sampling Interval μs
15	14	13	12	11	10	9	8	
0	0	0	0	0	0	0	0	341.00
0	0	0	0	0	0	0	1	682.67
0	0	0	0	0	0	1	0	1024.67
0	0	0	0	0	0	0	1	1365.33
.	.	.	.	.	.	.	.	.....
.	.	.	.	.	.	.	.	.....
1	1	1	1	1	1	1	1	87381.33

Table F.3 Derivative Term Sampling Interval Selection code

(Courtesy of Rajagopalan[41])

to f_{CLK} of 6MHz). The sampling time of the Derivative (D) term is programmable and ranges from $2048/f_{CLK}$ to $256*2048/f_{CLK}$. Bits 15-8 are used to set derivative sampling time as shown in Table F.3 [41]. A logic high on bits 3 to 0 indicates that the data downloaded are K_p, K_i, K_d and I_l (all coefficients are 16 bits words) respectively and the order of loading is the same as shown above. The downloaded coefficients are written to a primary buffer and are moved if the filter update command (04 Hex) is executed after checking busy bit.

The trajectory control commands consist of load trajectory (1F Hex) and start motion (01 Hex) with their control words shown in Table F.4 [41]. Bit 12 shows the direction of motion (logic high for clockwise rotation) in the velocity mode and bit 11 is for mode of operation (velocity or position). Bits 10-8 are to stop the motor with bit 10 for smooth stop and uses the programmed acceleration, bit 9 for panic stop to stop the motor at the highest possible deceleration and bit 8 is to stop the motor by applying a zero output to DAC (equivalent to turning the motor off). Bits 5 through 0 are to inform the nature of the data being downloaded ranging from absolute or relative acceleration, velocity or position. All the data are 32 bits and the order of loading is the same as mentioned above Also, similar to filter commands, the data are written to a primary buffer and then move to the secondary buffer.

Bit Position	Function
Bit 15	Not used
Bit 14	Not used
Bit 13	Not used
Bit 12	Forward direction - velocity mode only
Bit 11	Velocity mode selection
Bit 10	Smooth stop - use selected deceleration value
Bit 9	Stop abruptly - use maximum acceleration value
Bit 8	Turn off - zero output to the DAC, no feedback
Bit 7	Not used
Bit 6	Not used
Bit 5	Acceleration will be loaded (absolute)
Bit 4	Acceleration will be loaded (relative)
Bit 3	Velocity will be loaded (absolute)
Bit 2	Velocity will be loaded (relative)
Bit 1	Position will be loaded (absolute)
Bit 0	Position will be loaded (relative)

Table F.4 Trajectory Control Word Bit Allocation

Bit Position	Function
Bit 7	Motor Off
Bit 6	Breakpoint Reached (Interrupt)
Bit 5	Excessive Position Error (Interrupt)
Bit 4	Wraparound Occured (Interrupt)
Bit 3	Index Pulse Observed (Interrupt)
Bit 2	Trajectory Complete (Interrupt)
Bit 1	Command Error (Interrupt)
Bit 0	Busy Bit

Table F.5 Status Byte Bit Allocation

(Courtesy of Rajagopalan[41])

Bit Position	Function
Bit 15	Host Interrupt
Bit 14	Acceleration Loaded (not updated)
Bit 13	Trajectory Update Executed (filter not updated)
Bit 12	Forward Direction
Bit 11	Velocity Mode
Bit 10	On Target
Bit 9	Turn off - excessive position error
Bit 8	Eight Bit Output Mode
Bit 7	Motor Off
Bit 6	Breakpoint Reached (Interrupt)
Bit 5	Excessive Position Error (Interrupt)
Bit 4	Wraparound Occured (Interrupt)
Bit 3	Index Pulse Acquired
Bit 2	Trajectory Complete (Interrupt)
Bit 1	Command Error (Interrupt)
Bit 0	Acquire Next Index Pulse (Set Index Executed)

Table F.6 Signal Register Bit Allocation

(Courtesy of Rajagopalan[41])

The data reporting commands consist of read status byte, real and desired velocity, signal register, index signal position and integration sum limit. The status byte read operation has no command byte and is performed by simply reading the command port while the other read operations require the commands 08 Hex, 0A Hex, 07 Hex, 0B Hex, 09 Hex and 0D Hex, respectively, before reading data. The bytes are read from the most to the least significant.

F.2 Motion Controller Card and Interface with the IBM Bus

The communication between the LM628 chips and the host computer is provided by an interface card whose layout and circuitry are shown in Fig. F.2. The motion controller card has been designed and wire-wrapped to control four motors and its different segments are interface with the IBM Bus, motion controller and DAC, conditioning for servo amplifiers and encoder signals and safety features. As it is shown in Fig. F.2, the IBM BUS signals are driven by 74LS245 and 74LS244 bus drivers and the address decoding is performed by the use of two PAL16L8. There are a total of 12 addresses for chip selection as one command and data addresses for each motor (total of 8) and two common commands and data addresses for each pair of driving and steering motors (A&B, C&D) to facilitate their simultaneous motion.

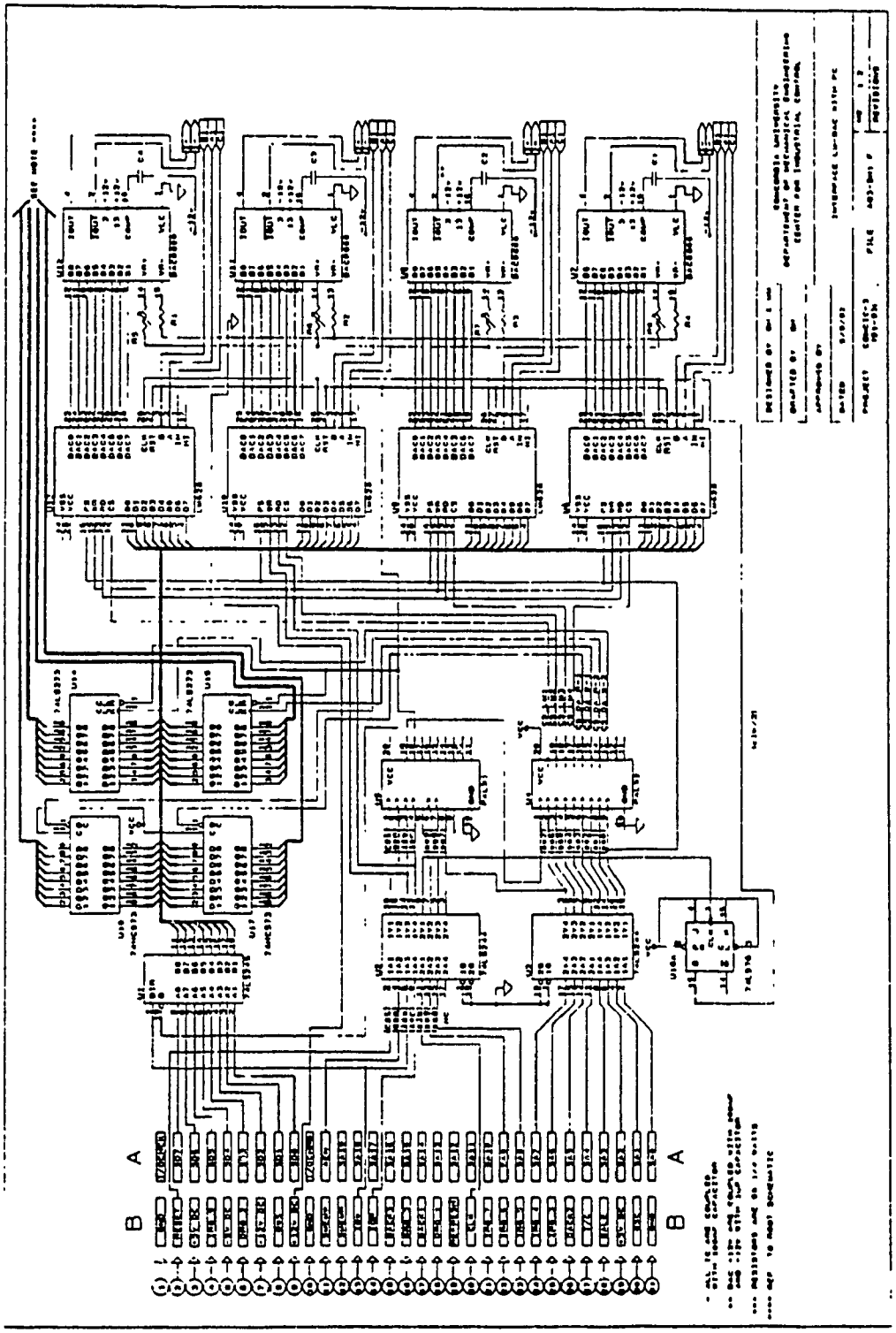

Fig. F.2 Interface circuitry

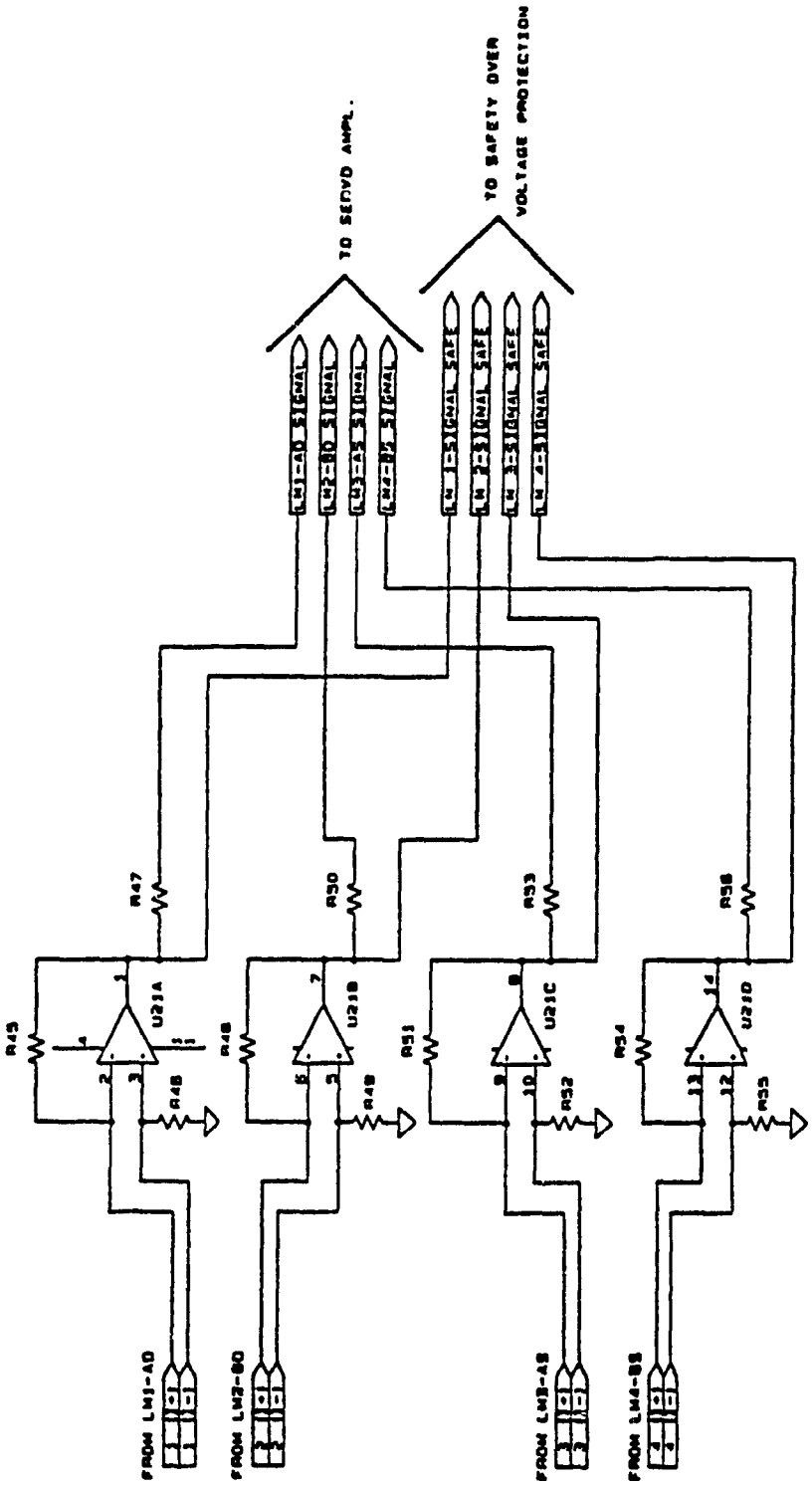

Fig. F.3 Interface with the Servo Amplifiers

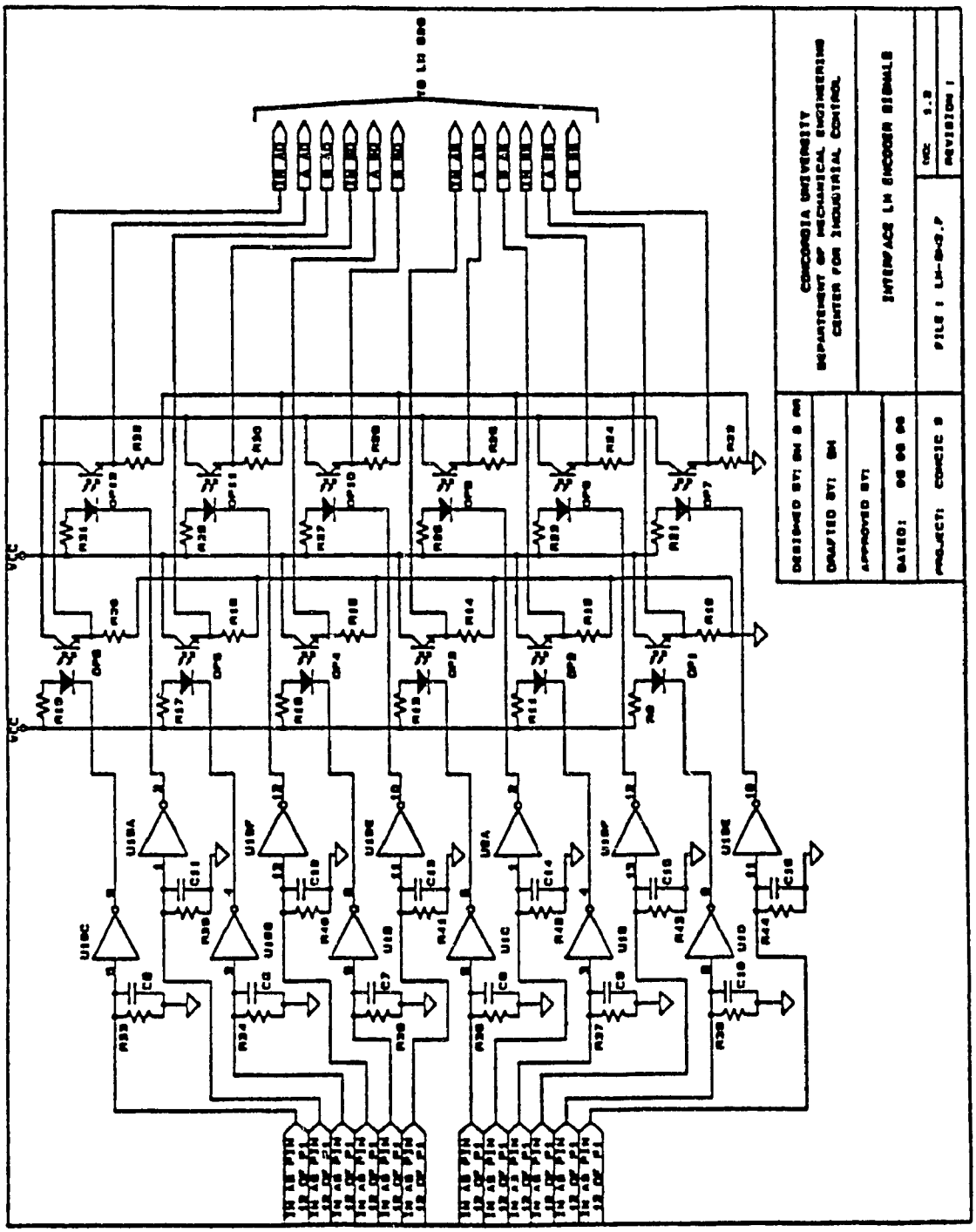

Fig. F.4 Interface with the Encoders

(Courtesy of Rajagopalan[41])

The signal conditioning circuits of the servo amplifier and encoder signals are shown in Fig. F.3-F.4. Two operational amplifiers are used to convert the current signal coming out of the DAC and to attenuate the signal in the range of -7.0 to 7.0 (as required by Galil servo amplifiers) respectively. Furthermore, since the encoder signals contain some elements of noise and they are directly connected to LM628 chips, a simple filter is used to remove the unwanted spikes.

F.3 Servo Amplifiers

The servo amplifiers employed for CONCIC III are off-the-shelf pulse width modulation amplifiers from Galil Motion Control [128] with the amplifier type ESA 15/75H meaning that the amplifier can deliver a maximum continuous current of 15A with the maximum operating voltage of 75 Volts. The minimum supply voltage is 20 Volts, the maximum peak current is 37A, the efficiency is %95 and a switching frequency is 20 KHz. The amplifier is H-type and can be set in current mode or voltage mode. In our case, the amplifiers are set in current mode with armature voltage feedback. As it is shown in Fig. F.4 [41], the armature current is obtained by measuring the voltage across a resistor and is compared with the output of an error amplifier. The resulting difference is processed by the current amplifier to provide a voltage command to the pulse width modulation section of the amplifier. It is necessary to set the continuous

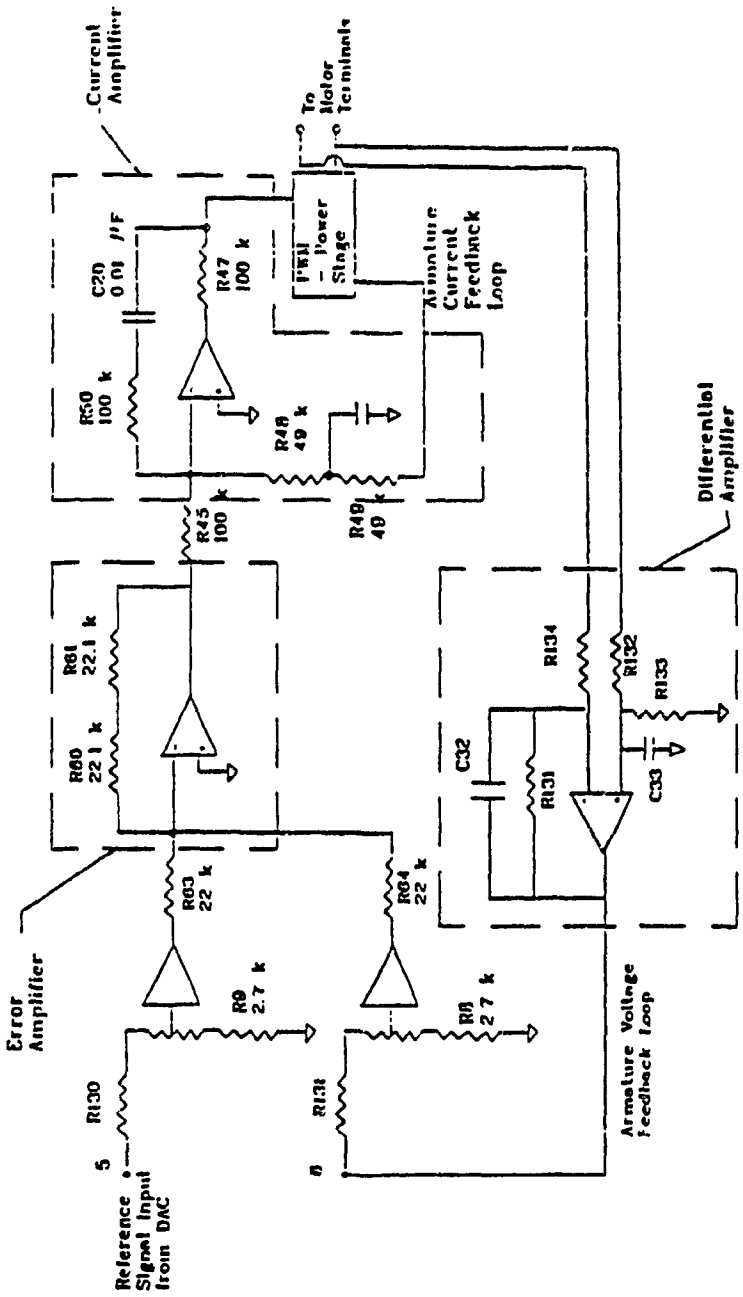

Fig. F.4 Servo Amplifier with Armatur· Voltage Feedback

(Courtesy of Rajagopalan[41])

and the peak current limits of the amplifiers based on the motor ratings. The current amplifier makes sure that the continuous current supplied to the motor does not exceed the current limit.

F.4 Position and Velocity Feedback Components

In closed-loop control systems, the feedback components are necessary to measure the position and velocity of the controlled system. This can be achieved by using analog devices such as tachometer (to provide velocity feedback) or potentiometer(to provide position feedback). For digital systems, the incremental encoder can be used to provide pulse trains whose frequency depends on the velocity of the motor and a decoding circuit to convert the pulses to speed or position information. In CONCIC III, the driving and steering motors employ the incremental encoders with quadrature output signals that provide the bi-directional control of the motors as well as enhancement in accuracy. For driving units, the encoders are from PMI motion technology and for steering motors, the encoders are from BEI motors. The detail specifications of the encoders are illustrated in Table F.7 [41].

F.5 Data Acquisition System Interface

Data acquisition system is provided to record the voltages and current of the steering and driving motors in real time. It is an interrupt driven data acquisition system whose circuit diagram is shown in Fig. F.5. The board consists of 12 bits analog to digital convertors (ADC) and the required signal conditioning circuitry to remove the noise. Figs. F.6-F.7 shows the ADC and host computer interfacing. The data conditioning circuitries are shown in Figs. F.6 (data conditioning for voltage) and F.7 (data conditioning for current). The board also houses a 8254 timer that is used to measure the timings of various cycle times, computations of actual velocities of the wheels, etc.

Encoder Specification for Drive Motors	
Company	PMI Motors
Type	Incremental Encoders with ABI signals
Model Type	M23
Output Waveform	Square wave ; 5Volt TTL Standard signal
Input Voltage	5 Volt ±5%
Resolution	1024 pulses per revolution
Hub Size	0.3750 inch diameter
Color Coding	
Output - A	White
Output - B	Blue
Index - I	Green
Ground	Black
Supply Voltage	Red
Specification	M23 - 1024 - ABI - 5 - S - C - .3750

Encoder Specification for Steer Motors	
Company	BEI Motors
Type	Incremental Encoders with ABI signals
Model Type	M23
Output Waveform	Square wave ; 5Volt TTL Standard signal
Input Voltage	5 Volt ±5%
Resolution	256 pulses per revolution
Hub Size	0.25 inch diameter
Color Coding	Terminals are marked on the enocder
Specifications	M23 - 256 - ABI - 5 - S - C - .2500

Table F.7 Specifications of the Encoders

(Courtesy of Rajagopalan[41])

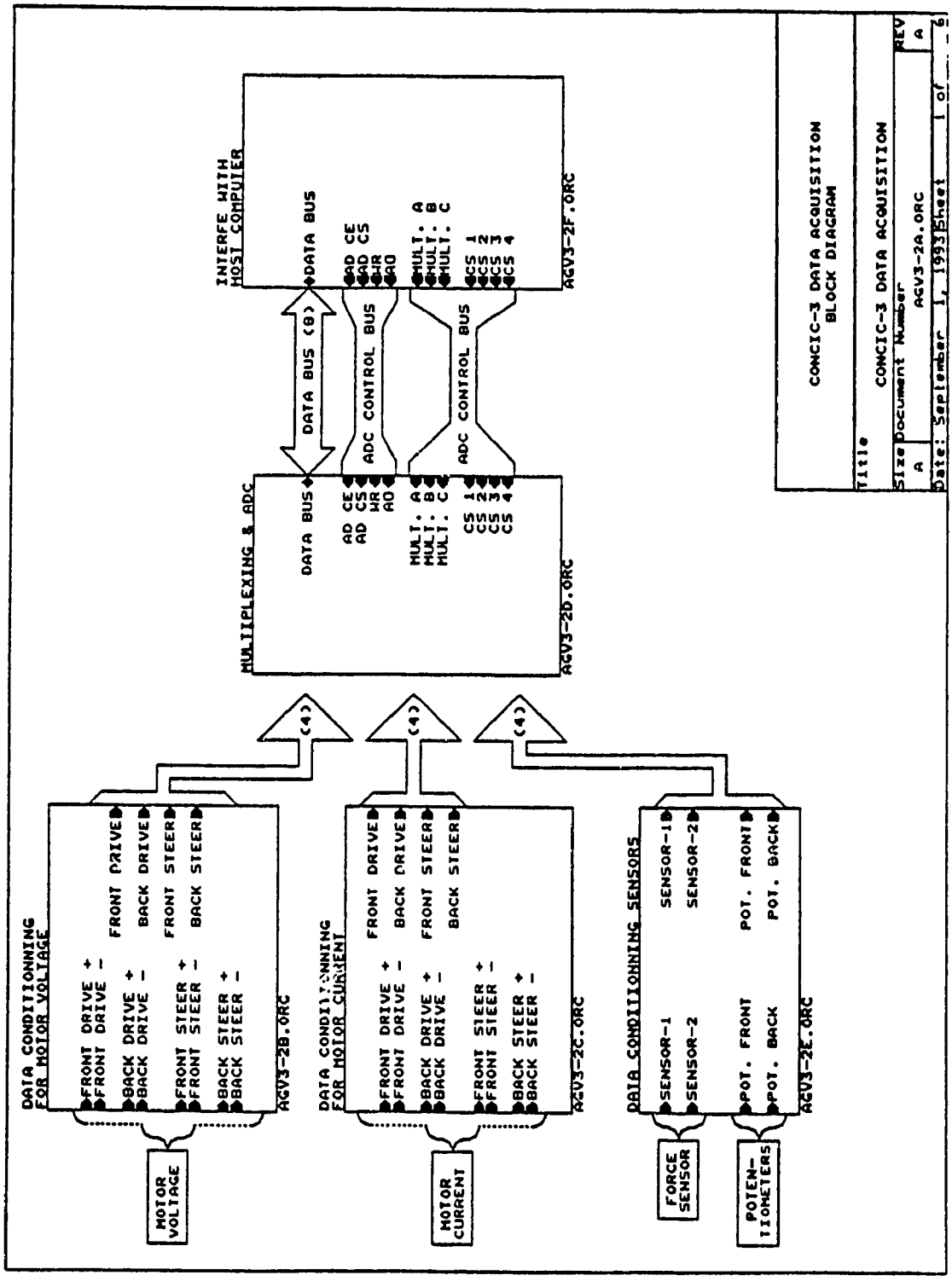

Fig. F.5 Data Acquisition Board

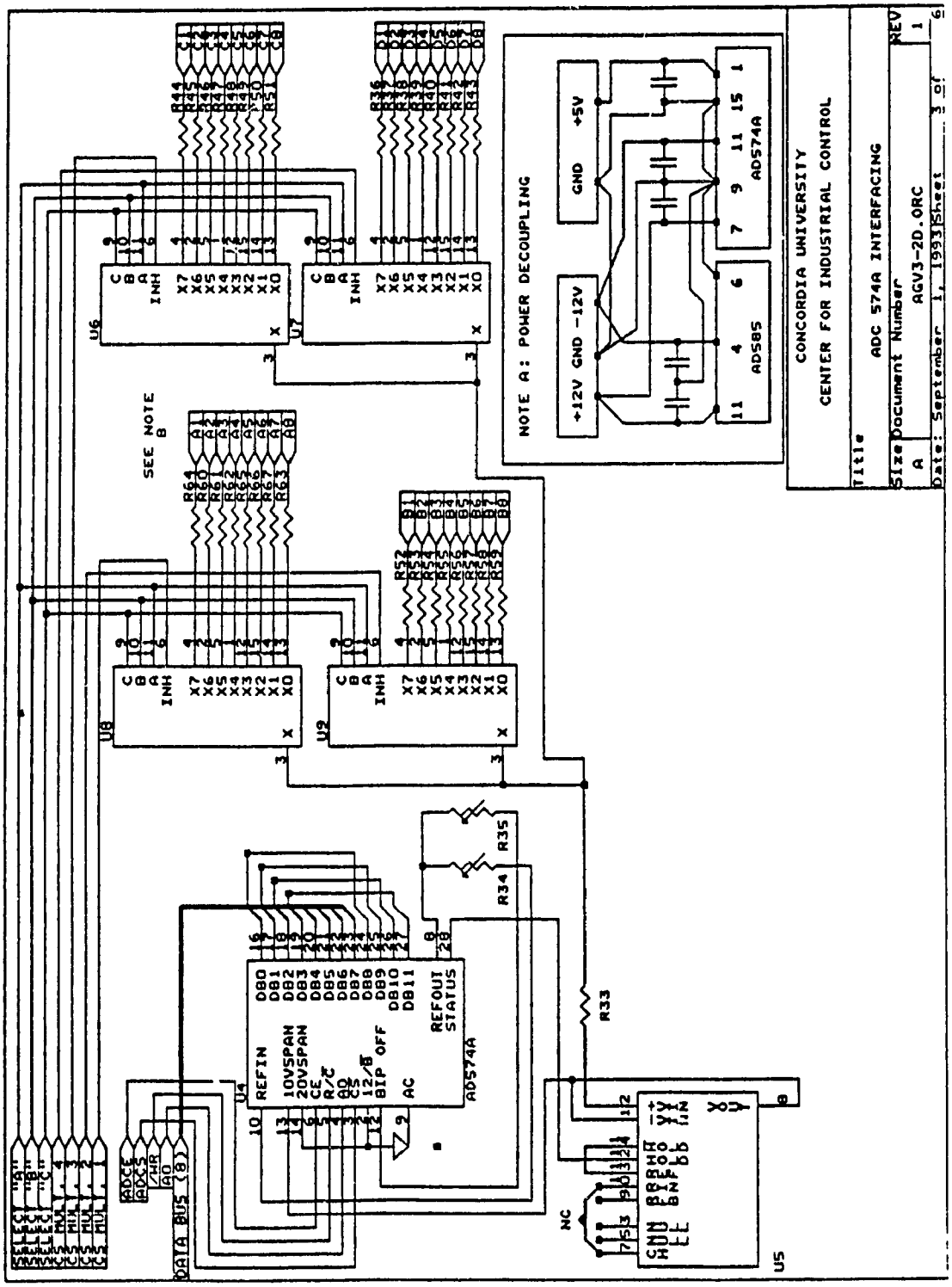

Fig. F.6 ADC 574A Interfacing

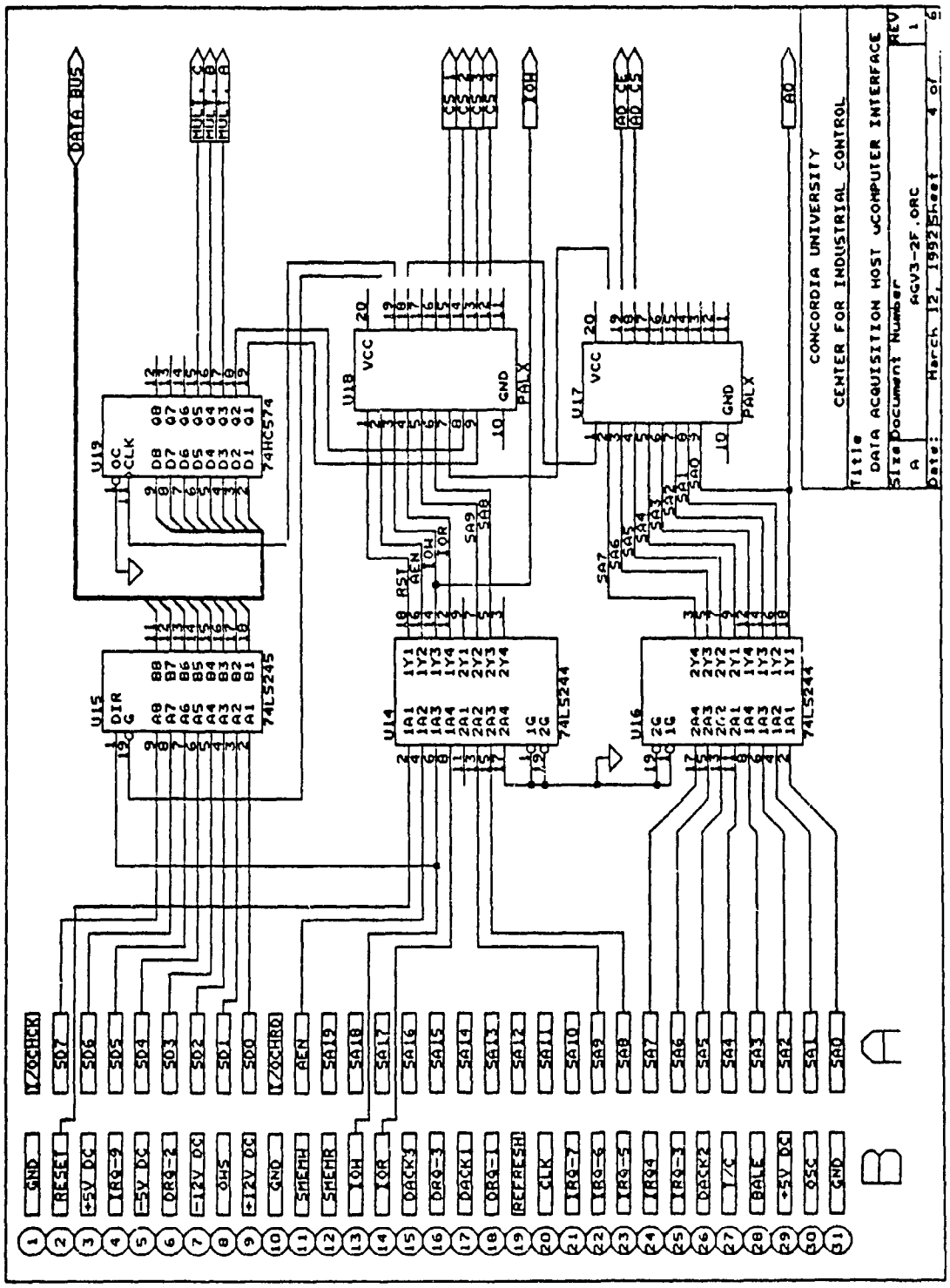

Fig. F.7 Data Acquisition and Host Computer Interfacing

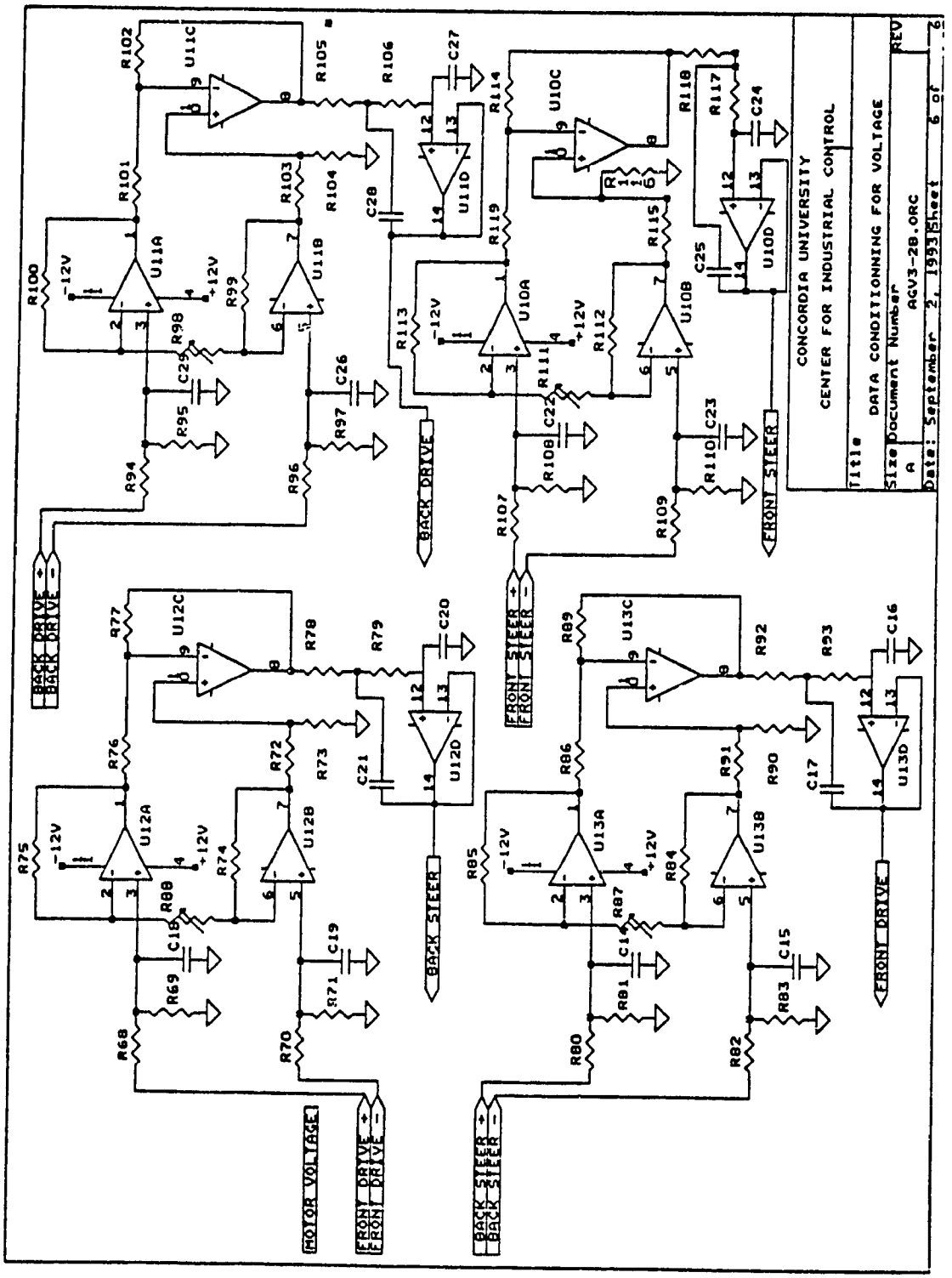

Fig. F.8 Data Conditioning for Voltage

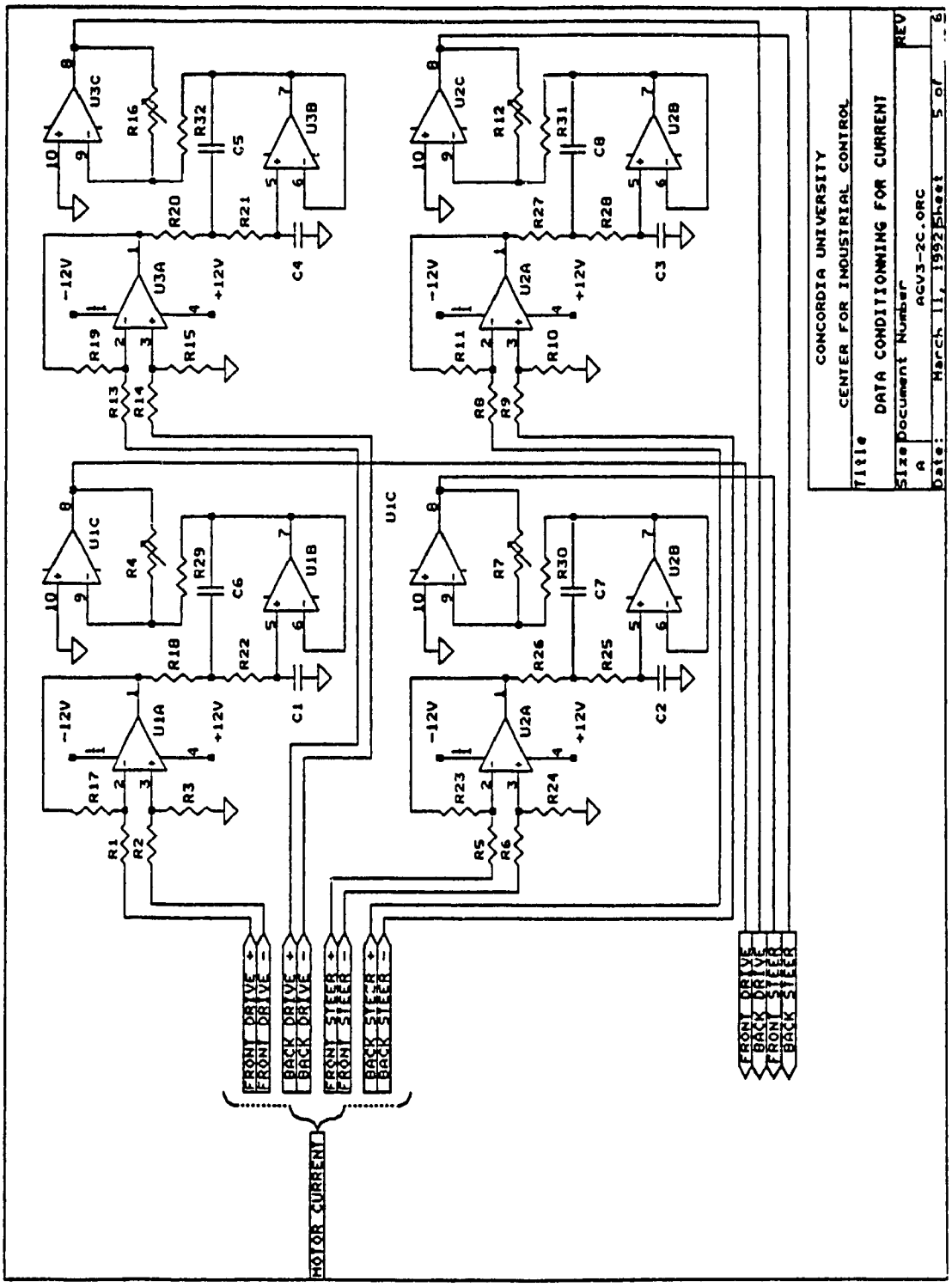

Fig. F.9 Data Conditioning for Current

APPENDIX-G

PATH RECONSTRUCTION SCHEME

In this appendix, the path reconstruction scheme employed for the motion of the vehicle is explained. It is intended to find the new position and orientation of the vehicle (posture) according to the readings of the encoder shafts of the front and rear driving and steering motors. Two successive motions of the vehicle are shown in Fig. G.1. U and W are the axis attached to the vehicle and X, Y are the fixed (world) coordinates. Points A,B and C are the initial positions of the front, rear and the centre of mass of the vehicle and the final positions of the same points are shown by A′, B′ and C′. Referring to this figure, the following relations can be written between the pairs (A,A′) and (B,B′) in (U,W) frame as:

$$U_{A'} = U_A + \Delta l_f \cos \delta_f \tag{G.1}$$

$$W_{A'} = W_A + \Delta l_f \sin \delta_f \tag{G.2}$$

and

$$U_{B'} = U_B + \Delta l_r \cos \delta_r \tag{G.3}$$

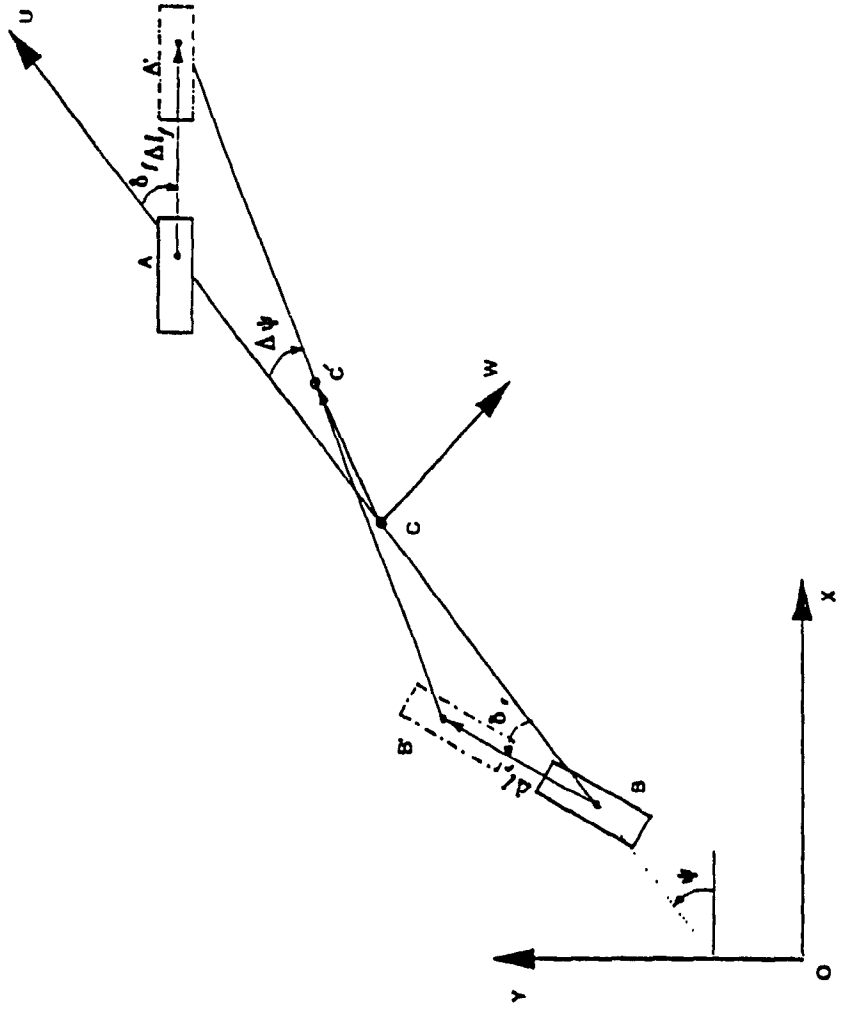

Fig. G.1 Incremental Motion of the Vehicle

$$W_{B'} = W_B + \Delta l_r \sin \delta_r \qquad \text{(G.4)}$$

where ($U_{A'}$, $W_{A'}$) and (UB', $W_{B'}$) are the new coordinates of Points A' and B'in (U,W) coordinate system. The incremental change in orientation of the vehicle ($\Delta\psi$) can be obtained from:

$$\Delta\psi = \tan^{-1} \frac{(W_{A'} - W_{B'})}{(U_{A'} - U_{B'})} \qquad \text{(G.5)}$$

Therefore, the new position and orientation of the centre of mass of the vehicle can be found from:

$$U_{C'} = U_{B'} + b \cos \Delta\psi \qquad \text{(G.6)}$$

$$W_{C'} = W_{B'} + b \sin \Delta\psi \qquad \text{(G.7)}$$

APPENDIX-H

DERIVATION OF EQUATIONS OF MOTION WITH KINEMATIC CONSTRAINTS

Thus far in the study of motion of automated vehicles, we have depended upon direct application of Newton's equations of motion by noting that given the external forces applied to the system, we can solve for the equations of motion. In this appendix, the formulation of equations of motion for the vehicle with the front and rear steering wheels will be presented by using Lagrangian formalism.

In the following sections, the equations describing the kinetic energy of the system will be presented. Also, the equations of the constraints to be satisfied for pure rolling and non-slippage motion of these vehicles will be given. Finally, the dynamic equations of the system will be derived.

H.1 Kinetic Energy of the System

Let the coordinates describing the configuration of the system be body axis (UCW) and the world coordinate (XOY) as it is done in chapter 4 (Fig.4.4). The kinetic energy of the vehicle can be expressed as:

$$T = \frac{1}{2} M (V_u^2 + V_w^2) + \frac{1}{2} I_z \Omega^2 \qquad \text{(H.1)}$$

where T is the kinetic energy of the vehicle, M and I_z are the mass and moment of inertia of the vehicle around its centre of mass C, V_u and V_w are the vehicle velocities in U and W directions, and Ω is the angular velocity of the vehicle.

In a similar manner, the kinetic energy of the front and rear wheels can be obtained as:

$$T_{kf} = \frac{1}{2} m_f (r_w \omega_f)^2 + \frac{1}{2} I_y \Omega^2 + \frac{1}{2} I_f \omega_f^2 \qquad \text{(H.2)}$$

or

$$T_{kf} = \frac{1}{2} (J_f + r_w^2 m_w) \omega_f^2 + \frac{1}{2} I_y \Omega^2 \qquad \text{(H.3)}$$

$$T_{kr} = \frac{1}{2}(J_r + r_w^2 m_w)\omega_r^2 + \frac{1}{2}I_y\Omega^2 \tag{H.4}$$

where m_w is the masse of the front and rear wheels (assumed equal), J_f and J_r are the moments of inertia of the front and rear wheels around their centres, ω_f, ω_r are the angular velocities of the front and rear wheels and I_y is the moment of inertia of the front and rear wheels about their axis of symmetry (in the plane of the wheel). Therefore the total kinetic energy of the system is:

$$\begin{aligned} T = & \frac{1}{2}M(V_u^2 + V_w^2) + \frac{1}{2}I_z\Omega^2 + I_y\Omega^2 \\ & + \frac{1}{2}(J_f + r_w^2 m_w)\omega_f^2 + \frac{1}{2}(J_r + r_w^2 m_w)\omega_r^2 \end{aligned} \tag{H.5}$$

or

$$\begin{aligned} T = & \frac{1}{2}M(V_u^2 + V_w^2) + \frac{1}{2}I\Omega^2 \\ & + \frac{1}{2}(I_f)\omega_f^2 + \frac{1}{2}(I_r)\omega_r^2 \end{aligned} \tag{H.6}$$

where

$$I = I_z + I_y \tag{H.7}$$

and

$$I_f = J_f + r_w^2 m_w$$
$$I_r = J_r + r_w^2 m_w \qquad \text{(H.8)}$$

H.2 Kinematic Constraints of the System

For the vehicle moving on a horizontal plane, the contact point between the wheels and the ground should satisfy the conditions of pure rolling and non-slippage. For the vehicle under consideration (front and rear steered; telescopic model), the fact that it should move in U- direction without slippage gives:

$$V_u - r_w \omega_r \cos \delta_{rw} = 0 \qquad \text{(H.9)}$$

There are rolling constraints to be satisfied such that the tangential velocity of each wheel rim must be equal to the linear velocity of the wheel rim with respect to the ground. Referring to Fig.4.6, one sees that this condition leads to two equations as:

$$V_w - r_w \omega_r \sin \delta_{rw} - b\Omega = 0 \qquad \text{(H.10)}$$

and

$$V_w + a\Omega - r_w \omega_f \sin \delta_{fw} = 0 \qquad \text{(H.11)}$$

the symbols used such as a, b, etc. are the same as in chapter 4. These are a set of nonholonomic constraints to be satisfied for no-slippage motion of the vehicle.

H.3 Derivation of Dynamic Equations

The general form of Lagrange equation is [131,132]

$$\frac{\partial T}{\partial q_k} - \frac{\partial}{\partial t}\left(\frac{\partial T}{\partial \dot{q}_k}\right) + \sum_{j=1}^{3} F_{jk}\lambda_j - Q_k = 0 \qquad \text{(H.12)}$$

where T is the kinetic energy, q_k are generalized coordinates, λ_j are Lagrange multipliers and F_{jk} are the coefficients of generalized coordinates (q_k) in j'th constraint equation and Q_k are the generalized forces.

For the system under consideration, one can specify the generalized coordinates as:

$$\left[\ q_1,\ q_2,\ q_3,\ q_4,\ q_5\ \right]^T = \left[\ x_u,\ y_u,\ \psi,\ \psi_f,\ \psi_r\ \right]^T \qquad \text{(H.13)}$$

where (x_u, y_u) are the coordinates of the centre of mass of the vehicle in body axis, ψ is the orientation angle of the vehicle, axis, ψ_f and ψ_r are the angular positions of the front and rear wheels, respectively. Therefore, with the above number of

generalized coordinates (five) and the number of constraint equations (three), namely equations (H.7-H.9), the system has two degrees of freedom. By substituting the expression for kinetic energy of the system (equation (H.7)) and employing constraint equations (equations (H.9) to (H.11)) in equation (H.12), one can get the following set of equations as:

$$M \dot{V}_u = \lambda_1 \tag{H.14}$$

$$M \dot{V}_w = \lambda_2 + \lambda_3 \tag{H.15}$$

$$I \dot{\Omega} = a\lambda_3 - b\lambda_2 \tag{H.16}$$

$$I_f \dot{\omega}_f = T_f - \lambda_3 r_w \sin \delta_{fw} \tag{H.17}$$

$$I_r \dot{\omega}_r = T_r - \lambda_1 r_w \cos \delta_{rw} - \lambda_2 r_w \sin \delta_{rw} \tag{H.18}$$

where T_f and T_r are the torques of the front and rear wheels corresponding to generalized forces (Q_5 and Q_6) and also $V_u = \dot{x}_u$, $V_w = \dot{y}_w$, $\Omega = \dot{\psi}$, $\omega_r = \dot{\psi}_r$, $\omega_f = \dot{\psi}_f$.

The above equations namely equations (H.14) to (H.18) (five equations), together with the equations of the constraints (three equations) should be solved

for eight unknowns (five generalized coordinates and three Lagrange multipliers) in order to specify the posture (position and orientation) of the vehicle at any instant.

Differentiating equations (H.10) and (H.11), one can get the expressions for ω_r, ω_f in terms of V_w and Ω as:

$$\dot{\omega}_r = \frac{(\dot{V}_w - b\,\dot{\Omega})\, r_w \sin \delta_{rw} - (V_w - b\Omega)\, r_w\, \dot{\delta}_{rw} \cos \delta_{rw}}{(r_w \sin \delta_{rw})^2} \quad \text{(H.19)}$$

$$\dot{\omega}_f = \frac{(\dot{V}_w + a\dot{\Omega})\, r_w \sin \delta_{fw} - (V_w + a\Omega)\, r_w\, \dot{\delta}_{fw} \cos \delta_{fw}}{(r_w \sin \delta_{fw})^2}$$

(H.20)

Differentiating equation (H.9) and combining the result with equation (H.14) we get:

$$\dot{V}_u = r_w\, \dot{\omega}_r \cos \delta_{rw} - r_w\, \dot{\delta}_{rw}\, \omega_r \sin \delta_{rw} \quad \text{(H.21)}$$

$$\lambda_1 = M\,(\, r_w\, \dot{\omega}_r \cos \delta_{rw} - r_w\, \dot{\delta}_{rw}\, \omega_r \sin\delta_{rw}) \quad \text{(H.22)}$$

Also, from equations (H.15) and (H.16), λ_2 and λ_3 can be found in terms of V_w and Ω as:

$$\lambda_2 = \frac{b\,M\,\dot{V}_w + I\,\dot{\Omega}}{(a+b)} \tag{H.23}$$

$$\lambda_3 = \frac{a\,M\,\dot{V}_w - I\,\dot{\Omega}}{(a+b)} \tag{H.24}$$

After substituting for ω_f, ω_r from equations (H.19-H.20) and λ_1, λ_2, λ_3 from equations (H.22-H.24) in equations (H.17-H.18) and doing the necessary manipulation, one can get:

$$a_1\dot{V}_w + a_2\dot{\Omega} + a_3 V_w + a_4\Omega = T_r\,(r_w \sin \delta_{rw})^2 \tag{H.25}$$

and

$$b_1\dot{V}_w + b_2\dot{\Omega} + b_3 V_w + b_4\Omega = T_f\,(r_w \sin \delta_{rw})^2 \tag{H.26}$$

where

$$a_1 = I_t\, r_w \sin \delta_{fw} + r_w^3\, a\, M\, \frac{(\sin \delta_{fw})^2 \sin \delta_{rw}}{(a+b)}$$

$$a_2 = I_t\, a\, r_w \sin \delta_{fw} - r_w^3\, I\, \frac{(\sin \delta_{fw})^2 \sin \delta_{rw}}{(a+b)}$$

$$a_3 = -I_t\, r_w \cos \delta_{fw}\, \dot{\delta}_{fw} + r_w^3\, M \cos \delta_{rw} (\sin \delta_{fw})^2\, \dot{\delta}_{rw}$$

$$a_4 = -I_t\, a\, r_w \cos \delta_{fw}\, \dot{\delta}_{fw} + r_w^3\, b\, M \cos \delta_{rw} (\sin \delta_{fw})^2\, \dot{\delta}_{fw} \qquad \text{(H.27)}$$

with

$$I_t = I + r_w^2\, M \cos^2 \delta_{rw} \qquad \text{(H.28)}$$

and

$$b_1 = r_w\, I \sin \delta_{rw} + \frac{b\, r_w^3\, M}{(a+b)} \sin^3 \delta_{rw}$$

$$b_2 = -I\, b\, r_w \sin \delta_{rw} + r_w^3\, I_t\, \frac{\sin^3 \delta_{rw}}{(a+b)}$$

$$b_3 = -I\, r_w \cos \delta_{rw}\, \dot{\delta}_{rw}$$

$$b_4 = +I\, b\, r_w \cos \delta_{fw}\, \dot{\delta}_{fw} \tag{H.29}$$

Equations (H.17) to (H.18) and (H.22) to (H.26) can be numerically integrated to find the position and orientation of the vehicle. Noting that the above equations are written in the vehicle body axis, the same transformations as in previous chapters can be used to find the position and orientation of the vehicle in world coordinate. As it is seen, throughout the derivations of equations of motion, stiffness properties of the wheels are totally neglected and in the final expressions some nonlinear terms are involved that makes the analysis and design of the controller difficult.